

**EVALUATION OF PERFORMANCE PARAMETERS OF
REDESIGNED HYBRID MUFFLER THROUGH
SIMULATION AND EXPERIMENTATION**

Thesis Submitted for the Award of the Degree of

DOCTOR OF PHILOSOPHY

in

Mechanical Engineering

By

Ujjal Kalita

Registration Number: 41700203

Supervised By

Dr. Manpreet Singh (20360)

School of Mechanical Engineering (Professor)

Lovely Professional University, Punjab



LOVELY PROFESSIONAL UNIVERSITY, PUNJAB

2023

DECLARATION

I, hereby declared that the presented work in the thesis entitled “**EVALUATION OF PERFORMANCE PARAMETERS OF REDESIGNED HYBRID MUFFLER THROUGH SIMULATION AND EXPERIMENTATION**” in fulfilment of degree of **Doctor of Philosophy (Ph. D.)** is outcome of research work carried out by me under the supervision **Dr. Manpreet Singh**, working as Professor in the **School of Mechanical Engineering** of Lovely Professional University, Punjab, India. In keeping with general practice of reporting scientific observations, due acknowledgements have been made whenever work described here has been based on findings of other investigator. This work has not been submitted in part or full to any other University or Institute for the award of any degree.



(Signature of Scholar)

Name of the scholar: Ujjal Kalita

Registration No.: 41700203

Department/school: Mechanical Engineering

Lovely Professional University,

Punjab, India

CERTIFICATE

This is to certify that the work reported in the Ph. D. thesis entitled “**EVALUATION OF PERFORMANCE PARAMETERS OF REDESIGNED HYBRID MUFFLER THROUGH SIMULATION AND EXPERIMENTATION**” submitted in fulfillment of the requirement for the reward of degree of **Doctor of Philosophy (Ph.D.)** in the Mechanical Engineering, is a research work carried out by __Ujjal Kalita__, 41700203_____, is bonafide record of his/her original work carried out under my supervision and that no part of thesis has been submitted for any other degree, diploma or equivalent course.



(Signature of Supervisor)

Name of supervisor: Dr. Manpreet Singh

Designation: Professor

Department/school: Mechanical Engineering

University: Lovely Professional University, Punjab

(Signature of Co-Supervisor)

Name of Co-Supervisor:

Designation:

Department/school:

University:

Abstract

Acoustics is a branch of science which deals with the behavior of sound. There are both wanted and unwanted sound across our environment. Noise is an unwanted sound which greatly affects the human health. As the number of automobiles is growing at an alarming rate in the modern day, a noise- and pollution-free environment is the most crucial factor. The sharp rise in automobile use significantly worsens noise pollution and puts people in danger. Because of this, the government now has to impose severe regulations on automakers to keep noise levels within the allotted ranges. Manufacturers are working hard to redesign various automotive parts that contribute to the overall sound level produced in the car in light of this. For instance, the overall sound level is influenced by the tyres, cooling system, intake and exhaust system, transmission system, and engine components. As exhaust sound contributes the most to the overall sound level of an automobile, an effort has been made in this study to reduce exhaust system noise by muffler redesign. The design was optimized and the muffler capability was increased using Taguchi-based design of experiments methodology. Initially, Comsol's pressure acoustic, frequency domain analysis was used to conduct pilot trials for choosing the number of baffles. Two baffles were chosen instead of three baffles based on the production of domes inside a particular frequency range that was identified through it. The position of the input and output tubes' baffles (L1 and L2), as well as the hole's position (HP), were selected as the control factors, and the range of these control factors was established using the two baffles. A signal to noise (S/N) ratio analysis in Minitab was then performed on the L9 trials obtained using the Taguchi method. As a result, we were given the appropriate dimension value of $L1 = 190$ mm, $L2 = 110$ mm and $HP = 10$ mm to get the maximum transmission loss. The significance and percentage contribution of the control factors to the performance of the muffler were then estimated using analysis of variance (ANOVA). The optimized reactive muffler's transmission loss (TL) value is validated by a transmission loss test using an impedance tube setup, and both findings demonstrated strong agreement with little difference in TL value. Then, Taguchi's DOE was used to transform the optimized reactive muffler into a hybrid muffler by adding a layer of Glasswool absorption material inside of it. The thickness of absorption material in each chamber of the hybrid muffler were selected as the main control factors. The L16 trial experiments was obtained using the Taguchi

method and signal to noise ratio analysis was performed. This gave the optimum dimension value of thickness of absorption material in each chamber. The optimum value of thickness in chamber 1 is zero, whereas in second and third chamber it is found to be 35 mm. The ANOVA was then conducted for predicting the significance of this control factors. Using this optimized value of absorption layer thickness the hybrid muffler was tested in Comsol Multiphysics. These findings were supported by an experimental setup using impedance tubes. The results showed a significant improvement in maximum transmission loss value as compared to the optimized reactive muffler and existing muffler. The TL value of an existing muffler produced through modelling and experiment was compared with the results achieved for the optimized reactive and hybrid muffler. With a wider frequency spectrum for the third dome, the improved hybrid muffler demonstrated a noticeable development in terms of maximum TL and superior performance overall. In order to comply with government standards and lowering an automobile's overall sound level, a hybrid muffler may therefore be a preferable option. The pressure acoustic, frequency domain analysis was also suggested in the study as an effective way for assessing muffler performance.

As part of this analysis, vibration signals were also collected in each chamber of the hybrid muffler, and their impact on the muffler's sound pressure level was examined. During the experimentation, vibration signals are acquired with the help of accelerometer, by placing it at three positions namely inlet tube, center and outlet tube of muffler. Next, the FFT analysis was performed followed by wavelet analysis and from this analysis, Fejer-Korovkin wavelet was selected as the most suitable wavelet for analysis of vibration signal. Using this wavelet, the rms, standard deviation, kurtosis, Shannon entropy and log energy entropy for all the signals are investigated. Finally, comparing the sensitivity analysis for the Shannon entropy of the signals and sound pressure level of the hybrid muffler helps in identifying the position, having greatest impact of vibration on muffler.

Keywords: Reactive Muffler, Hybrid muffler, Transmission Loss, Pressure acoustic frequency domain analysis, COMSOL Multiphysics, Impedance tube, Vibration

Acknowledgement

Firstly and foremost, I am profoundly grateful to my respected supervisor Dr. Manpreet Singh, Professor, Department of Mechanical Engineering, LPU, Phagwara, Punjab for his constant involvement, energetic efforts and proficient guidance.

This work would not have been possible without the encouragement and expert guidance of my supervisor. His enthusiasm and optimism made this experience enjoyable. His feedback and guidance throughout my Ph.D. work and editorial comments were also valuable for writing this thesis. I feel lucky to have got an opportunity to work with him.

I humbly express my sincere thanks to Dr. Paresh Shravage, Director (Alfaacoustics, Pune), for providing me the guidance and facility to carry out the experimental work in his industry.

Finally, I would like to take this opportunity to express my gratitude to my family members for their love, unfailing encouragement and continuous support especially to my parents, wife and son throughout this journey.

TABLE OF CONTENTS

DECLARATION	ii
CERTIFICATE	iii
Abstract	iv
Acknowledgement	vi
TABLE OF CONTENTS.....	vii
LIST OF TABLES.....	xi
LIST OF FIGURES	xii
CHAPTER 1. INTRODUCTION.....	1
1.1 Acoustics	1
1.2 Analogies used in acoustics.....	2
1.3 Acoustic Wave Propagation Theory	3
1.4 Processing of acoustic signal.....	4
1.4.1 Wavelet.....	6
1.4.2 Statistical Analysis.....	8
1.5 Muffler	10
1.5.1 Reactive or reflective muffler:	12
1.5.2 Dissipative or absorptive muffler:	12
1.5.3 Hybrid Muffler:.....	13
1.6 Design prerequisites of muffler.....	15
1.7 Performance measurement parameters of muffler	16
1.7.1 Aerodynamic Performance parameter:	16
1.7.2 Acoustic Performance parameter	17
1.8 Sound Absorption Material	18
1.8.1 Parameters for defining liquid properties of absorption material	20

1.8.2	Parameters to define the coupling between the fluid and the structure of the material	21
CHAPTER 2. REVIEW OF LITERATURE.....		26
2.1	Muffler design modification.....	26
2.2	Numerical techniques and muffler designing.....	34
2.3	Optimization technique	42
2.4	Vibration characteristics in muffler.....	45
CHAPTER 3. RESEARCH GAP IDENTIFICATION AND MOTIVATION OF THE STUDY		47
CHAPTER 4. RESEARCH OBJECTIVES		49
CHAPTER 5. THEORETICAL BACKGROUND AND ANALYSIS OF MUFFLER ..		50
5.1	Analytical method for calculating transmission loss.....	50
5.2	Transfer matrix method for calculating transmission loss	52
5.3	Implementation of Transfer Matrix Method (TMM) in reactive muffler	53
5.4	Implementation of Transfer Matrix Method (TMM) in hybrid muffler.....	55
CHAPTER 6. ANALYSIS OF EXISTING MUFFLER		58
6.1	Aerodynamic Analysis of Existing muffler	58
6.2	Acoustic Analysis of Existing muffler	63
6.3	Experimental Validation of simulation results.....	66
6.3.1	Fabrication of the existing muffler and experimental set up	66
6.3.2	Experimental Results	76
6.3.3	Comparison of simulation and experimental results for existing muffler ..	77
CHAPTER 7. OPTIMIZATION OF REACTIVE MUFFLER		79
7.1	Criteria for selection of number of baffles	79
7.2	Range selection for hole position and baffles position	81

7.3	Application of Taguchi approach.....	84
7.3.1	Aerodynamic Performance analysis of the trial experiments	85
7.3.2	Acoustic performance analysis of the trial experiments	90
7.3.3	Signal to noise ratio	91
7.3.4	Analysis of variance.....	93
7.4	Experimental validation of simulation results.....	95
7.4.1	Fabrication of optimized reactive muffler and experimentation.....	95
7.4.2	Experimental Results	97
7.4.3	Comparison of simulation and experimental result of reactive muffler .	98
7.5	Comparison of the existing muffler and the optimized reactive muffler	99
CHAPTER 8. OPTIMIZATION OF HYBRID MUFFLER		101
8.1	Variation of Sound absorption material	101
8.2	Optimization of absorption layer thickness in chambers	103
8.3	Application of Taguchi approach.....	104
8.3.1	Acoustic performance analysis of the trial experiments	104
8.3.2	Signal to noise ratio	108
8.3.3	Analysis of variance.....	109
8.4	Experimental validation of simulation results.....	112
8.4.1	Fabrication and experimentation of Hybrid Muffler	112
8.4.2	Comparison of simulation and experimental result for hybrid muffler	116
8.5	Comparison of optimized reactive type muffler and hybrid type muffler	116
8.6	Sensitivity analysis of the performance parameter of hybrid muffler.....	117
CHAPTER 9. VIBRATION ANALYSIS OF OPTIMIZED HYBRID MUFFLER.....		120
9.1	Vibration response.....	120
9.2	Selection of wavelet and decomposition level for vibration signal	129

9.3 Statistical analysis	131
CHAPTER 10. CONCLUSIONS	139
REFERENCES	143
APPENDICES	161
1. Analytical method for calculating transmission loss	161
2. Transfer matrix method for calculating transmission loss	162
3. Aerodynamic performance analysis using finite element analysis	165
4. Parameters used in the setup of aerodynamic performance analysis	168
5. TL for the trial experiments of optimized reactive muffler	173
LIST OF ABBREVIATIONS	174
NOMENCLATURE	175
LIST OF PUBLICATIONS	177
LIST OF CONFERENCES	179
LIST OF PATENTS	180
COPYRIGHT	181
LIST OF CERTIFICATION COURSES	182

LIST OF TABLES

Table 1.1. Electro-acoustic analogies	3
Table 6.1. Criteria's used for selecting muffler testing parameters	72
Table 6.2. Recommended maximum frequency based on microphone diameters	72
Table 6.3. Details of Impedance tube setup	75
Table 7.1. Control parameters and levels	84
Table 7.2. L9 orthogonal array matrix	85
Table 7.3. Material Properties	85
Table 7.4. Pressure drop and acoustic power level in trial experiment models	90
Table 7.5. L9 Taguchi Table with S/N ratio	92
Table 7.6. ANOVA values obtained through MINITAB	93
Table 7.7. Calculation of percentage contribution from the variance analysis	93
Table 7.8. Transmission loss values at different frequency range	100
Table 8.1. Sound absorption materials with its properties	102
Table 8.2. Control parameters and levels	104
Table 8.3. L16 Orthogonal array matrix	104
Table 8.4. L16 Taguchi Table with S/N ratio	108
Table 8.5. ANOVA values obtained through MINITAB	109
Table 8.6. Calculation of percentage contribution from the variance analysis	109
Table 8.7. TL values at diverse frequency range	117
Table 8.8. Variation and percentage change of sound pressure level in hybrid muffler	118
Table 9.1. Energy values from FFT curve	128
Table 9.2. Decomposition of signals using Symlet ("sym"), N = 4	129
Table 9.3. Decomposition of signals using Daubechies ("db"), N = 4	129
Table 9.4. Decomposition of signals using Fejer-Korovkin ("fk"), N = 4	129
Table 9.5. Decomposition of signals using Coiflets ("coif"), N = 4	130
Table 9.6. Maximum energy to entropy for various wavelets	130
Table 9.7. Determination of statistical parameter for raw signals obtained for 5 sec	131
Table 9.8. Determination of statistical parameter for defected signals obtained for 5 sec	131
Table 9.9. Percentage change of statistical parameters	137

LIST OF FIGURES

Figure 1.1. Spherical wave propagation	3
Figure 1.2. Plane wave propagation.....	4
Figure 1.3. Sound wave propagation, vibration signal	6
Figure 1.4. Schematic of discrete wavelet transformation.....	7
Figure 1.5. Classification of types of muffler	11
Figure 1.6. Reactive muffler of WagonR [41]	12
Figure 1.7. Dissipative muffler (Source: Silex Exhaust Silencers, Inc.)	13
Figure 1.8. Hybrid muffler (Source: Silex Exhaust Silencers, Inc.)	14
Figure 1.9. Noise reduction curve for the three types of muffler of Silex Exhaust Silencer Ltd.	15
Figure 1.10. Woven Glass Fiber and Glasswool.....	19
Figure 5.1. Schematic of simple reactive or simple expansion muffler.....	51
Figure 5.2. Pictorial representation of an element for transfer matrix.....	52
Figure 5.3. Line Diagram of the reactive muffler	53
Figure 5.4. Equivalent circuit demonstration of the reactive muffler.....	53
Figure 5.5. Line Diagram of the hybrid muffler	55
Figure 6.1. Schematic view of four-chamber reactive muffler	59
Figure 6.2. Geometry of the four chamber reactive muffler.....	61
Figure 6.3. Front view and side view of meshed model	61
Figure 6.4. Pressure contour for the existing reactive muffler	62
Figure 6.5. Velocity contour for the existing reactive muffler	63
Figure 6.6. Sketch of the four chamber reactive muffler in COMSOL	64
Figure 6.7. Mesh model of in COMSOL	65
Figure 6.8. TL curve obtained in COMSOL Multiphysics	66
Figure 6.9. Baffle plates with tubes	67
Figure 6.10. (a) Mild steel sheet with the sheet cutting machine, (b) cutted rectangular sheet for muffler construction.	68
Figure 6.11. (a) Sheet in rolling machine, (b) rectangular sheet after rolling.....	69
Figure 6.12. Fabrication process of existing muffler with the baffles and tubes placed inside muffler.....	69

Figure 6.13. Schematic diagram of impedance tube with microphone holders.....	70
Figure 6.14. (a) Alfaacoustics Power Amplifier, (b) Alfaacoustics Four-channel Data Acquisition System	73
Figure 6.15. GRAS ¼” pressure field microphones	73
Figure 6.16. Alfaacoustics Impedance tube	74
Figure 6.17. Two impedance tube with the DAQ and power amplifier connected for calibration	74
Figure 6.18. Inner view of the impedance tube.	74
Figure 6.19. Parameters for experimentation.....	75
Figure 6.20. Experimental setup with muffler attached.....	76
Figure 6.21. TL curve for existing reactive muffler through experimentation	77
Figure 6.22. Comparison of TL obtained through simulation and experimentation for existing reactive muffler	78
Figure 7.1. Assessment of TL curve for muffler with rise in number of baffles	80
Figure 7.2. TL curve for double baffle muffler with variation in hole position	81
Figure 7.3. Pilot tests with deviation in position of baffle from inlet tube (L1).....	82
Figure 7.4. Pilot tests with deviation in position of baffle from outlet tube (L2).....	83
Figure 7.5. Pressure and velocity contour for trial experiment 1.....	86
Figure 7.6. Pressure and velocity contour for trial experiment 2.....	86
Figure 7.7. Pressure and velocity contour for trial experiment 3.....	87
Figure 7.8. Pressure and velocity contour for trial experiment 4.....	87
Figure 7.9. Pressure and velocity contour for trial experiment 5.....	87
Figure 7.10. Pressure and velocity contour for trial experiment 6.....	88
Figure 7.11. Pressure and velocity contour for trial experiment 7.....	88
Figure 7.12. Pressure and velocity contour for trial experiment 8.....	89
Figure 7.13. Pressure and velocity contour for trial experiment 9.....	89
Figure 7.14. Comparison of TL for all trial experiments.....	91
Figure 7.15. S/N ratio curve obtained through Minitab software	92
Figure. 7.16. Schematic view of the optimized reactive muffler.....	94
Figure 7.17. 3D view of the optimized reactive muffler in COMSOL.....	94
Figure 7.18. Mesh model of the optimized reactive muffler	95

Figure 7.19. TL curve for optimized reactive muffler through simulation.....	95
Figure 7.20. Baffles with tubes and muffler after welding all the components.....	97
Figure 7.21. Experimental setup with optimized reactive muffler	97
Figure 7.22. Transmission Loss curve obtained for optimized muffler through experimentation.....	98
Figure 7.23. Comparison of TL obtained for optimized muffler through simulation and experimentation.....	99
Figure 7.24. Comparison of TL for four chamber reactive muffler and optimized reactive muffler (a) through simulation (b) experimentation	100
Figure 8.1. Combination of reactive muffler and sound absorption material	101
Figure 8.2. TL curve for the muffler using various sound absorption materials	102
Figure 8.3. TL curve on variation of absorption material layer thickness in first chamber	103
Figure 8.4. TL curve for the 16 trial experiments.....	107
Figure 8.5. Comparison of TL curve for the trial experiments.....	107
Figure 8.6. S/N ratio curve obtained through Minitab software	108
Figure 8.7. Schematic diagram of the optimized hybrid muffler.....	110
Figure 8.8. Three-dimensional diagram of the optimized hybrid muffler	110
Figure 8.9. Meshed model of the optimized hybrid muffler.....	111
Figure 8.10. (a) Pressure and (b) velocity variation for the optimized hybrid muffler....	111
Figure 8.11. TL curve for the hybrid muffler acquired through simulation	112
Figure 8.12 Glasswool sound absorption material.....	114
Figure 8.13 Implementing the sound absorption material inside the muffler.....	114
Figure 8.14 Hybrid muffler after welding all components	114
Figure 8.15. Transmission loss curve acquired through experimentation for hybrid muffler	115
Figure 8.16. TL curve obtained through simulation and experimentation for hybrid muffler	116
Figure 8.17. Comparison of TL acquired for optimized reactive muffler and hybrid muffler through (a) simulation (b) experimentation	116
Figure 8.18. Schematic of hybrid muffler with vibration sensor placed position.....	118

Figure 9.1. PCB Piezotronics accelerometer	120
Figure 9.2. Three channel NI Data acquisition system	121
Figure 9.3. NI DAQ system connected with BNC cable	121
Figure 9.4. Signals at the inlet, center and outlet at frequency of 550 Hz	122
Figure 9.5. Signals at the inlet, center and outlet at frequency of 1400 Hz	123
Figure 9.6. Signals at the inlet, center and outlet at frequency of 2200 Hz	124
Figure 9.7 FFT curve formed at 550 Hz for the signals acquired at the inlet tube, center and outlet tube.....	126
Figure 9.8.FFT curve formed at 1400 Hz for the signals acquired at the inlet tube, center and outlet tube.....	127
Figure 9.9. FFT curve formed at 2200 Hz for the signals acquired at the inlet tube, center and outlet tube.....	128
Figure 9.10. RMS curve for the signals at 550 Hz, 1400 Hz and 2200 Hz	133
Figure 9.11. Standard deviation curve at frequencies of 550 Hz, 1400 Hz and 2200 Hz.....	133
Figure 9.12. Kurtosis curve at frequencies of 550 Hz, 1400 Hz and 2200 Hz	134
Figure 9.13.Shannon Entropy curve at frequencies of 550 Hz, 1400 Hz and 2200 Hz..	135
Figure 9.14. Log Energy Entropy curve at frequencies of 550 Hz, 1400 Hz and 2200 Hz	135
Figure 12.1.Equivalent circuit representation for a distributed element.....	163
Figure 12.2. Equivalent circuit representation for an in-line lumped element	163
Figure 12.3. Equivalent circuit representation for a shunt lumped element	164
Figure 12.4. Steps for FEA in ANSYS Fluent.....	166
Figure 12.5. Fluent launcher interface for selecting module	167
Figure 12.6. Steps used in setup and solution stage of fluent interface	167
Figure 12.7. TL curve for all the trial experiments.....	173

CHAPTER 1. INTRODUCTION

1.1 Acoustics

Acoustics is the study of science that deals with the control, production, reception, transmission and the behavior of sound. It has been evolved from the Greek work 'akoustos' which means "heard". It was originated with the experiments on the properties of vibrating strings performed by Pythagoras in and around 6th Century B.C. and evolved the tuning system. Aristotle in 4th Century B.C. based upon his philosophy advocated that sound waves transmits in air through the motion of air and it propagates faster at high frequencies than low frequencies. Vitruvius in 1st Century B.C. proved that the theories of Aristotle were incorrect and provided new mechanism for transmitting of sound waves [1]. He gave a detailed concept on echo, reverberation and interference. This were described in modern architectural acoustics. Boethius a roman philosopher suggested the human sensitivity of pitch and also the science related to musical sound [2]. Galileo Galilei is considered to be the father of modern study of acoustics. He improved the theories of science related to vibrations i.e. correlation between frequency and pitch in 16th Century B.C [3]. Marsenne also worked parallel on this concept of vibrations. Later Boyle discussed about the medium in which sound waves propagates and justified that for transmission of sound waves, air is considered as the medium. Subsequently several other scientists and researchers over the years are continuously working in the field of Acoustics. Many mathematical theories and principles were invented which are now used in development of different industrial components [4]–[8]. Helmholtz invented the Helmholtz resonator for implementing in a silencing system [9]. He also implemented the elliptic partial differential equation in developing the 3D wave propagation equation, which the basic equation for acoustics. This equation is also known the Helmholtz Equation. While studying about the acoustics of muffler, this equation is considered as the basic equation of designing it. The 1-D or 3-D Helmholtz wave equation is considered as the main wave equation in this present thesis for study related to muffler. The concept of vibrations and mathematical theories were also added to the study [10].

The book on Acoustics by Beranek is very helpful for different researchers in knowing the use of theory of electro-acoustic in acoustic measurements while Whitham gave a detailed

explanation on the mathematical concept behind the linear and non-linear wave equation [11], [12].

Acoustics is the science of sound, and it has a wide range of applications across various fields. Some important applications of acoustics are discussed herewith. Acoustics is crucial in designing spaces that provide optimal sound quality for musical performances and recording. Understanding the acoustics of musical instruments helps in their design and improvement. It plays a role in the design of devices like telephones, microphones, and speakers. In underwater acoustics, sonar systems use sound waves to detect and locate objects underwater. It can be used to study celestial objects and phenomena, such as solar seismology to understand the sun's interior. It is used in medical ultrasound imaging to visualize internal body structures, monitor pregnancies, and more. It is used to reduce noise pollution in urban areas, workplaces, and transportation systems. Architects use acoustics to create spaces with optimal sound quality for their intended purpose. Acoustic techniques are used to inspect and test materials and structures without causing damage. Acoustic measurements can assess the quality of products in industries like automotive and aerospace. In automotive industry, acoustics helps in reducing noise inside vehicles for a quieter and more comfortable ride. It helps in designing quieter and more efficient engines. Acoustics is used in headphones to cancel out external sounds for better listening experiences and also adjust sound quality in audio equipment. Thus acoustics is a fundamental field of study in physics and engineering programs at universities and research institutions. It is also used for experiments in various scientific disciplines.

1.2 Analogies used in acoustics

Power dissipated in an electrical system is mainly analogous the acoustics impedance of a system. The expressions for it are shown in Eq. 1 and Eq. 2.

$$\text{Power dissipation, } P = V^2 / 2R \quad (1)$$

$$\text{Acoustic impedance (Z)} = \frac{\rho c}{A} \quad (2)$$

Its unit is Pa.s/m³ or Rayls/m²

The electro-acoustic analogies are described in Table 1.1

Table 1.1. Electro-acoustic analogies

S. No.	Acoustical Terms			Electrical Terms		
	Variables	Symbol	Unit	Variables	Symbol	Unit
1	Acoustic Impedance	Z	$m^{-1}.s^{-1}$	Electrical Impedance	Z	Ohms
2	Mass Velocity	V	$m.s^{-1}$	Current	I	Ampere
3	Pressure	P	$N.m^{-2}$	Voltage	V	Volt

1.3 Acoustic Wave Propagation Theory

A sequence of pressure changes are caused by a wave that is propagating from a sound source. These slight changes aid in the wave's propagation in that direction. In reality, there are two ways that these waves can spread. Spherical wave propagation refers to the first scenario, in which the sound source is kept in an open area, and plane wave propagation, in which the sound source is constrained by a specific path [13], [14].

Spherical Wave propagation :

Sound waves travel spherically from a point source in all directions as demonstrated in Figure 1.1. Moving away from the sound source causes its intensity to lessen. This sort of sound transmission results in a natural reduction of sound intensity and is inversely proportionate to the distance from the sound source [13].

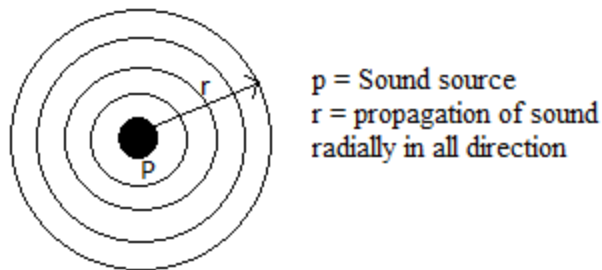


Figure 1.1. Spherical wave propagation

Plane Wave propagation :

The wave is intended to propagate in one direction during this form of propagation. The wave particles continue to move parallel to one another as seen in Figure 1.2. Until the duct is constrained by specific limits, a sound wave propagating through a pipe or duct will travel a long distance without suffering significantly from intensity loss. These limitations aid in lowering sound pressure, which in turn causes a large decrease in sound intensity [13].

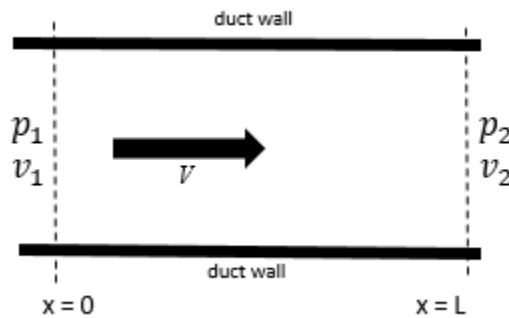


Figure 1.2. Plane wave propagation

1.4 Processing of acoustic signal

Acoustics is basically a vibrational energy, which propagates in a medium. The acoustic and vibration are always interrelated to each other and greatly creates an impact i.e. the sound produced by a listening device or by any vehicles. A sound from a source makes the adjacent particles to vibrate and the acoustic energy keeps on propagating from one particle to the next in the said medium and transmits to the surrounding air [13], [15]. Thus the sound energy travels to long distance because of the vibration of sound particles. In case of plane wave propagation, the sound particles vibrates in longitudinal direction from the sound source as shown in Figure 1.3.

Signal processing is the study or extraction of information from a signal propagating from an acoustic source. This helps in acquiring information from any acoustic signals, even in case of noisy environment. Signals are generally the foundation of information processing, transmission and storage of information [16]–[18]. These signals can be analyzed by three different techniques and are known as time-domain analysis, frequency-domain analysis and time-frequency domain analysis.

Time-domain analysis: It refers to the analysis of signals or systems in the time domain, which is the representation of signals or systems in terms of time. In other words, time domain analysis involves studying the behavior of signals or systems as a function of time. One of the most common techniques used in time domain analysis is the time-domain waveform analysis, which involves analyzing the shape and amplitude of a signal as it varies over time. [16], [18].

Frequency-domain analysis: Frequency domain analysis refers to the analysis of signals or systems in the frequency domain, which is the representation of signals or systems in terms of their frequency components. In other words, frequency domain analysis involves studying the behavior of signals or systems in the frequency domain, rather than the time domain. The most common technique used in frequency domain analysis is the Fourier transform, which is a mathematical tool that transforms a signal from the time domain to the frequency domain. The Fourier transform allows us to break down a complex signal into its individual frequency components, which can then be analyzed separately. In this analysis, a set of sinusoids are joined together in place of the measured signal to create waveforms that are identical to the original signals [16], [18].

Time-frequency domain analysis: It is a signal processing technique used to analyze non-stationary signals that vary over time and frequency. This technique provides a way to examine a signal's energy distribution in the time-frequency domain by decomposing the signal into its constituent frequencies and analyzing how those frequencies change over time. The Fourier transform, which transforms a time-function into an integral of sine waves with different frequencies, is one example of this type of transform. Whereas the inverse of this Fourier transform will convert the said frequency back to time-domain. These different signal processing methods could be further analyzed through wavelet analysis.

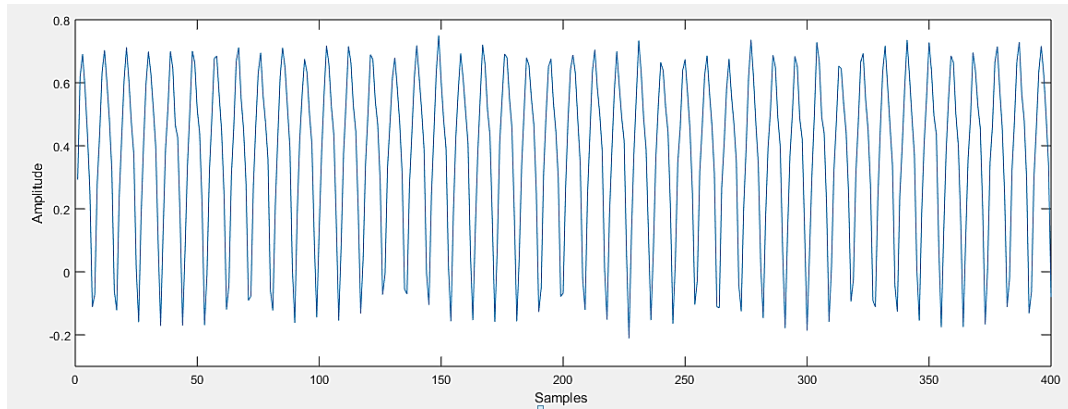


Figure 1.3. Sound wave propagation, vibration signal

1.4.1 Wavelet

Wavelets are mathematical functions used in wavelet analysis to decompose signals and data into a set of frequency and time-localized components. Wavelets are typically derived from a single "mother" wavelet function by scaling and translating it to create a set of wavelets at different scales and positions. Wavelets are well-suited for analyzing signals with transient or localized features, as they can provide a more detailed representation of the signal at different scales than traditional Fourier analysis. Wavelets have applications in a wide range of fields, including signal and image processing, data compression, and time series analysis.

1.4.1.1 Wavelet Analysis

Wavelet analysis is a mathematical technique used to analyze signals and data by decomposing them into a set of wavelet functions at different scales or resolutions. Unlike Fourier analysis, which uses a fixed set of sinusoidal functions to represent a signal, wavelet analysis uses functions that are both time and frequency-localized. This makes wavelets well-suited for analyzing signals with transient or localized features, such as audio signals, images, and financial data. Wavelet analysis is used in a wide range of applications, including signal and image processing, data compression, and feature extraction.

There are two main types of wavelet analysis: continuous wavelet transform (CWT) and discrete wavelet transform (DWT).

1. Continuous Wavelet Transform (CWT): The CWT decomposes a signal into wavelet functions that are continuously scaled and translated. The resulting wavelet coefficients represent the correlation between the wavelet function and the signal at each

point in time and scale. The CWT is useful for analyzing signals with continuous spectral content, such as audio signals and time-varying signals.

2. Discrete Wavelet Transform (DWT): The DWT is a digital version of wavelet analysis that involves decomposing a signal into a set of wavelet functions that are both time and frequency localized. Unlike the CWT, the DWT uses a discrete set of scales and translations to decompose the signal into wavelet coefficients. The DWT is widely used in signal and image processing applications because it is computationally efficient and provides a flexible representation of the signal at different scales. It is also known as Multi-resolution wavelet analysis which decompose the variability of the data into physically meaningful and interpretable parts [19]. The schematic of a discrete wavelet transform is shown in Figure 1.4.

The DWT process involves a series of steps:

- i. Wavelet Selection: Choose a suitable mother wavelet that matches the characteristics of the signal. Different wavelets are better suited for specific types of signals, such as those with sharp transients or smoothly varying trends.
- ii. Decomposition: The signal is passed through a series of filters, typically a high-pass filter (detail) and a low-pass filter (approximation). The signal is then down-sampled to retain only a subset of samples, effectively reducing its resolution.
- iii. Recursion: The low-pass output from the previous step becomes the input for the next level of decomposition. This recursive process is repeated iteratively to create multiple levels of decomposition, generating approximation and detail coefficients at each level [20], [21].

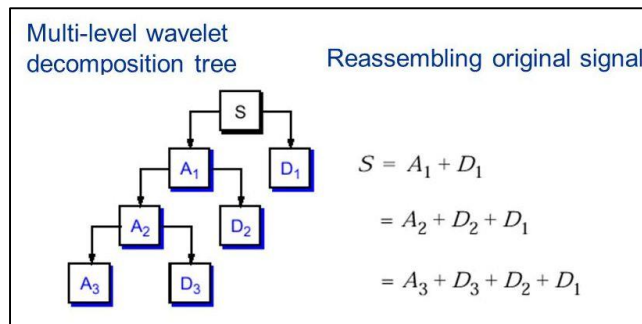


Figure 1.4. Schematic of discrete wavelet transformation

1.4.1.2 Wavelet family:

Various types of wavelets are available for analyzing the received signals. Some of the type of wavelets commonly used by researchers are discussed herewith [22]–[24].

Orthogonal wavelet family: These type of transformation preserves energy and these wavelets with compact support are not symmetric. The various wavelets which supports this family are

Symlets (“sym”): Its main feature is that the wavelet is least asymmetric and having nearly linear phase. It is represented as “symN” where $N = 2, 3, 4 \dots 45$ and N is known as vanishing moments.

Daubechies (“db”): Its main feature is that the energy of the wavelet is concentrated near the start of their support and is having nonlinear phase. It is represented as “dbN” where $N = 2, 3, 4 \dots 45$.

Fejer-Korovkin (“fk”): Its main feature is that filters are constructed to minimize the difference between an ideal sinc lowpass filter and valid scaling filter. They are generally useful in discrete wavelet platform transform. It is represented as “fkN” where $N = 4, 6, 8, 14, 18, 22$.

Coiflets (“coif”): Its main feature is that scaling function and the wavelets are having the same number of vanishing moments. It is represented as “coifN” where $N = 1, 2, 3, 4, 5$.

1.4.2 Statistical Analysis

Root mean square (RMS): In the context of vibration analysis, the root mean square (RMS) value of a vibration signal is a measure of the overall amplitude or energy content of the signal. It is calculated by taking the square root of the average of the squared values of the signal over a given time interval [25], [26]. Mathematically it can be determined by Eq.3.

$$\text{RMS} = \sqrt{\frac{\sum_{k=1}^n A_k^2}{n}} \quad (3)$$

Where “ A_k ” is the amplitude of the signal and “ n ” is the total number of data points.

The RMS value is often used as a measure of the severity of vibration in mechanical systems, as it provides a way to quantify the total energy being transmitted through the

system. The RMS value is a statistical measure that provides information on the overall level of vibration, but it does not give any insight into the frequency content of the signal. Standard Deviation (σ): It is a statistical measure that describes the amount of variation or dispersion in a set of data. It is calculated as the square root of the variance, which is the average of the squared differences from the mean. Mathematically, it can be determined by Eq. 4.

$$\sigma = \sqrt{\frac{\sum_{k=1}^n (A_k - \bar{a})^2}{n}} \quad (4)$$

Where \bar{a} is the average value of the amplitude of the acquired signal.

A higher standard deviation indicates that the data is more spread out, while a lower standard deviation indicates that the data is more clustered around the mean.

Kurtosis: It is statistical parameter used for measuring a time domain signal. It describes the "peakedness" or "flatness" of a probability distribution relative to the normal distribution. It measures how much of the distribution's variance is in the tails, compared to the variance in the central part of the distribution. Mathematically, it can be determined by Eq. 5.

$$\text{Kurtosis} = \frac{\frac{1}{n} \sum_{k=1}^n (A_k - \bar{a})^4}{\left[\frac{1}{n} \sum_{k=1}^n (A_k - \bar{a})^2 \right]^2} \quad (5)$$

According to the earlier research, it was found that a component is considered to be in good condition if the value of Kurtosis of the signal is nearly close to three or less than three. But a Kurtosis value greater than three designates that the component is damage. This Kurtosis factor gives the overall condition of the system only, not the percentage of defect in the component. A distribution with high kurtosis has more of its variance in the tails, which results in a sharper peak and heavier tails, while a distribution with low kurtosis has more of its variance in the center, which results in a flatter peak and lighter tails. The normal distribution has a kurtosis of 3, so distributions with kurtosis greater than 3 are said to be "leptokurtic," while distributions with kurtosis less than 3 are said to be "platykurtic." Skewness: It is a statistical parameter to measure the symmetry of the signal. Mathematically, it can be determined by Eq. 6.

$$\text{Skewness} = \frac{\frac{1}{n} \sum_{k=1}^n (A_k - \bar{a})^3}{\sigma^3} \quad (6)$$

The skewness follows the normal distribution curve and is found to be zero. So, skewness should be zero for any signal having symmetric data. If the skewness value is negative, then the data of signals are skewed towards left of the normal distribution curve. Whereas if skewness value is positive than the signal data are skewed towards right of normal distribution curve.

In the context of vibration analysis, skewness can provide valuable information about the underlying physical mechanisms that generate the signal. A positively skewed vibration signal may indicate the presence of a fault, while a negatively skewed signal may indicate the presence of a misalignment.

Shannon Entropy (SE): It is a measure of the amount of uncertainty or randomness in a system. It is calculated based on the probability distribution of the system's states. To perform a sensitivity analysis on Shannon entropy, we need to identify the input variables that affect the probability distribution and hence the entropy. This parameter is named after Claude Shannon and it is determined mathematically for random signal 'x' with 'N' number of outcomes as x_0, x_1, x_2, \dots and with probability of $P(x_i)$ is expressed as shown in Eq.7 and Eq.8 is a more simplified form of it [25], [27], [28].

$$S(x) = -\sum_{i=0}^{N-1} P(x_i) \log_2 [P(x_i)] \quad (7)$$

Here $P(x_i) = r_i/N$, r_i is incident rate and $N = \sum_{i=0}^{N-1} r_i$

$$\text{Eq.7 can be rewritten as } S(x) = \log_2 N - \frac{1}{N} \sum_{i=0}^{N-1} r_i \log_2 r_i \quad (8)$$

1.5 Muffler

A muffler also known as “silencer” is a device that is used to reduce the noise generated by an internal combustion engine by decreasing the sound pressure level of the exhaust gases. When exhaust gases are released from an engine, they generate sound waves that propagate through the air. A muffler works by providing a series of chambers and baffles that cause the sound waves to bounce and collide with each other, canceling out some of the noise energy and decreasing the sound pressure level of the exhaust gases that are released. Some of the typical acoustic components utilized in mufflers include baffles, perforated tubes, uniform tubes, Helmholtz resonators, angle plates, absorption materials, etc. These different aspects of muffler were discussed in the book on acoustics by M L Munjal [29], [30].

Two of the famous researchers from Reeves Pulley Company, Milton O. Reeves and Marshall T. Reeves of the Columbus, Indiana were continuously working on the exhaust muffler. On 11th May, 1897, they patented the first exhaust muffler for engines [31]. Later various other eminent scientists and researchers such as George W Moores in 1920, Oldberg in 1936, Phelan in 1963, Kaari in 1968 etc.[32]–[35] and many others have patented their exhaust mufflers. Houdry, a Frenchman in 1962 patented a catalytic exhaust muffler for application in the automotive exhaust pipes. This muffler also helped in reducing the exhaust gas pollution released through these pipes with the help of catalytic process [36], [37]. More and more inventions were made by different scientists and different types of mufflers were constructed [38], [39]. One of the most recent patent in the field of exhaust system was made by Abdulhadi et al. in 2021 [40].

Mufflers are mostly classified into two type's i.e. reactive muffler and dissipative muffler. Whereas a combined reactive muffler and dissipative muffler exist which forms a third type of muffler known as hybrid muffler. Mufflers could be further classified based on different parameters as shown in Figure 1.5.

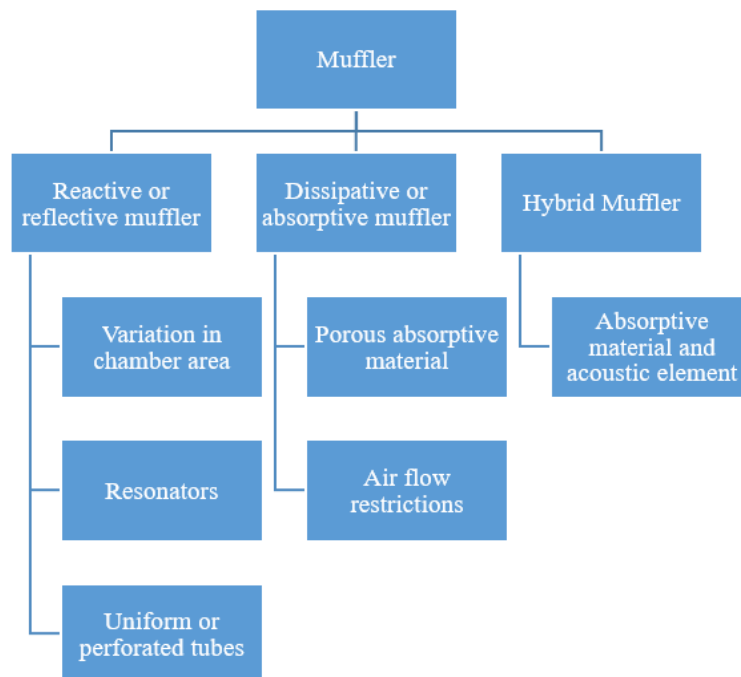


Figure 1.5. Classification of types of muffler

1.5.1 Reactive or reflective muffler:

It is a type of muffler in which the high pressure gases from the exhaust system is passed through the acoustic elements placed inside it. This acoustic elements reflects the sound incident on it and because of the impedance mismatch at the junction of those elements large amount of sound waves are reflected back to the source reducing the noise. Perforated tube, baffles, uniform tube, Helmholtz resonator, quarter-wave resonator etc. are some of the acoustic elements used inside this muffler [29]. Use of this elements creates an impact on the performance of the muffler. This type of mufflers performs better at low to mid frequencies. Simple expansion chamber is the most elementary form of reactive muffler and it is single chambered. The advantage of this muffler is that it involves less maintenance and also it is quite economical. However, it provide little attenuation at some of the frequency ranges which is a major drawback of this muffler. Implementation of baffles inside the simple expansion chamber converts it into a multi-chambered muffler. A model of reactive muffler use in Maruti WagonR is shown in Figure 1.6.



Figure 1.6. Reactive muffler of WagonR [41]

1.5.2 Dissipative or absorptive muffler:

It is type of a muffler in which the high pressure gases from exhaust system is incident on it and is dissipated or converted into heat energy because of the absorptive material present inside it. The sound absorption materials are either lined along the duct surface from inside or the chambers are totally filled with the material. Depending on the properties and characteristics of the materials, it will dissipate the sound and will ultimately reduce the

noise. Absorptive material also absorbs the noise from exhaust because of viscous and thermal dissipation and are porous in nature. Glasswool, Rockwool, glass fiber etc. are some of the most commonly used absorption material [42]–[44]. This mufflers performs better at high frequencies [45]. Further in these mufflers, flow reversal or twist or turn of the exhaust gases doesn't occur due to which the back pressure or pressure drop is comparatively low [30]. This is one of the main advantage of this muffler whereas one of the major drawback of this muffler is the generation of large wavelength for the sound waves, which affects the attenuation. A typical dissipative muffler used by Silex exhaust silencers, Inc is shown in Figure 1.7.



Figure 1.7. Dissipative muffler (Source: Silex Exhaust Silencers, Inc.)

1.5.3 Hybrid Muffler:

This is a combination of both the dissipative muffler and reactive muffler. This muffler absorbs as well as reflects the exhaust gases, which enters the muffler. This muffler is used for reducing the broadband noise. This type first come into existence back in 1930s where the main chamber of a three-pass muffler is packed with absorption material and was developed by Peik [46]. Sterrett et al. also proposed a design of hybrid muffler consisting of two dissipative chamber and a reactive type of resonator [47]. Hybrid mufflers are mainly designed to overcome the deficiency cause by dissipative and reactive type muffler. As we have found that dissipative muffler is essential for reducing noise at high frequency and reactive muffler is effective at low frequency. But the hybrid muffler is effective for

reducing noise at all form of frequencies. Finite element method (FEM), Boundary Element Method (BEM) are the multidimensional numerical methods which are effective for such complex geometries [48], [49]. This type of mufflers are having some specific properties and acoustic filters which helps in reducing the noise from the exhaust of engine. Some of these acoustic filters are absorption material, perforated tube etc. Air flow resistivity (σ), material density are some of the main absorption material properties [50] and back pressure, transmission loss (TL), insertion loss (IL), level difference (LD) are the performance parameters of the muffler. Thus, designing a hybrid muffler is complex and it requires a proper knowledge of acoustic characteristics and the combination of reactive, dissipative and interacting ducts. A thorough study on this type of muffler is still of much importance because the noise reduction should be done in wide frequency range. A typical hybrid muffler used by Silex exhaust silencers, Inc is shown in Figure 1.8 and a comparison curve between these mufflers is shown in Figure 1.9.



Figure 1.8. Hybrid muffler (Source: Silex Exhaust Silencers, Inc.)

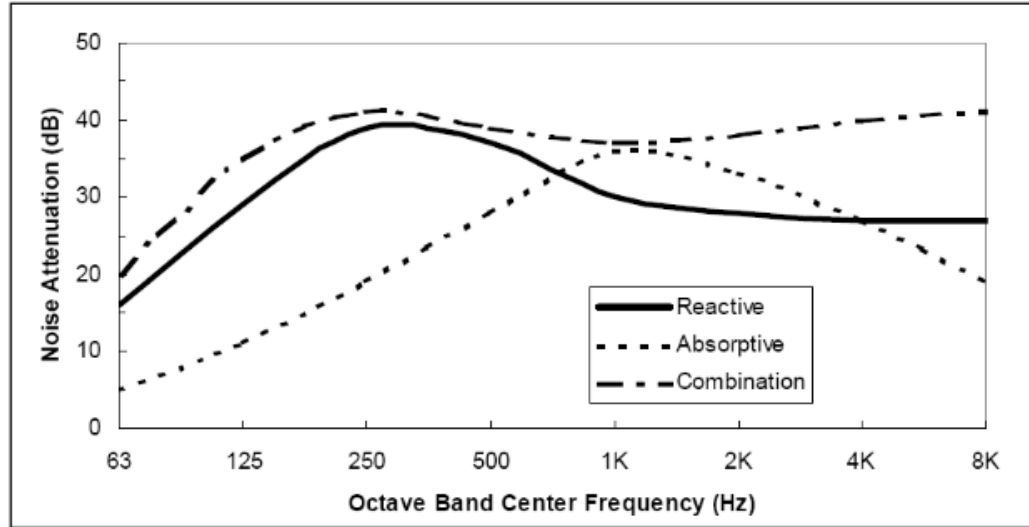


Figure 1.9. Noise reduction curve for the three types of muffler of Silex Exhaust Silencer Ltd.

1.6 Design prerequisites of muffler

The muffler is designed in such a way that it satisfy the consequent five prerequisites which are discussed herewith [30], [51]–[53].

1. Acceptable performance in noise reduction

Noise reduction is the fundamental requirement of muffler. In case of an IC engine of automotive vehicle, generation of maximum amount of noise is generally observed in first few orders of engine's rotational frequency. So, the designed muffler should be able to attenuate the noise in that specific range of frequencies.

2. Low Back pressure

Back pressure plays significant role in the performance of engine. Backpressure is produce because of the restrictions in the flow of gases inside muffler created due to presence of acoustic elements. Increase in backpressure shrinks the volumetric efficiency of engine and

further increases specific fuel consumption. An IC engine can operate with back pressure ranging around 25 – 30 kPa. The muffler must be designed in such a way that it produce minimum amount of back pressure.

3. Dimensions of muffler

Automotive vehicle is having specific restrictions in considering the physical dimension of muffler. It is selected according to the available space and should satisfy the acoustic requirements.

4. Mechanical and material requirements

The material used in muffler should have the capability to resist the heat as well as it should be corrosion resistant because the gases leaves the exhaust system at high pressure and temperature. Further on the basis of absorption materials, acoustic materials the performance of muffler varies. Thus this prerequisite should be considered in designing.

5. Economical requirements

This is one of the most critical requirement of automotive industry. This includes the initial, manufacturing, maintenance and operating cost. Further the strict environment rules or noise criteria regarding the noise pollution or the gases coming out is also taken into consideration.

1.7 Performance measurement parameters of muffler

Mainly the performance of a muffler is categorized into two types: Aerodynamic performance parameter and acoustic performance parameter based on the work carried by various researchers [30], [54].

1.7.1 Aerodynamic Performance parameter:

The performance of a muffler depends on the acoustic pressure variation inside the muffler. The exhaust gas comes out of the engine at high pressure and enters the muffler. Due to the flow restriction caused by the acoustic elements, change in pressure and velocity is noticed from inlet to the exit of muffler. This change affects the performance of muffler and it may lead to increase or decrease in noise at the exit section of muffler. This performance parameters could be evaluated through different numerical techniques.

Computational Fluid dynamics (CFD) analysis is one of the most suitable numerical techniques which is performed in ANSYS Fluent.

Back pressure: It is the key aerodynamic performance parameter of muffler. It is formed due to various bents and obstructions present inside the muffler or any inside any constrained specimens such as ducts or pipes [54], [55].

Exhaust back pressure: The combustion produced in an engine produces high pressure gases. This high pressure gases are discharged through the exhaust system and during this process, the exhaust pipe or duct produced the back pressure. This exhaust back pressure can be described as the gauge pressure at the exit of a naturally aspirated engine. There are two basic characteristic of this pressure i.e. pressure always streams from high to low pressure and further pressure is a scalar quantity. [54].

To calculate the engine exhaust back pressure we use the following Eq. 9.

$$P = (L * \rho * Q^2 * 3.6 * 10^{-6}) / d^5 + \text{Muffler resistance} \quad (9)$$

Here P = back pressure in kPa

L = Length of the chamber in m.

Q = Exhaust gas flow in kg/m³

ρ = density of gas in kg/m³

d = inside diameter of chamber in mm.

T = exhaust temperature in °C

P_s = Muffler resistance

Pressure drop: It is the difference between the sound pressures from inlet to the outlet section of muffler. It can also be calculated through flow transfer matrix (T_{flow}) [54].

$$T_{flow} = \begin{bmatrix} 1 & R_f \\ 0 & 1 \end{bmatrix}$$

Here R_f represents flow resistance and whereas 0 and 1 represents that when a continuous flow passes from inlet to outlet, there is no resistance produced in the flow in the direction opposite to the outlet [56].

1.7.2 Acoustic Performance parameter

It is the key performance parameter for obtaining the amount of noise reduced by muffler. Further it also witness the sound pressure level (SPL) towards the exit of muffler. There

are generally three main acoustic parameters, designating the acoustical performance of muffler [29], [30], [54], [57], [58]. They are:

- 1) Transmission Loss (TL)
- 2) Insertion Loss (IL)
- 3) Level Difference (LD)

1. Transmission Loss: It is the ratio of incident pressure (sound wave) on the inlet section to the transmitted pressure (sound wave) at the outlet section of muffler. This performance parameter works individually and is independent of the source or acoustic termination properties of muffler [30], [54].

Mathematically, it can be determined as shown in Eq. 10 and Eq. 11.

$$TL = 10 \log \frac{\text{Incident Sound Pressure } (p_i)}{\text{Transmitted Sound pressure } (p_t)} \quad (10)$$

$$TL = 10 \text{Log} \left(\left| \frac{p_i}{p_t} \right|^2 \right) + 10 \text{Log} \left(\frac{S_o}{S_i} \right) \quad (11)$$

Here, S_i , S_o designates the cross-sectional area of the inlet and outlet section of muffler.

2. Insertion Loss: It is the variation in acoustic power produced at the exhaust system without implementation of acoustic filter and the acoustic power for the exhaust system with implementation of acoustic filter [30], [54].

Mathematically, Eq.12 represents

$$IL = L_{w1} - L_{w2} = 10 \log \left(\frac{W_1}{W_2} \right) \quad (12)$$

Here W_1 and W_2 represents the acoustic power of the system without acoustic filter and with filter respectively.

3. Noise Reduction or Level Difference: The variation in sound pressure level's at any two random points, one located in exhaust pipe and other on tail pipe [29], [30], [54].

Mathematically, Eq.13 represents

$$LD \text{ or } NR = 10 \text{Log} \left| \frac{p_n}{p_1} \right| \quad (13)$$

Here n and 1 represents the selected section on exhaust pipe and tail pipe respectively.

1.8 Sound Absorption Material

Sound absorption materials are used for dissipating the sound waves propagating from any source. The sound waves propagating from a source would be either reflected or absorbed

when it encounters any object. The sound absorption material will absorb the sound waves and converts it into a small amount of heat energy. The performance of a muffler increases with the implementation of absorption material [43], [59]. It can be placed as a lining along the duct surface or can be put as a whole inside the chamber. The performance of the material depends upon its various properties and characteristics and it could be determined mathematically as well as experimentally by using two-cavity method as suggested by Delany and Bazley in his work [60]. Some of the most common types of sound absorption materials used in mufflers are Glasswool, glass fiber, Rockwool, polyester etc. as shown in Figure 1.10 [61]–[64]. The flow resistivity and the density of these materials plays an important role towards the performance of the muffler. When absorption material is incorporated inside muffler, its operative expansion area decreases and as a whole it absorbs the sound waves and reflects very little.

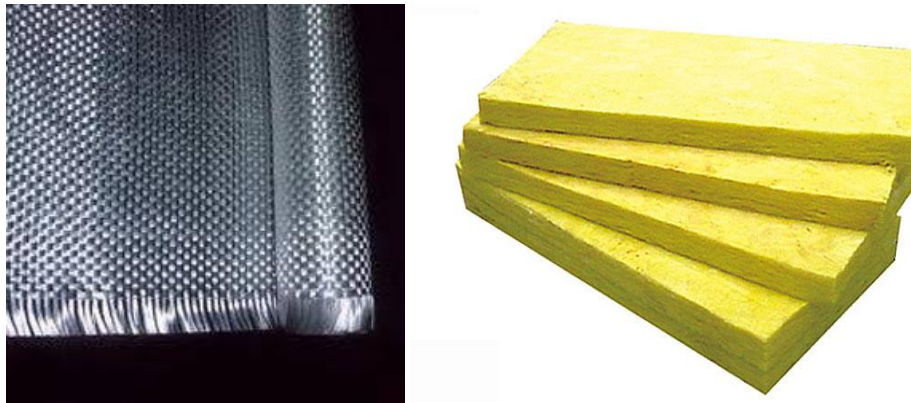


Figure 1.10. Woven Glass Fiber and Glasswool

According to Delany and Bazley [60], the complex acoustical impedance (\bar{Z}) and wave number (\bar{k}) of the absorption material are determined mathematically through Eq. 14 and Eq. 15 [60], [65], [66].

The complex acoustical impedance, \bar{Z} , and the wave number, \bar{k} , can be determined as

$$\frac{Z_c}{Z_o} = 1.0 + 0.0954 \left(\frac{\rho_o f}{\sigma} \right)^{-0.754} - j0.085 \left(\frac{\rho_o f}{\sigma} \right)^{-0.732} \quad (14)$$

$$\frac{k_c}{k_o} = 1.0 + 0.16 \left(\frac{\rho_o f}{\sigma} \right)^{-0.577} - j0.189 \left(\frac{\rho_o f}{\sigma} \right)^{-0.595} \quad (15)$$

The effectiveness and absorption capacity of the materials depends on its different parameters.

1.8.1 Parameters for defining liquid properties of absorption material

a) Mass volume: It is the mass per unit volume of a body and is generally stated in kg/m^3 .

b) Ratios of specific heat (γ): It is the ratio of specific heat at constant pressure (C_p) to constant volume (C_v) [67]. Mathematically it is shown in Eq. 16.

$$\text{i.e.} \quad \gamma = \frac{C_p}{C_v} \quad (16)$$

The unit of specific heat is $\text{J}/(\text{kgK})$

For monoatomic gas, $\gamma = 1.33$

For diatomic gas, $\gamma = 1.4$

For triatomic gas, $\gamma = 1.67$

c) Sound velocity: As we know in acoustics the process of propagation is isentropic. Isentropic process is characterized by the law $p=C\rho^\gamma$ given by Kinsler et al.[10]

Where p = pressure, ρ = density, C = constant which depend on the gas and γ = ratio of specific heat.

Sound velocity or sound speed (c) is the velocity of the fluctuating pressure wave travelling in a particular medium. It can also be defined as the sqrt of the ratio of partial derivative of pressure to partial derivative of density at constant entropy and is expressed in Eq. 17 and Eq. 18.

$$\text{i.e.} \quad c = \sqrt{\frac{\partial P}{\partial \rho}} \quad (17)$$

For perfect gas, speed of sound is given by

$$c = \sqrt{\gamma RT} \quad (18)$$

Where γ = specific heat constant

R = specific gas constant = $287 \text{ J}/(\text{kgK})$

T = temperature

The speed of sound for air at 0°C is 340 m/s .

In terms of bulk modulus, the speed of sound in a medium can be determined as

$$c = \sqrt{K/\rho} \quad (19)$$

Here c is speed of sound, K is bulk modulus and ρ is density of material.

d) Dynamic viscosity (η)

Viscosity is defined as the density of fluid by which it offers resistance to the fluid flow. The unit of dynamic viscosity is centipoises (CP) and in MKS system its unit is Pascal. Sec (Pa.s). In general, at 0 °C, dynamic viscosity of air is 1.72×10^{-5} Pa.s.

e) Prandtl Number (Pr)

The Prandtl number, denoted as Pr, is a dimensionless number that appears in the study of heat transfer in fluids. It is named after the German physicist and engineer Ludwig Prandtl. It is defined as the ratio of momentum diffusivity (kinematic viscosity) to thermal diffusivity and mathematically defined as shown in Eq. 14 [66].

$$\text{Pr} = \frac{\eta / \rho}{k / \rho C_p} = \frac{\eta C_p}{k} \quad (20)$$

Here k represents thermal conductivity and its unit is watt/m²K

At 0°C, for air Pr is 0.708.

Mathematically, the parameters used for determining liquid properties of absorption materials were given from Eq. 16 to Eq. 20.

1.8.2 Parameters to define the coupling between the fluid and the structure of the material

a) Porosity (ϕ):

The porosity of a sound absorption material refers to the percentage of open space or voids within the material. This open space allows sound waves to enter the material and be absorbed or dissipated through friction and conversion to heat energy. The porosity of a sound absorption material is an important factor in determining its acoustic properties. Generally, a higher porosity will lead to better sound absorption because it allows more sound waves to enter the material and be dissipated. However, the material must also have sufficient thickness and density to effectively absorb sound. The porosity is determined mathematically as shown in Eq.21 [66], [67].

$$\phi = \frac{V_f}{V_t} \quad (21)$$

Here V_f = Air volume quotient and V_t = Total volume. Porosity of the material range between 0 and 1. The material with porosity 1 is fully plastic material [68].

b) Resistivity (σ):

The resistivity of a sound absorption material refers to its ability to resist the flow of sound waves through the material. The resistivity of a sound absorption material depends on its density, thickness, and composition. Materials with higher density and thickness typically have higher resistivity and are better at blocking sound, while materials with lower density and thickness typically have lower resistivity and are better at absorbing sound. Under certain frequency, viscous layer thickness is given by

$$\delta = \sqrt{\frac{2\eta}{\omega\rho_0}} \quad (22)$$

According to Darcy, the flow resistivity is the inversely proportional to permeability and is given as [64]

$$\sigma = -\frac{\Delta p}{l} \frac{S}{Q} \quad (23)$$

Here l is porous material thickness

S is section material and

Q is volumetric flow and $Q = C_{\text{permeability}} S \frac{\Delta p}{l}$

Δp = pressure difference

Unit of resistivity is Rayls/m or Ns/m⁴

For a porous material, intrinsic permeability is given by

$$k_i = \frac{\eta}{\sigma} \quad \text{in m}^2. \quad (24)$$

For some of absorbing materials; $10^3 \text{ Nm}^{-4}\text{s} < \sigma < 10^6 \text{ Nm}^{-4}\text{s}$

There are two means of measuring flow resistivity.

By constant flow

By variable flow

Measurement by constant flow

When two materials are placed serially the first material is taken as the reference material and the second material resistivity is calculated from these according as

$$\sigma = R_2 \frac{S}{l} \quad (25)$$

To determine R_2

$$\frac{\Delta p_1}{R_1} = \frac{\Delta p_2}{R_2} \quad (26)$$

Thus, air flow resistivity is

$$\sigma = R_1 \frac{\Delta p_2 S}{\Delta p_1 l} \quad (27)$$

Here R_1 and R_2 are the resistance to the flow for material 1 and 2.

Δp_1 and Δp_2 are the pressure difference in material for 1 and 2.

S and l are the section and thickness of the material.

It is one of the most important properties of sound absorption materials that describe the sound absorbing characteristics of the muffler i.e. the acoustic properties of the muffler. According to Conrad (1983) [68], when sound waves enters the material through convoluted passages it causes friction which reduces the amplitude. By these the acoustic energy is transformed into heat energy (Conrad, 1983). This friction quantity is also defined airflow resistance and is defined as

$$\sigma = \frac{\nabla p}{\Delta T u} \text{ MKS. Rayls/m} \quad (28)$$

Where u = particle velocity in samples, m/s

∇p = difference in sound pressure in sample thickness

ΔT = variation in layer of thickness, m

According to ASTM D-1564-1971, flow resistance can be tested and determined as

$$\sigma = \frac{P}{vl} \quad (29)$$

Here P = difference in static pressure between the faces of the sample

v = velocity of air, m/s

l = sample thickness, m

c) Tortuosity (α_∞)

Tortuosity also known as structure shape factor defines the irregular shape and non-uniform distribution of the pore present in poro-elastic material [66], [67].

Tortuosity is given by

$$\alpha_\infty = \phi \frac{R_e}{R_{e0}} \quad (30)$$

Here R_{e0} = resistivity without a porous material and R_e = resistivity with porous material.

d) Refraction index ($n(\omega)$):

Sound absorption materials typically have a refractive index close to that of air, as they are designed to attenuate sound waves passing through them rather than refracting them.

The refractive index is a measure of how much a material slows down the speed of light or sound when it passes through it. In general, the refractive index of a material is related to its density, stiffness, and other physical properties. Sound absorption materials are typically made of porous or fibrous materials that trap sound waves and convert their energy into heat through friction and vibration. The exact refractive index of a sound absorption material can vary depending on its composition, thickness, and other factors, but it is generally close to 1.0, which is the refractive index of air. Refraction index in terms of an acoustic medium (c_o) and porous medium ($c(\omega)$) is

$$n(\omega) = \frac{c_o}{c(\omega)} = 1 + \frac{c_o \Delta t(\omega)}{1} \quad (31)$$

When the refraction index is squared then the equation becomes

$$n^2(\omega) = \alpha_\infty \left[1 + \delta \left(\frac{1}{\Lambda} + \frac{\gamma - 1}{\Lambda' \sqrt{Pr}} \right) \right] \quad (32)$$

Here δ = maximum viscous layer.

Λ = characteristic viscosity and Λ' = thermal length.

e) Viscous characteristics length:

The effect of viscosity at high frequencies is called viscous characteristics length (Λ).

This is associated with flow direction or flow path.

According to Dauchez [69], it is expressed as

$$\Lambda = 2 \frac{\int_{V_f} |U_m|^2 dV}{\int_{S_i} |U_m|^2 dS} \quad (33)$$

Where S_i = area interaction between the fluid and the structure.

U_m = microscopic speed of the fluid.

f) Thermal characteristic length

Thermal characteristic length is the thermal change between two solid and fluid phases flowing at high frequency range. According to Dauchez (1999), thermal limit layer is the component on which the thermal characteristics length depends [69].

$$\delta' = \frac{\delta}{\sqrt{Pr}} \quad (34)$$

Where δ is viscous limit layer and Pr is Prandtl Number

Therefore, thermal characteristic length (Λ') is given by

$$\Lambda' = 2 \left(\frac{V_f}{S_i} \right) \quad (35)$$

Here V_f is fluid volume.

g) Transition frequency:

It is defined by taking into consideration the thermal effects at low frequencies and high frequencies.

$$f_{Tt} = \frac{\eta \phi^2 \Lambda'^2}{8\pi k_o r^2 \rho_o Pr} \quad (36)$$

Where ρ_o = density of fluid

η = Viscosity of fluid

ϕ = porosity

Pr = Prandtl number

Eq. 21 to Eq. 36 were the various mathematical relations used for determining the parameters used to define the coupling between the fluid and structure of the absorption material.

CHAPTER 2. REVIEW OF LITERATURE

Over the decade, various researchers and scientists were continuously working on improving the performance of exhaust system in automotive vehicles. According to earlier researches, the exhaust radiated noise contributes around 25.1%, whereas tire or road noise, production clear air duct noise, induction snorkel airborne noise and other noises contributes around 19%, 13% and 9% respectively towards the overall automotive noise [70]. Few other researchers have also mentioned about the percentage contribution of different noise produced by vehicle in their work [71]–[73]. Thus, the exhaust system noise is the major contribuent towards the overall sound level of an automotive vehicle. These research shows that the noise produced by exhaust system is major concern for the automotive industry. So, study is going on in improving the performance of muffler, which is the main acoustic filter used in the exhaust system. Few of the works carried out by different researchers are discussed in this section.

2.1 Muffler design modification

Researchers are continuously working on improving the design of muffler using various techniques. In this regards, different types of mufflers are used by various researchers. Some of these works carried out on these mufflers are discussed herewith.

Around the middle of the 20th century, Davis et al. employed an experimental verification to validate their one-dimensional acoustic approach for calculating transmission loss. Theoretical and practical testing was done on 77 distinct combinations of single- and multi-chamber resonators mounted to tailpipes. The overall noise level was seen to be significantly lower in all of the cases. Four distinct muffler-tailpipe configurations for a helicopter were shown, and their results were compared to the noise spectrum of an unmuffled aircraft. The analysis revealed that even the tiniest muffler tested was able to lower the helicopter's total noise level [74].

The combined dissipative and reactive muffler utilised in IC engines was the focus of research by Nakra et al. The characteristics of noise attenuation have been covered. They observed that the combination muffler, which is a parallel composition of backflow and absorption type muffler, gave high noise dissipation over a broad frequency range as

compared to different kinds of muffler. The performance parameters in their work were theoretically determined and were then verified by experimentation [75].

Munjal discussed the various facets of muffler design in his article. It provides information about the muffler's performance parameters as well as the various methods employed to determine the parameters. It was found that various numerical methods, including the boundary element method and the finite element approach, are helpful for figuring out the performance parameters. This book also reinforced the notion that one of the most effective methodologies for determining the transmission loss (TL) of mufflers is the transfer matrix approach. muffler [29], [30].

Munjal earlier made a review on the different advances made in the field of acoustics of flow ducts for heating, ventilation and air-conditioning systems and exhaust mufflers. For explaining his research findings, works were performed on reflective muffler. Frequency domain one-dimensional analysis was initially performed on the reflective muffler and the results were verified through the numerical analysis. His work concluded with the details of works that could be carried out in future in the field of acoustics of ducts and mufflers [76].

Bilawchuk and Fyfe in their work used different numerical methods for obtaining the transmission loss of the muffler. They took a simple expansion chamber and determined the performance parameter by using a traditional laboratory method i.e. FEM and BEM, three point method and four-pole transfer matrix method. They used SYSNOISE for FEM numerical method and their results showed that this method is most suitable for calculating the performance parameter. These work concluded that the three-point method is the fastest method for obtaining these parameters [77].

Xu et al. in their study used two-dimensional analytical approach for evaluating the performance of a dissipative expansion chamber muffler. The performance of the muffler were determined by variation in thickness of absorption material, variation in chamber diameter and change in absorption material properties. From their analysis it was observed that with the increase in flow resistivity value of absorption material, increase the TL value. Further it was observed fiber layer thickness of 4.5 cm gave the maximum TL and lastly with area ratio of 8, the maximum TL was obtained [78].

Gerges et al. had a discussion about muffler modelling techniques. The two techniques employed are boundary element methods and FEM. In their research, they talked about how to calculate the TL in a muffler using the transfer matrix technique (TMM). They have also experimentally supported these findings [79].

Mehdizadeh and Paraschivoiu used three-dimensional finite method and was implemented on a packed muffler. Parallel baffle plates were used on parallel baffle silencer and three layers of polyester lining having flow resistivity of 16000 MKS Rayls/m was used. From the theoretical and experimentation it was observed a quite promising result in terms of TL. The maximum transmission loss (TL) of 75 dB was obtained in packed muffler as compared to 52 dB in parallel baffle silencer [80].

Lee et al. in his work on the recent development on muffler primarily focused on reducing the exhaust noise by optimizing the structure of the muffler. In his various works, different designs of reactive and dissipative mufflers were studied. His study notified that airflow velocity is one of the main parameter which influence the performance of the muffler [81].

Erol and Ahmetoglu in their study used Finite element method and experimentation was performed for obtaining the performance of a circular fully filled dissipative muffler. Fiber material i.e. Rockwool and perforation ratio in pipes inside the muffler were the main acoustic elements considered for attenuating the muffler. Msc-Actran was used for determining the TL values which were validated through experimentation. It was observed that muffler with 500 perforated holes gave maximum TL of around 90 dB and absorption material of 10 mm thickness gave the maximum TL of around 83 dB [82].

Ji et al worked on three-pass perforated tube mufflers and used one-dimensional time domain approach. The transmission loss for it was obtained using the GT Power software. Their worked showed that using end resonators in muffler reduce the exhaust noise at low frequency whereas creating a hole in the baffle of resonator, shift the peak of maximum TL to higher frequency [65], [83].

Anderson worked on reflective muffler, absorptive muffler, plug flow muffler and an expansion chamber with resonator. He used a three-dimensional linear pressure acoustic module in Comsol for obtaining the transmission loss of the muffler and these results were

validated through experimentation. A flow acoustic test rig was used for performing the experimentation [84], [85]. Anderson et al. patented an acoustic test rig consisting of impedance tube and sample holder in it [86].

Elnady et al. in their work used perforated tubes and duct segments in their muffler and used the transfer matrix method in the segmentation approach for determining the performance. Further analytical method was also used for evaluation and convergence test was also performed for obtaining the accurate number of segment. The results obtained from these analysis were compared with the three dimensional finite element analysis and experimentation was performed for validation [87]–[89].

Munjal and Chaitanya talked about extended concentric tube resonators in their work and the one-dimensional formulation approach was employed for evaluation. The intake and outlet free extended length of the perforated duct were changed. Further the effectiveness of the muffler was assessed by changing the porosity, thickness, chamber to hole diameter ratio and hole diameter. Through experimentation, the one-dimensional method's results were confirmed [90].

A newly created muffler with outstanding performance that passes air via various chambers was built by Ying Li Shao. To calculate the insertion loss of the muffler, he used the concepts of counter-phase counteract and split gas rushing [91]. Later, Zhang et al. employ a similar idea known as split-stream rushing in his exhaust system. The performance parameters of a split stream rushing muffler were mathematically analyzed, then empirically confirmed, using the acoustic wave theory. A newly created structure effectively reduces noise in the high frequency region. Low exhaust resistance and little turbulence are produced by this revolutionary design. muffler [92].

Kamarkhani and Mahmoudi worked on both reactive and absorptive muffler. They investigated the effect of baffle and perforations on muffler by using COMSOL software. TL for the muffler with and without the baffle are analyzed and it is observed that from both simulation and experimental method muffler with baffle and perforation gives us better sound reduction [93].

Rojan et al. worked on the performance of a motorcycle muffler and is obtained by optimizing the back pressure. In this study the diameter of hole of perforated tube is modified and to obtain the pressure variation CFD analysis is performed. The variation in hole diameter affect the back pressure in muffler. It was found that perforated tube with largest hole diameter produces lowest back pressure [94].

Zhang et al. used a reactive muffler with side outlet and obtained the performance parameter and noise reduction of the muffler. They have used a theoretical technique i.e. transfer matrix method (TMM) for determining the TL and the result was verified with experimental results. The quadrapole parameters are obtained using TMM and experiment was performed in impedance tube set up [95].

Lee in his work had discussed about the topology optimization method for determining the transmission loss and insertion loss. Mathematical expressions for performance parameters were developed from the available acoustic equations and are implemented on simple expansion chamber. These performance parameter were again obtained by mounting the muffler on a duct. His work results in development of a new muffler design methodology for getting accurate performance parameter values [96], [97]. Similar work was earlier performed by Jin Woo Lee in which work on reactive muffler, where topology optimization was implemented. The results obtained from this method was validated through experimentation [98].

Terashima et al. discussed about perforated silencer where the three-dimensional finite element approach was used for investigating the TL. Eight different models were investigated which consists of models such as perforated tube with uniformly distributed holes, perforated inner concentric tube etc. Geometric parameters were modified and the TL were determined through three dimensional FEM using the four-node tetrahedral element in SIMCENTER 3D Siemens software. The results obtained were experimentally validated using the Bruel and Kjaer Impedance tube set up [57].

Liu et al in their work discussed about sound absorption on a porous material perforated with holes. In their work the radii of the perforated holes were varied. The TMM was implemented to obtain a relation between the sound pressure and particle velocity [45]. Various other researchers are also continuously using different numerical techniques and

design parameters, acoustic elements such as baffles, uniform tubes for designing the reactive or dissipative muffler and its acoustic and aerodynamic performance parameters are obtained [99]–[102].

The simple dissipative and reactive mufflers have been the subject of research by several scientists, but there are also some scientists who have combined these two mufflers or integrated various acoustic filters to create a new kind of muffler. The 1930s saw the introduction of the concept of a hybrid muffler. Piek created a three-pass muffler in 1935 with an inner chamber coupled to a perforated steel tube. A sound-absorbing material such as slag wool, steel wool, or micaceous material was utilized to fill the inner chamber, which has an octagonal-shaped shell, which is where the perforated tube is located [46]. A muffler made of many reactive chambers coupled with a Helmholtz resonator and a single dissipative chamber was created by Sterrett et al. in 1998. They employed porous ceramic material, fiber glass, or steel wool to fill the dissipative chamber, which was made out of perforated and uniform tubes for the reactive chamber [103]. Several patents have been filled over the years by various researchers employing absorption materials in their mufflers. Such as Nelson (1937) used four parallel and juxtaposed ducts inside the chamber and the remaining space was filled with sound and gas pressure absorption material such as mineral wool, pumice [104]. Schimdt (1937) invented a muffler where multiple perforated tubes are used and were placed lateral to the inlet or outlet tube. The sound absorption materials were also placed laterally and filled the remaining space of chamber of muffler [105]. Similar inventions were made by other researchers Manning (1939), Wolfhugel (1983), Fukuda (1986), Hetherington (1989), Garey (1990), Udell (1990), Valdaman (2000), Zhang (2010) etc. with changes in their acoustic filters inside the chambers [39], [106]–[112].

Different researchers were also performed over the years in attaining an adequate design of hybrid muffler using the acoustic filters, some of which are discussed in this section.

Craggs in his work has discussed about the application of absorption material as a lining in an expansion chamber and the performance was determined theoretically. His work showed that implementation of absorption material increase the magnitude of transmission loss i.e. the performance parameter. Further with increase in thickness of absorption

material inside chamber the performance increase with reduction in number of domes and the band of frequencies producing maximum transmission loss increased [113].

Selamet et al. worked on the hybrid muffler where they projected the TL of the muffler by using BEM. The muffler is composed of two single-pass perforated tube and the chambers was filled with fibrous material. In between the two chambers, a Helmholtz resonator was used and evaluated for determining the performance parameter. They demonstrated the effectiveness of hybrid muffler theoretically and experimentally and showed that implementation of Helmholtz resonator improve performance at low frequencies whereas absorption material improve it at high frequencies. [49] .

Chiu and colleagues optimized the muffler's form. There are five main kinds of hybrid mufflers that use Helmholtz resonators, dissipative and reactive units, and other components. The broad frequency noise hybridized with pure tones is suppressed by these mufflers. In their research, the four-pole transfer matrix system and the theory of plane waves were used to evaluate the acoustical performance. The Simulated Annealing (SA) algorithm serves to simulate the metals' softening process. The size and design specifications of the muffler are also optimized using this method, which lowers the sound pressure level at the muffler outlet. As a consequence of their analysis, the sound power levels for the various mufflers were reduced from 146 dB to 35.9, 32.0, 41.1, 31.1, and 40.3 dB(A) [114], [115].

Stebalj et al. worked on an adaptive muffler, which is the combination of a conventional muffler with a Helmholtz resonator and there was a variation in its geometry. Both simulation and experimental work were performed on wide range of frequencies. Their work suggested that change in volume of chamber of muffler creates an impact and helps in increasing the performance of adaptive muffler [116].

Pal worked on dissipative, hybrid, and simple mufflers. Glass wool is employed as the porous material in his work, and variations are made in the porous material's thickness and the air gap inside the muffler. He used the CAD programme "CATIA" to complete the 3D modelling. In his work, hybrid muffler design is used to optimize the muffler design. Using ANSYS software, the transmission loss performance metric is calculated. This outcome was confirmed by an experimental process. The experimentally determined TL value and

the anticipated TL value were found to be well within ± 3 dB, validating his study and demonstrating an increase in TL at higher frequency ranges. His research also came to the conclusion that porous media cannot have a thinner thickness than air media [117].

The hybrid muffler was the focus of Gupta et al. They combine a number of perforated tubes and perforated baffles with absorbent materials like asbestos, Rockwool, glass fiber, etc. in their work. They have assessed the transmission loss of the muffler using both experimental and FEA analysis. Analyses of 1-D waves were used to validate experimental results. They use Rockwool and glass fibre in their developed muffler, and it was discovered that using these absorptive materials caused the TL to rise by 9.23 dB and 32.7 dB, respectively [118], [119].

Huang et al in their work investigated the TL of three-pass perforated (TPP) reactive muffler and hybrid muffler. The effect of perforated tube, sound absorption materials and bulkhead on the acoustic performance parameter i.e. TL of the mufflers are determined numerically in COMSOL Multiphysics. Whereas the aerodynamic parameter i.e. pressure drop is obtained from ANSYS software. Both the results were compared and verified and it was observed that the TPP tube with hybrid muffler perform better as compared to all the other type of mufflers. In this hybrid muffler, sound absorption material is placed in the center chamber [120], [121].

Reactive and hybrid mufflers were both the subject of research by Kalita et al. The pressure drop and transmission loss for each reactive muffler were calculated in their work using several acoustic elements at first. The transmission loss (TL) was computed using COMSOL software, whereas the pressure drop was done using ANSYS Fluent. According to their investigation, the reactive muffler with a double baffle and tube exhibits a pressure drop that is 29.1% higher than that of the existing muffler with three baffles. In addition, the pressure drop rose by an additional 5% when an absorption material lining was added to a reactive muffler with double baffles as opposed to one without. Also, this hybrid muffler's sound pressure level is decreased to about 47 dB [122], [123]. Kalita et al in his previous work had discussed about the different available sound absorption porous materials. They also implemented it in a simple expansion chamber muffler and predicted one of the most suitable absorption material that could be used in muffler [43], [124]

Patne et al. worked on a multi-chambered reactive muffler and a muffler with absorptive lining of thickness 10 mm placed inside it. Initially, transmission loss was obtained for the multi-chambered muffler and later on sound absorptions materials i.e. Glasswool, polyurethane (PT foam), rockwool were implemented and obtained the TL. Absorption lining were varied for 0 mm thickness to 15 mm thickness. These analysis were performed using pressure acoustic in COMSOL and results were verified with referred experimental results. It shows that the average TL increased by maximum 8% on implementing the 10 mm absorptive lining inside the multi-chambered reactive muffler [125].

In their research, Zaw et al. talked about how the Helmholtz resonator affects how well a muffler works. To create a hybrid muffler, they paired the expansion chamber with a Helmholtz resonator. This muffler's TL was determined using the transfer matrix approach, and its accuracy was tested using the two-load method with an impedance tube setup. The investigation looked into how the performance was affected by the resonator's neck's length and diameter. Reducing the length and the diameter of the neck was found to increase the TL [126].

Fan and Ji worked on a two pass perforated hybrid mufflers where an one-dimensional analytical approach was used to determine the TL i.e. the acoustic performance parameter. Long fiber glasswool was used and its acoustic wave number and impedance was obtained through experimentation in impedance tube set up. By variation in the geometric parameters such as the length of extended tube, outlet tube and perforation in the bulkhead, the TL was determined through analytical approach and experimentation in impedance tube set up [127].

From the different literature survey related to hybrid muffler, few of the important aspects about sound absorption materials and different sound absorption materials used by various researchers are discussed herewith.

2.2 Numerical techniques and muffler designing

Finite Element Method (FEM) is the most advanced technique used for the muffler analysis. Muffler is a multi-chambered acoustic filter and the acoustic waves passing through it is complex, so this technique is commonly used. The finite element method was originally developed for the structural analysis but it was later stretched to the acoustic

analysis by Gladwell [128] and Craggs [113] . This technique was implemented in mufflers by Young and Crocker [129]. This method is used in the muffler for its dominant three dimensional effects.

The finite element analysis procedure consists in discretizing the chamber into number of finite elements of equivalent length. A field function is selected for the exact and approximate field analysis within the element. The element matrices are evaluated by the variational principle or residual methods.

The algebraic equation for the finite element system is formulated and the various unknown pressures and velocities at the nodes are calculated. Finally, after computing the acoustical performance parameters in the form of four pole parameters, the transmission loss is determined.

Advantage of finite element method

It doesn't depend on the geometry of the muffler and the properties of the medium.

The boundary conditions for pressure or velocity could be placed anywhere in the system.

Any desirable degree of accuracy could be obtained by increasing the number of elements into which the element is subdivided.

The finite element software's available are FEMLAB, ABACUS, MSc.ACTRAN, ANSYS and COMSOL MULTIPHYSICS [130]–[132].

Finite element analysis could be performed through different simulation software package for different physical and engineering applications. COMSOL Multiphysics software allows for using coupled systems of partial differential equation and also it has various modules for analyzing various systems. The pressure acoustic frequency domain module is used in this thesis for acquiring the performance parameters of the muffler. This module is applicable for devices which produces measures and utilizes acoustic waves. Here the model is analyzed using the time harmonic pressure acoustic interface in the frequency domain and modified Helmholtz equation as shown in Eq. 37 and for this acoustic pressure is considered [84], [133].

$$\nabla \left(-\frac{\nabla p}{\rho} \right) - \frac{\omega^2 p}{c_s^2 \rho} = 0 \quad (37)$$

Here ρ = density, c_s = speed of sound and ω = angular frequency.

For the highly porous material, Delany and Bazley's equation are used for determining the complex wave number (k_c) and complex impedance (Z_c) of the absorption material which estimates the acoustic parameters as the function of frequency and air flow resistance.

The pressure and velocity variation inside the muffler could also be obtained by finite element analysis. The computation fluid dynamic analysis is mainly performed for obtaining these parameters and over the years, researchers are continuously using these while designing the muffler. Few of these techniques implemented by researchers in their work are discussed herewith.

Wiemeler et al. devised a new empirical formula for estimating the flow sound levels in muffler components. A curve in the exhaust pipe was built once the CFD analysis for the model was completed, establishing a flow velocity of 0.3 Mach number. In order to achieve a local velocity of 0.23 Mach, the curve was further modified. The sound power level (SPL) at the exhaust system revealed a reduction of 6 dB. It was an efficient instrument for flow noise optimization [134].

Fang et al. performed their research work on determining pressure loss for a muffler based on CFD and experimentation. It was found that by increasing the inlet velocity through the muffler, the pressure loss for the muffler was also increasing. High inlet velocity resulted in high pressure loss. Further it was observed that an error of 19.54% was observed between the simulation and experimental result of pressure loss [135], [136].

Roy has used Lab View simulation software to conduct mathematical modelling as part of his research, which was then numerically evaluated. He worked with various muffler models that had absorption material of various thicknesses. To determine the transmission loss characteristics in the mufflers, several acoustic filters, including perforated tubes with different sized holes, baffles, and uniform tubes, were used and tested [54].

Chen et al. worked on reactive muffler, which was implemented with a selective catalytic converter in it. The exhaust back pressure was calculated for it using a two-load method. During this evaluation three-dimensional finite element method (FEM) was also initially used for back pressure calculation. The results were compared with the experimentation

using transfer matrix. The results showed that selective catalytic reduction muffler performs better and improves the NO_x emission and increase efficiency of engine[137]

Liu et al. used multi-dimensional computational fluid dynamics approach in their work for obtaining the transfer matrix of their muffler. 6 different muffler models were fabricated and were tested with mean and without mean flow. Both simulation and experimentation was performed on the models and the results showed good agreement between them. Ultimately, using Thevenin's theorem the noise at the exhaust system using the muffler is determined [138], [139]

For study, Xu and Zhou gave a double mode muffler some thought. In their investigation, CFD software was used to analyze the pressure loss and internal flow characteristics of the muffler. The pressure changes inside the muffler from input to output are clearly seen by the CFD analysis. outlet [140].

Wang et al. worked on reactive muffler where they implemented perforated tubes inside the muffler. To determine the performance parameter numerical method such as transfer impedance approach was implemented. Further their work resulted in simple boundary element method (BEM) for obtaining the performance for small perforated sample [141].

Saripalli in his work had taken a reactive muffler used in Maruti Ciaz for the purpose of optimization. CFD analysis was performed on it and the effect of baffles on the variation of pressure and velocity of the muffler is determined. Two mufflers are compared and the pressure drop in each muffler is obtained [142].

Puneetha et al. have studied the effect of back pressure in muffler. In their work four different models of reactive muffler were considered and the back pressure for those mufflers were obtained through CFD analysis. This analysis was performed in Acusolve CFD software by considering the mass flow rate as the main parameter at the inlet of the muffler. From the analysis, the total pressure drop across the mufflers were obtained [143]

Guhan et al. focused on reducing the weight of muffler by optimizing the muffler volume. Pressure and velocity variation is found for the newly designed muffler by CFD analysis. It was observed that by reducing the length of muffler and increasing the number of holes

in perforated tube the weight of muffler is reduced by 2%. Earlier they discussed about a muffler used in three-cylinder LCV exhaust system [144], [145].

According to Talegaonkar et al. research's the main source of noise pollution is exhaust system noise. They contend that since a fast car produces high pressure, noise reduction should also be significant. Back pressure is a performance attribute that is crucial to an engine's operation. Traditional or hybrid mufflers have fixed noise attenuation and lower back pressure. Their research demonstrates to us clearly that reduced back pressure is necessary for good acceleration. They used a butterfly valve to determine the muffler's ability to reduce noise in their work. The results indicated that the valve should be opened for improved performance; this lowers back pressure but does not significantly lower noise, which is only around 40% lower than when the valve is closed. [146].

Prajapati and Desai in their work discussed about a conventional muffler of Maruti Suzuki WagonR. By taking the parameters of conventional muffler, the new mufflers are modelled and CFD analysis are performed determining the pressure drop inside the newly designed muffler. Comparison is made on the amount of noise reduction; pressure drop in the muffler. The optimized design is found this CFD analysis. In this work, six proposed design of the muffler was tested and the reactive muffler was taken as a reference muffler for comparing the results. CFX of Ansys is used for the simulation under the same boundary condition. They observed that Design -1 and design - 6 are having more pressure loss. As a result of their work they concluded that the Design-1 Muffler had a maximum pressure loss when compared to other designs due to its smaller pipe diameter. Design – 6 muffler was attached with a resonator at the tile of the muffler because of this, there was an increase in pressure loss but an increase in back pressure [41]

Milad et al. in their research, used a straightforward expansion chamber with a mix of reactive and dissipative muffler. Both the simulation and the experiment have been done by them. The acoustic behavior were assessed in the simulation using the Ansys's software, and the outcomes were contrasted with those from the experimental approach. After first evaluating the acoustic behavior of a straightforward expansion chamber, perforated tubes are inserted, and the resulting acoustic behavior are then watched to see how they evolve. For their study, several hole sizes and densities were used. It was observed that the

transmission loss value varied depending on the frequency range, with the high frequency range experiencing the highest TL. [147].

Prasad and Thiagarajan worked on a reactive muffler, which was designed in CAD software and numerical simulation was performed on COMSOL Multiphysics. They observed that the reduction of noise is inversely proportional to the back pressure. During their analysis tetrahedral mesh elements are used and four elements per wavelength are preferred for FEA. The TL was calculated and it was observed that maximum TL of 90 dB was observed at the tailpipe at 1350Hz [148].

Tutunea et al. in their work justified that CFD analysis of mufflers is difficult to perform and use for design. Because of the high subsonic compressible flow, low-velocity wake regions, and high regions of high vortices produced in muffler. In their work the exhaust muffler was designed in SolidWorks and the material used was Steel Stainless 302. The model was analyzed in Solidworks with Cosmos flow. After the analysis done by them, they observed the change in the velocity field, pressure, density, and temperature in the exhaust muffler. It was observed that in the inlet pipe the temperature and pressure are high whereas on the other hand the outlet pipe had decreased temperature and pressure [149].

Pangavhane et al. discussed the effect of change in dimensions of perforation diameter and change in porosity and how it affects the muffler. They observed that the smallest diameter has high backpressure and vice versa. Three types of mufflers were tested in this experiment with varying porosity. Further high back pressure affects the engine performance (reduced power, high fuel consumption, and emission). As a result of their work they observed that the CFD analyses and experimental values don't have a big difference while tested in a muffler [150].

Rao and Verma emphasized on the design method on current CAE gear for optimization of typical gadget layout. In the work for creating a muffler layout, a realistic technique was used for optimizing the product development time and the fee required was investigated, taking into consideration noise & back pressure. The method has been advanced because of maximum layout and degrees of freedom and a much less fee was required for muffler layout with the aid of using balancing numerous parameters [151].

Vijay and Doere worked on double expansion chamber muffler. In their work bulkheads were used for creating the chambers which act as the reactive dampers. Three models with different combinations are analyzed in COMSOL Multiphysics. They found that out of the three models, model 3 providing broadband transmission losses in the considered frequency range [152].

Krishnan in his research work discussed the three different types of muffler and their results were compared with a muffler used in WagonR. The mufflers were designed using Creo and the outer dimensions for all three mufflers were kept same, but the internal profiles were varied. These mufflers were analyzed in finite element analysis software COMSOL Multiphysics after carrying out the meshing. After analyzing and observing, it was found that out of three mufflers, reactive mufflers are giving good results in acoustic pressure, sound pressure level, transmission loss [153].

Bendhia et al. implemented ducts with a defined length while designing the muffler. In their study, they suggested a numerical technique that combines modal decomposition at the duct's inlet and exit with finite elements in the muffler. But the challenge with this approach is to produce a mesh that takes into account the various scales required in the construction of such a system. In the muffler the perforations are on a small scale, the inner tube is on a medium scale, and the cavity is on used as a large scale [154] .

Kore et al. in their work demonstrated how CFD can be utilized to assess the mean flow and sound absorption of a reactive muffler. The expansion chamber, which has a quick change in cross-sectional area and reflects sound waves to the engine, was the main muffler considered for study. The insertion loss, back pressure, size, robustness, sound quality, breakout noise from the muffler shell were investigated and all the other performance affecting factors must be considered while designing a muffler. The analysis showed that the maximum transmission loss is nearly constant since they used Alfa Romeo's muffler, which also has a constant size, for the CFD analysis [155]

Trivedi et al. in their study placed a perforated tube inside the reactive muffler. During their work flow analysis is performed using real gas. Pressure and velocity variation was determined and the results obtained from simulation was compared with the experimental results and the most optimized reactive muffler was obtained [156], [157].

Patil and Chaudhary worked on the production of exhaust back pressure on a four-stroke CI engine. CFD analysis was performed for determining pressure variation in the exhaust system. It was observed that by placing the muffler away from engine the backpressure could be reduced [158].

Puhan et al. in their work considered an exhaust muffler used in TATA INDICA, where the dimension of the hole and cross-section of perforated pipe were modified. CFD analysis was performed using ANSYS and the results were compared with existing muffler of the car. Change in cross-section of perforated pipe from circular to elliptical results in reduction of backpressure by 75% and on changing dimension of hole, it reduce by 38% [159].

Torregrosa et al. used a generic adjustable expansion chamber for their experiment. In their research, it was found that when the first and second axisymmetric natural modes of the structure are excited, the influence of structural vibration becomes significant. Their primary goal is to characterize an adjustable expansion chamber using time-domain CFD methods. They used the finite element discretization method. The outcomes were contrasted with those of the frequency domain FEM solution. The outcome demonstrates that the computing demands of the time-domain CFD method are significantly greater than those for the same shape when utilizing a frequency-domain FEM approach. [160].

George and Raj in their work reviewed the different performance parameters of mufflers. Back pressure, pressure drop, transmission loss was reviewed. It was found that CFD analysis is one of the best methods for determining the back pressure or pressure drop through simulation and harmonic analysis is performed for determining transmission loss [161].

Mann et al. in their work had specified about the flow fluctuation produce at the exhaust system by the engine. They specified that back pressure is produce which reduces the efficiency of engine. In order to reduce the number of physical experiments, initially Lattice Boltzmann method solver was used by them in the simulation software. On getting the most optimized muffler, experimentation was performed in it and obtained the performance parameters [162].

Mohamad et al. in their study, performed analysis on a muffler used at the exhaust of formula race car. Perforated pipe were used inside the reactive muffler and also the volume of muffler were varied. CFD analysis is performed for determining the flow properties i.e. pressure, velocity inside the muffler. The optimization of muffler ultimately result in optimization of SPL at the exit of muffler [163].

Hujare et al. worked on a single chamber and double chamber reactive muffler and determine the TL for the mufflers. During their work the TL was obtained by creating pores at the inlet pipe and the outlet pipe of the muffler. COMSOL Multiphysics was used for determining the performance parameters and the results were validated through experimentation. The results showed the effect on pores on TL value at different target frequencies [164].

Saadabadi et al. worked on a high-performance muffler used in KTM390 engine. During this study the overall length of muffler, presence of baffle, baffle distance, baffle hole diameter, baffle hole offset are the main parameters considered for study. COMSOL software was used for determining the transmission loss of the muffler within a specific frequency range of 75-300 Hz and 300 Hz-1500 Hz. Further the aerodynamic performance analysis was performed and it was observed that the efficiency of the new and organized muffler increased by 41.2% in terms of back pressure [165].

Song et.al worked on designing a low cost suction muffler used in compressor of refrigerator. The transmission loss is calculated for the muffler theoretically using LMS.Virtual lab software and if further experimented using transmission loss test bench. It was observed that the result of highest TL obtained theoretically showed a variation of around 10 dB as compared to experimentation [166].

From this literature surveys, it was observed that FEM technique and COMSOL Multiphysics software were mainly developing in recent years and used by researchers.

2.3 Optimization technique

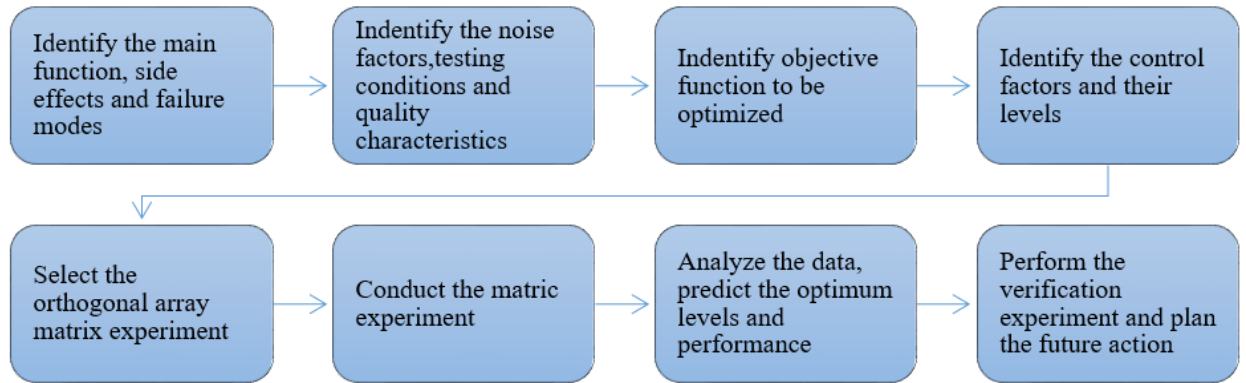
From the aforementioned literature study, the different numerical methodologies and experimental methods are utilized for identifying the most suited muffler is noticed. Only

a small number of researchers continue to use optimization techniques for muffler design. In this part, the optimization methods that were applied are briefly reviewed.

Design of Experiments (DOE) is a statistical method used for optimizing the design of any structure. This technique or statistical method use the available input variables during the process of optimization. For optimizing any system, it initially screen's out the entire possible factor which will affect the performance of the system. When the system is having large number of input variables, then its primary objective is to scale down the number of factors based upon its effect. This DOE requires cautious planning and sensible layout of the experiment and also expert analysis of the results. The DOE methodology proposed by Taguchi is considered to be one of the best methodologies in the process of optimizing any system. This is known as Taguchi method or Taguchi technique [167], [168].

Taguchi Method: It is a Design of Experiment (DOE) technique that is employed in the creation of high-caliber systems. It is a straight forward, effective, and methodical process for arriving at an optimized design with high performance, minimal expense, and highest quality. To determine the relevance or importance of the chosen parameter, this method is quite helpful. Factorial design could also be utilized to optimize a muffler. However, because the muffler design calls for more experiments than necessary to identify the parameters, fractional factorial design may also be utilized. A method of investigating and identifying every conceivable situation in an experiment with several components is called factorial design. Experiments are used to evaluate the impact of certain parameters on performance [169], [170]. The signal to noise (S/N) ratio calculates how much the experimental findings deviate from the target values. Analysis of Variance (ANOVA) analysis is carried out after achieving the S/N ratio. It analyses the data and makes the necessary judgments about the importance of the parameter taken into account for design optimization. This procedure follows the flowchart's eight phases to produce the intended outcome [168], [171].

Eight steps of Taguchi method are



The Taguchi approach has been discussed by several scholars in relation to muffler design, engine performance, and pollutant emission conditions. They are covered in this section, among others.

Sanjay et al. has talked about how to improve the suction muffler in a reciprocating compressor that is hermetically enclosed. For calculating the transmission loss and pressure drop in the muffler, their work took into account the effects of variations in the insertion tubes' lengths, cross-sectional areas, and chamber volumes. Using Taguchi's DOE methodology, it was assessed how important these variables were. Software called SYSNOISE and FLUENT were used to study the acoustic and aerodynamic parameters, respectively. Through the use of experimental methods, these findings have been confirmed [172].

Patil et al. in their research, used the Taguchi approach to optimize the two chamber reactive muffler's design. The study's control criteria include chamber length and the inner radius of holes. The transmission loss was the observed metric identified in SYSNOISE, and the L9 orthogonal array was used in their research. An improved reactive muffler is first created using the Taguchi method, and the outcomes of the experiments are then compared [170].

Yang and Tsai worked on a muffler used in a 40 HP blower used in generator. Different acoustic elements were used according the range of frequencies at which it operates. The muffler used for reducing noise at low frequency was constructed with micro-perforated plates and multiple resonant chambers. Whereas glass fiber blankets of different grades and densities were implemented on those muffler, which are used for high frequencies.

Statistical method i.e. taguchi method was used during the optimization of the mufflers and their analysis resulted in reduction of noise from 111 dB to 78 dB at the exhaust for the newly designed muffler [173]. Naikwad also utilized the taguchi method for optimizing a dual chambered muffler [174].

From the literature survey, it was observed that design of experiment (DOE) is one of the efficient technique used by researchers in recent years for optimization of their muffler design.

2.4 Vibration characteristics in muffler

Various structural, thermal and vibration loads are also acting on the mufflers which are generated for the engine, high pressure exhaust gases and also from road excitations. The vibrations causes localized stresses in the muffler. According to the researches, vibration analysis helps in reducing the crack initiation, improve life of the muffler and also increases efficiency. Stiffeners were used by various researchers for reducing the intensity of vibration in the muffler. Jagtap and Khairnar in their work have performed the vibration through experimentation for obtaining the natural frequencies [175], [176]. Ambesange and Jagtap also worked on performing the FFT analysis in muffler. The natural frequencies were determined using the model analysis method. This analysis results were verified and validated through experimentation [177]. Few other researchers have also performed vibration analysis in order to dampened the noise produce mainly at the exhaust [178]–[180].

Mohanty and Fatima [181], [182] in their work had discussed about the different techniques that could be used for noise and vibration and controlling these vibrations. Taking into consideration the rules and regulation set by different legislative bodies, they suggested some of the numerical techniques which could be implemented by manufacturing industries. Their work revealed that computer aided numerical techniques is effective method for designing and analysis the noise and vibration. Mohanty further in his various works, mentioned about the application of vibration techniques on different types of muffler and for maintaining the noise and pressure fluctuation at the exhaust of vehicles [15], [183], [184].

Barbieri et al. in their work had specified that measurement of the acoustic performance parameters of different mufflers are influenced by the wave propagation. So, bi-spectrum and kurtosis approach was used for detecting the amount of error occurred in the transmission loss value of the muffler. These experiments were performed in a bipartite chamber and a chamber inserted with concentric perforated tube using two microphone method [185], [186]

Patekar and Patil worked on modelling the exhaust system of an automotive vehicle. During the designing, a muffler used in two-wheeler is considered. The specific properties of material are considered and finite element analysis (FEA) was performed using ANSYS for obtaining its performance parameters. Modal analysis is next performed with FFT analyzer for determining the effect of vibration on the muffler. These modal analysis was performed for diminishing the effect of resonance in muffler [187].

Sunil and Suresh also worked on determining the natural frequencies, mode shapes obtained through vibration testing in an automotive muffler. To attain a desired noise level at the exhaust system, knowing the accurate mode shape is of prime importance. The natural frequencies in the reactive muffler is obtained through simulation using MSC NASTRAN software and the results were verified experimentally using FFT analyzer [188].

Mittal and More in their work discussed the effect of vibration in the exhaust system. According to them pressure wave generated from the engine and pressure fluctuations at the exhaust port highly affect the performance of muffler. FEA technique was used by them for reducing the resonance produce by this pressure fluctuations. ANSYS is mainly used for performing the modal analysis of the muffler. The results obtained were validated through physical experimentation i.e. through FFT and impact hammer test [189]. Similarly, many other researchers such as Schwarz, Jie, Reddy had also worked on performing the modal analysis of muffler and determined the natural frequencies in the muffler in their individual works [190]–[192].

CHAPTER 3. RESEARCH GAP IDENTIFICATION AND MOTIVATION OF THE STUDY

It has been determined from numerous reviews of the literature that car exhaust makes an extremely loud noise. This loud noise causes significant noise pollution which is detrimental for human health. According to a report published by the World Health Organization (WHO) and European Union (EU), 40% of the EU inhabitants are exposed to road noise of 55 dB or more at night. Whereas 20% of this is subjected to noise levels over 65 dB during the day [193]. As a consequence of it, various health issues such as high blood pressure, noise-induced hearing loss (NIHL), cardiovascular issues etc.

Looking into this conditions new regulations had been taken into consideration by the European Commission to reduce the desired noise produced by different passenger cars, commercial vehicles, buses, lorries, etc. All passenger vehicles are required to reduce the lower noise limit of vehicles by 2 dB(A) in two steps in accordance with the regulation put up by the EU. Numerous other legislative organizations and governing bodies had published this in the official journals. EU noise policy established a promise to considerably reduce noise pollution in the Union in its programme on Environment Action through 2020. By 2020, its value would be somewhat closer to those set forth by the World Health Organization [194]–[196].

Indian Standards state that a vehicle's maximum noise level should not exceed 80 dB. In order to gather real-time noise monitoring data, the Central Pollution Control Board (CPCB), New Delhi, has started the National Ambient Noise Monitoring Network (NANMN) in India's main cities. Although there are now no restrictions in place in India, they are expected to be adopted very soon in an effort to limit vehicle noise and to demand extremely low levels of emission vehicles [197], [198]. The implementation of strict rules and regulations set by the legislative bodies had put forward a design constraint for the manufacturing industries while developing a new design of muffler. The new acoustic muffler should be very much helpful for reducing the unwanted noise produce by exhaust system as well as satisfy the rules of regulatory bodies. So, wide scope is available for improving the design of muffler as per the regulations.

Reviews of the literature have revealed that reactive and dissipative mufflers are the two main types of mufflers being considered by many researchers for parameter

optimization. Yet very few researchers have studied combination of dissipative and reactive muffler (hybrid muffler) for adjusting the settings to increase the performance. But, when it comes to lowering sound levels, the results of the hybrid muffler are found to be very much promising. Due to the complexity of the design of hybrid muffler, very few researchers had attempted to design it. This leads a wide scope for researcher to design and construct a simple hybrid muffler. Researchers typically alter designs in optimization without taking into account any particular criteria or parameter and instead use boundary conditions to gauge performance.

The sound from exhaust system propagates through the muffler because of pressure fluctuations which is basically the vibration of the sound particles. Thus vibration is one of the main effect due to which the noise is generated, but the effect of this vibration on the performance of muffler is not yet been explored

Motivation of the work

According to studies conducted by several researchers, the exhaust system and tail pipe independently provide the most noise to the overall sound level, each at a rate of about 25.1%. In contrast, the contribution of the tire, duct or intake system, induction snorkel system is roughly 19.1%, 13.5%, and 8.7%, respectively [70], [71]. The noise from the exhaust system is seriously affecting human health and contributing to conditions including stress, hypertension, high blood pressure, heart disease, and noise-induced hearing loss (NIHL). Looking into this issues various governing bodies all over the world had become strict on implementing regulations towards reducing the noise coming from the exhaust system. In India also legislative bodies had become strict on emission sound from vehicles putting strict regulations for automotive manufacturers. In light of this, manufacturers and researchers are putting a lot of effort into redesigning the exhaust system because it offers a lot of room for development and adds greatly to the overall sound of the car. Further the vibration characteristics of this exhaust system could also be studied. This has given me a motivation towards doing my research in this field, so that a better exhaust system could be manufactured which would be helpful for automotive industry as well as beneficial for the society.

CHAPTER 4. RESEARCH OBJECTIVES

This research work is based on dissipative, reactive and hybrid muffler. The objectives of this study are

- ❖ Optimization of reactive muffler on the basis of simulation and its validation experimentally.
- ❖ Different type of absorption material with variable density would be tested for best outcomes through simulation and these results would be validated experimentally.
- ❖ Combination of the reactive muffler and absorption material i.e. a hybrid muffler for the best results would be tested through simulation and will be validated experimentally.
- ❖ Effect of vibration on the acoustic behavior at the upstream and downstream section of the muffler would also be investigated and will be correlated with acoustic parameters.

CHAPTER 5. THEORETICAL BACKGROUND AND ANALYSIS OF MUFFLER

A sequence of pressure changes are produced whenever an audio wave travels. The wave propagates in a certain direction due to these minor fluctuations, which follow a linear equation with a steady state term and a first order fluctuation. The wave equation, or Eq. 38, is a representation of pressure variation [13], [14].

$$\frac{\partial^2 p}{\partial t^2} = c^2 \nabla^2 p \quad (38)$$

Where p is acoustic pressure, c is speed of sound, ∇^2 is Laplacian Operator and

$$\nabla^2 = \frac{\partial^2}{\partial x^2} + \frac{\partial^2}{\partial y^2} + \frac{\partial^2}{\partial z^2}$$

Practically, there are two ways that waves can spread. First, spherical wave propagation occurs when the sound source is retained in an open area, and second, plane wave propagation occurs when the sound source is constrained by a specific path [13].

5.1 Analytical method for calculating transmission loss

Simple expansion chambers are used as sound attenuators for creating reactive mufflers. It can have an equal inlet and output tube cross-section at both chamber ends and can be either cylindrical or elliptical in shape. When designing, only a few presumptions from the theory of the acoustic field are often taken into account. [30], [199]. The assumptions are

1. Viscosity effect is neglected.
2. Gravity effect is neglected.
3. Radiation and convection of sound through duct surface are neglected.
4. There is no reflected wave and zero mean flow at exit of muffler.

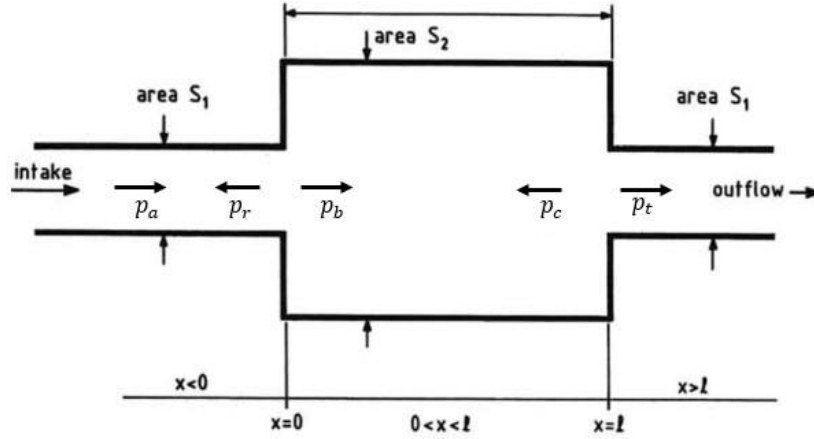


Figure 5.1. Schematic of simple reactive or simple expansion muffler

The cross-section of a straight forward expansion chamber muffler is shown in Figure 5.1. At the intersection of the inlet tube and outlet tube, the incident pressure (p_i), reflected pressure (p_r), transmitted pressure (p_t) and (p_b), (p_c) which represent the pressure in the main chamber, are given as follows [13].

$$p_i = A_i e^{i\omega(t-\frac{x}{c})} \quad \text{in } x < 0 \quad (39)$$

$$p_b = A_b e^{i\omega(t-x/c)} \quad \text{in } 0 < x < l \quad (40)$$

$$p_r = A_r e^{i\omega(t+x/c)} \quad \text{in } x < 0 \quad (41)$$

$$p_c = A_c e^{i\omega(t+x/c)} \quad \text{in } 0 < x < l \quad (42)$$

$$p_t = A_t e^{i\omega(t-\frac{x-l}{c})} \quad \text{in } x > l \quad (43)$$

The boundary conditions for pressure and velocity displacement are met by the Eqs. (39–43). These boundary conditions are used for the incident, reflected and transmitted wave and the transmission loss is finally calculated as

$$TL = 10\log_{10} \left[1 + \frac{1}{4} \left(m - \frac{1}{m} \right)^2 \sin^2 kl \right] \quad (44)$$

Where $m = \text{expansion ratio} = S_1/S_2$ and S_1, S_2 are the cross-section areas of inlet tube and chamber respectively.

The one who wants to know the calculation can refer section 1 in Appendices.

5.2 Transfer matrix method for calculating transmission loss

The TL of a muffler is dependent on each of its component parts, and it may be calculated using the transfer matrix approach. In the transfer matrix approach, matrices are built utilizing two state variables: mass velocity (v) and acoustic pressure (p) [79], [85]. The state variables are related from one end of the element to the other end of the element for an element shown in Figure 5.2 is through Eq. (45).

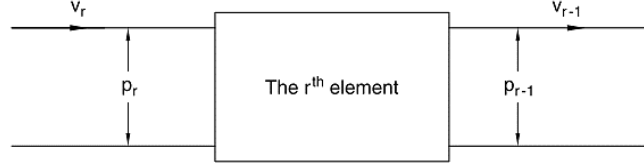


Figure 5.2. Pictorial representation of an element for transfer matrix.

$$\begin{pmatrix} p_r \\ v_r \end{pmatrix} = \begin{pmatrix} A \ 2 \times 2 \ transfer \ matrix \\ for \ the \ r^{th} \ element \end{pmatrix} \begin{pmatrix} p_{r-1} \\ v_{r-1} \end{pmatrix} \quad (45)$$

Here $[p_r, v_r]$ symbolizes the state vector on upstream point 'r' and $[p_{r-1}, v_{r-1}]$ symbolizes state vector on downstream point 'r-1'. The transfer matrix for this r^{th} element is represented by $[T_r]$.

Thus, Eq. (45) can be rewritten as shown in Eq. (46)

$$\begin{pmatrix} p_r \\ v_r \end{pmatrix} = [T_r] \begin{pmatrix} p_{r-1} \\ v_{r-1} \end{pmatrix} \quad (46)$$

The transfer matrix for r^{th} element can be expressed as $[T_r] = \begin{pmatrix} E_{11} & E_{12} \\ E_{21} & E_{22} \end{pmatrix}$

Where E_{11}, E_{12}, E_{21} and E_{22} are also identified as four pole parameters and each pole parameter is having its own implication.

Using Eq. (46), the four pole parameter are stated as

$$E_{11} = \left. \frac{p_r}{p_{r-1}} \right|_{v_{r-1}=0}, \quad E_{12} = \left. \frac{p_r}{v_{r-1}} \right|_{p_{r-1}=0}, \quad E_{21} = \left. \frac{v_r}{p_{r-1}} \right|_{v_{r-1}=0}, \quad E_{22} = \left. \frac{v_r}{v_{r-1}} \right|_{p_{r-1}=0} \quad (47)$$

For the elements or sub-elements positioned inside the muffler, the transfer matrix is obtained using the four pole parameters given in Eq. (47). According to the principle of the transfer matrix, there are three different sorts of muffler elements: distributed, in-line, and shunt or branch lumped. Standard wave relations are used to define the transfer matrix for these components [29], [30], [76]. Using these relations, the transfer matrix is created for different acoustic elements and its transmission loss is obtained through Eq. (48).

$$TL = 20 \log \left[\left(\frac{Y_1}{Y_r} \right)^{1/2} \left| \frac{1}{2} \left[\left(E_{11} + \frac{E_{12}}{Y_1} \right) + Y_r \left(E_{21} + \frac{E_{22}}{Y_1} \right) \right] \right| \right] \quad (48)$$

Here, Y_r represents the characteristic impedance.

The one who wants to know the process of calculation can refer section 2 under Appendices.

5.3 Implementation of Transfer Matrix Method (TMM) in reactive muffler

A line diagram for an idealized three-chamber reactive muffler that includes all of the parts are depicted in Figure 5.3. The 11 elements are numbered 1 through 11 and are given matching lengths from l_1 to l_{11} in the diagram. The muffler's entry point and exit point, which are connected to the engine exhaust and outlet, respectively, are represented by elements 0 and 12. Figure 5.4 depicts the comparable circuit schematic for the entire three-chamber reactive muffler. Additionally, the line diagram designates the position of the baffle from the inlet tube, baffle from the outlet tube, and the hole position as L1, L2, and HP, respectively.

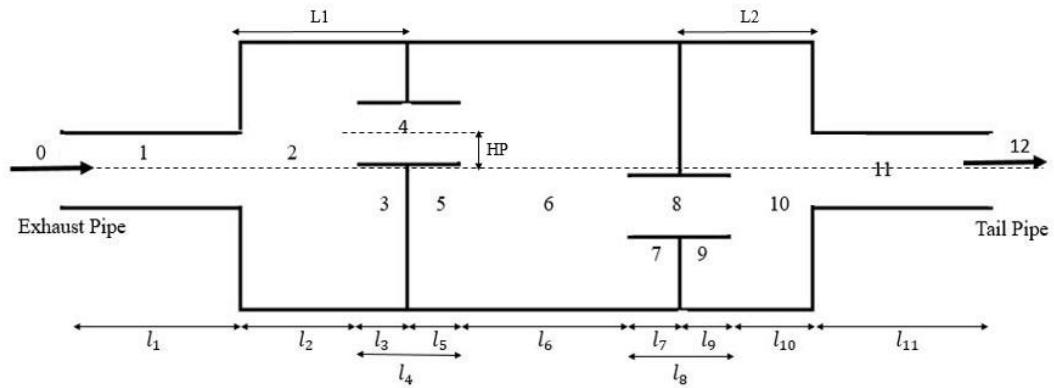


Figure 5.3. Line Diagram of the reactive muffler

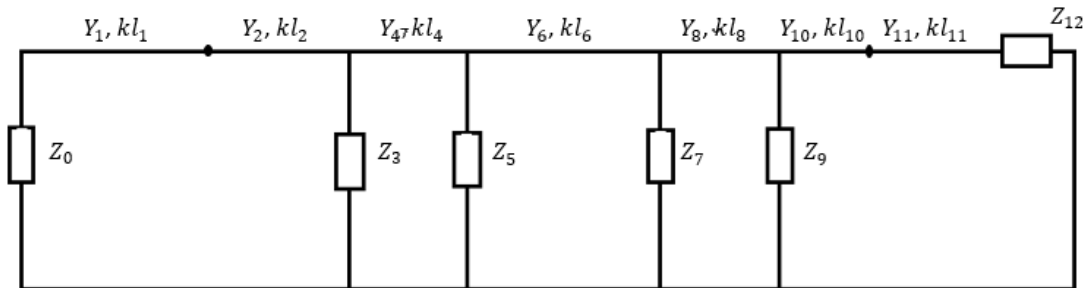


Figure 5.4. Equivalent circuit demonstration of the reactive muffler

The elements 0, 3, 5, 7 and 9 behave according to the branch lumped element idea, while elements 1, 2, 4, 6, 8, 10, and 11 behave according to the distributed element notion.

Element 12 behaves according to the in-line element principle. The decision to use a certain element is decided based on its shape, which was already presented in the previous section. The transfer matrices for one element from each of the categories of dispersed (element 1), branch lumped (element 3), and in-line (element 12) are shown in Eqs. (49), (50), and (51), respectively.

$$\text{Transfer matrix } [M_1] = \begin{pmatrix} \cos(kl_1) & jY_1 \sin(kl_1) \\ \frac{j\sin(kl_1)}{Y_1} & \cos(kl_1) \end{pmatrix} \quad (49)$$

$$\text{Transfer matrix } [M_3] = \begin{pmatrix} 1 & 0 \\ 1/Z_3 & 1 \end{pmatrix} \quad (50)$$

$$\text{Transfer matrix } [M_{12}] = \begin{pmatrix} 1 & Z_{12} \\ 0 & 1 \end{pmatrix} \quad (51)$$

As a result, $[M_r]$ can represent the full transfer matrix for the muffler and create it by multiplying the transfer matrices of each component that is connected to the muffler. Eqs. (52) and (53), respectively, show the entire transfer matrix..

$$\begin{pmatrix} p_0 \\ v_0 \end{pmatrix} = [M_0] [M_1] [M_2] [M_3] [M_4] [M_5] [M_6] [M_7] [M_8] [M_9] [M_{10}] [M_{11}] [M_{12}] \begin{pmatrix} p_{12} \\ v_{12} \end{pmatrix}$$

i.e. $\begin{pmatrix} p_0 \\ v_0 \end{pmatrix} = [M_r] \begin{pmatrix} p_{12} \\ v_{12} \end{pmatrix}$ (52)

$$\begin{aligned} [M_r] = & \begin{pmatrix} 1 & 0 \\ 1/Z_0 & 1 \end{pmatrix} \begin{pmatrix} \cos(kl_1) & jY_1 \sin(kl_1) \\ \frac{j\sin(kl_1)}{Y_1} & \cos(kl_1) \end{pmatrix} \begin{pmatrix} \cos(kl_2) & jY_2 \sin(kl_2) \\ \frac{j\sin(kl_2)}{Y_2} & \cos(kl_2) \end{pmatrix} \begin{pmatrix} 1 & 0 \\ 1/Z_3 & 1 \end{pmatrix} \\ & \begin{pmatrix} \cos(kl_4) & jY_4 \sin(kl_4) \\ \frac{j\sin(kl_4)}{Y_4} & \cos(kl_4) \end{pmatrix} \begin{pmatrix} 1 & 0 \\ 1/Z_5 & 1 \end{pmatrix} \begin{pmatrix} \cos(kl_6) & jY_6 \sin(kl_6) \\ \frac{j\sin(kl_6)}{Y_6} & \cos(kl_6) \end{pmatrix} \begin{pmatrix} 1 & 0 \\ 1/Z_7 & 1 \end{pmatrix} \\ & \begin{pmatrix} \cos(kl_8) & jY_8 \sin(kl_8) \\ \frac{j\sin(kl_8)}{Y_8} & \cos(kl_8) \end{pmatrix} \begin{pmatrix} 1 & 0 \\ 1/Z_9 & 1 \end{pmatrix} \begin{pmatrix} \cos(kl_{10}) & jY_{10} \sin(kl_{10}) \\ \frac{j\sin(kl_{10})}{Y_{10}} & \cos(kl_{10}) \end{pmatrix} \\ & \begin{pmatrix} \cos(kl_{11}) & jY_{11} \sin(kl_{11}) \\ \frac{j\sin(kl_{11})}{Y_{11}} & \cos(kl_{11}) \end{pmatrix} \begin{pmatrix} 1 & Z_{12} \\ 0 & 1 \end{pmatrix} \end{aligned} \quad (53)$$

The total transfer matrix $[M_r]$ can be determined by multiplying the transfer matrices of each individual element, and it can then be written as follows in Eq. (54), along with those properties.

$$[M_i] = \begin{pmatrix} E_{11} & E_{12} \\ E_{21} & E_{22} \end{pmatrix} \quad (54)$$

The TL can be calculated using these four characteristics of the entire transfer matrix, which are known as the four pole parameters.

The three-chamber muffler's TL may be calculated using four pole characteristics as shown in Eq.(55) using the basic TL equation.

$$TL = 20 \log_{10} \left[\left(\frac{Y_t}{Y_i} \right)^{1/2} \left| \frac{E_{11} + \frac{E_{12}}{Y_t} + E_{21} Y_i + \frac{Y_i}{Y_t} E_{22}}{2} \right| \right] \quad (55)$$

Where Y_t and Y_i represents the characteristic impedance of the incident pressure wave and transmitted pressure wave respectively.

5.4 Implementation of Transfer Matrix Method (TMM) in hybrid muffler

The reactive muffler in Figure 5.3 has been changed into a hybrid muffler by adding a layer of sound-absorbing material in the second and third chambers. Figure 5.5 depicts the line diagram of this hybrid muffler, which lists all of the elements and their respective lengths from l_1 to l_{15} . There are 15 different elements in all. The muffler's entry point and exit point, which are connected to the engine exhaust and outlet, respectively, are represented by elements 0 and 16.

Additionally, the line diagram designates the location of the baffle from the input tube, exit tube, hole position, absorption material layer in chamber 2 and chamber 3 as L1, L2, HP, A2 and A3 respectively.

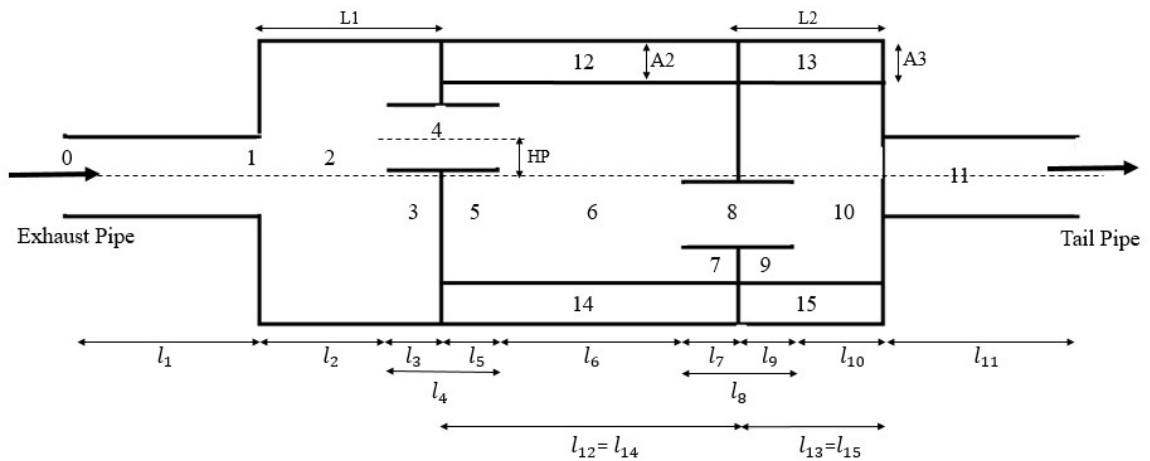


Figure 5.5. Line Diagram of the hybrid muffler

The behavior of the elements from 0 to 11 are already discussed in the previous section in reactive muffler, whereas the elements 12, 13, 14 and 15 works on the principle of absorption material.

Let T_{abs} represents the 2 x 2 matrix of the uniform absorptive material in muffler of the i^{th} acoustic element between the section (j_k) , relating the state variable P_r and v_r where j represents the reactive element and k represents absorptive element [30], [49].

$$T_{abs} = \begin{pmatrix} \cos(k_w l_r) & jY_w \sin(k_w l_r) \\ \frac{j \sin(k_w l_r)}{Y_w} & \cos(k_w l_r) \end{pmatrix}$$

Where k_w = Complex wave number

Y_w = characteristic impedance of the acoustic lining

Thus, the transfer matrix for one of the absorption elements (i.e. element 12) can be written as shown in Eq. (56).

$$\text{Transfer matrix } [M_{12}] = \begin{pmatrix} \cos(k_w l_{12}) & jY_{12} \sin(k_w l_{12}) \\ \frac{j \sin(k_w l_{12})}{Y_{12}} & \cos(k_w l_{12}) \end{pmatrix} \quad (56)$$

As a result, by multiplying the transfer matrices of each individual component connected to the muffler, the complete transfer matrix for the hybrid muffler can be represented by $[M_{hm}]$. The hybrid muffler's equation for calculating the state variables through TMM is

$$\begin{pmatrix} p_0 \\ v_0 \end{pmatrix} = [M_0][M_1][M_2][M_3][M_4][M_5][M_6][M_7][M_8][M_9][M_{10}][M_{11}][M_{12}][M_{13}][M_{14}][M_{15}] \begin{pmatrix} p_{16} \\ v_{16} \end{pmatrix} \quad (57)$$

$$\text{i.e. } \begin{pmatrix} p_0 \\ v_0 \end{pmatrix} = [M_{hm}] \begin{pmatrix} p_{16} \\ v_{16} \end{pmatrix} \quad (58)$$

Thus, the complete TMM for the hybrid muffler is

$$[M_{hm}] = \begin{pmatrix} 1 & 0 \\ 1/Z_0 & 1 \end{pmatrix} \begin{pmatrix} \cos(kl_1) & jY_1 \sin(kl_1) \\ \frac{j \sin(kl_1)}{Y_1} & \cos(kl_1) \end{pmatrix} \begin{pmatrix} \cos(kl_2) & jY_2 \sin(kl_2) \\ \frac{j \sin(kl_2)}{Y_2} & \cos(kl_2) \end{pmatrix} \begin{pmatrix} 1 & 0 \\ 1/Z_3 & 1 \end{pmatrix} \\ \begin{pmatrix} \cos(kl_4) & jY_4 \sin(kl_4) \\ \frac{j \sin(kl_4)}{Y_4} & \cos(kl_4) \end{pmatrix} \begin{pmatrix} 1 & 0 \\ 1/Z_5 & 1 \end{pmatrix} \begin{pmatrix} \cos(kl_6) & jY_6 \sin(kl_6) \\ \frac{j \sin(kl_6)}{Y_6} & \cos(kl_6) \end{pmatrix} \begin{pmatrix} 1 & 0 \\ 1/Z_7 & 1 \end{pmatrix} \\ \begin{pmatrix} \cos(kl_8) & jY_8 \sin(kl_8) \\ \frac{j \sin(kl_8)}{Y_8} & \cos(kl_8) \end{pmatrix} \begin{pmatrix} 1 & 0 \\ 1/Z_9 & 1 \end{pmatrix} \begin{pmatrix} \cos(kl_{10}) & jY_{10} \sin(kl_{10}) \\ \frac{j \sin(kl_{10})}{Y_{10}} & \cos(kl_{10}) \end{pmatrix}$$

$$\begin{aligned}
& \begin{pmatrix} \cos(kl_{11}) & jY_{11}\sin(kl_{11}) \\ \frac{j\sin(kl_{11})}{Y_{11}} & \cos(kl_{11}) \end{pmatrix} \begin{pmatrix} \cos(k_w l_{12}) & jY_{12}\sin(k_w l_{12}) \\ \frac{j\sin(k_w l_{12})}{Y_{12}} & \cos(k_w l_{12}) \end{pmatrix} \begin{pmatrix} \cos(k_w l_{13}) & jY_{12}\sin(k_w l_{13}) \\ \frac{j\sin(k_w l_{13})}{Y_{13}} & \cos(k_w l_{13}) \end{pmatrix} \\
& \begin{pmatrix} \cos(k_w l_{14}) & jY_{12}\sin(k_w l_{14}) \\ \frac{j\sin(k_w l_{14})}{Y_{14}} & \cos(k_w l_{14}) \end{pmatrix} \begin{pmatrix} \cos(k_w l_{15}) & jY_{12}\sin(k_w l_{15}) \\ \frac{j\sin(k_w l_{15})}{Y_{15}} & \cos(k_w l_{15}) \end{pmatrix} \begin{pmatrix} 1 & Z_{16} \\ 0 & 1 \end{pmatrix} \quad (59)
\end{aligned}$$

By multiplying each individual element's transfer matrix, the full transfer matrix $[M_{hm}]$ indicated in Eq. (59) may be generated. It can then be written as follows in Eq. (60) with its unique properties.

$$[M_{hm}] = \begin{pmatrix} E_{11} & E_{12} \\ E_{21} & E_{22} \end{pmatrix} \quad (60)$$

The TL of the hybrid muffler may be calculated using these four characteristics of the full transfer matrix, which are referred to as four pole parameters.

The TL of the hybrid muffler may be calculated utilizing four pole properties using the fundamental TL calculation, as illustrated in Eq. (61).

$$TL = 20 \log_{10} \left[\left(\frac{Y_t}{Y_i} \right)^{1/2} \left| \frac{E_{11} + \frac{E_{12}}{Y_t} + E_{21}Y_i + \frac{Y_i}{Y_t}E_{22}}{2} \right| \right] \quad (61)$$

Where Y_t and Y_i represents the characteristic impedance of the incident pressure wave and transmitted pressure wave respectively.

CHAPTER 6. ANALYSIS OF EXISTING MUFFLER

A muffler follows the principle of plane wave propagation in which the wave propagate through the passages of duct and ultimately reduces the exhaust system noise. The performance of this muffler greatly depends on the passages created by the acoustic elements inside it. A small change in design parameters in any of these acoustic elements, differs its performance. Over the years various scientists and researchers have worked on the performance of muffler and used the various multi-dimensional analytical approaches for evaluating it. But it becomes very tedious for evaluating the complex, complicated designed mufflers as well as greater diversity was seen between the analytical and experimental results.

In the past few years, with the development of new generation of computers and increase in its speed, scientists and researchers started utilizing different numerical simulation techniques. This techniques are providing better solution for the complex structure, due to which it is greatly accepted. FEM is one of the numerical technique, which is being widely used now-a-days during the design process. A muffler size varies from small to large, its testing procedure is complex as well as costly, so this technique is very much beneficial for accurately predicting the performance of muffler before construction. The FEM involves in discretizing the muffler chamber into number of finite elements of equivalent length. A field function is then selected for the exact and approximate field analysis within the element and finally the element matrices are evaluated by the variational principle or residual methods. Further the algebraic equation for the finite element system is formulated and the various unknown pressures and velocities at the nodes are determined [45], [98], [200].

The finite element analysis could be performed through various computational software's such as ANSYS, COMSOL, FEMLAB, ABACUS, MSc.ACTRAN etc [201]–[203]. In this study, ANSYS and COMSOL are the two main software's considered for carrying out the aerodynamic and acoustic performance parameters of the muffler respectively.

6.1 Aerodynamic Analysis of Existing muffler

ANSYS is a finite element analysis software which composed of more than thousands and lakhs of lines of coding for carrying out the final outcome. It is most suitable for

computational work from the last 36 years. Now a days, ANSYS is used in almost all the engineering department i.e. Aerospace, Automobile, Mechanical, Biomedical etc. for optimizing and designing the structures [204], [205]. This could be used for determining both the aerodynamic and acoustic performance parameters. The steps for performing the aerodynamic performance analysis using finite element analysis is discussed under appendices in section 3.

In the current study, an elliptical type, four-chamber reactive muffler employed in a four-cylinder, petrol engine producing 91 bhp at 6000 rpm was taken into consideration for optimization [142]. This is selected from the literature survey performed for the work performed by various researchers. It has an exterior configuration, or a total length of 500 mm for the chambers, and an elliptical cross-section with dimensions of 112 mm for the semi-major axis and 78 mm for the semi-minor axis, respectively [122]. In Figure 6.1, its schematic representation is displayed. It was observed that multi-chambered mufflers with different acoustic elements in it, used in vehicles performs better than the other cross-section mufflers. But due to the design complexity, manufacturers are taking time during the construction as well as it increases the cost. Looking into these factors, the muffler shown in Figure 6.1 used in a four-cylinder petrol engine is considered for study.

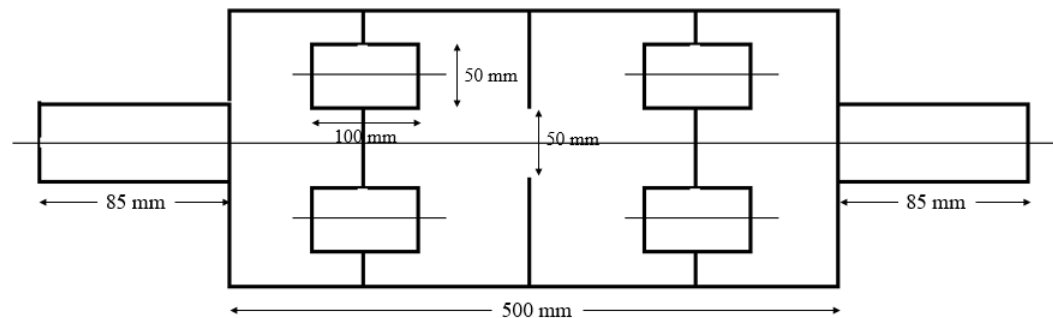


Figure 6.1. Schematic view of four-chamber reactive muffler

Calculating the volume of muffler

The volume of the muffler is estimated using acoustic theory.

Swept volume per cylinder: $0.25 \times (3.14 \times 73^2 \times 82)$, (V_s) = 0.343201 Lt.

Total swept volume is equal to 4×0.3432 litres, or 1.3728 litres.

$0.5 \times V_s \times n = 0.686402$ Lt is the volume to be taken into account for the computation.

Volume of the silencer must be between 12 and 25 times the volume being considered [29], [30].

Volume can be changed according on the available space.

Factor taken into account is 20

Silencer volume is determined by factor and considered volume and it equals 13.728 L (0.01372 m³).

Volume can be changed according on the available space.

Configuration internally and conceptual designs

Size of the intake pipe Calculations:

Hypothetical cylindrical diameter for a volumetric muffler.

V_m equals $0.25 \times \pi \times d^2 \times l$ or $0.013728 = 0.25 \times \pi \times d^2 \times 0.5$

$d = 0.187 \text{ m} = 187 \text{ mm}$.

According to the specifications for the supercritical grade of mufflers, the body's diameter should be around three times that of the exhaust pipe.

$D_{\text{exhaust}} = 62.33 \text{ mm}$ when $d = 3 * d_{\text{exhaust}} = 187$

The dimensions of the muffler are crucial factors when creating one.

By taking into account the elliptical shape of the current muffler

Semi-major axis: 112 millimeters equals 0.112 metres

Semi-minor axis: 78 mm equals 0.078 metres

Muffler length is 500 mm, or 0.5 metres.

The present elliptical muffler's volume (V_m) is equal to $(\pi abh) = 3.14 \times 0.112 \times 0.078 \times 0.5 = 0.01372 \text{ m}^3$.

Now, while performing the FEM analysis of this existing muffler in ANSYS, few assumptions are followed.

1. Fluid is compressible and it allows very small change in pressure with respect to main pressure.
2. Fluid is inviscid and viscosity causes no dissipation.
3. Uniform mean pressure and uniform mean density.

Steps for aerodynamic analysis

ANSYS Workbench is used for performing the analysis. In this computational software, different modules are available, of which the fluent module is considered for the flow analysis. The steps followed are discussed in this section.

Step 1: Geometry of the existing reactive muffler.

The geometry of the reactive muffler is constructed in the design modular interface with the available tools. During this process different constraints were used and the diagram for the muffler is shown in Figure 6.2.

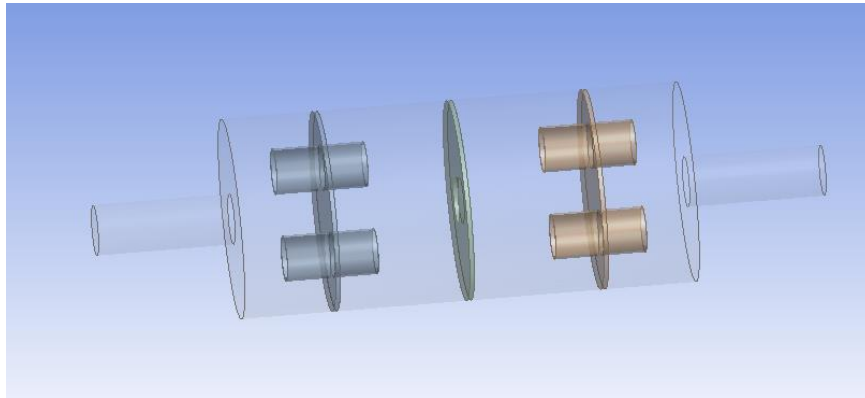


Figure 6.2. Geometry of the four chamber reactive muffler

Step 2: Meshing of the muffler

It is the method of dividing the model into small finite elements. The muffler model is now divided into finite number of small elements. Upon completion of meshing the inlet and outlets are named as well as the other sections are also named accordingly as shown in Figure 6.3. The element size of mesh is finalized as 5 mm by performing the grid independence test.

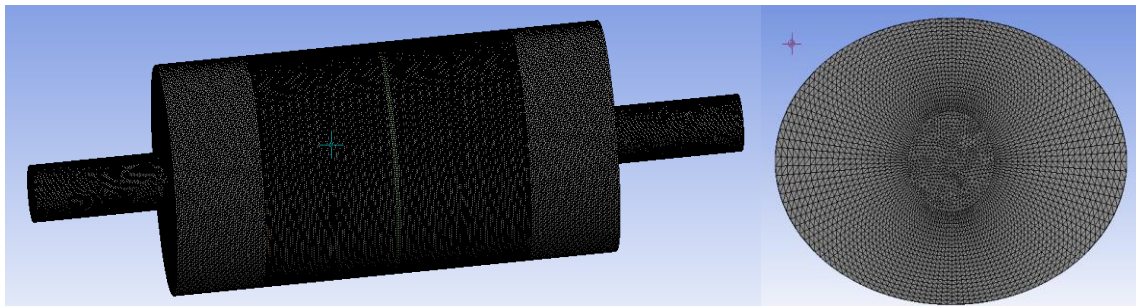


Figure 6.3. Front view and side view of meshed model

Grid Independence Test

Mesh convergence test or grid independent test is performed to choose the mesh size, as size of the mesh plays a major role in the simulation results. The test was performed for mesh sizes varying from 3mm to 5 mm and the total pressure and acoustic power level were determined. The total pressure was found to be varying from 6792.4 Pa to 6792.91 Pa and the acoustic power level varied from 54.55 dB to 55.87 dB. Thus, not much variation

was observed in these values and to reduce the simulation time, a mesh size of 5 mm was chosen for carrying out the analysis.

Step 3: Setup

The meshed model is now imported in the setup of fluent and the various working conditions are implemented. Initially the model dimension is selected as 3D and double precision option is selected in the fluent launcher interface. Next the pressure based solver was considered for the flow analysis as the flow velocity in the muffler is around Mach number of 0.11. During this step initially the steady state pressure based solver is used by considering the absolute velocity formulation module. Next the physical parameters and materials used in the model and its properties are implemented in the interface. The model is then implemented with two boundary conditions. Velocity inlet boundary condition of 40 m/s and pressure outlet boundary condition of 0 is applied at the inlet and outlet section of muffler. This is later on solved using the pressure velocity coupling method.

One can refer the details of steps and values used during the analysis under section 4 in appendices.

Step 5: Results

The pressure and velocity contour obtained for the model is shown in Figure 6.4 and 6.5.

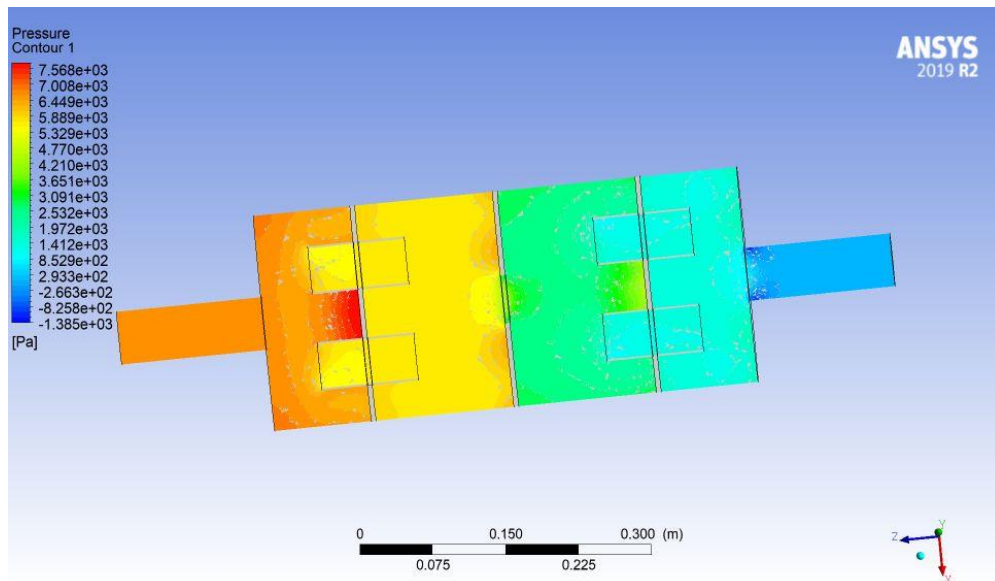


Figure 6.4. Pressure contour for the existing reactive muffler

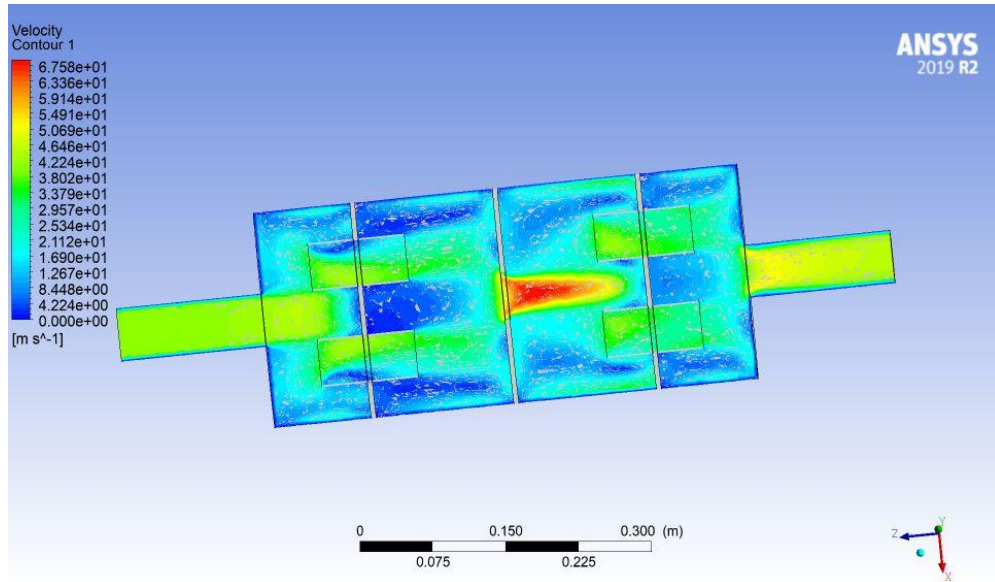


Figure 6.5. Velocity contour for the existing reactive muffler

The analysis depicts that the pressure at the inlet section of the muffler is 6792.9 Pa, whereas at outlet section it is 0. Thus the difference in pressure i.e. pressure drop between this section of muffler is found to be 6792.9 Pa whereas the velocity contour depicts that the maximum velocity of 67.58 m/s is observed at the position of hole in the center baffle.

6.2 Acoustic Analysis of Existing muffler

COMSOL Multiphysics is a simulation software or finite element analysis (FEA) software which is used for solving various coupled and Multiphysics problems. This is also capable of solving problems which are based on advanced numerical methods. These problems are solved by using the different partial differential equations. It is a user-friendly software which can be used for performing the model of the component as well as performing the complete analysis. Out of the various modules available in this FEA software, the pressure acoustic module is implemented for obtaining the acoustic noise level of muffler in this work. So this software is mainly used for determining the acoustic performance parameter of muffler [148], [206], [207].

Transmission Loss (TL), the main acoustic performance parameter of muffler is obtained by using the acoustic sound power at the inlet and outlet section of the system. According to Reynold's, the sound power could be determined through Eq. (62) [208], [209].

$$W = \int \frac{p_{rms}^2}{\rho c} \cdot dS \quad (62)$$

Where p_{rms} = root mean square pressure, S = area of the surface through which sound is propagating, ρ = density, c = speed of sound.

Thus, the TL can be obtained by using Eq. (63)

$$TL = 10 \log \frac{W_i}{W_t} \quad (63)$$

Where, W_i = Incident sound power, W_t = transmitted sound power.

The steps followed for TL calculation is discussed in this section.

Step 1: Selection of model wizard and space dimensions.

Step 2: Selection of module according to the analysis that need to be performed. In this work, module used is acoustics and the physical interface used is pressure acoustic, frequency domain (acpr) for obtaining the TL for the muffler.

Step 3: Creating the geometry

The geometry of the model can be either imported to the interface or it can be sketched with the in-built tools available for modeling. Here, in this study the model is sketched in the interface as shown in Figure 6.6.

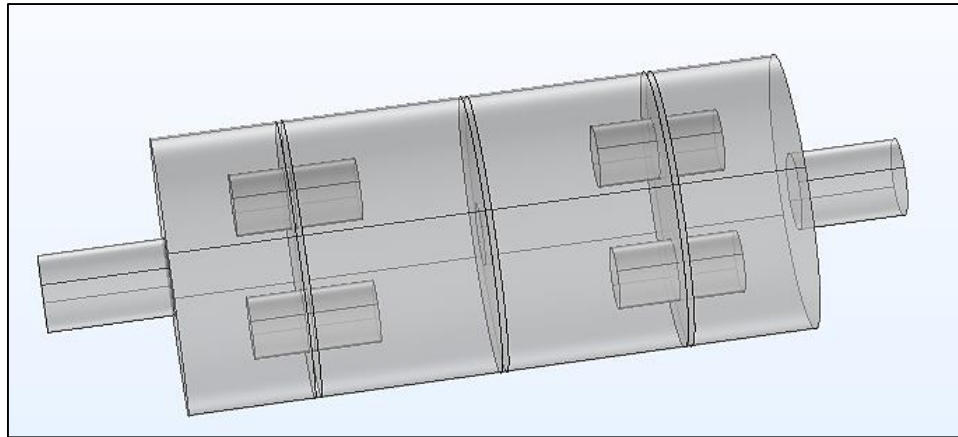


Figure 6.6. Sketch of the four chamber reactive muffler in COMSOL

Step 4: Application of Material Properties

Material Contents				
Property	Variable	Value	Unit	
<input checked="" type="checkbox"/> Density	rho	1.2256	kg/m ³	
<input checked="" type="checkbox"/> Speed of sound	c	343	m/s	
Coefficient of thermal expansi...	alpha_...	alpha_p...	1/K	
Mean molar mass	Mn	0.02897	kg/mol	
Bulk viscosity	muB	muB(T)	Pa·s	
Relative permeability	mur_i...	1	1	
Relative permittivity	epsilo...	1	1	
Dynamic viscosity	mu	1.81e-5	Pa·s	
Ratio of specific heats	gamma	1.4	1	
Electrical conductivity	sigma...	0[S/m]	S/m	
Heat capacity at constant pres...	Cp	1005	J/(kg·K)	
Thermal conductivity	k_iso ;...	0.0285	W/(m·...	
Refractive index, real part	n_iso ;...	1	1	

Family: Air

Material Contents				
Property	Variable	Value	Unit	
<input checked="" type="checkbox"/> Density	rho	7900	kg/m ³	
<input checked="" type="checkbox"/> Speed of sound	c	343	m/s	
Heat capacity at constant pres...	Cp	500	J/(kg·K)	
Thermal conductivity	k_iso ;...	16.27	W/(m·...	

Family: Steel

Step 5: Meshing

The model is next meshed in the COMSOL meshing module using extremely fine module as shown in Figure 6.7.

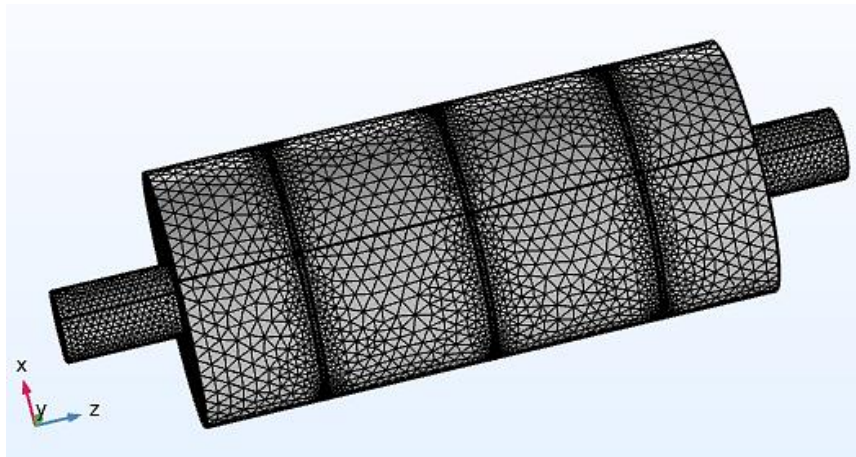


Figure 6.7 Mesh model of in COMSOL

Step 6: Boundary conditions

Radiation boundary condition is used in the inlet surface and outlet surface of the muffler.

Step 7: Solution

Frequency domain is used for performing the analysis and ultimately determining the TL for the muffler. The analysis was performed for frequencies ranging from 5 Hz to 2000 Hz with step size of 5 Hz.

Step 8: Results

The TL obtained for the existing muffler from this analysis is shown in Figure 6.8.

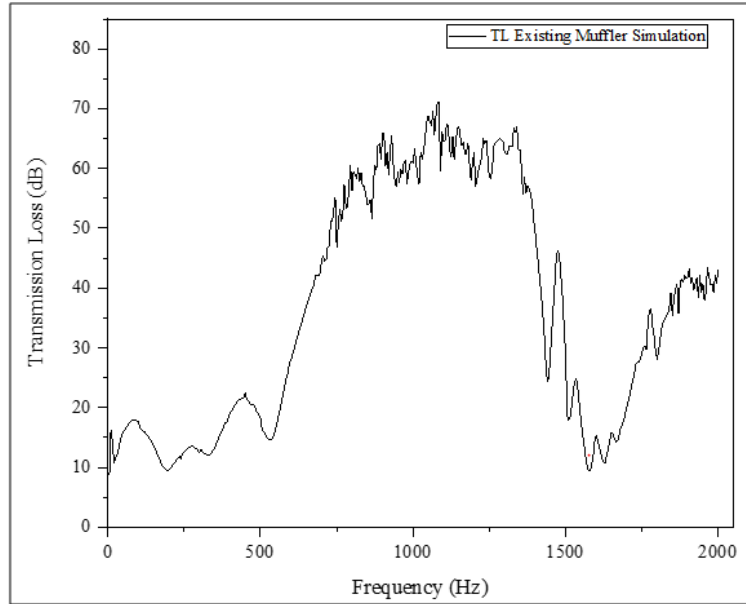


Figure 6.8.TL curve obtained in COMSOL Multiphysics

Figure 6.13 shows that the TL value is not much at low frequencies but with the increase in frequency, the TL also increases and the maximum TL obtained is about 71.04 dB at 1085 Hz.

6.3 Experimental Validation of simulation results

6.3.1 Fabrication of the existing muffler and experimental set up

Initially, the different materials that would be required for fabricating the muffler are determined through literature reviews. It was observed that mild steel, stainless steel are some of the materials commonly used for constructing the exhaust system components. In this study mild steel is used for fabricating the different components used in muffler. Mild steel is composed of iron and carbon and it is strong and durable. It is less expensive than most of the other materials such as stainless steel. One of the drawback of mild steel is that it doesn't resist corrosion and in order to overcome it, the exhausts parts could be painted with high temperature paint.

Once the muffler is fabricated, non-destructive test (NDT) is performed to check the manufacturing defects. Tap or coin test is one such old and simple NDT in which through the sections of the component is tapped by small hammer or coin and defect is judged by the sound produced in that position. A dull sound indicate the presence of a defect at that

position due to which the sound at that position is dampened. This tap test could be performed manually as well as it could be performed through automatic tap testing instrument such as Mitsui Woodpecker [210]–[213].

The steps followed for the fabrication are mentioned in this section.

Step 1: A rectangular sheet of 2 mm thickness is cutted from a big sheet according to the dimension of the muffler i.e. 500 mm x 602 mm. The sheet is then rolled in the shape of the ellipse according to dimension of semi-major and semi-minor axis of 112 mm and 78 mm respectively in a roller machine and is welded.

Step 2: Five small rectangular plates of dimensions 240 mm x 170 mm were cutted from big sheet. These plates were taken for covering the ends of muffler chamber and for constructing the baffles.

Step 3: The five plates were first given the shape of the ellipse according to the dimension of the muffler chamber. Next two holes of 50 mm diameter is made on two plates which would be used as a baffle and a hole was made on the center plate. Further holes were also made on two other plates according to the dimension of inlet and outlet tubes.

Step 4: The inlet and outlet tubes made of mild steel having length of 150 mm were taken and welded with the two plates which would be connected for covering the muffler chamber.

Step 5: Two tubes of 100 mm length were welded on each baffles as shown in Figure 6.9.



Figure 6.9. Baffle plates with tubes

Step 6: All the baffles were next welded according to its respective position and also the inlet and outlet baffles were properly welded and final welded muffler is shown in Figure 6.10.

The complete fabricated model with the steps followed were shown in Figure 6.11 and 6.12 respectively.

Step 7: Non-destructive test for checking the manufacturing defects on muffler. Tap or coin test was performed on the muffler to know the defect on the points of welding of baffles and tubes.



Figure 6.10. (a) Mild steel sheet with the sheet cutting machine, (b) cutted rectangular sheet for muffler construction.



Figure 6.11. (a) Sheet in rolling machine, (b) rectangular sheet after rolling



Figure 6.12. Fabrication process of existing muffler with the baffles and tubes placed inside muffler

Experimental Setup

Different researchers have used different experimental set up for evaluating the acoustic performance parameters. Few researchers have initially developed a low cost impedance tube set up for measuring the TL of muffler. From the literature review, it is found that over the years various industries are also manufacturing the commercial experimental set up for measuring the acoustic performance parameter of the muffler [86], [214]–[219]. In this work, transmission loss would be experimentally calculated for all the mufflers using an impedance tube set up.

Impedance tube set up: The impedance tube is used for measuring the acoustic properties such as absorption coefficient, impedance of perforation and transmission loss of material and mufflers. The construction of Commercial impedance is complex and is very costly. Initially our task is to construct a low-cost impedance tube set up according to our designed muffler. From the work done by different researchers, it is found that in our work for determining the acoustic parameters, different impedance tube set up should be constructed. One setup should be constructed by considering the effect of mean flow and the other in absence of mean flow [214], [217].

Construction of test set up: The complete test set up consists of the following components.

1. Signal generator
2. Power amplifier
3. Speaker
4. Multichannel signal analyzer
5. Acoustic element
6. USB data acquisition system.

Practical considerations for designing impedance measuring tube

These considerations are taken according to American Standard for measurement i.e. ASTM E1050 and ISO 10534-2. Figure 6.13 shows a schematic diagram of an impedance tube and Table 6.1 and 6.2 gives the various design criteria of the impedance tube and microphones [220].

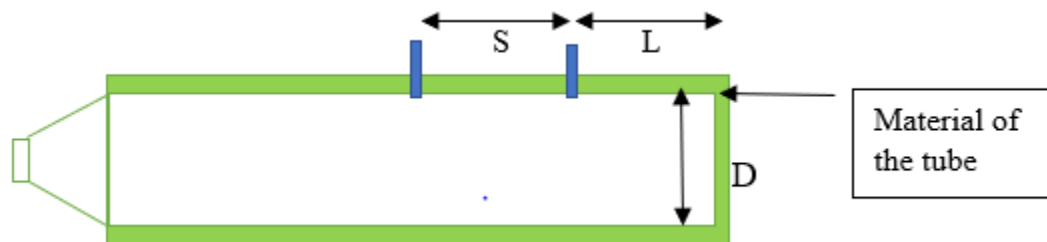


Figure 6.13. Schematic diagram of impedance tube with microphone holders

1. Material of the tube:

1. Tube should be heavy i.e. thickness of wall should be heavy, high weight. Because of heavy weight outside noise doesn't come inside.

2. Damping of material should be high. High frequency will produce high excitation of vibration, so materials used should have high damping.
2. Microphone Distance (Value of S)
 - S should be greater than 1% of the wavelength (λ) for lower frequency limit (f_l).
 - S should be lower than 80% of the wavelength for upper frequency limit (f_u).
3. Diameter of the tube(D):
 - Diameter of tube is calculated by
$$f_u < 0.586c_0/D$$
4. Space between microphone and speaker
 - Length between microphone M_1 and speaker should be more than $3D$.

Table 6.1.Criteria's used for selecting muffler testing parameters

S.No	Particular	Formula used
1	Selection of Operating frequency range (f)	$f_l < f < f_u$ The signal processing system's precision sets a limit on the tube's ability to operate at lower frequencies, f_l and the tube's maximum operating frequency is f_u
2	f_u upper working frequency	$f_u = 1.84c_o / \pi D$ D is the diameter of the tube, If “f” is below “ f_u ”.
3	Spacing between microphones	It is recommended to choose as following: $S = 0.45c_o / f_u$ where, S is the spacing between microphones
4	The lower working frequency, f_l ,	$f_l = 0.01c_o / s$

Table 6.2.Recommended maximum frequency based on microphone diameters

Nominal Diameter (in.)	Diaphragm Diameter (mm)	Maximum frequency(Hz)
1”	22.70	3000
½”	12.20	5600
¼”	5.95	11500

Configuration of test set up: The impedance tube can be used for measuring the acoustic properties such as absorption coefficient, impedance of perforation and transmission loss of material and mufflers. The construction of Commercial impedance tube set up is complex and is very costly. Here Alfaacoustics's Impedance tube set up [221] was used for carrying out the experimentation. The set up composed of two impedance tubes, four-microphones, power amplifier, data acquisition system, a laptop with Alfa Acoustic Labview software for acquiring the data. The setup is constructed as per ASTM E2611[222], [223] and Figure 6.14 – 6.18 represents its various components.



Figure 6.14. (a) Alfaacoustics Power Amplifier, (b) Alfaacoustics Four-channel Data Acquisition System



Figure 6.15. GRAS 1/4" pressure field microphones

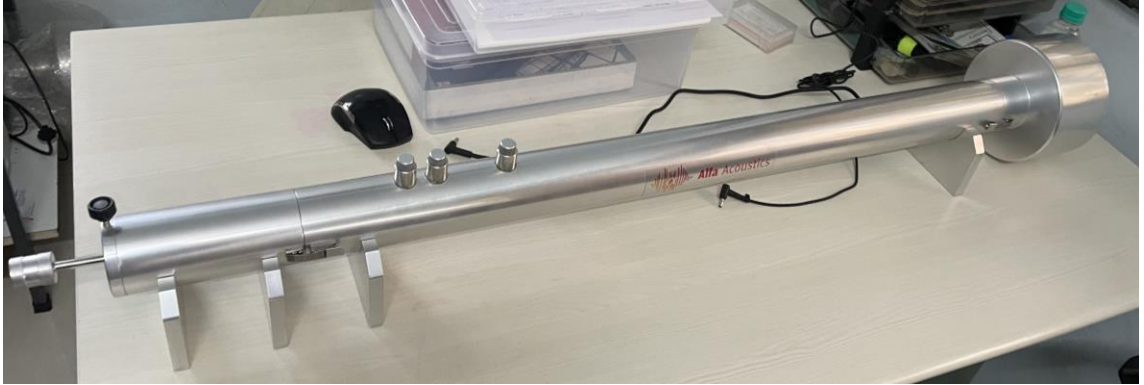


Figure 6.16. Alfaacoustics Impedance tube

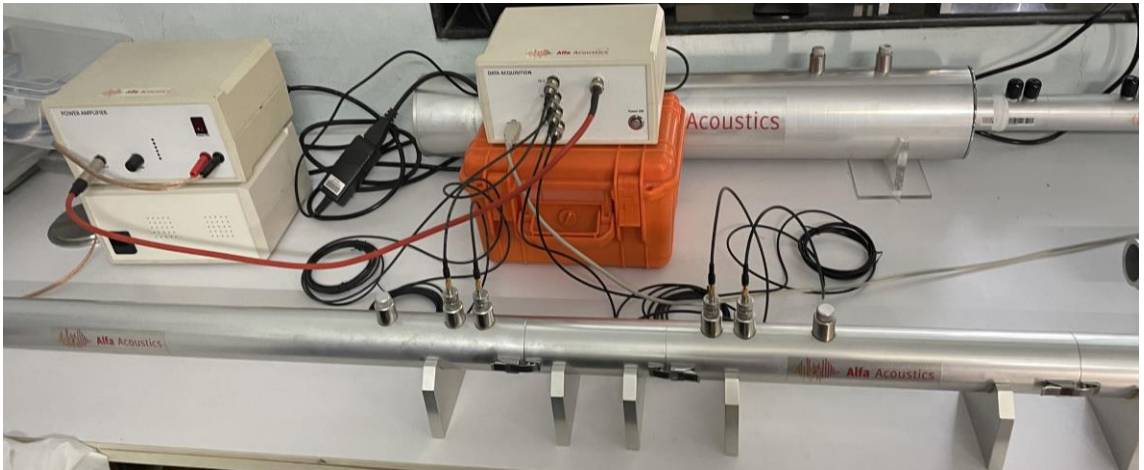


Figure 6.17. Two impedance tube with the DAQ and power amplifier connected for calibration

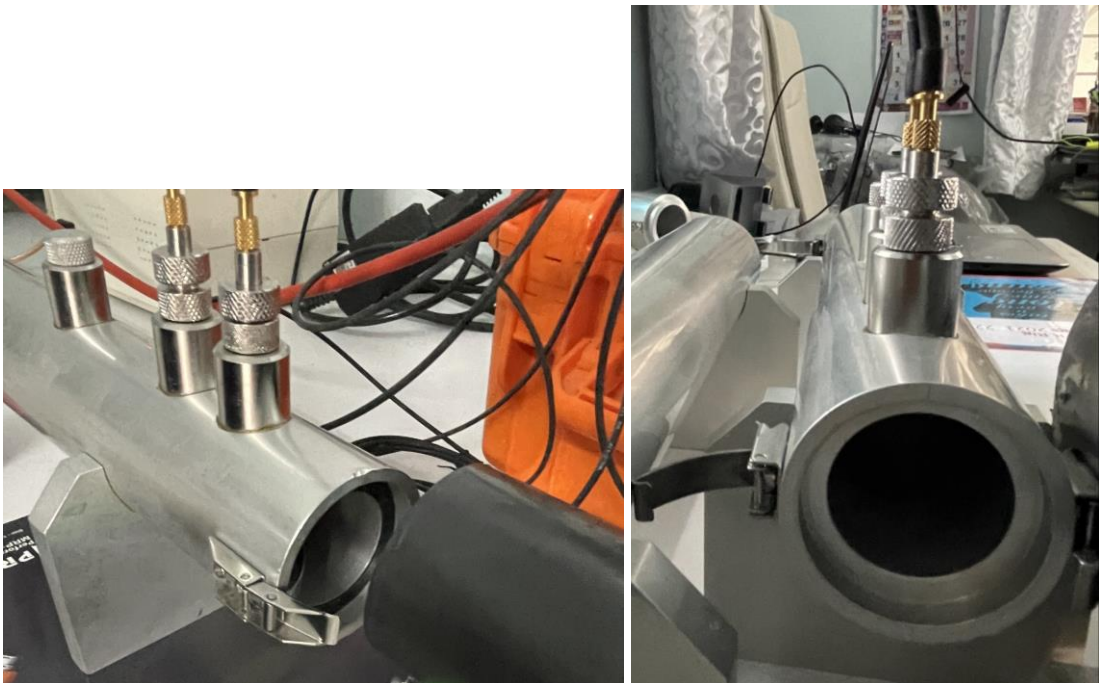


Figure 6.18. Inner view of the impedance tube.

Table 6.3. Details of Impedance tube setup

Impedance tube set	
Tube	Small
Internal Diameter (mm)	34.9
Sound absorption standards	ASTM E1050/ ISO 10534-2
Sound transmission loss standards	ASTM E2611
Frequency range	10 – 5000 Hz
Microphones	¼” pressure field, 4 numbers
Power Amplifier	40 Watts
Data Acquisition System	4 channel - 2 output
Loudspeaker	4” diameter, 15 Watts, 6 Ohm

The details of components and composition of the impedance tube set up is shown in table 6.3 and the parameters and condition taken for experimentation are shown in Figure 6.19.

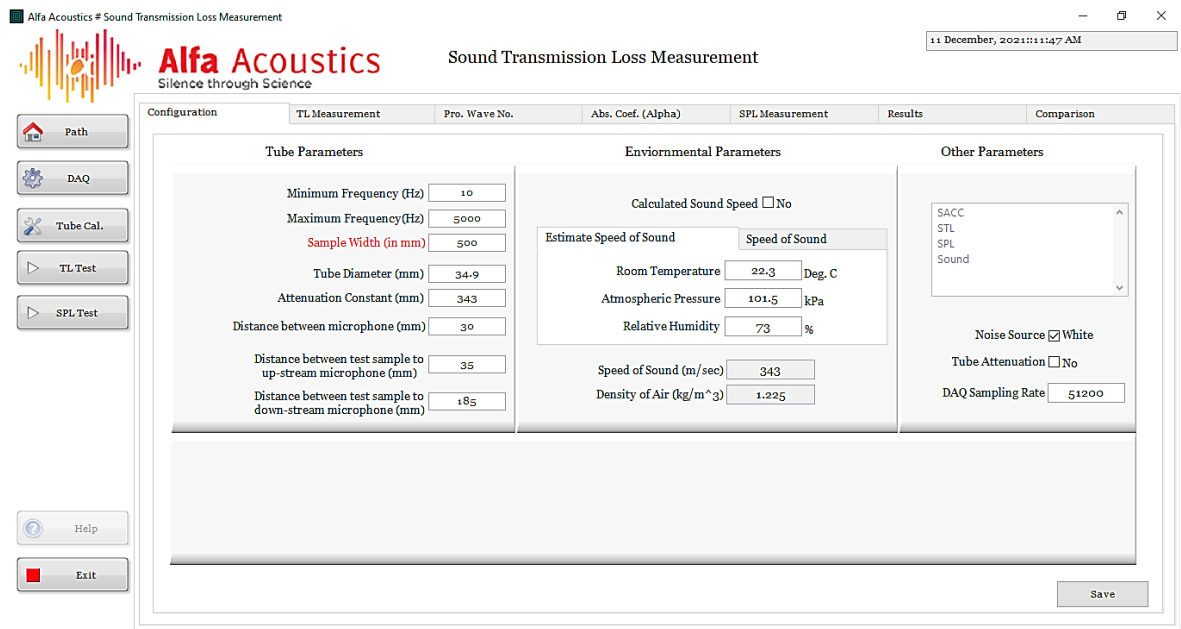


Figure 6.19. Parameters for experimentation

The experimental set up with the muffler attached is shown in below Figure 6.20.

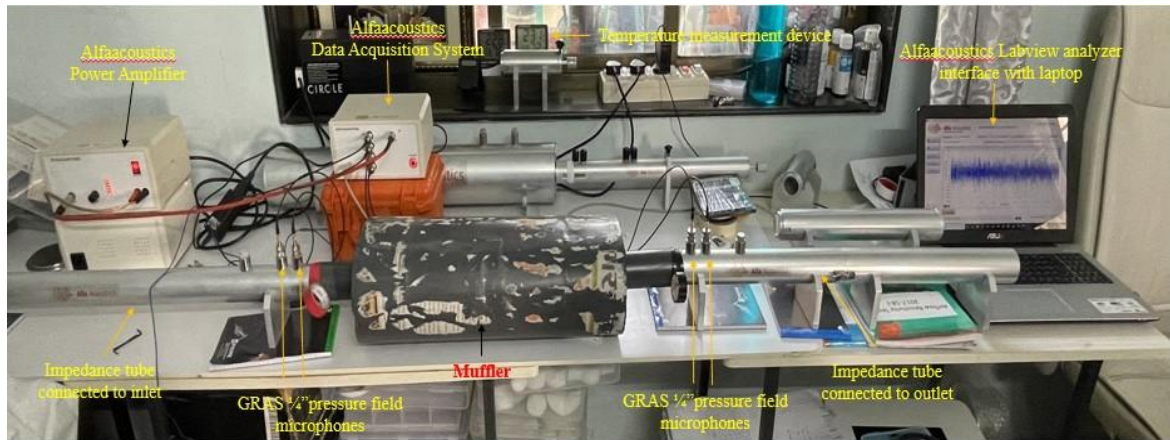


Figure 6.20. Experimental setup with muffler attached

6.3.2 Experimental Results

The Existing muffler is now tested in the impedance tube set up for entire range of frequencies ranging from 0 to 2000 Hz. During the experimentation, it is important to identify the uncertainty to obtain reliable and accurate results. The International Organization for Standardization (ISO) provides guidelines for estimating the uncertainty of measurement for different types of tests, including the measurement of transmission loss of mufflers. The specific standard that provides guidance on measurement uncertainty for transmission loss of mufflers is ISO 3744:2010 "Acoustics - Determination of sound power levels of noise sources using sound pressure - Engineering methods for an essentially free field over a reflecting plane [224] ."

Section 10.3 of the standard provides guidance on estimating the uncertainty of measurement for transmission loss measurements of mufflers using the standing wave tube (SWT) method. The standard states that the uncertainty of measurement for transmission loss is typically in the range of ± 0.5 dB to ± 1 dB, but it can be higher or lower depending on the specific test conditions and other factors that can influence the measurement.

The transmission loss (TL) for the existing muffler is acquired through impedance tube set up. To know the accuracy of the experiment, the testing was performed three times and the transmission loss curve ultimately obtained and is shown in Figure 6.21.

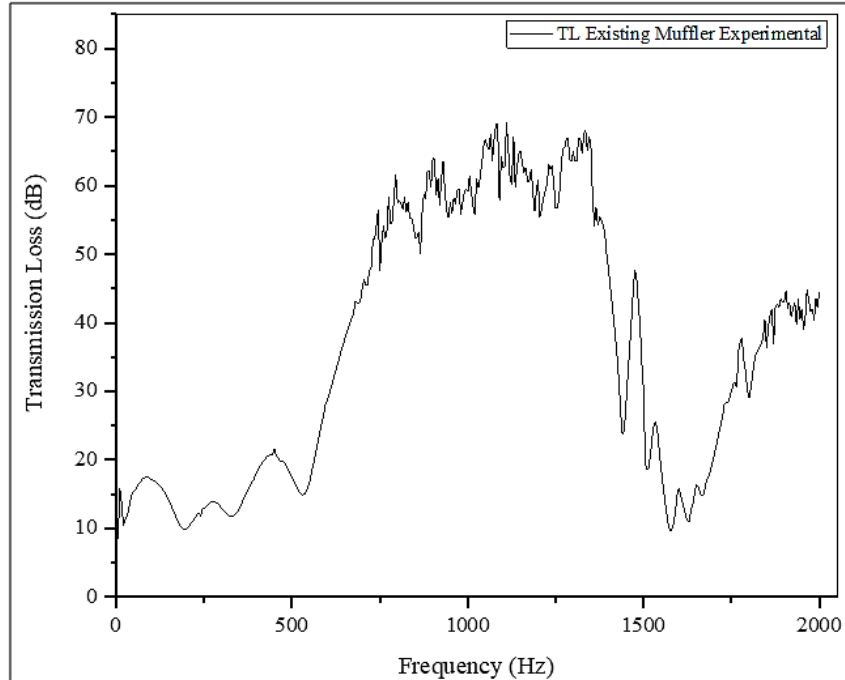


Figure 6.21. TL curve for existing reactive muffler through experimentation

Figure 6.21 depicts the variation of TL and it was observed that TL value is not much at low frequency but with the increase in frequency, there was a rise in TL value till 1400 Hz. But after this the TL value again decreased at high frequency and maximum TL obtained is about 69.26 dB at 1085 Hz.

6.3.3 Comparison of simulation and experimental results for existing muffler

The existing muffler was built in accordance with the schematic view in Figure 6.1, and Comsol Multiphysics pressure acoustic, frequency domain analysis was used to determine TL for various frequencies. Additionally, it was tested using an impedance tube configuration, and the outcome was compared to that of the simulation. These is depicted in Figure 6.22.

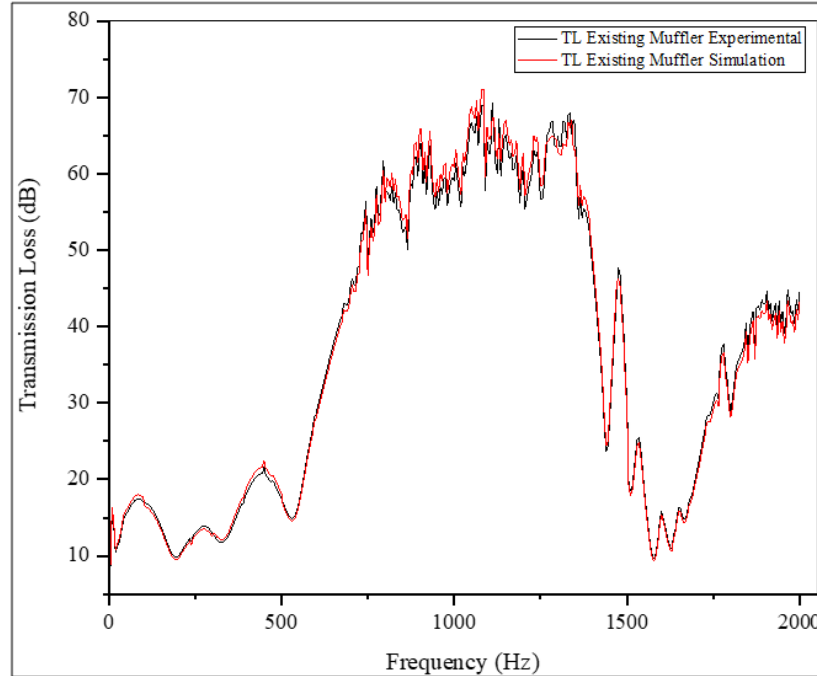


Figure 6.22. Comparison of TL obtained through simulation and experimentation for existing reactive muffler

With only roughly 2.5% of the maximum TL differing between the experimental and simulation results, the experimental result was in satisfactory correlation with the simulation result.

Limitation of the study

Muffler is installed in the exhaust system of vehicle and it should be installed within its designated space. Due to the space constraint, outer dimension of existing muffler should be kept fixed for a particular vehicle. For different vehicle, mufflers should be designed separately with respect to the volume of muffler fixed for particular engine. Further during the manufacturing process, it becomes very difficult to manufacture the muffler accurately as in the CAD software. The baffles, tubes all need to be welded together and it becomes difficult to provide a fine finish to this portion, as in machines also little bit tolerance is provided. This lead to a variation in the simulation and experimental results.

Future scope of the study

- Insertion loss which is one of the performance parameter of muffler could be calculated, which requires a practical environment for obtaining the sound level produced by exhaust system of vehicle.
- Designed a universal type muffler which could be used for either diesel engine or petrol engine vehicle for reducing the exhaust noise.

CHAPTER 7. OPTIMIZATION OF REACTIVE MUFFLER

In the current study for the purpose of optimization, an existing elliptical type muffler, as depicted in Figure 6.1 was taken into consideration. The previous section included the analysis of this muffler's aerodynamic and acoustic performance. Pilot experiments were first carried out to improve the acoustic performance of this four-chambered reactive muffler. Pilot experiments were done to determine the number of baffles with a single hole in each baffle in order to reduce the complexity of the construction. Following the determination of the total number of baffles, pilot tests were carried out to determine where to place the holes and where to place each baffle. One parameter was changed at a time while the other two corresponding parameters were kept fixed during the range selection of each parameter.

The next sections display the selection criteria and the outcome produced by Comsol Multiphysics software employing pressure acoustic frequency domain.

7.1 Criteria for selection of number of baffles

Previous study by a number of researchers shows that adding baffles to an expansion chamber significantly enhances the performance of a muffler [130], [225]. However, the length to lateral dimension ratio of a muffler was taken into consideration while deciding how many baffles to include [226], [227]. Three baffles were employed in the existing design, but before deciding on the final number, a pilot experiment was run on four cases: no baffle, one baffle, two baffles, and three baffles. The existing muffler's external geometry was maintained during study, and all of the baffles were positioned at equal intervals with holes in the center. All four cases underwent pressure acoustic frequency domain analysis, and TL was determined at various frequencies. Figure 7.1 provides a graphical representation of the results.

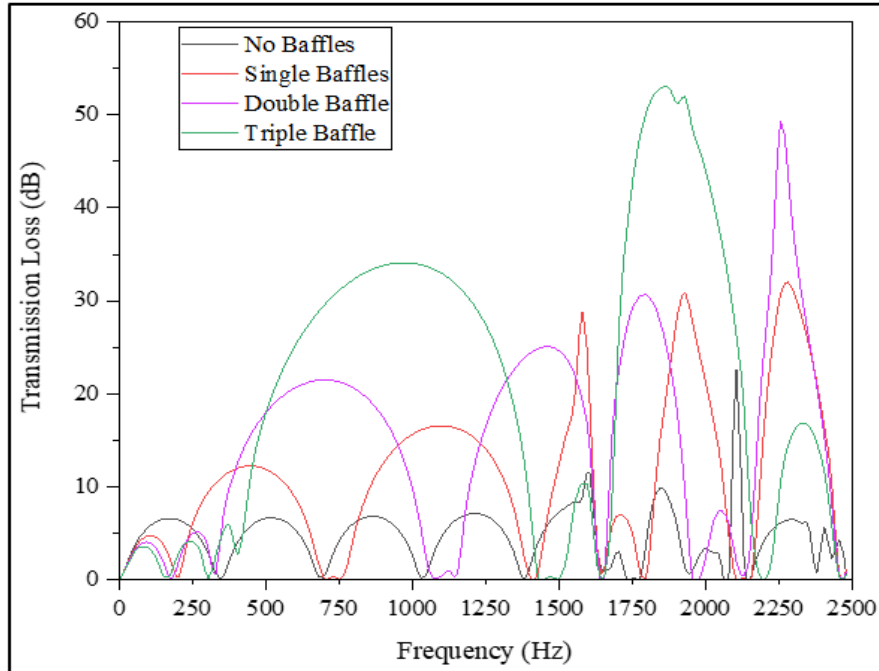


Figure 7.1. Assessment of TL curve for muffler with rise in number of baffles

The graph shows that for a straightforward expansion chamber without baffles, domes with the same frequency bands were made, with about the same degree of TL for each dome. In comparison to the case with no baffle, a second dome's TL significantly increased with the addition of one baffle, and the frequency spectrum also widened. This increase in transmission loss is due to the attenuation of sound energy as it passes through a medium. This attenuation is caused by scattering, which occurs because the sound waves encounters small obstacles or irregularities in the medium due to the baffles, causing them to change direction. Similarly, from the third dome onward, a considerable rise in the TL and widening of the frequency range were seen when two baffles were introduced. Later, with the addition of three baffles, the point of amplitude and frequency band increase migrated to the fourth dome. At higher frequencies, the larger domes produced by many baffles nearly completely cover the smaller domes produced by a straightforward expansion chamber. When the first crossover was noticed from the single baffle muffler at 250 Hz frequency, the TL performance was unquestionably greater for a simple expansion chamber. Due to their low sound pressure levels and typical origin in primary firing frequencies, the lower frequencies can be avoided from a design standpoint. Up until the three baffle muffler TL line crossed it over at 500 Hz frequency, the two baffle muffler's TL line was crossing over the single baffle muffler's TL line at 380 Hz and performing

better in terms of TL. Each of these four cases was shown to have a distinct frequency range where their TL performance was superior to that of other cases. As a result, it is not advisable to considerably reduce the number of baffles from the initial design. Keeping into this factor, the final design must take into account two baffles. Another factor in the decision to choose a two-baffle muffler over a three-baffle muffler was that it was shown to function better in the frequency ranges of 0-500 Hz and 1320-1705 Hz.

7.2 Range selection for hole position and baffles position

The simple expansion chamber's two finalized baffles were then used to do a pressure acoustic frequency domain study by moving the hole. The baffles were drilled with holes that were evenly separated from the center and in the opposite direction, starting from the center position and increasing by 5 mm up to a maximum of 60 mm.

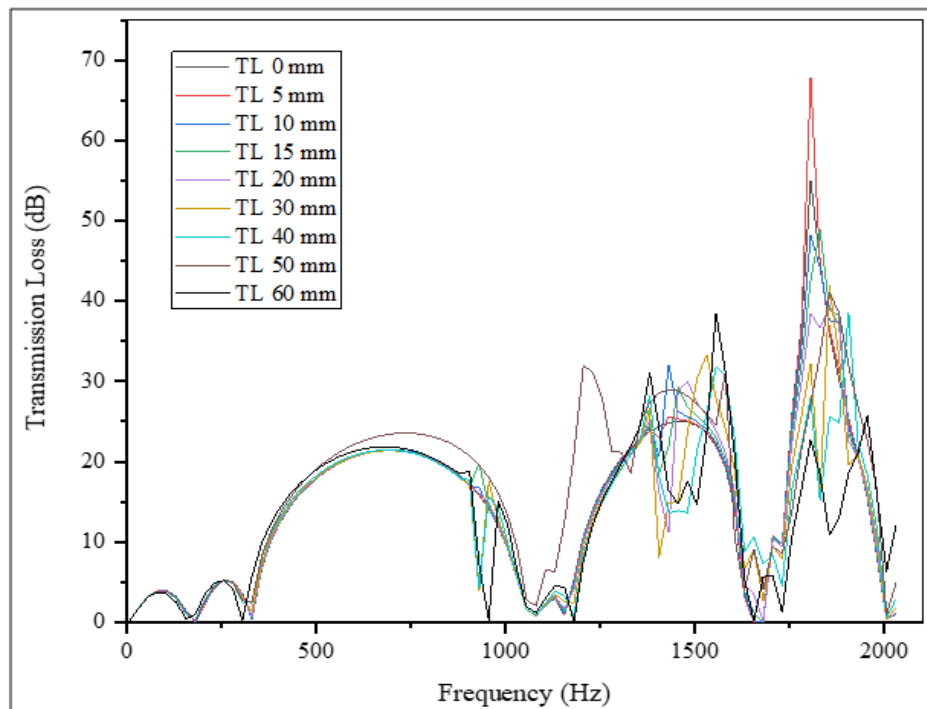


Figure 7.2. TL curve for double baffle muffler with variation in hole position

In Figure 7.2, graphs representing the transmission loss for each hole site were calculated and shown. At low frequencies, transmission loss did not vary greatly, but from medium to high frequencies, there was a noticeable increase in TL. At 1770 Hz frequency, a maximum transmission loss of about 70 dB was noted for a hole position 5 mm from the center axis. The two transmission loss values that came after the maximum were 55 dB and

49 dB, respectively, at the center and 10 mm from the center of the hole. Finally, the range of hole position is from center to 10 mm based on the highest transmission loss. The works conducted by various researchers are taken into consideration while choosing the ranges based on the maximum TL for the parameter. [80], [228]–[230].

Baffle position optimization

In this series of trials, the inlet tube's position was kept constant while the position of the baffle right next to it was altered. The first baffle was modified from 40 to 240 mm with increments of 10 mm, and the transmission loss results are shown in Figure 7.3 over the useful range of 130 mm to 240 mm. The findings of transmission loss for the effective range of 40 mm to 130 mm are shown in Figure 7.4. Next, the position of the second baffle next to the outlet tube was similarly changed in the range of 40 mm to 240 mm with increments of 10 mm.

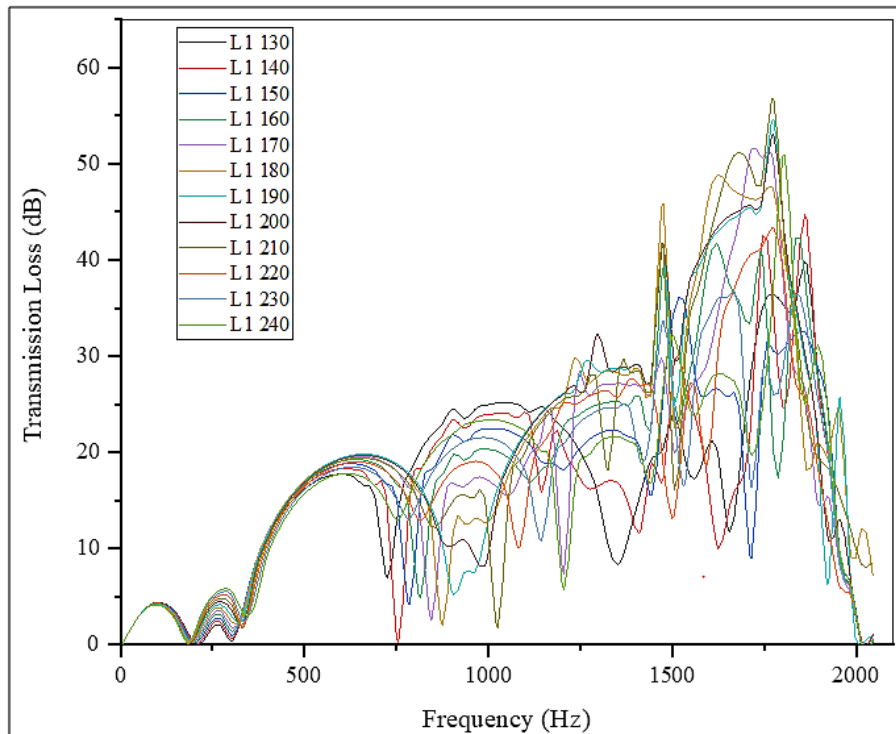


Figure 7.3. Pilot tests with deviation in position of baffle from inlet tube (L1)

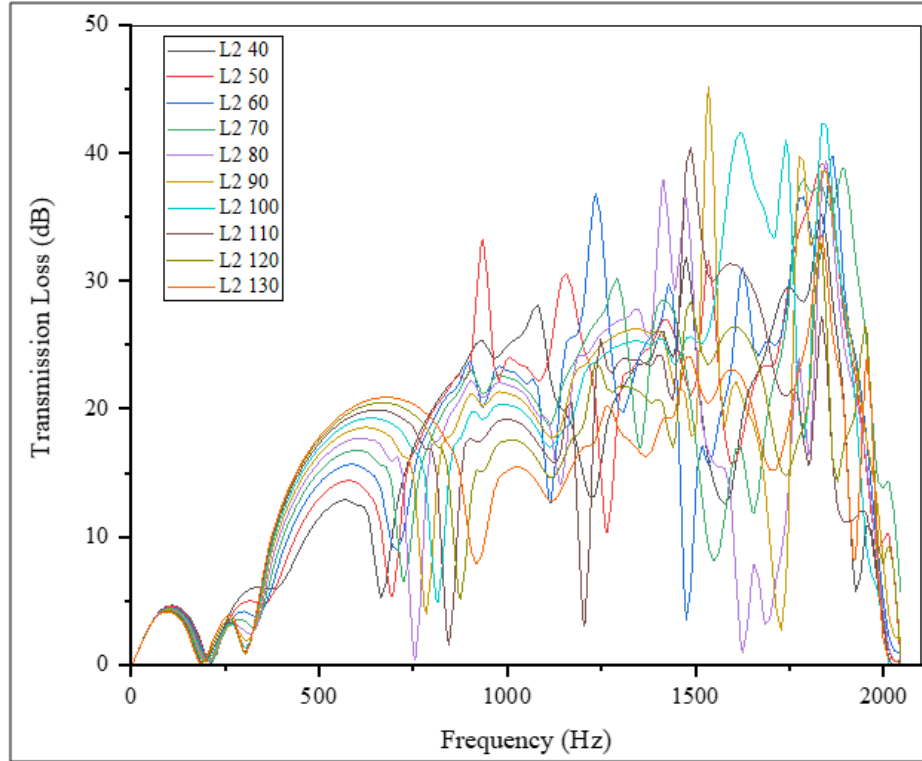


Figure 7.4. Pilot tests with deviation in position of baffle from outlet tube (L2)

For the lower frequency range, the transmission loss showed very little variation in relation to changes in the position of the baffle near the entrance tube. However, for the following placements of 210 mm, 190 mm, and 200 mm, the maximum transmission losses in higher frequency bands were observed to be 57 dB, 54.6 dB, and 53 dB, respectively. Similar to this, the maximum transmission loss was measured as 45.2 dB, 42.4 dB, and 39.2 dB for the respective positions of 90 mm, 100 mm, and 110 mm with respect to the position of the second baffle. In order to lessen the burden of transporting a large set of experiments, Taguchi-based DOE technique was used to determine the range of all three parameters based on the greatest transmission loss.

From Figure 7.3 and Figure 7.4 it was observed that changing baffle position towards the inlet tube provides better transmission loss value as compared to change in baffle position from the outlet tube. The position of the baffle relative to the inlet tube can influence the interaction of sound waves within the muffler. If the baffle is positioned optimally in the inlet section, it can help create phase cancellations and reflections that effectively interfere with and attenuate certain frequency components of the sound waves. This will ultimately slow down the turbulence. If the length of chamber increases i.e. if L1

increases than L2 decreases and vice versa. This increase in L1 will decrease the length L2 and will achieve maximum transmission loss. Whereas if we increase in L2, L1 will decrease by an affecting the value of transmission loss. Adjusting the baffle position from the inlet allows for tuning the device to target specific frequency bands more effectively, resulting in improved transmission loss for those frequencies. Properly positioning the baffle within the inlet can help achieve better acoustic impedance matching between the incoming sound waves and the internal structure of the muffler and also slow down turbulence. By keeping this in mind the displacement of baffle from inlet (L1) is increased to higher amount as compared to displacement of baffle for outlet (L2).

7.3 Application of Taguchi approach

To lessen the difficulty of conducting numerous trials while optimizing the muffler, the Taguchi-based design of experiment (DOE) technique was used. Three parameters with three levels of variation were subjected to the taguchi DOE technique, which resulted in a reduction of the number of tests to nine. Pilot tests were used to determine the level fluctuation in the previous sections. Table 7.1 displays all components and levels of variation in their entirety. The L9 orthogonal array matrix, which was built to specify the nine trial experiments that must be conducted, is displayed in Table 7.2.

Table 7.1. Control parameters and levels

FACTORS/LEVELS	A	B	C
L1 (Position of baffle from inlet tube)	190	200	210
L2 (Position of baffle from outlet tube)	90	100	110
HP (Hole position from center of baffle)	0	5	10

Table 7.2.L9 orthogonal array matrix

S.No	L1	L2	HP
1	190	90	0
2	190	100	5
3	190	110	10
4	200	90	5
5	200	100	10
6	200	110	0
7	210	90	10
8	210	100	0
9	210	110	5

7.3.1 Aerodynamic Performance analysis of the trial experiments

The aerodynamic performance analysis is performed on the nine trial experiments as represented in table 7.2. Pressure drop or backpressure is the main aerodynamic performance parameter. This analysis were performed in ANSYS Workbench software using the fluent module. During this analysis, pressure based solver is considered and the velocity inlet of 40 m/s and pressure outlet of 0 are considered as the boundary conditions and the material properties considered are shown in Table 7.3. Using these conditions, the pressure variation, velocity variation and the pressure drop for all the trials were obtained as shown in this section.

Table 7.3. Material Properties

Material	Density (kg/m ³)	Specific heat (J/[kg*k])	Thermal conductivity (W/[m*k])
Steel	7900	500	16.27
Air	1.2256	1005	0.02975

Pressure variation and Velocity variation in trial experiments

Using the velocity inlet boundary condition of 40 m/s, the pressure and velocity variation inside the muffler was obtained. It was observed that pressure is maximum in the first chamber but as it passes through the tube in first chamber the pressure decreases with the increase in velocity in that section. The pressure further decrease in the second chamber and ultimately reaches to minimum pressure towards the outlet section of the muffler. Whereas the velocity increased more in the tube joining the second and third chamber. In

each of the cases, same behavior was observed with variation in magnitude of pressure and velocity. Ultimately, the amount of pressure drop from inlet section to outlet section was observed and it signifies the most effective muffler for reduction of maximum amount of noise. Figure (7.5 – 7.13) shows the pressure contour and velocity contour obtained for all the nine trial experiments.

Trial 1: L1 = 190, L2 = 90, HP = 0.

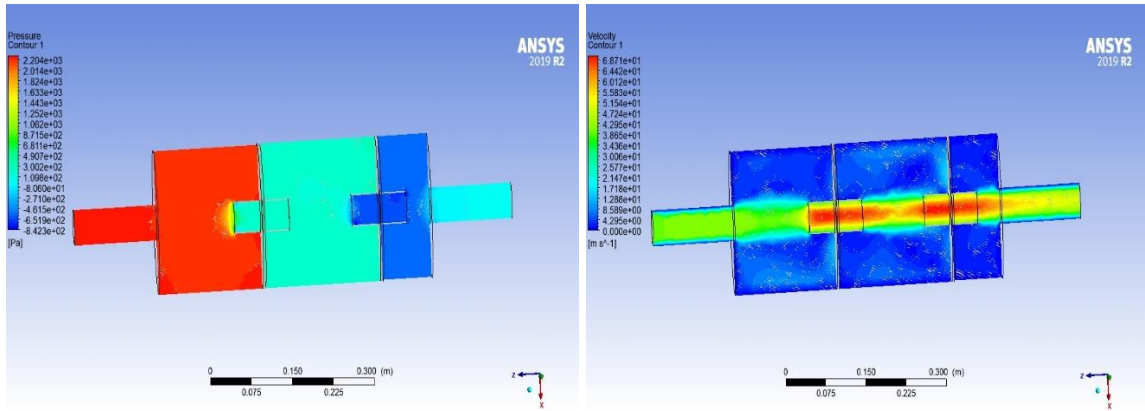


Figure 7.5. Pressure and velocity contour for trial experiment 1

The maximum and minimum pressure was observed to be 2.204 kPa and -0.08 kPa respectively and the maximum velocity is 68.71 m/s as found in Figure 7.5.

Trial 2: L1 = 190, L2 = 100, HP = 5

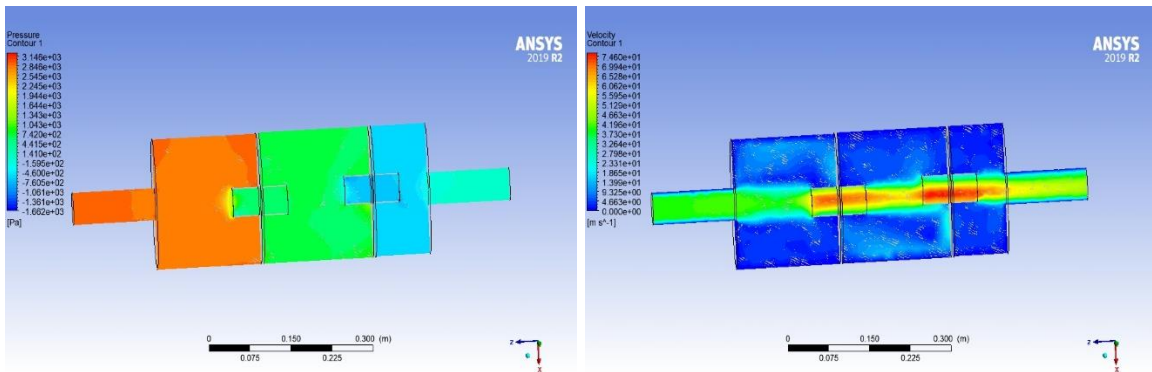


Figure 7.6. Pressure and velocity contour for trial experiment 2

The maximum and minimum pressure was observed to be 3.416 kPa and -0.00166 kPa respectively and the maximum velocity is 74.6 m/s as found in Figure 7.6.

Trial 3: L1 = 190, L2 = 110, HP = 10

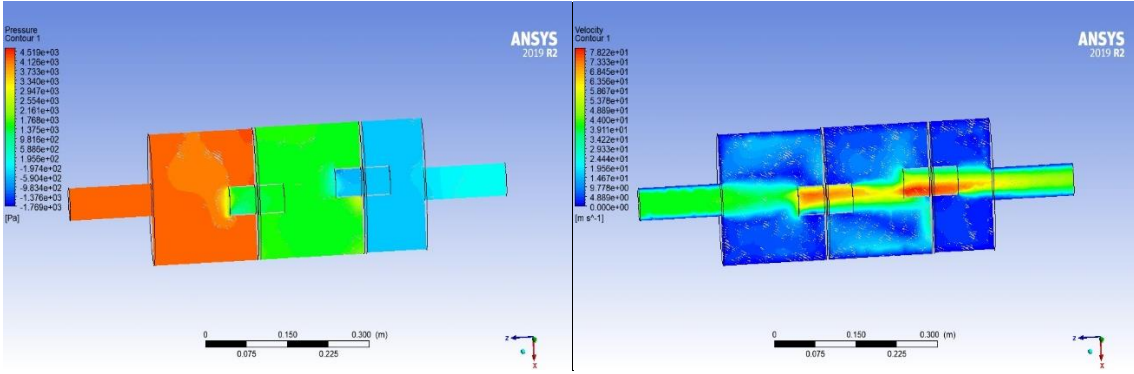


Figure 7.7. Pressure and velocity contour for trial experiment 3

The maximum and minimum pressure was observed to be 4.519 kPa and -0.00177 kPa respectively and the maximum velocity is 78.22 m/s as found in Figure 7.7.

Trial 4: L1 = 200, L2 = 90, HP = 5

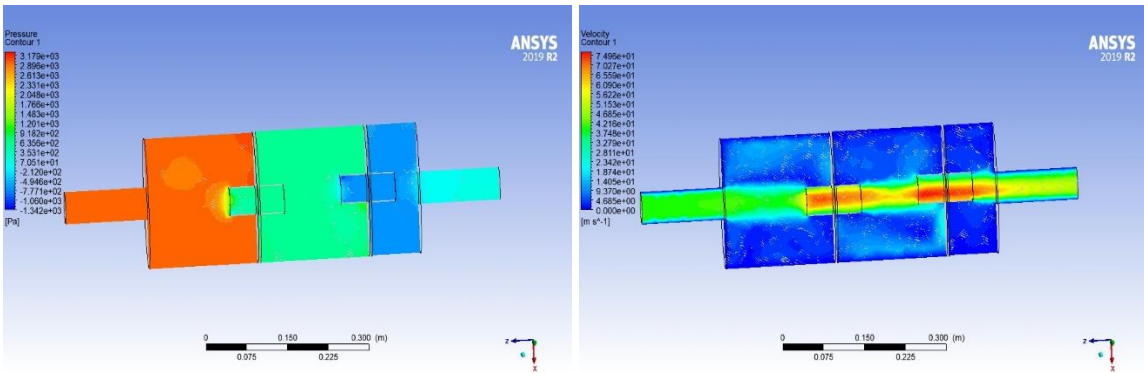


Figure 7.8. Pressure and velocity contour for trial experiment 4

The maximum and minimum pressure was observed to be 3.179 kPa and -0.00134 kPa respectively and the maximum velocity is 74.96 m/s as found in Figure 7.8.

Trial 5: L1 = 200, L2 = 100, HP = 10

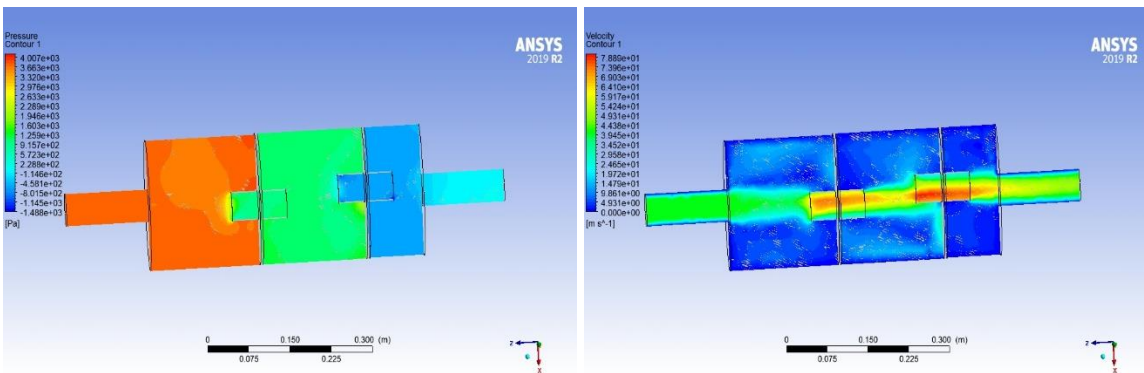


Figure 7.9. Pressure and velocity contour for trial experiment 5

The maximum and minimum pressure was observed to be 4.007 kPa and -0.00149 kPa respectively and the maximum velocity is 78.89 m/s as found in Figure 7.9.

Trial 6: L1 = 200, L2 = 110, HP = 0

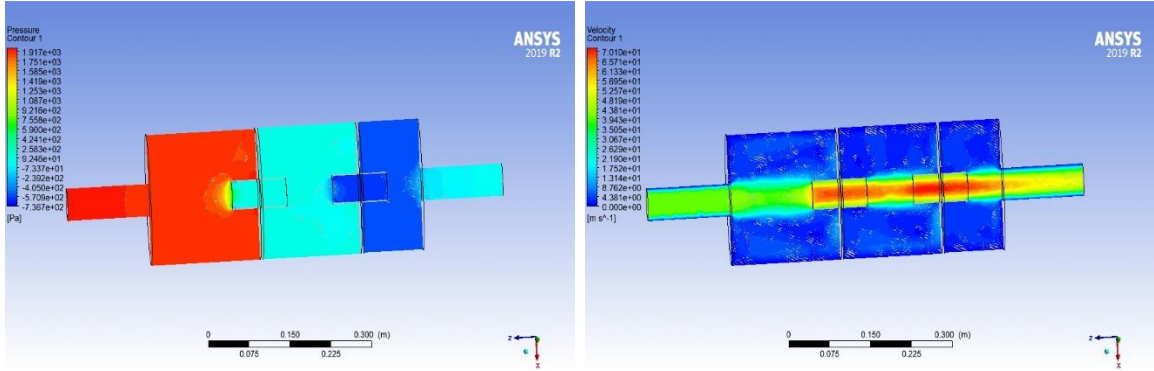


Figure 7.10. Pressure and velocity contour for trial experiment 6

The maximum and minimum pressure was observed to be 1.917 kPa and -0.0737 kPa respectively and the maximum velocity is 70.10 m/s as found in Figure 7.10.

Trial 7: L1 = 210, L2 = 90, HP = 10

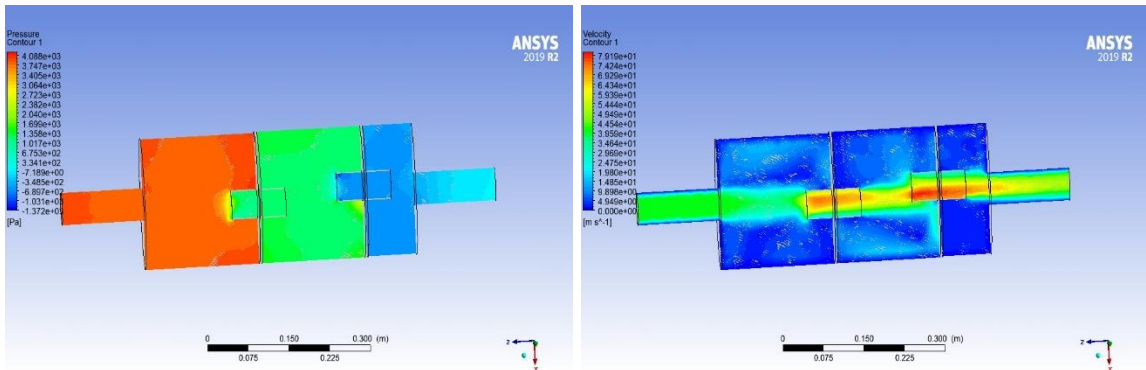


Figure 7.11. Pressure and velocity contour for trial experiment 7

The maximum and minimum pressure was observed to be 4.088 kPa and -0.00137 kPa respectively and the maximum velocity is 79.19 m/s as found in Figure 7.11.

Trial 8: L1 = 210, L2 = 100, HP = 0

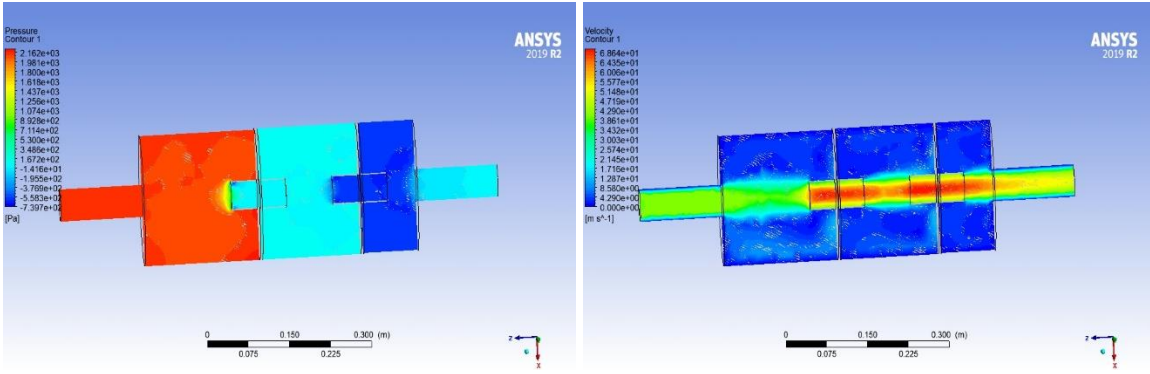


Figure 7.12. Pressure and velocity contour for trial experiment 8

The maximum and minimum pressure was observed to be 2.162 kPa and -0.074 kPa respectively and the maximum velocity is 68.64 m/s as found in Figure 7.12.

Trial 9: L1 = 210, L2 = 110, HP = 5

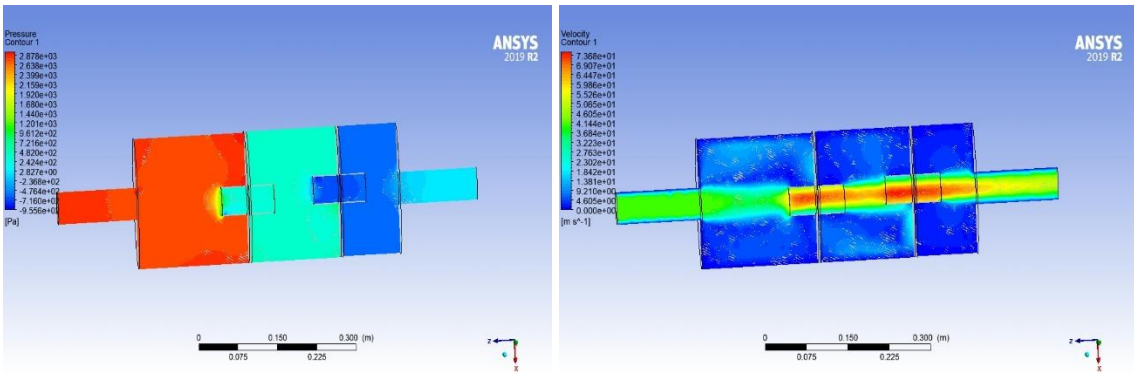


Figure 7.13 Pressure and velocity contour for trial experiment 9

The maximum and minimum pressure was observed to be 2.878 kPa and -0.096 kPa respectively and the maximum velocity is 73.68 m/s as found in Figure 7.13.

From the above analysis, the pressure drop for each of the cases and change in acoustic power level observed in each cases were determined as shown in table 7.4.

Table 7.4. Pressure drop and acoustic power level in trial experiment models

S. No. of trails	Pressure Drop (Pa)	Acoustic Power Level at inlet (dB)	Acoustic Power Level at outlet (dB)	Change in acoustic power level (dB)
Trial 1	2248.98	39.1712	66.96	27.79
Trial 2	2878.1	39.1417	71.79	32.65
Trial 3	4193.5	39.175	72.65	33.48
Trial 4	2966.98	39.175	71.510	32.335
Trial 5	3708.48	39.167	72.258	33.091
Trial 6	1948.89	39.171	69.23	30.059
Trial 7	3877.19	39.167	74.829	35.66
Trial 8	2159.06	39.1598	68.277	29.117
Trial 9	2826.89	39.158	71.761	32.603

From the above aerodynamic analysis table 7.4, it was observed that the muffler with dimension of L1= 190 mm, L2 = 110 mm and HP = 10 mm, i.e. trail 3 is producing the maximum pressure drop of 4.198 kPa and the change in acoustic pressure level is also maximum of about 33.48 dB. Thus, from aerodynamic performance analysis also, it was observed this muffler model is the best optimized reactive muffler.

7.3.2 Acoustic performance analysis of the trial experiments

The acoustic performance analysis is performed on the nine trial experiments as represented in table 7.2. Transmission loss is the main acoustic performance parameter, which was performed in COMSOL Multiphysics software using the pressure acoustic module. During this analysis pressure incident of 1 Pa was considered as the boundary conditions. The transmission loss curve for the nine trial experiments are shown in Figure 7.14. Whereas for reference one can refer the transmission loss curve of individual trial experiments in appendix under section 5. It was observed that not much variation was observed in TL values at low frequencies till 300 Hz. But afterwards the TL is increasing and maximum TL was observed at around 900 Hz. The TL value then keep on varying in an uneven manner for the higher frequencies as shown in Figure 7.14.

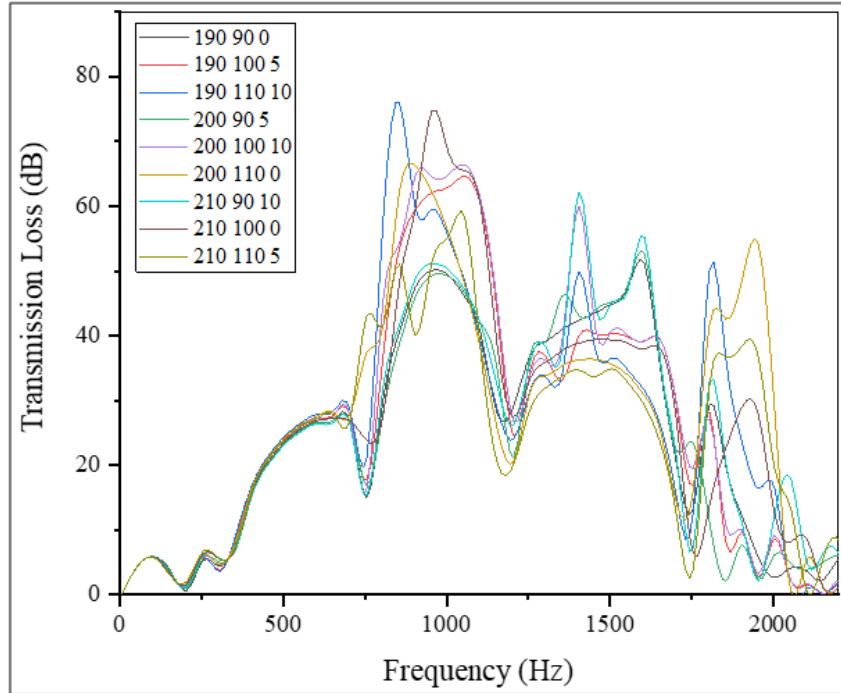


Figure 7.14. Comparison of TL for all trial experiments

7.3.3 Signal to noise ratio

Fluent and pressure acoustic frequency domain in ANSYS and Comsol Multiphysics, respectively, were used to determine the pressure drop and transmission loss for the chosen set of trials. The TL values obtained from the trial tests were then fed into the Minitab Programme, and S/N ratio was calculated, taking into account TL as the primary performance parameter of the muffler. Because higher transmission loss denotes stronger noise decrease capability of the muffler, "bigger the better" qualities were taken into consideration when computing the S/N ratio [168]. The mathematical result of the S/N ratio was shown in Eq. (64).

$$\eta = -10 \log \left[\left(\frac{1}{n} \right) * \Sigma \left(\frac{1}{y_i^2} \right) \right] \quad (64)$$

Where η = resultant S/N ratio, n = number of observations, y = respective responses.

The outcome of S/N ratio calculated through Minitab software and presented in table 7.5 and its plot was shown in Figure 7.15.

Table 7.5. L9 Taguchi Table with S/N ratio

S. No.	L1	L2	HP	TL	Sq.TL	S/N ratio	Mean
1	190	90	0	25.529	651.73	28.1407	25.529
2	190	100	5	26.131	682.83	28.3431	26.131
3	190	110	10	26.600	707.56	28.4976	26.600
4	200	90	5	25.459	648.16	28.1168	25.459
5	200	100	10	26.012	676.62	28.3035	26.012
6	200	110	0	26.376	695.69	28.4242	26.376
7	210	90	10	25.263	638.22	28.0497	25.263
8	210	100	0	25.718	661.42	28.2047	25.718
9	210	110	5	26.068	679.54	28.3222	26.068

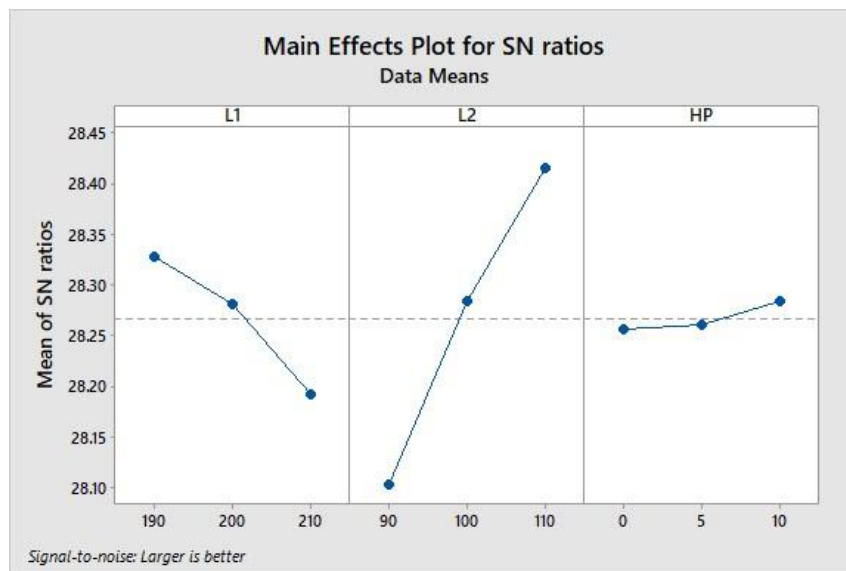


Figure 7.15. S/N ratio curve obtained through Minitab software

Figure 7.15's S/N ratio curve, which was derived using MINITAB, shows that S/N ratio values varied greatly for L1 and L2, whereas they varied little for HP. The L1 parameter's S/N ratios peaked at 190 mm, the L2 parameters at 110 mm, and the HP parameter's at 10 mm. The levels of 190 mm, 110 mm, and 10 mm for the parameters L1, L2, and HP were therefore regarded as the most ideal levels for creating the greatest TL value.

It was observed from S/N ratio curve that the peak value of S/N ratio was attained with reduced dimension of L1 and increased dimension of L2 value. As the dimension increases, the signal have to travel a longer distance or cross more complex paths. This lead to greater signal attenuation, i.e. the signal becomes weaker as it propagates through the medium. If

the noise level remains relatively constant, the weakened signal will result in a lower S/N ratio. Moreover signals scatter or diffuse due to interactions with obstacles with increase in dimension. This scattering can cause the signal to spread out and become less focused, making it more susceptible to noise interference and thus reduce the S/N ratio. Whereas adjusting the baffle position (L2) lead to specific acoustic reflections or focusing effects that concentrate the desired signal at the measurement points. This potentially lead to a more focused signal with less noise, leading to increase the S/N ratio.

ANOVA analysis is now perform to identify the importance and contribution of the parameters.

7.3.4 Analysis of variance

By taking into account the 95% confidence level or a probability value (p) less than 0.05 for the control parameters, the one-way ANOVA analysis was carried out to support the significance of the selected control parameters. The analysis was carried out using the Minitab Programme, and table 7.6 shows the outcomes.

Table 7.6. ANOVA values obtained through MINITAB

Source	DF	Seq SS	Adj SS	Adj MS	F	P
L1	2	0.028267	0.028267	0.014134	47.35	0.021
L2	2	0.147530	0.147530	0.073765	247.13	0.004
HP	2	0.001275	0.001275	0.000637	2.14	0.319
Residual Error	2	0.000597	0.000597	0.000298		
Total	8	0.177669				

Table 7.7. Calculation of percentage contribution from the variance analysis

S. No	Factors	Degree of freedom(DF)	Total Sum of squares	Mean Square variance	Percentage contribution(P)
1	L1	2	0.028267	0.014134	15.909922
2	L2	2	0.147530	0.073765	83.036433
3	HP	2	0.001275	0.000637	0.717626
	Residual Error	2	0.000597	0.000298	0.336018
	Total	8	0.177669		100

The results of the ANOVA study supported the conclusion that L1 and L2 were significant control factors, and table 7.7 lists their percentage contribution to the

performance of the muffler. L2 was shown to have a maximum contribution of 83.04% in TL for all the parameters, compared to L1's 15.91% and HP's 0.7%.

Figures 7.16 and 7.17 depict the final, optimized reactive muffler based on the findings of the simulation. Figure 7.18 also depicts the optimized reactive muffler's mesh model. The S/N ratio analysis and maximum transmission loss reported in table 7.5 were used as the foundation for determining the ideal settings. The condition's chosen final optimal parameters are L1=190 mm, L2=110 mm, and HP=10 mm. Figure 7.19 displays the outcomes of the pressure acoustic frequency domain study used to determine the entire set of TL for the chosen reactive muffler. At a frequency of 1090 Hz, the maximum TL for the chosen optimal muffler is achieved close to 73.33 dB.

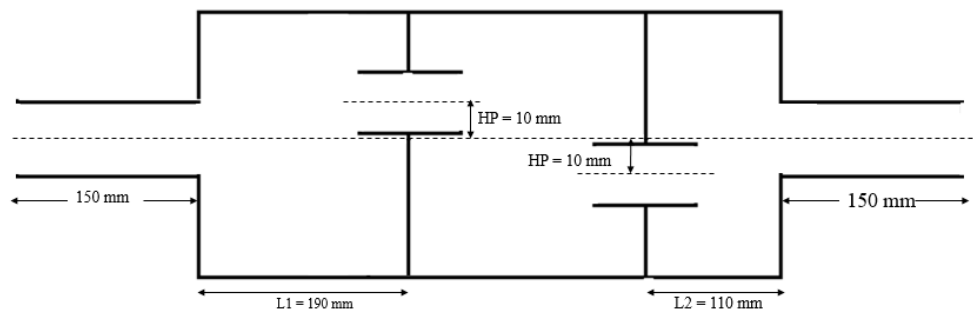


Figure. 7.16. Schematic view of the optimized reactive muffler

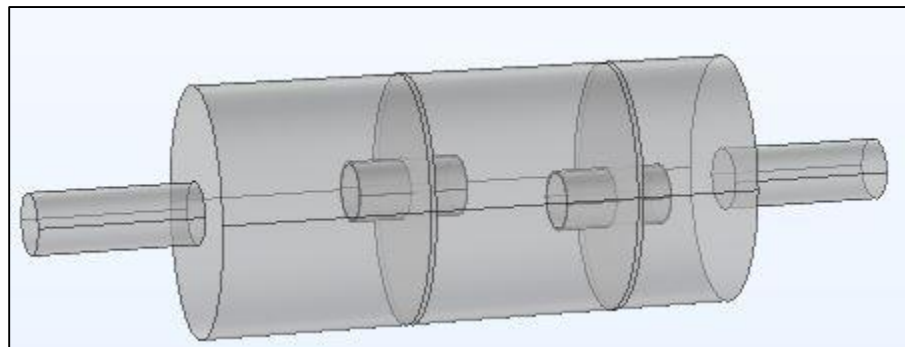


Figure 7.17. 3D view of the optimized reactive muffler in COMSOL

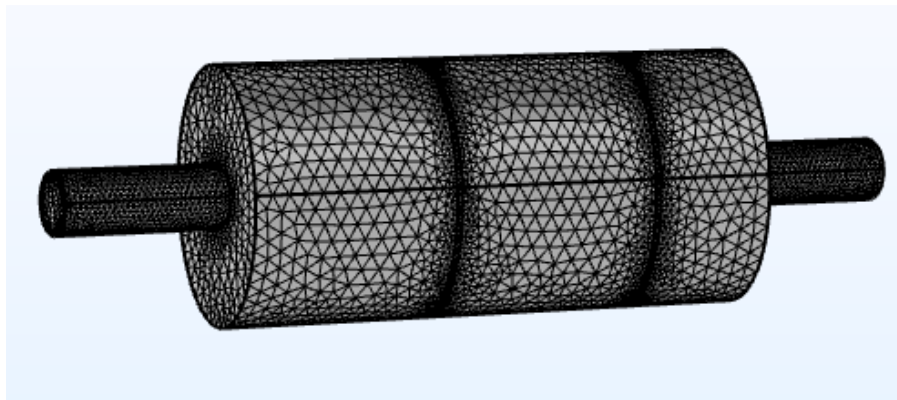


Figure 7.18. Mesh model of the optimized reactive muffler

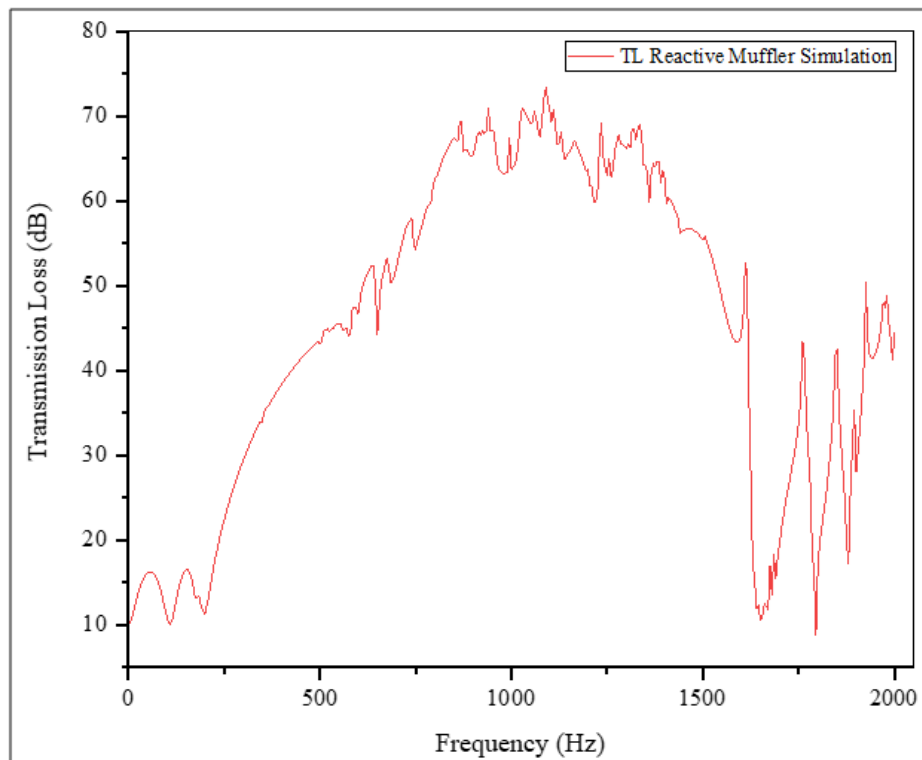


Figure 7.19. TL curve for optimized reactive muffler through simulation

7.4 Experimental validation of simulation results

In this section the experimental validation was carried out for the optimized reactive muffler selected on the basis of simulation results. The optimized reactive muffler were initially fabricated and then tested in Alfa acoustics impedance tube setup.

7.4.1 Fabrication of optimized reactive muffler and experimentation

The steps followed for the fabrication are mentioned in this section.

Step 1: A rectangular sheet of 2 mm thickness is cutted from a big sheet according to the dimension of the muffler i.e. 500 mm x 602 mm. The sheet is then rolled in the shape of the ellipse according to dimension of semi-major and semi-minor axis of 112 mm and 78 respectively in a roller machine and is welded.

Step 2: Four small rectangular plates of dimensions 240 mm x 170 mm were cutted from big sheet. These plates were taken for covering the ends of muffler chamber and for constructing the baffles.

Step 3: The four plates were first given the shape of the ellipse according to the dimension of the muffler chamber. Next a hole of 50 mm diameter is made on two plates which would be used as a baffle and hole were made on the other two plates according to the dimension of inlet and outlet tubes.

Step 4: The inlet and outlet tubes made of mild steel having length of 150 mm were taken and welded with the two plates which would be connected for covering the muffler chamber.

Step 5: Two tubes of 100 mm length were welded with the baffles.

Step 6: The two baffles were welded inside the muffler chamber. One at distance of 190 mm from left hand end of muffler chamber i.e. from the inlet section and the next at a distance of 110 mm from the right hand end of muffler i.e. from the outlet section.

Step 7: The plates with the inlet and outlet tube of muffler were welded with the muffler chamber.

The complete welded optimized reactive muffler is shown in Figure 7.20.

Step 8: Non-destructive test for checking the manufacturing defects on muffler. Tap or coin test was performed on the muffler to know the defect on the points of welding of baffles and tubes. Further leakage test was also performed to check the welding of the acoustic elements.



Figure 7.20. Baffles with tubes and muffer after welding all the components

Experimentation of Optimized reactive muffler

A four-microphone impedance tube, a power amplifier, a data gathering device, and a laptop running Alfa Acoustic Labview software made comprised the impedance tube setup, as illustrated in Figure 7.21. The setup for measuring TL was built in accordance with the ASTM E2611 standards and ISO 3744-2010 [224], which were covered in the previous section.

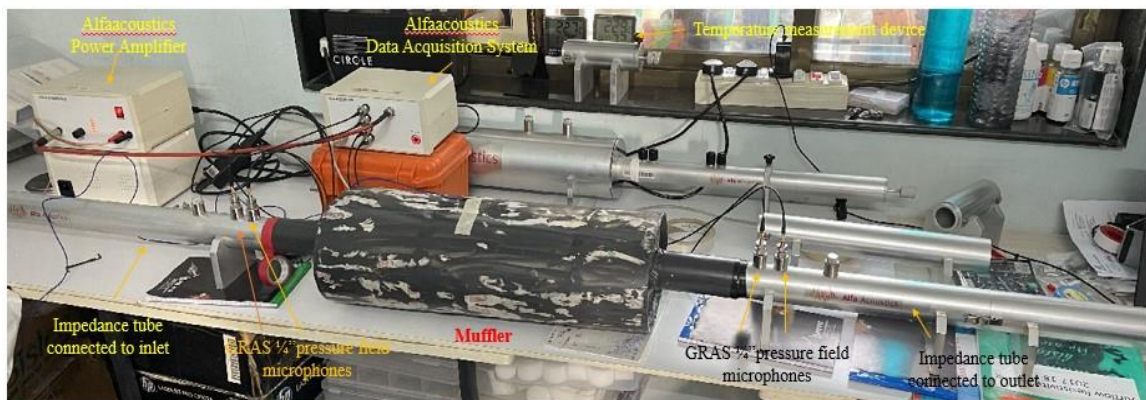


Figure 7.21. Experimental setup with optimized reactive muffler

7.4.2 Experimental Results

The experiment was performed three times on the same parameters to check the uncertainty and accuracy of the transmission loss of the muffler. Figure 7.22 displays the final experimental outcome for the optimized reactive muffler. The optimized reactive muffler was subjected to testing in order to determine the TL at various frequencies.

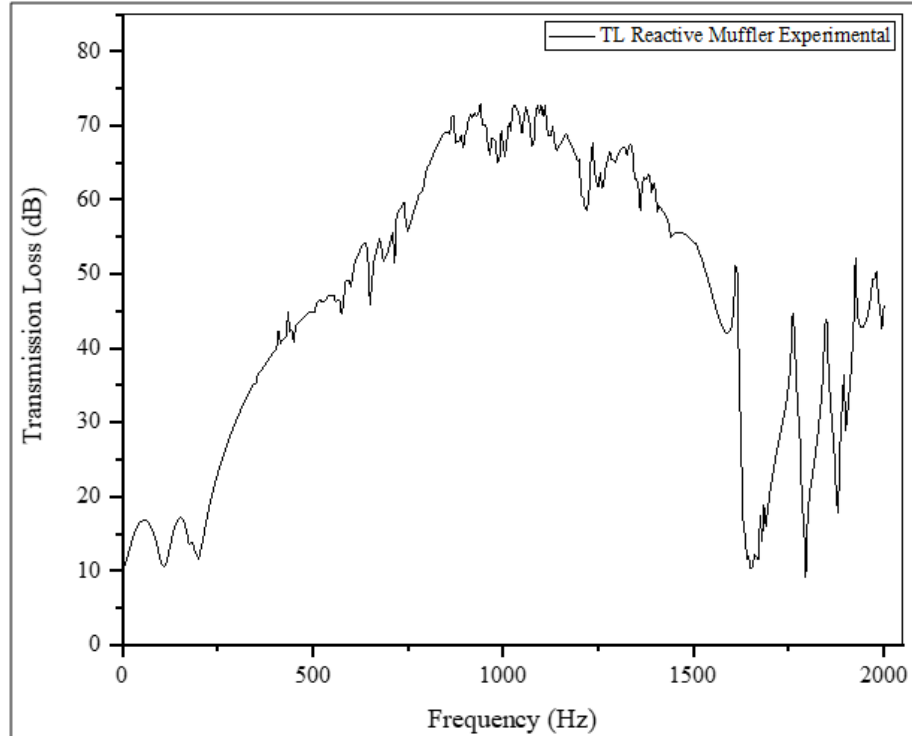


Figure 7.22. Transmission Loss curve obtained for optimized muffler through experimentation

The Transmission loss value was initially low at low frequencies, but with the increase in frequency the transmission loss value also increased and maximum transmission loss of 72.94 dB was achieved at 1090 Hz. This TL increased due to scattering, which occurs as the sound waves encounter small obstacles or irregularities in the medium due to baffles and tubes, causing them to change directions. Thus the reflection of the scattering waves, ultimately increases the TL of the muffler at that frequency.

7.4.3 Comparison of simulation and experimental result of reactive muffler

The outcomes of the experiment were then compared with those of the simulation, and both results demonstrated strong agreement, with the maximum TL showing variation of only around 0.5%, as seen in Figure 7.23.

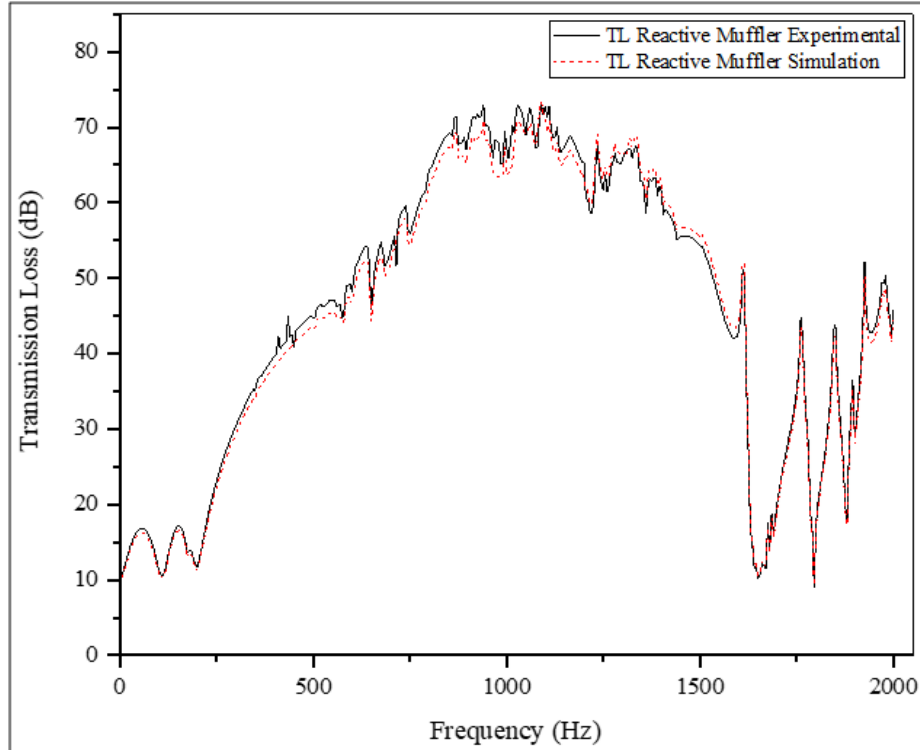


Figure 7.23. Comparison of TL obtained for optimized muffler through simulation and experimentation

7.5 Comparison of the existing muffler and the optimized reactive muffler

The optimized reactive muffler and the existing reactive muffler underwent simulation and experimental testing. Figure 7.24 (a) and (b) illustrate the simulation and experiment results for conventional and improved mufflers, respectively. In terms of maximum TL and frequency band widening, it can be seen that the transmission loss for the optimized reactive muffler was superior to the existing reactive muffler. For the purpose of comparing the maximum TL over three frequency bands, the numbers are shown in table 7.8. The results of the optimized muffler were superior to those of the current muffler in terms of maximum TL for all frequency bands. Additionally, it has been noted that the third dome of the optimized muffler widens in accordance with the outcomes of simulation and experimentation, fully enclosing the second, third, and fourth domes of the original muffler. The frequency range of the third dome for the optimum muffler was discovered to be between 200 and 1650 Hz. The maximum TL performance of the optimized muffler was found to be better, and the broadening of the third dome gave it an advantage over the conventional muffler in terms of performing better throughout a larger frequency range.

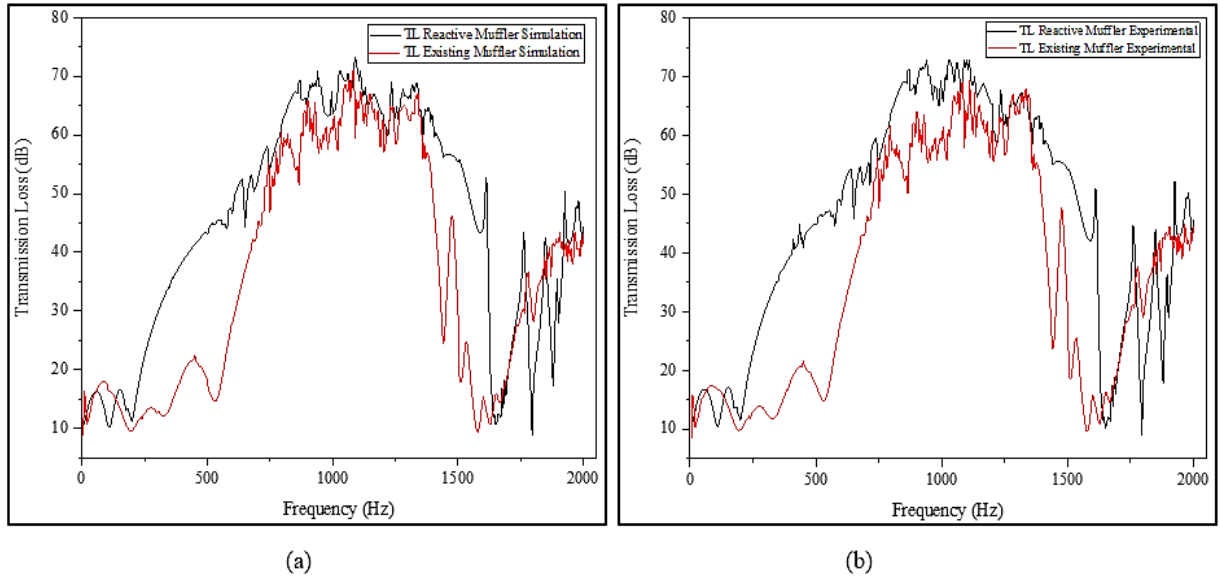


Figure 7.24. Comparison of TL for four chamber reactive muffler and optimized reactive muffler (a) through simulation (b) experimentation

Table 7.8. Transmission loss values at different frequency range

Frequency Ranges	Maximum Transmission Loss in dB			
	Existing muffler simulation	Optimized reactive muffler simulation	Existing muffler experiment	Optimized reactive muffler experiment
5 Hz -500 Hz	22.45	43.47	21.59	44.99
505 Hz – 1500 Hz	71.04	73.33	69.26	72.94
1505 Hz – 2000 Hz	43.48	55.24	44.82	53.63

CHAPTER 8. OPTIMIZATION OF HYBRID MUFFLER

A reactive and absorptive or dissipative muffler are combined to create a hybrid muffler, which combines the characteristics of the two types of mufflers. The chapter's optimized reactive muffler is now filled with a layer of sound-absorbing material, transforming it into a hybrid type of muffler as depicted in Figure 8.1 in this section. The thickness of the absorption layer in chambers 1, 2, and 3 are designated as A_1 , A_2 , and A_3 , correspondingly.

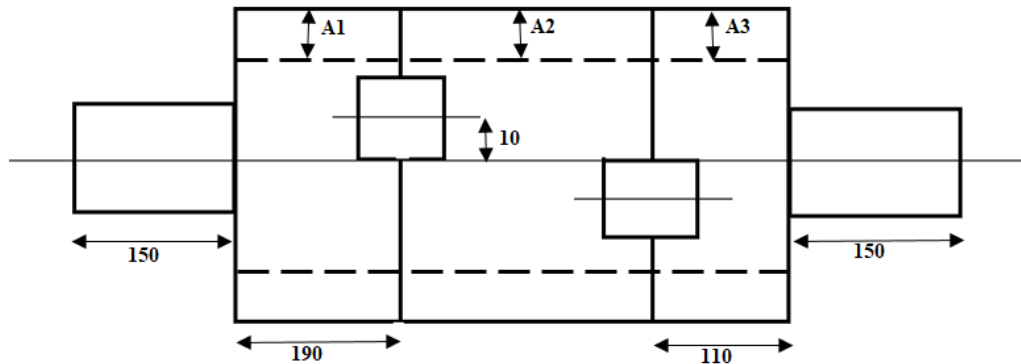


Figure 8.1. Combination of reactive muffler and sound absorption material

This part underwent optimization in order to provide an optimal layer of absorption material in each chamber, which would finally provide the hybrid muffler with its best performance. To choose the most appropriate absorption material in this technique, pilot experiments were first conducted on a variety of sound-absorbing materials. The range of absorption material in each chamber was then chosen through pilot experiments using pressure acoustic frequency domain analysis. One parameter was changed at a time while the other two corresponding parameters were kept fixed during the range selection of each parameter. The results are displayed in the parts that follow. After choosing the range of absorption material, DOE's Taguchi technique is used to create the optimal layer of absorption material in each chamber.

8.1 Variation of Sound absorption material

To find the best sound absorption material in terms of maximum transmission loss value, many types of sound absorption materials are used inside a basic expansion muffler. According to earlier studies by several academics, Glasswool, Rockwool, and glass fibres were among the most often used materials inside the muffler. Different grades of

glasswool, rockwool, polyester, and melamine were employed inside the muffler for this study, and pressure acoustic frequency domain analysis was used to determine the TL. Table 8.1 lists the various classes of these materials along with their characteristics, and Figure 8.2 displays the TL determined in each case.

Table 8.1. Sound absorption materials with its properties

Material	Flow Resistivity (Pa.s/m ²)	Density (kg/m ³)
Glasswool TP 1	5000	13
Glasswool Acoustic guard	5800	14
Glasswool SSP1	11000	20
Glasswool 701	14000	24
Glasswool Fire & Sound guard	20000	40
Rockwool KR S	9500	32
Rockwool KR SK	10300	40
Rockwool KR L	13800	50
Rockwool KR M	14400	60
Polyester Isobond WLG 040	5000	20
Polyester Isobond WLG 035	10000	40
Melamine	12000	9

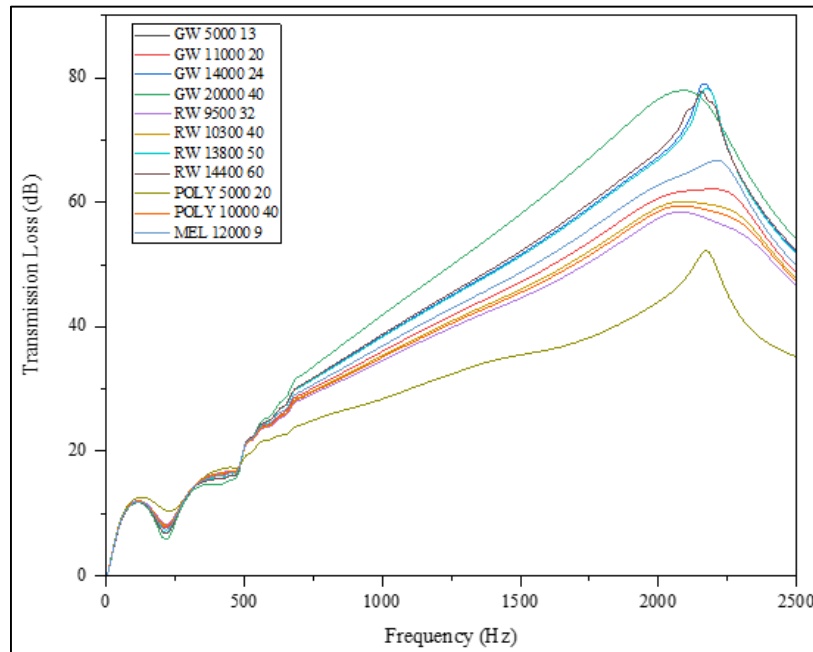


Figure 8.2. TL curve for the muffler using various sound absorption materials

The transmission loss values provided in Figure 8.2 showed that the highest transmission loss was 78.92 dB while using Glasswool 701 grade with flow resistivity of 14000 Pa.s/m²

and density of 24 kg/m^3 within the simple expansion chamber. In the muffler, it can therefore be utilized as an absorption layer.

8.2 Optimization of absorption layer thickness in chambers

The layers in each chamber of the reactive muffler that had been optimized were taken into account as the control parameters for the hybrid muffler's optimization. Through the use of pressure acoustic frequency domain analysis, pilot tests were used to define the range or amounts of these control parameters for the investigation. During the pilot studies, glasswool with a flow resistivity of $14000 \text{ Pa} \cdot \text{s/m}^2$ and a density of 24 kg/m^3 was used as the absorption medium inside the muffler. Pilot tests were first conducted with an absorption material thickness in the first chamber that ranged from 5 mm to 50 mm with a 5 mm step size.

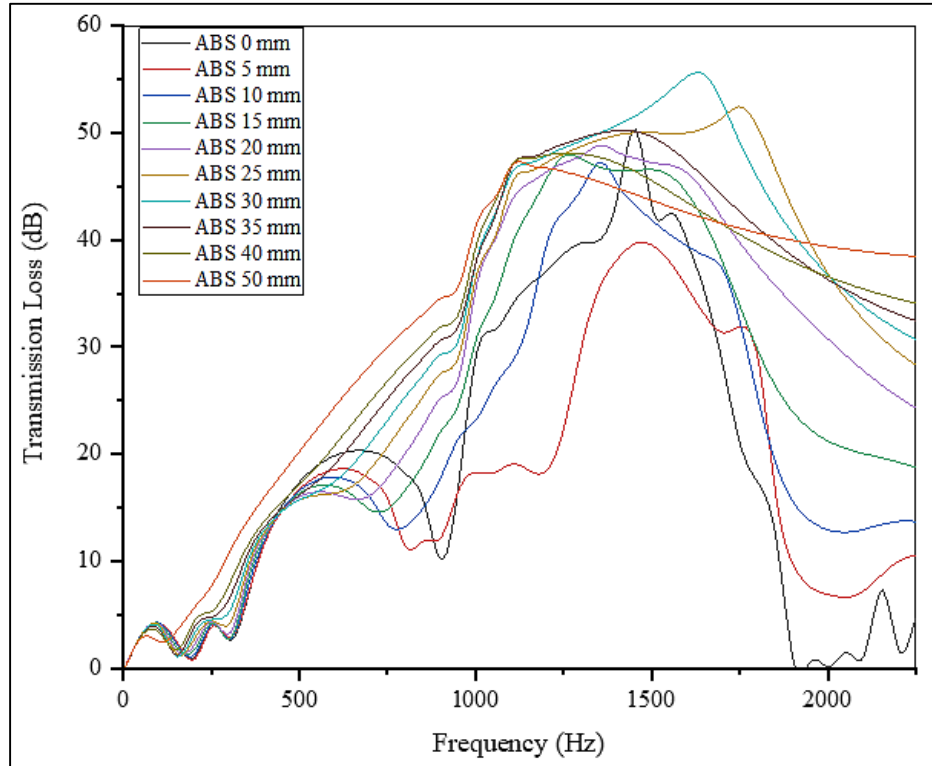


Figure 8.3. TL curve on variation of absorption material layer thickness in first chamber

The transmission loss curve in Figure 8.3 showed that the muffler's TL value grew as the thickness of the absorption material increased, reaching a maximum TL of 56 dB at 30 mm thickness. However, once the thickness is increased beyond 30 mm, the transmission loss value starts to decrease. Thus, the final levels chosen for optimization range in thickness

from 25 mm to 35 mm, with 0 mm level also being taken into consideration. Similar to this, the absorption layer for each of the other two chambers was selected for the pilot testing, with final levels ranging from 25 mm to 35 mm.

8.3 Application of Taguchi approach

To lessen the difficulty of conducting numerous trials while optimizing the muffler, the Taguchi-based design of experiment (DOE) technique was used. Three parameters with four levels of variation were subjected to the taguchi DOE technique, which resulted in a reduction of the number of tests to sixteen. As was previously mentioned, pilot experiments were used to determine the level fluctuation. Table 8.2 displays the entire set of variables and the degree of variance. The sixteen trials that must be conducted are specified by the L16 orthogonal array matrix, which was afterwards produced and is depicted in table 8.3.

Table 8.2. Control parameters and levels

FACTORS/LEVELS	A	B	C	D
A1 (Liner in first chamber)	0	25	30	35
A2 (Liner in second chamber)	0	25	30	35
A3 (Liner in third chamber)	0	25	30	35

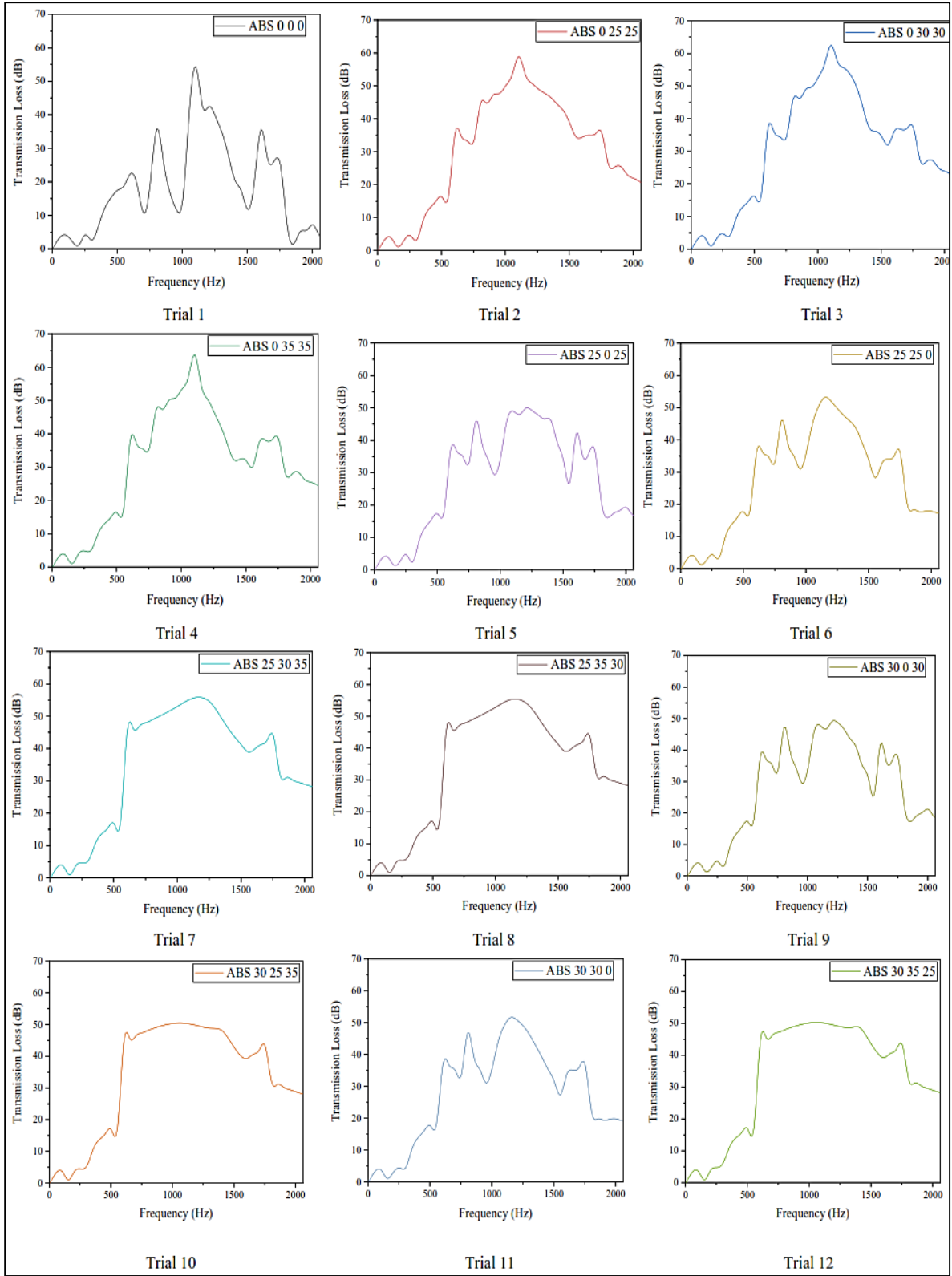
Table 8.3. L16 Orthogonal array matrix

S.No	A1	A2	A3
1	0	0	0
2	0	25	25
3	0	30	30
4	0	35	35
5	25	0	25
6	25	25	0
7	25	30	35
8	25	35	30
9	30	0	30
10	30	25	35
11	30	30	0
12	30	35	25
13	35	0	35
14	35	25	30
15	35	30	25
16	35	35	0

8.3.1 Acoustic performance analysis of the trial experiments

In the COMSOL Multiphysics Programme, 16 trial tests from the L16 orthogonal array matrix (i.e., table 8.3) are subjected to pressure acoustic frequency domain analysis. With

a step size of 25 mm for each experiment, the TL is determined throughout the complete frequency range from 0 to 2000 Hz. Figures 8.4 and 8.5 show the TL curves for each trial experiment and a comparison of all the studies, respectively.



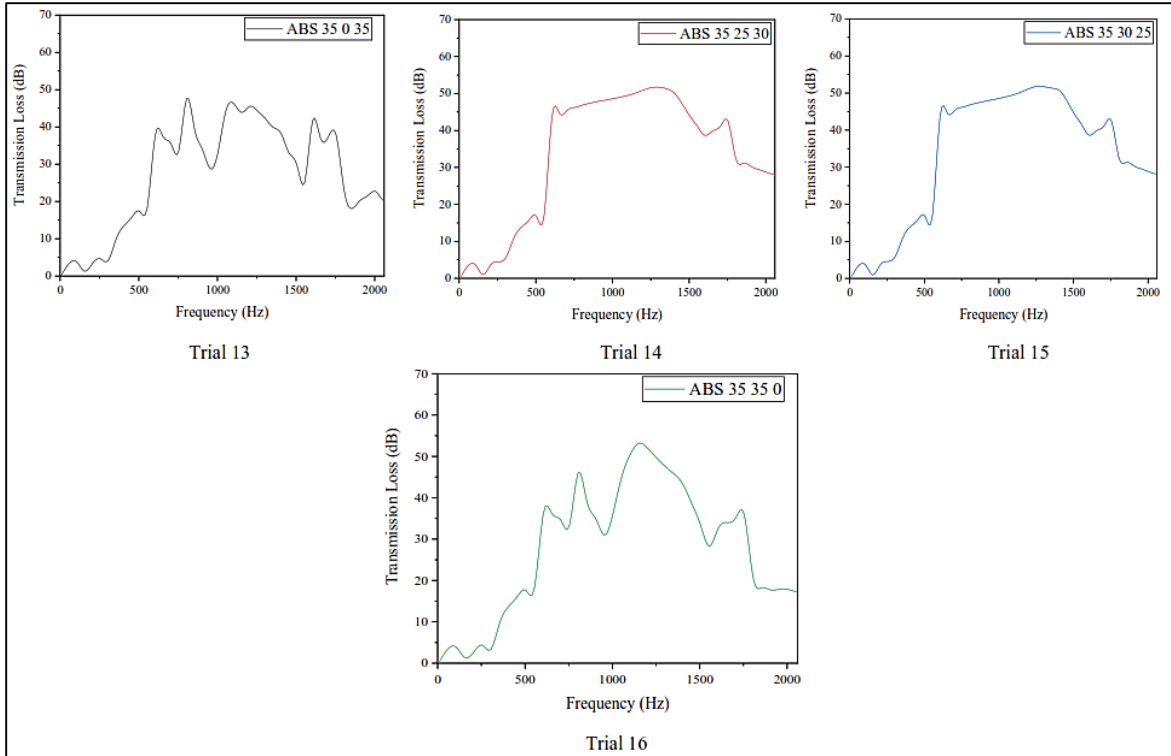


Figure 8.4. TL curve for the 16 trial experiments

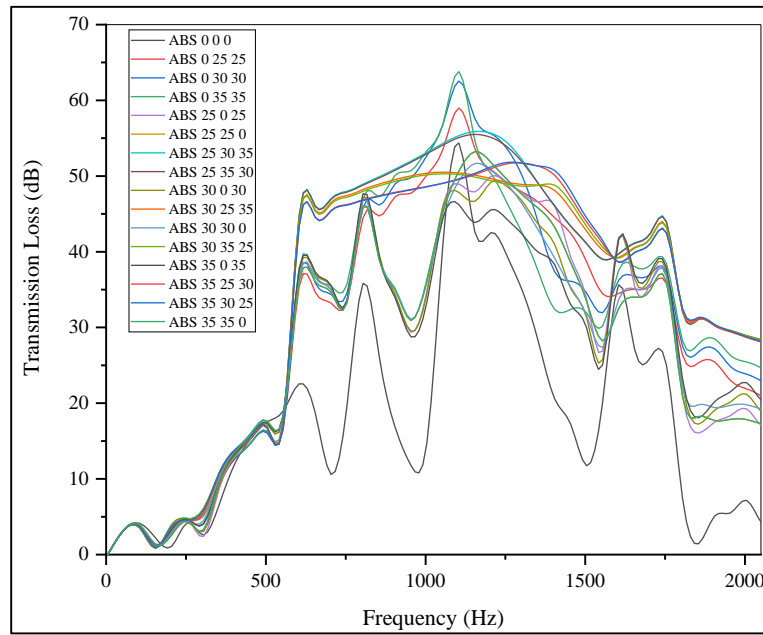


Figure 8.5. Comparison of TL curve for the trial experiments

The Figure 8.5 depicts that the maximum transmission loss was obtained for trial 4, when the absorption material layer of 35 mm was considered in the second and third chamber as compared to all the other cases.

8.3.2 Signal to noise ratio

As demonstrated in the preceding section, Comsol Multiphysics's pressure acoustic frequency domain analysis was used to compute the transmission loss for this particular set of trials. The S/N ratio was calculated using the Minitab software after the transmission loss values from these trials were entered. Table 8.4 and Figure 8.6 both display the outcome of the Minitab software's evaluation of the S/N ratio.

Table 8.4. L16 Taguchi Table with S/N ratio

S. No.	A1	A2	A3	TL	Sq. TL	S/N ratio	Mean
1	0	0	0	54.295	2947.947	34.6952	54.295
2	0	25	25	58.97	3477.461	35.41262	58.97
3	0	30	30	62.535	3910.626	35.92246	62.535
4	0	35	35	63.75	4064.063	36.0896	63.75
5	25	0	25	48.915	2392.677	33.78884	48.915
6	25	25	0	50.705	2570.997	34.10102	50.705
7	25	30	35	55.34	3062.516	34.86078	55.34
8	25	35	30	55.08	3033.806	34.81988	55.08
9	30	0	30	47.81	2285.796	33.59037	47.81
10	30	25	35	50.42	2542.176	34.05206	50.42
11	30	30	0	49.39	2439.372	33.87278	49.39
12	30	35	25	50.19	2519.036	34.01234	50.19
13	35	0	35	46.185	2133.054	33.29002	46.185
14	35	25	30	49.56	2456.194	33.90263	49.56
15	35	30	25	49.645	2464.626	33.91751	49.645
16	35	35	0	50.705	2570.997	34.10102	50.705

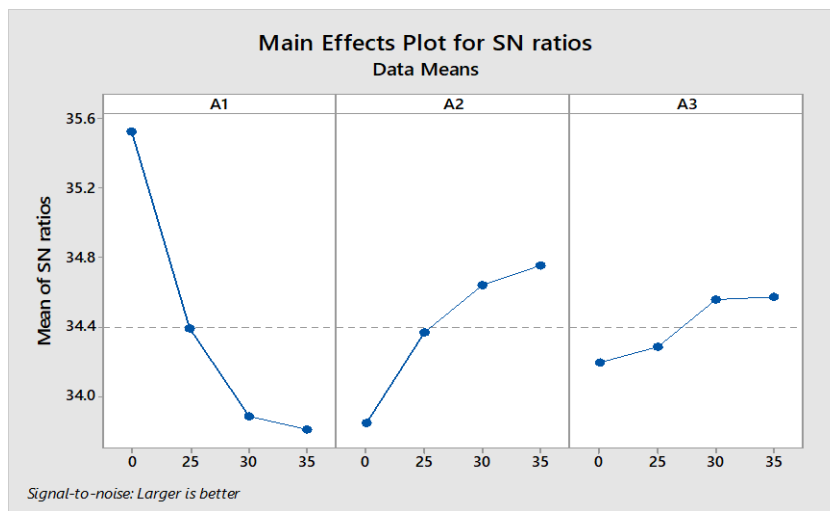


Figure 8.6. S/N ratio curve obtained through Minitab software

According to the transmission loss data from the sixteen trail trials, the highest S/N ratio was recorded when the layer of absorption material in the first chamber was zero, or empty. The maximum S/N ratio in the second and third chambers, however, is 35 mm and 35 mm, respectively. This means that these parameters are the best ones for causing the most transmission loss. The performance of the muffler was then evaluated using an ANOVA analysis to identify the importance and contribution of these characteristics.

8.3.3 Analysis of variance

By taking into account the 95% confidence level or a probability value (p) less than 0.05 for the control parameters, the one-way ANOVA analysis was carried out to support the significance of the selected control parameters. The analysis was carried out using Minitab software, and table 8.5 shows the outcomes.

Table 8.5. ANOVA values obtained through MINITAB

Source	DF	Seq SS	Adj SS	Adj MS	F	P
A1	3	7.6079	7.60789	2.53596	168.05	0.000
A2	3	1.9968	1.99679	0.66560	44.11	0.000
A3	3	0.4479	0.44788	0.14929	9.89	0.010
Residual Error	6	0.0905	0.09054	0.01509		
Total	15	10.1431				

Table 8.6. Calculation of percentage contribution from the variance analysis

S.No.	Factors	Degree of freedom (DF)	Total Sum of squares	Mean Square variance	Percentage contribution
1	A1	3	7.6079	2.53596	75.005
2	A2	3	1.9968	0.66560	19.686
3	A3	3	0.4479	0.14929	4.416
	Residual Error	6	0.0905	0.01509	0.892
	Total	15	10.1431		100

It can be seen from the ANOVA summary table 8.5 created with Minitab software that all three control parameters are significant ($p < 0.05$), satisfying the 95% confidence level requirement for significance. According to Table 8.6, A1 has the most impact with a percentage contribution of 75%, while A2 and A3 each have percentage contributions of 19.686% and 4.416%. Figure 8.7 depicts the schematic layout of this improved hybrid muffler.

As a result, in the section that follows, the pressure drop and transmission loss for the optimized hybrid muffler with absorption layers of $A1 = 0$ mm, $A2 = 35$ mm, and $A3 = 35$ mm are calculated.

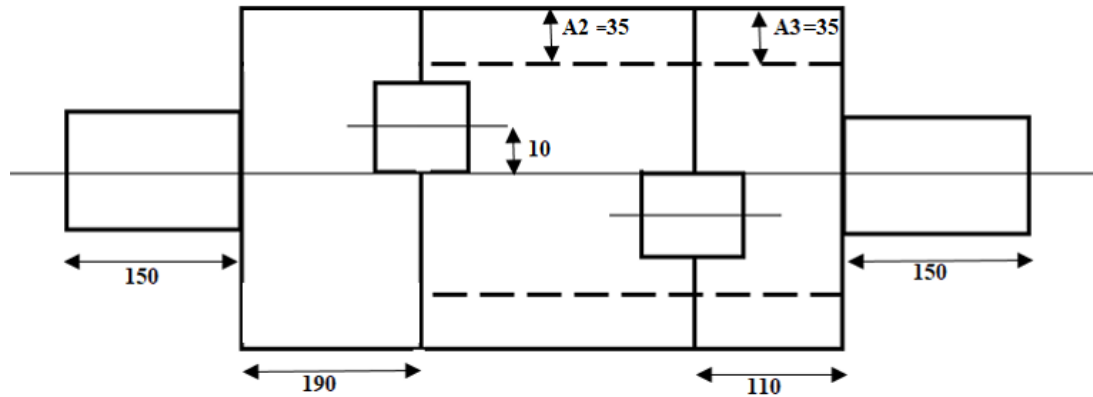


Figure 8.7. Schematic diagram of the optimized hybrid muffler

8.3.3.1 Aerodynamic analysis of the optimized hybrid muffler

The aerodynamic analysis for the optimized hybrid muffler is performed by using the fluent module in ANSYS Workbench. During this analysis, velocity inlet and pressure outlet are the main boundary conditions used. Using the same procedure as described in Chapter 5, the pressure variation, velocity variation and acoustic power distribution inside the muffler is observed. Figure 8.8 and 8.9 shows the three-dimensional model and meshed model of the hybrid muffler.

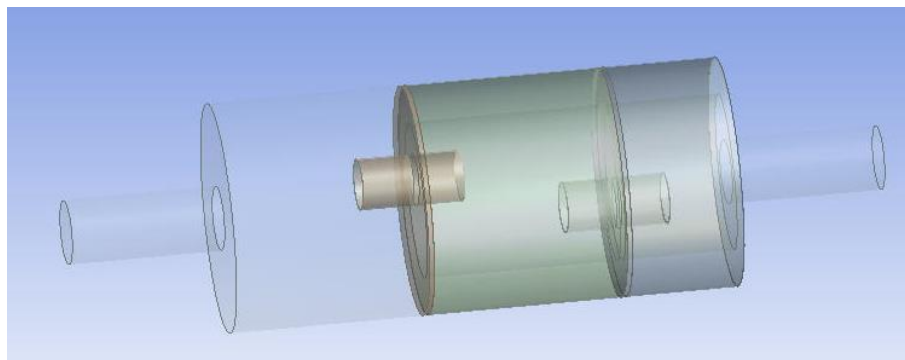


Figure 8.8. Three-dimensional diagram of the optimized hybrid muffler

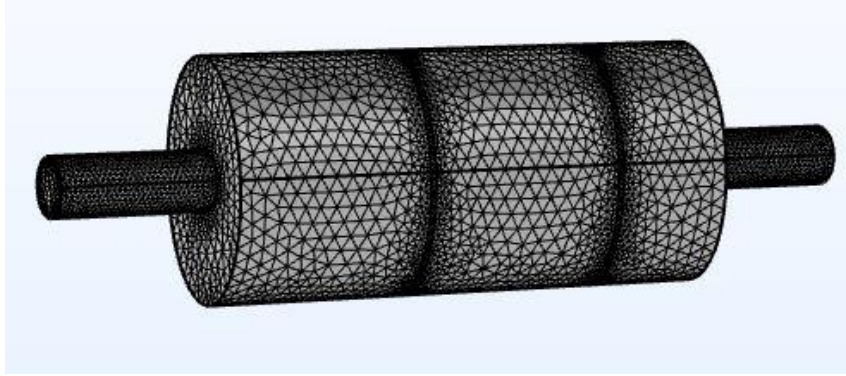
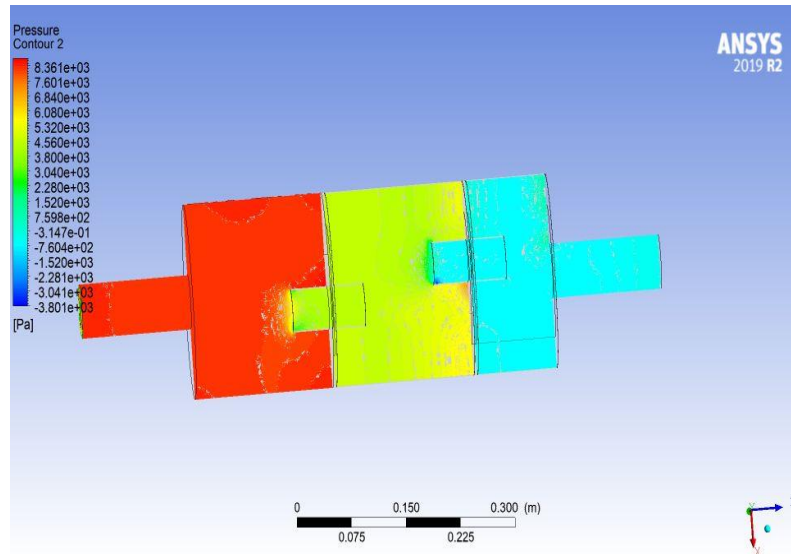
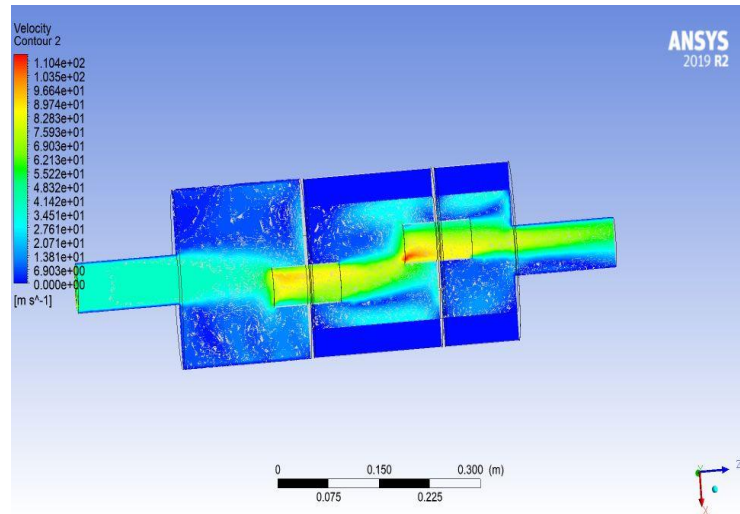


Figure 8.9. Meshed model of the optimized hybrid muffler



(a)



(b)

Figure 8.10. (a) Pressure and (b) velocity variation for the optimized hybrid muffler

The Figure 8.10 depicts that the pressure drop from inlet to the outlet of the muffler is around 8361 Pa and the maximum velocity of around 110 m/s is observed near the inner tube placed in the second baffle.

8.3.3.2 Acoustic analysis of the optimized hybrid muffler

The acoustic analysis for the optimized hybrid muffler is performed by using the pressure acoustic frequency domain module in COMSOL Multiphysics. During this analysis, pressure incident is the main boundary conditions used. Using the same procedure as described in Chapter 5, the transmission loss is obtained for the muffler.

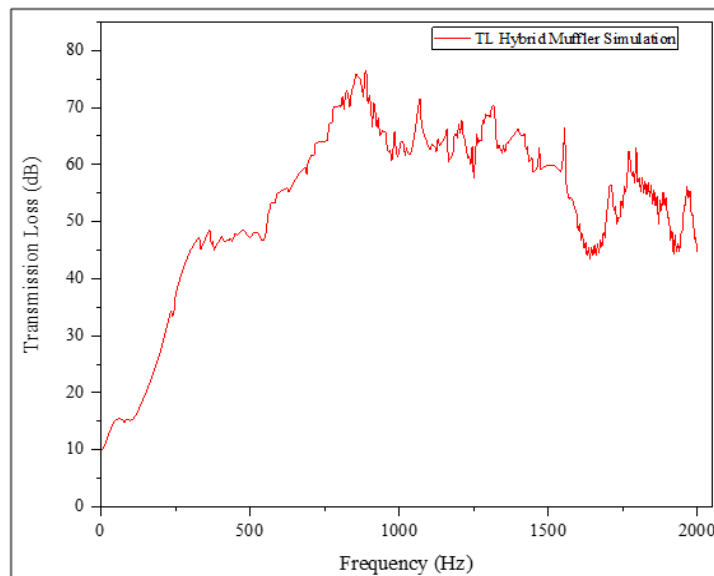


Figure 8.11. TL curve for the hybrid muffler acquired through simulation

The transmission loss curve showed that TL value is low at low frequencies, but with the increase in frequency the TL value is also increasing and maximum TL of 77.59 dB was obtained at frequency of 900 Hz. Further it was observed that the TL value is high from the mid to high frequencies as compared to TL in low frequency range.

8.4 Experimental validation of simulation results

The hybrid muffler is now fabricated and experimented in the impedance tube setup.

8.4.1 Fabrication and experimentation of Hybrid Muffler

Followed steps were taken for constructing the hybrid muffler.

Step 1: A rectangular sheet of 2 mm thickness is cutted from a big sheet according to the dimension of the muffler i.e. 500 mm x 602 mm. The sheet is then rolled in the shape of

the ellipse according to dimension of semi-major and semi-minor axis of 112 mm and 78 respectively in a roller machine and is welded.

Step 2: Four small rectangular plates of dimensions 240 mm x 170 mm were cutted from big sheet. These plates were taken for covering the ends of muffler chamber and for constructing the baffles.

Step 3: The four plates were first given the shape of the ellipse according to the dimension of the muffler chamber. Next a hole of 50 mm diameter is made on two plates which would be used as a baffle and hole were made on the other two plates according to the dimension of inlet and outlet tubes.

Step 4: The inlet and outlet tubes made of mild steel having length of 150 mm were taken and welded with the two plates which would be connected for covering the muffler chamber.

Step 5: Two tubes of 100 mm length were welded with the baffles.

Step 6: The two baffles were welded inside the muffler chamber. One at distance of 190 mm from left hand end of muffler chamber i.e. from the inlet section and the next at a distance of 110 mm from the right hand end of muffler i.e. from the outlet section.

Step 7: A layer of glasswool sound absorption material was inserted between the two baffles by cutting the muffler covering from one side and afterwards it was again welded.

Step 8: The plates with the inlet tube was initially welded with the muffler chamber and by putting a layer of glasswool between the baffle and plate with outlet tube, the plate was welded.

Step 9: Non-destructive test for checking the manufacturing defects on muffler. Tap or coin test was performed on the muffler to know the defect on the points of welding of baffles and tubes. Further, leakage test was also performed to test to leakage of the muffler near the weldings.

The total fabrication process is shown from Figure (8.12 – 8.14).



Figure 8.12 Glasswool sound absorption material



Figure 8.13 Implementing the sound absorption material inside the muffler



Figure 8.14 Hybrid muffler after welding all components

Experimentation of hybrid muffler

The optimized hybrid muffler has now been constructed as depicted in Figure 8.13 and 8.14, and it has been tested in an impedance tube setup, in similar way as the optimized reactive muffler was used. The process and the many factors that were taken into account throughout the study were the same as those that were employed in the case of the improved reactive muffler. Figure 8.15 displays the transmission loss that was discovered through experimentation after undergoing the uncertainty and accuracy of the experiment.

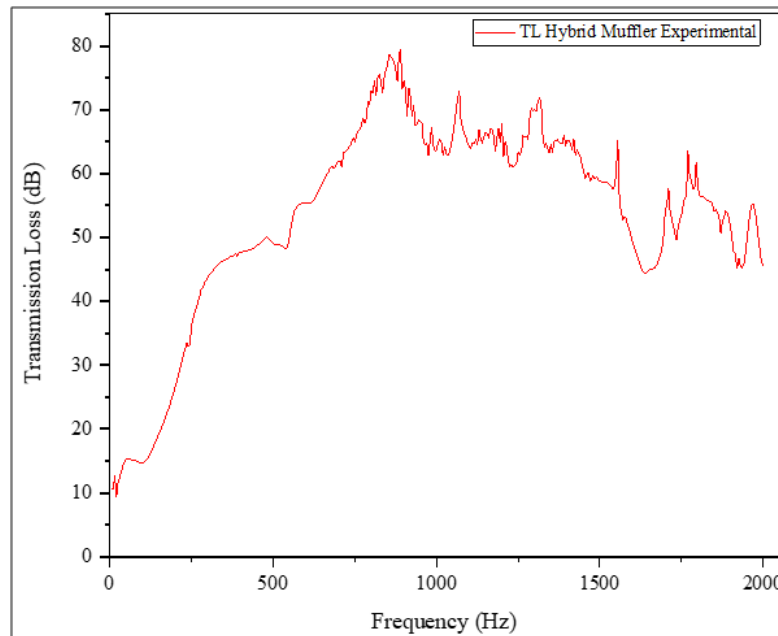


Figure 8.15. Transmission loss curve acquired through experimentation for hybrid muffler

8.4.2 Comparison of simulation and experimental result for hybrid muffler

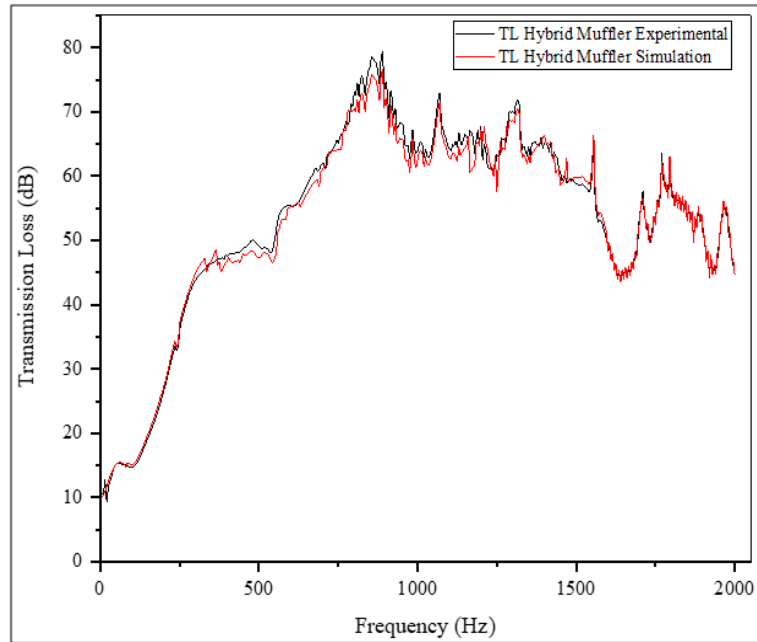


Figure 8.16. TL curve obtained through simulation and experimentation for hybrid muffler

The TL curve, presented in Figure 8.16, revealed that the maximum TL is 79.36 dB at frequency of 900 Hz. It also demonstrated strong agreement with the simulation result, with a deviation of only about 2.28%.

8.5 Comparison of optimized reactive type muffler and hybrid type muffler

Simulation and testing were done on both the hybrid and the upgraded reactive mufflers. Figures 8.17 (a) and (b) make it clear that the hybrid's transmission loss outperformed the optimized reactive muffler in terms of maximum TL as well as frequency spectrum broadening.

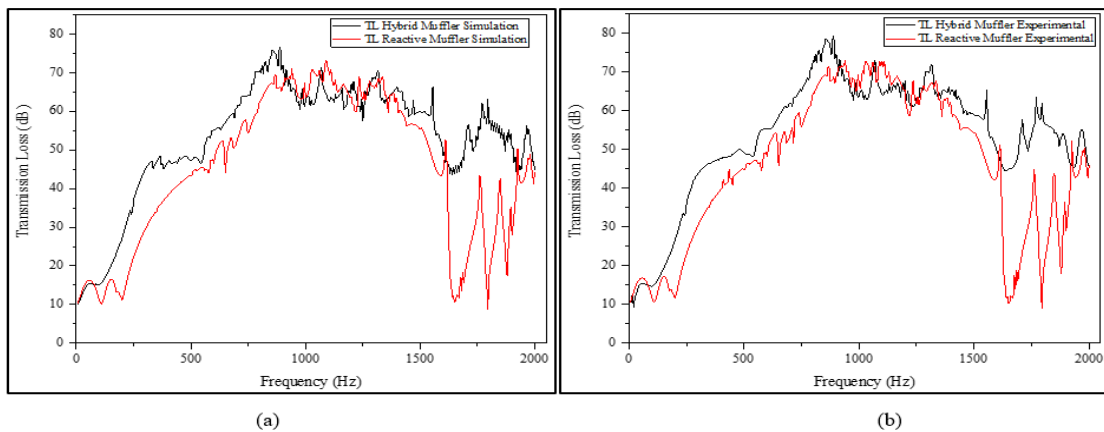


Figure 8.17. Comparison of TL acquired for optimized reactive muffler and hybrid muffler through (a) simulation (b) experimentation

According to the transmission loss curve, the third dome of the improved reactive muffler increases in size from 200 Hz to 1650 Hz. The second dome of the hybrid muffler, in contrast, entirely encloses the second and third domes of the optimal reactive muffler with a broadening of the second dome's frequency from 100 Hz. From 0 to around 900 Hz, the hybrid muffler's TL was found to be superior to the reactive mufflers; however, there was little difference in TL values between the two in the 900 Hz to 1350 Hz frequency range. Beyond 1350 Hz, it was discovered that the hybrid muffler's TL value was consistently superior to that of the reactive muffler. The increase in transmission loss is due to the attenuation of sound energy as it passes through a medium. This attenuation is caused by various mechanisms such as absorption, due to the presence of sound absorption material. As shown in table 8.7, the transmission values discovered through modelling and experiments for both the optimized reactive muffler and hybrid muffler were grouped from low frequency to high frequency. According to table 8.7, hybrid mufflers outperform optimal reactive mufflers in terms of maximum transmission value across all frequency ranges.

Table 8.7. TL values at diverse frequency range

Frequency Ranges	Maximum Transmission Loss in dB			
	Optimized reactive muffler simulation	Optimized hybrid muffler simulation	Optimized reactive muffler experiment	Optimized hybrid muffler experiment
(5 - 500)Hz	43.37	48.57	44.99	50.02
(505 – 1500) Hz	73.33	77.59	72.94	79.36
(1505 – 2000) Hz	55.24	66.48	53.63	65.17

8.6 Sensitivity analysis of the performance parameter of hybrid muffler

The sound pressure level is obtained for the hybrid muffler using the pressure acoustic frequency domain analysis in Comsol Multiphysics. These sound pressure level are noted at the three positions i.e. at inlet tube, center and outlet tube with respect to frequencies where the vibration sensor was fitted during experimentation as shown in Figure 8.18.

For determining the sensitivity of the sound pressure level from inlet to the outlet, chain base indexing concept is implemented in this study. Here the value of sound pressure level obtained at the inlet tube is considered as the reference value. The variation of sound pressure level at the center and outlet tube of the muffler is determined by implementing

the chain base indexing concept. Equation shows the relation used for chain indexing and table 8.8 shows the percentage change in sound pressure level value for the signals at those positions.

Applying the chain base index concept, percentage (%) change in sound pressure level (SPL) is calculated as shown in Eq. (65).

$$\% \text{ change in SPL at center} = \frac{(\text{SPL for signal taken at inlet tube} - \text{SPL for signal taken at center})}{\text{SPL for signal taken at inlet tube}} \times 100 \%$$

And (65)

$$\% \text{ change in SPL at outlet tube} = \frac{(\text{SPL for signal taken at center} - \text{SPL for signal taken at outlet tube})}{\text{SPL for signal taken at center}} \times 100 \%$$

Next, the percentage change in variation of sound pressure level for inlet tube to outlet tube were determined using the chain base indexing method as shown in equation and values obtained are depicted in in table 8.8.

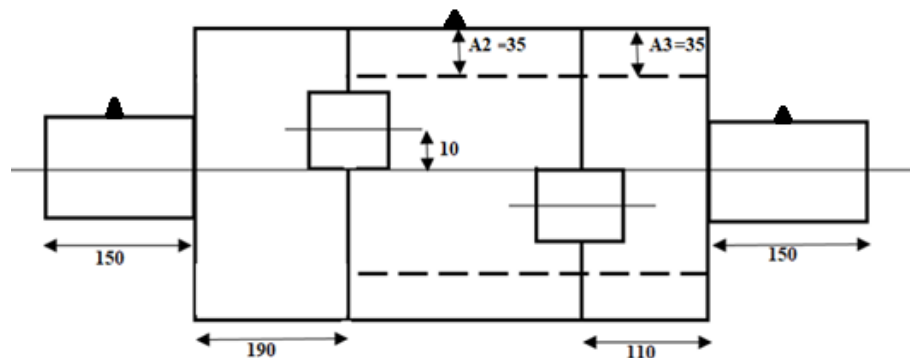


Figure 8.18. Schematic of hybrid muffler with vibration sensor placed position

Table 8.8. Variation and percentage change of sound pressure level in hybrid muffler

Frequency (Hz)	Position	Sound Pressure Level (dB)	Percentage change by chain base method	Percentage decrease of SPL
550	Inlet tube	96.89		
550	center	45.00	53.56	
550	Outlet tube	30.55	32.11	68.47
1400	Inlet tube	92.82		
1400	center	49.00	47.21	
1400	Outlet tube	32.22	34.24	65.29
2200	Inlet tube	89.30		
2200	center	52.00	41.77	
2200	Outlet tube	33.80	35.00	62.15

The high pressure gases from the exhaust system of vehicle enters the hybrid muffler and at the inlet tube, sound pressure level was observed to be 96.89 dB, 92.82 dB and 89.3 dB at 550 Hz, 1400 hz and 2200 Hz respectively. As it moves through the chamber, sound pressure level was observed to be decreasing and minimum sound pressure level was observed at the outlet tube. The overall sound pressure level decrease by 68.47%, 65.29% and 62.15 % respectively from the inlet tube to the outlet tube.

The significance of this decrease in sound pressure level in a muffler is that it reduces the overall noise level generated by the engine. The benefit of this is that it improved the driver and passenger comfort, reduce noise pollution in the environment. Further, it helped in maintaining regulations governing the maximum noise level that a vehicle is allowed to generate.

CHAPTER 9. VIBRATION ANALYSIS OF OPTIMIZED HYBRID MUFFLER

9.1 Vibration response

The impedance tube set up was used for determining the transmission loss of a muffler. During this process, an accelerometer (Figure 9.1) as well as a separate NI DAQ (Figure 9.2 and 9.3) was also fitted across the muffler at different position along with the impedance tube set up for acquiring the amount of vibration produce in the muffler in the sections. In this study, the vibrations signals are noted at three different position i.e. at inlet tube, center and at outlet tube respectively of the muffler. The mufflers were tested for frequencies ranging from 10 Hz to 3000 Hz and for determining the effect of vibration produce by the exhaust gases, signals are noted at various frequencies. The signals obtained at frequencies of 550 Hz, 1400 Hz and 2200 Hz are shown from Figure (9.4 – 9.6).

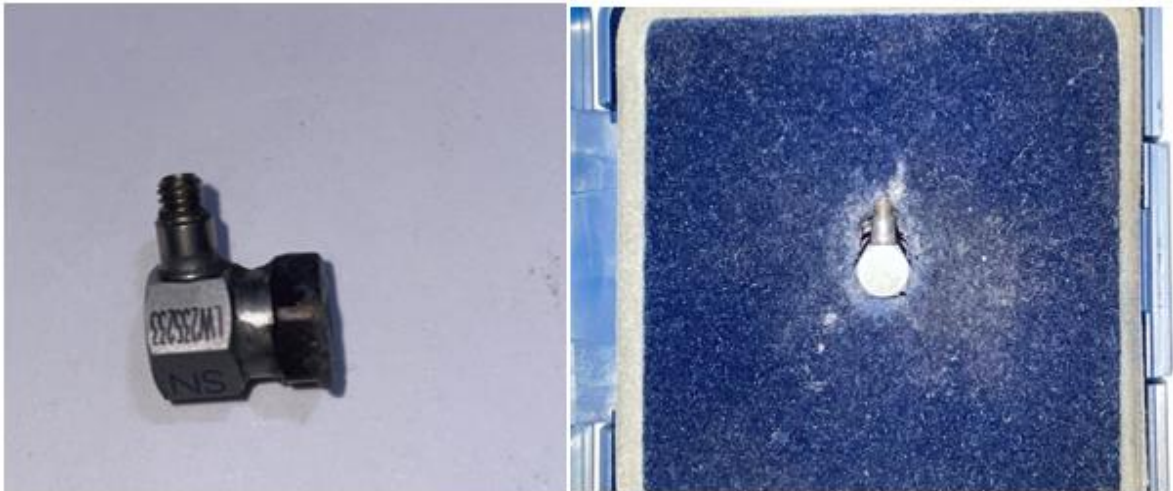


Figure 9.1. PCB Piezotronics accelerometer

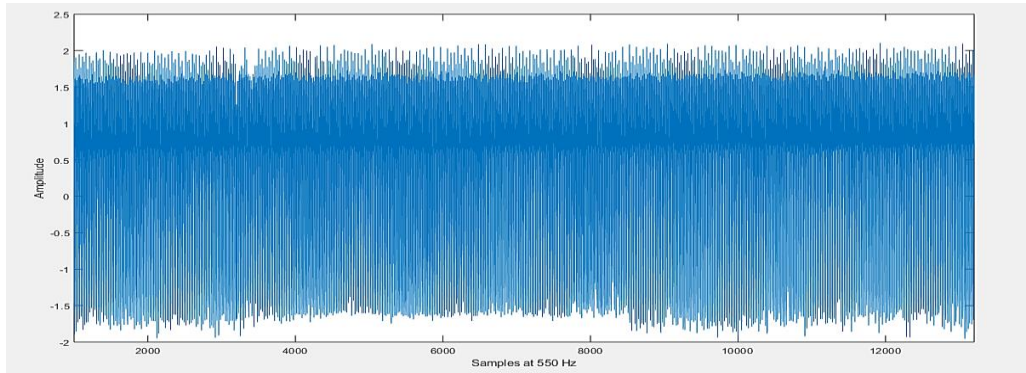


Figure 9.2. Three channel NI Data acquisition system

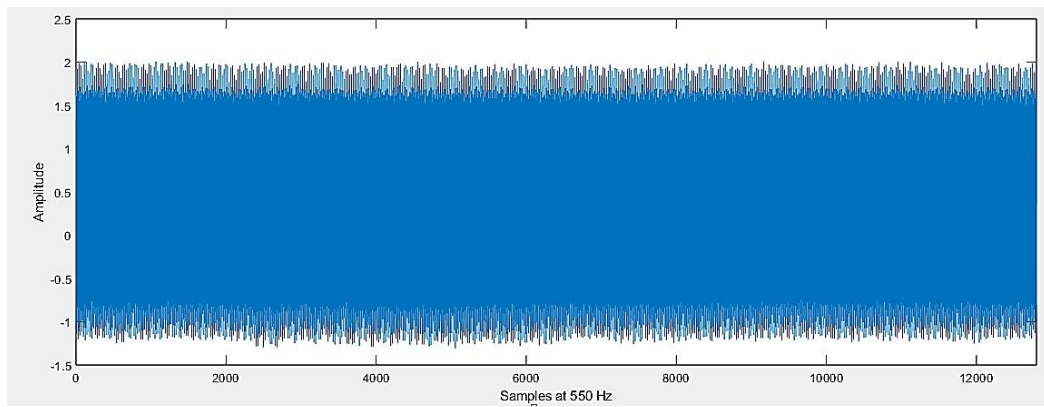


Figure 9.3. NI DAQ system connected with BNC cable

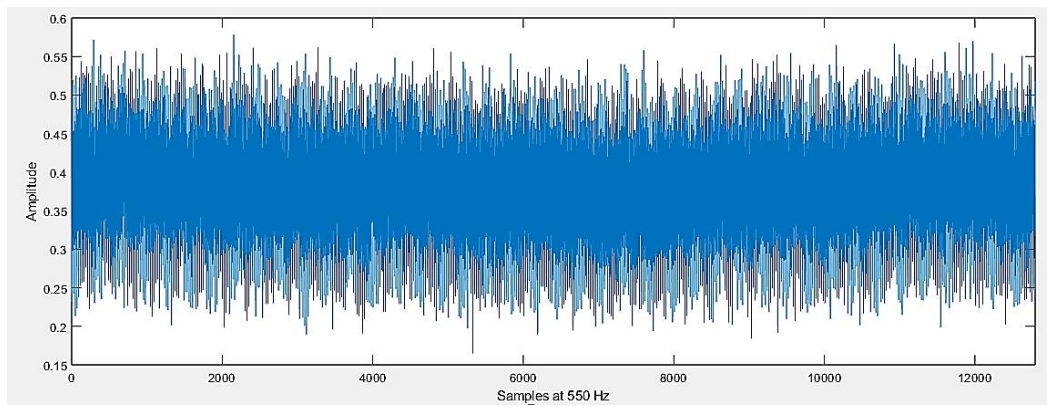
Vibration Signals at 550 Hz



(a)



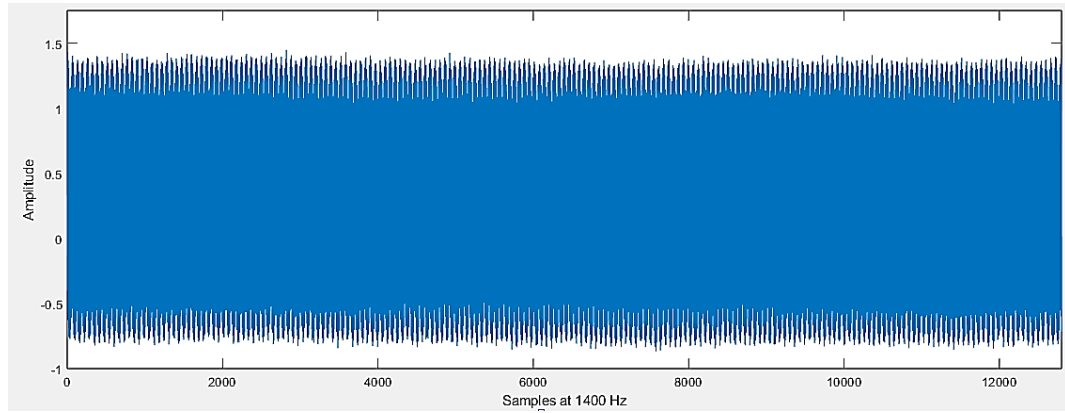
(b)



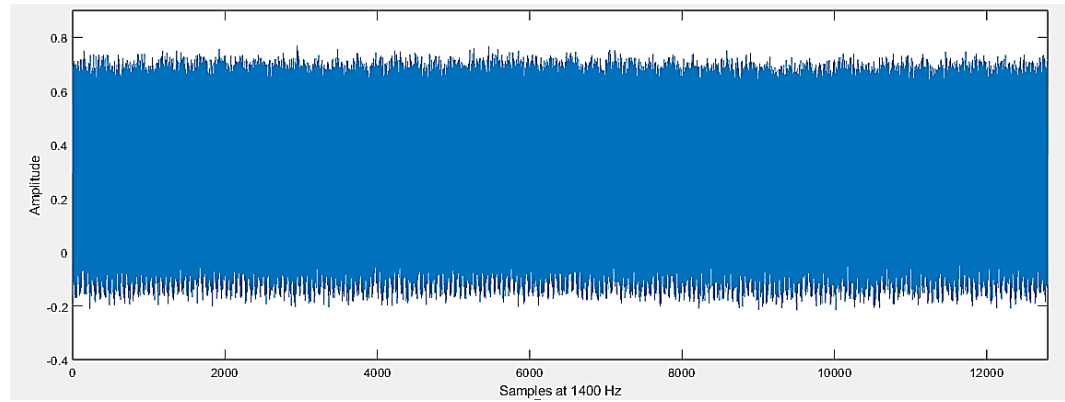
(c)

Figure 9.4. Signals at the inlet, center and outlet at frequency of 550 Hz

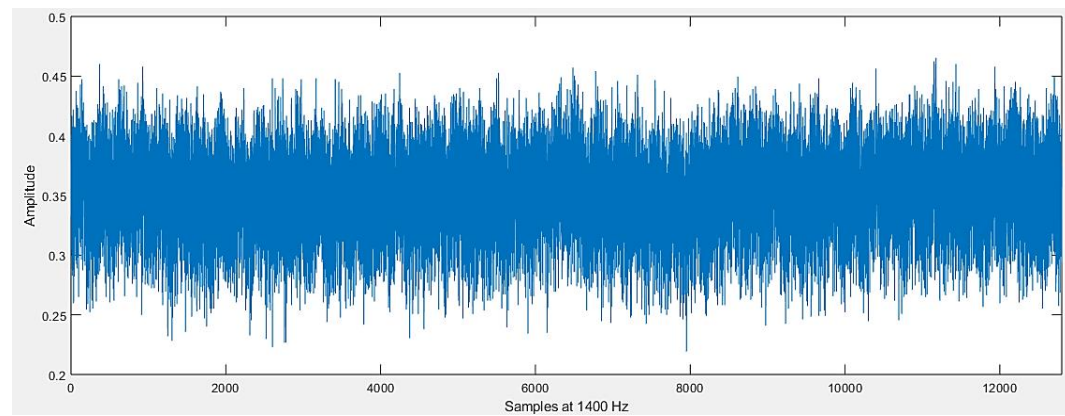
Vibration Signals at 1400 Hz



(a)



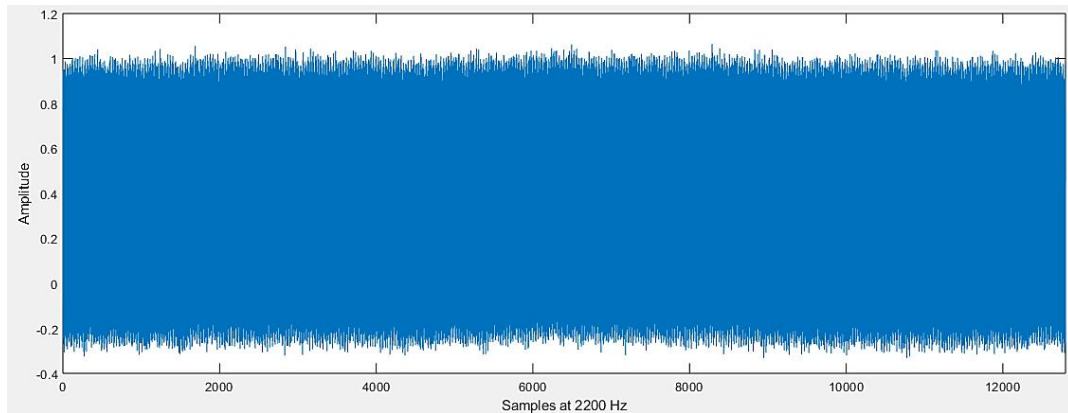
(b)



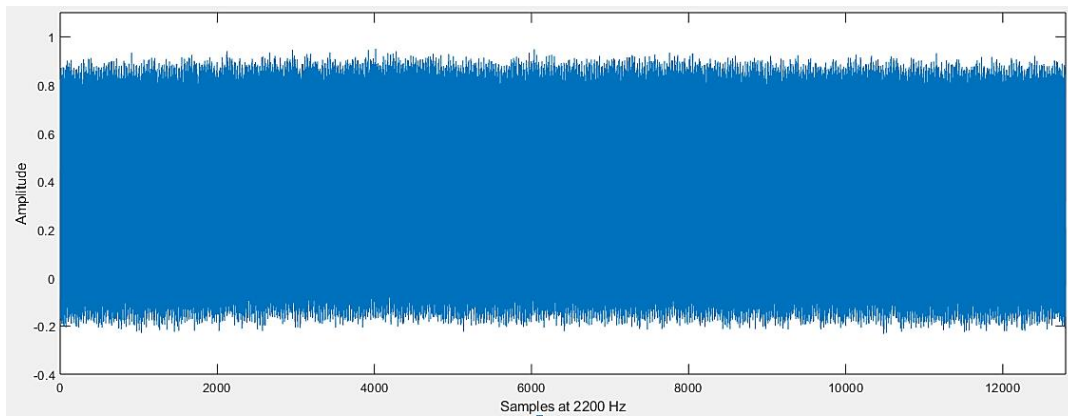
(c)

Figure 9.5. Signals at the inlet, center and outlet at frequency of 1400 Hz

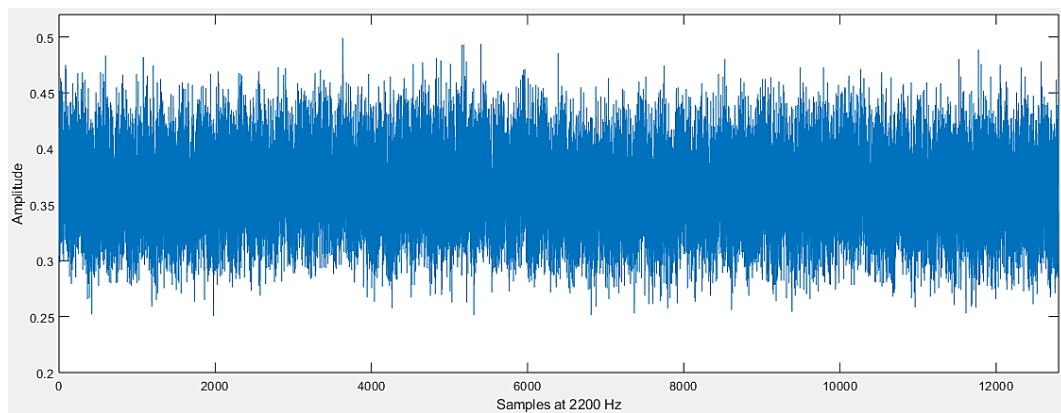
Vibration signals at 2200 Hz



(a)



(b)



(c)

Figure 9.6. Signals at the inlet, center and outlet at frequency of 2200 Hz

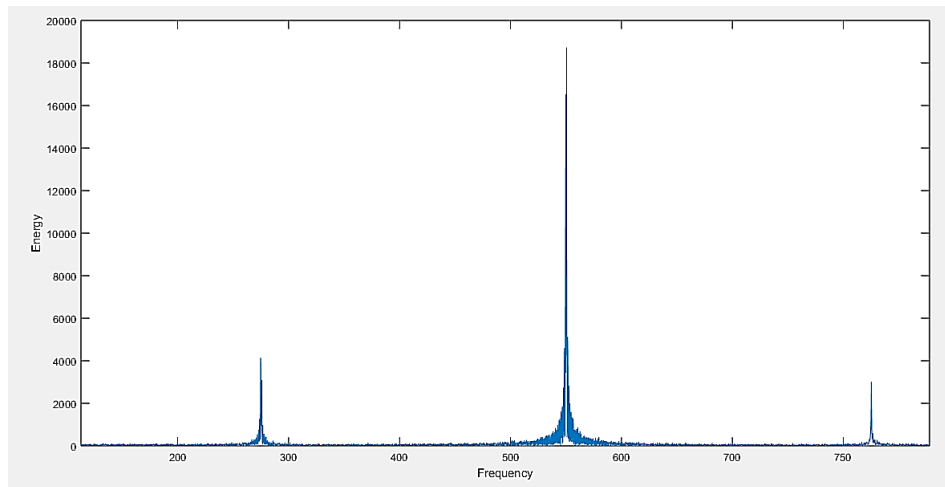
Figure (9.4 – 9.6) shows the behavior of signals acquired at different positions of the muffler. It represents the amplitude of the signals with respect to the number of samples (12800 samples/sec). It depicts that for each frequency the amplitude of the signals is

maximum towards the inlet tube and along the length of the muffler, the amplitude is decreasing. Maximum amplitude is at the inlet position and minimum amplitude is observed at the outlet for all the frequencies considered for study.

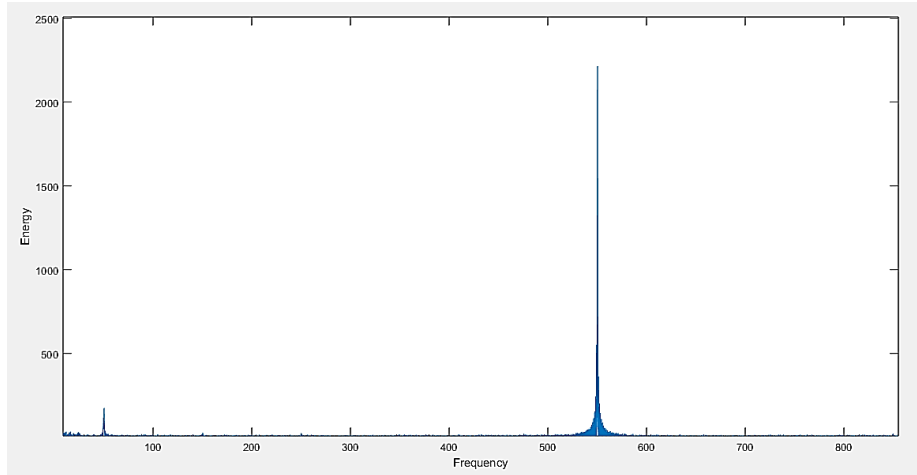
FFT (Fast Fourier Transform) Analysis:

FFT (Fast Fourier Transform) analysis is often used to analyze vibration signals because it can reveal important information about the frequency content of the signal. Vibration signals are typically time-varying signals, which means that the amplitude of the signal changes with time. By performing an FFT analysis on a vibration signal, we can transform it from the time domain to the frequency domain, which allows us to see the spectral content of the signal. The frequency content of a vibration signal can provide important information about the machinery or structure that is producing the signal. FFT analysis is particularly useful for detecting and analyzing vibration signals in machinery and structures because it can help identify specific frequencies that may indicate the presence of faults or abnormalities. By analyzing the vibration signal in the frequency domain, we can identify these frequencies and use this information to diagnose problems and make informed decisions about maintenance and repairs. The FFT algorithm is widely used in many software packages for data analysis and visualization.

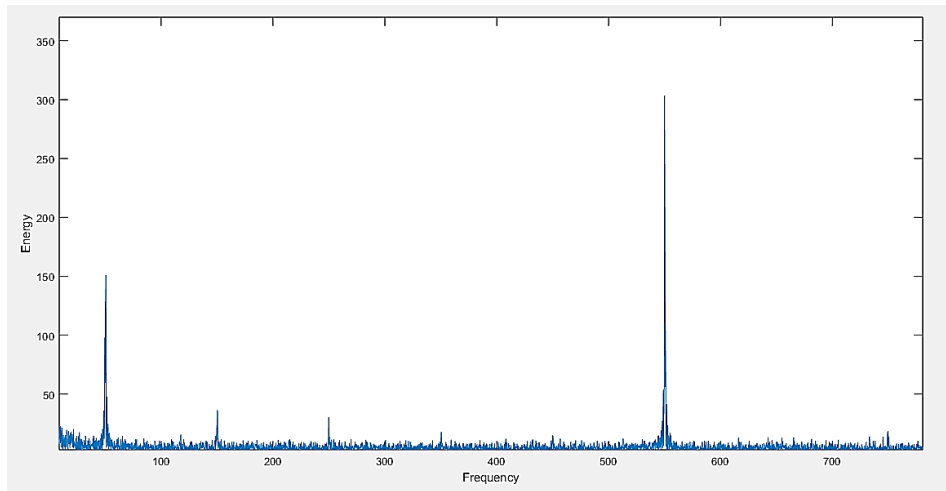
FFT analysis is performed for the signals acquired at inlet tube, center and outlet tube to identify the specific frequencies that may indicate the presence of faults or abnormalities.



(a)

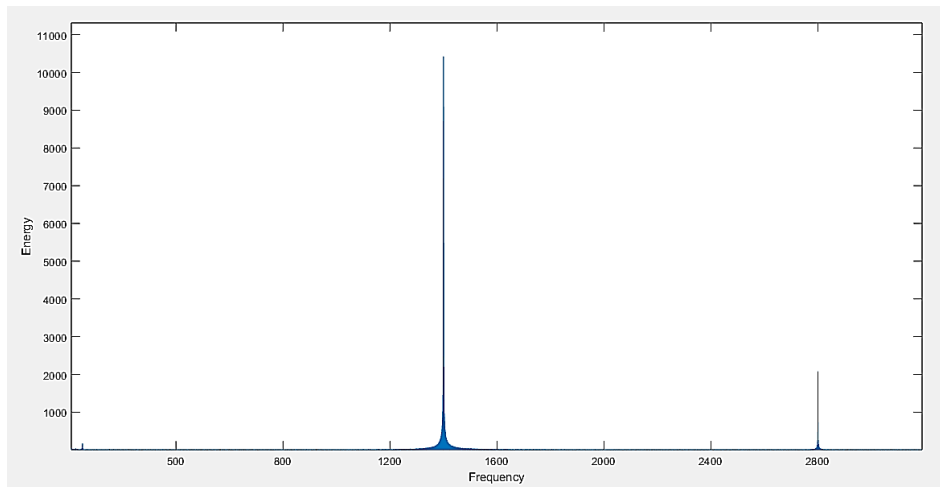


(b)

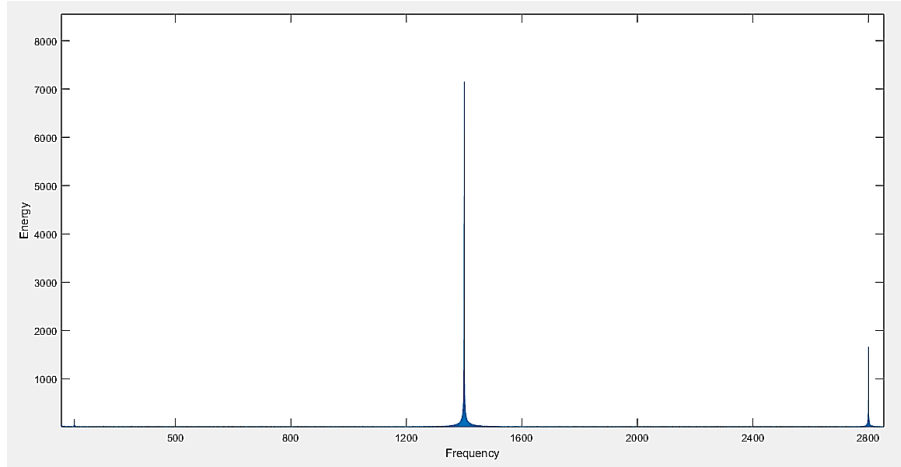


(c)

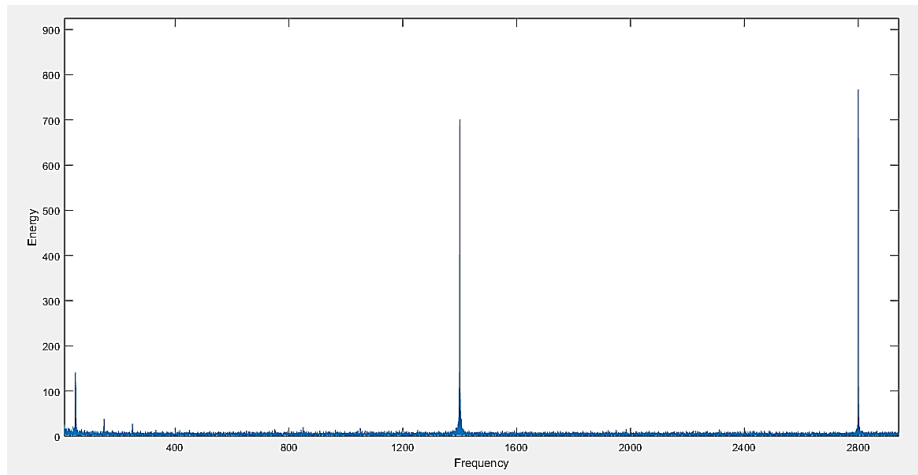
Figure 9.7 FFT curve formed at 550 Hz for the signals acquired at the inlet tube, center and outlet tube.



(a)

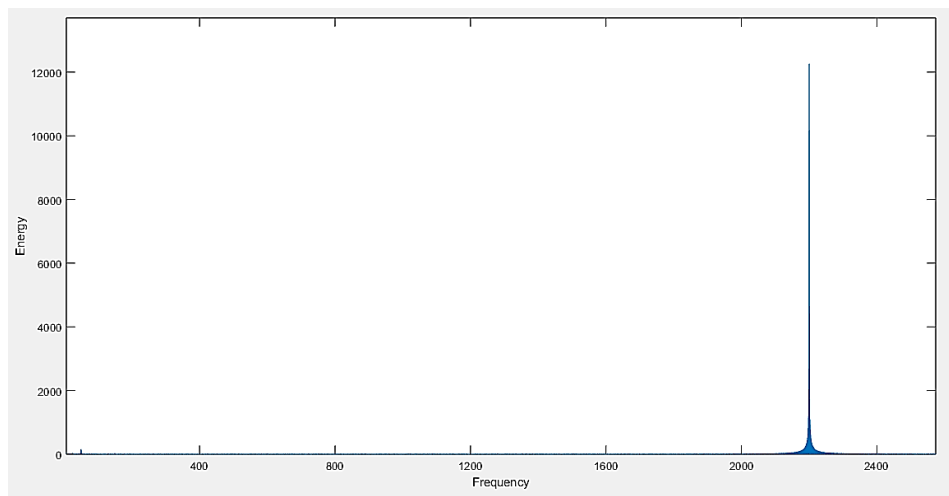


(b)

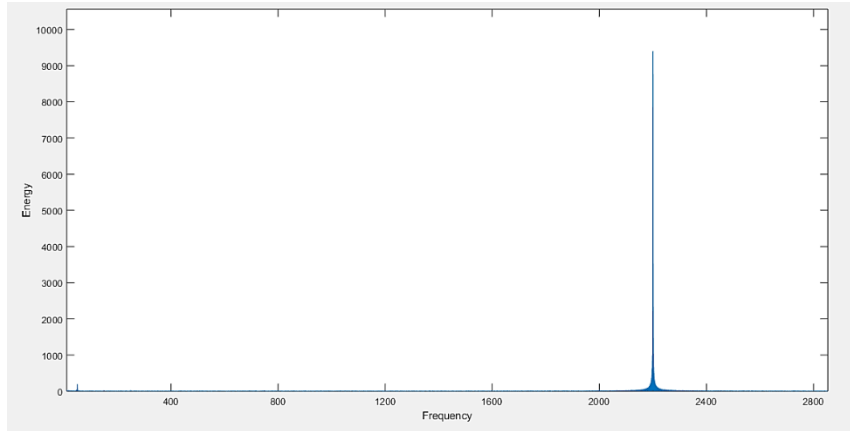


(c)

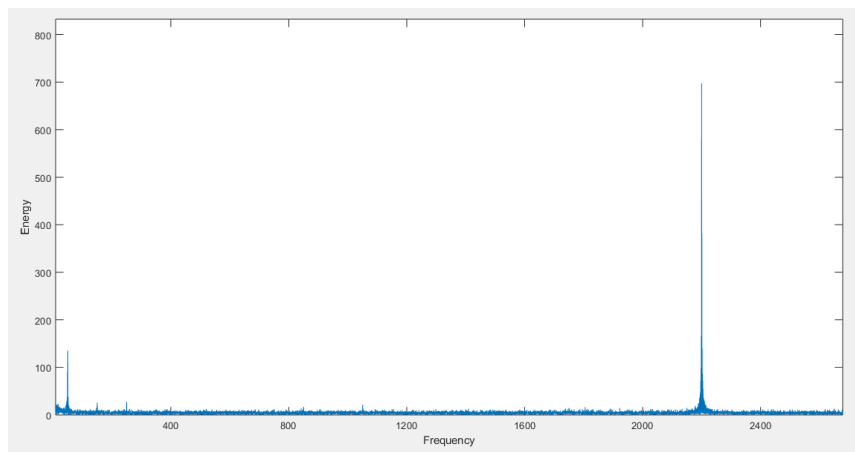
Figure 9.8. FFT curve formed at 1400 Hz for the signals acquired at the inlet tube, center and outlet tube



(a)



(b)



(c)

Figure 9.9. FFT curve formed at 2200 Hz for the signals acquired at the inlet tube, center and outlet tube

Figure (9.7 – 9.9) shows the FFT curve obtained at the three positions i.e. inlet tube, center and outlet tube and it was observed that the energy decreased from inlet tube to the outlet tube at all the frequencies. Table 9.1 represents the energy level acquired at various position in the muffler.

Table 9.1. Energy values from FFT curve

Frequency (Hz)	Energy		
	Inlet tube	Center	Outlet tube
550	19000	6250	320
1400	10500	7000	750
2200	12100	9500	700

9.2 Selection of wavelet and decomposition level for vibration signal

Selecting the best suited wavelet and level, at which best performance would be achieved is of prime importance. So, analysis is performed for a signal taken at the inlet position at 1400 Hz. The energy and entropy of the signal are determined applying different wavelets in MATLAB R2018b software. During this analysis, “*Symlet, Daubechies, Fejer-Korovkin, Coiflets*” are the wavelets considered for study. Initially, for selecting the best suited level, analysis was performed for all the levels and decomposition of the signals as shown from table (9.2-9.5). Later, by selecting the level producing maximum energy, the type of wavelet which produce maximum energy to entropy ratio is determined.

Decomposition of signals using Symlet (“sym”), N = 4

Table 9.2. Decomposition of signals using Symlet (“sym”), N = 4

Levels	Energy				
	Ea	Ed			
	approx., a	d ₁	d ₂	d ₃	d ₄
4	64.67	1.7618	10.8204	22.7296	0.014
3	64.6554	1.7634	10.8304	22.7508	
2	87.3991	1.7644	10.8365		
1	98.2351	1.7649			

Decomposition of signals using Daubechies (“db”), N = 4

Table 9.3. Decomposition of signals using Daubechies (“db”), N = 4

Levels	Energy				
	Ea	Ed			
	approx., a	d ₁	d ₂	d ₃	d ₄
4	64.6698	1.7593	10.8193	22.7387	0.0129
3	64.6517	1.7608	10.8288	22.7587	
2	87.4038	1.7617	10.8345		
1	98.2379	1.7621			

Decomposition of signals using Fejer-Korovkin (“fk”), N = 4

Table 9.4. Decomposition of signals using Fejer-Korovkin (“fk”), N = 4

Levels	Energy				
	Ea	Ed			
	approx., a	d ₁	d ₂	d ₃	d ₄
4	64.9913	4.0816	12.6681	18.1812	0.0777
3	65.0599	4.0827	12.6715	18.1860	
2	83.2438	4.0832	12.6730		
1	95.9166	4.0834			

Decomposition of signals using Coiflets (“coif”), N = 4

Table 9.5. Decomposition of signals using Coiflets (“coif”), N = 4

Levels	Energy				
	Ea	Ed			
	approx., a	d ₁	d ₂	d ₃	d ₄
4	64.7222	1.5399	8.1532	25.5537	0.0310
3	64.6703	1.5435	8.1724	25.6138	
2	90.2696	1.5458	8.1845		
1	98.4530	1.5470			

Table (9.2-9.5) depicts that the maximum energy is produced by the signals at level 1 using all the wavelets. Using level 1, the maximum energy to entropy ratio is determined for all the wavelets at different vanishing moments and shown in table 9.6.

Table 9.6. Maximum energy to entropy for various wavelets

Type of Wavelet	Vanishing moment, N	Energy		Entropy	Maximum Energy to Entropy ratio
		Ea	Ed		
Symlet (sym)	2	97.21	2.79	6.9547	13.9776
	3	97.97	2.03	6.8894	14.2204
	4	98.2351	1.7649	6.8521	14.3365
	5	98.34	1.66	6.8267	14.4052
	6	98.39	1.61	6.8062	14.45594
	7	98.42	1.58	6.7901	14.49463
	8	98.44	1.56	6.7757	14.52839
Daubechies (db)	1	94.71	5.29	7.124	13.2945
	2	97.21	2.79	6.9547	13.9776
	3	97.97	2.03	6.8894	14.2204
	4	98.23	1.77	6.8521	14.33575
	5	98.34	1.66	6.8267	14.4052
	6	98.39	1.61	6.8062	14.45594
	7	98.42	1.58	6.7901	14.49463
	8	98.44	1.56	6.7757	14.52839
	10	98.48	1.52	6.7541	14.58077
Fejer-Korovkin (fk)	4	95.92	4.08	7.0394	13.62616
	6	98.19	1.81	6.8665	14.29986
	8	98.33	1.67	6.819	14.42
	14	98.52	1.48	6.7226	14.65504
	18	98.62	1.38	6.6847	14.75309
	22	98.69	1.31	6.6587	14.82121
Coiflets (coif)	1	97.29	2.71	6.9478	14.00299
	2	98.26	1.74	6.8459	14.35312
	3	98.4	1.6	6.7982	14.47442
	4	98.45	1.55	6.7672	14.54811
	5	98.49	1.51	6.7455	14.60085

Using the signal multi-resolution analysis in MATLAB, the maximum energy to entropy ratio values are obtained for all the four wavelets considered for study. The results showed that maximum energy to entropy ratio is obtained for Fejer-Korovkin (fk) wavelet. The maximum energy to entropy ratio of 14.82 is obtained when the vanishing moment was considered to be 22. Thus, this wavelet is considered to be most suitable for application as compared to all the other cases.

Fejer-Korovkin (fk) wavelet is now selected from the preliminary analysis and the different statistical parameters are determined for the received vibration signals. In the hybrid muffler, 9 different signals are acquired at frequencies of 550 Hz, 1400 Hz and 2200 Hz respectively by placing the accelerometer at inlet tube, center and outlet tube.

9.3 Statistical analysis

The values for the various statistical parameters i.e. root mean square (RMS), standard deviation (σ), Kurtosis and Skewness for the nine defected signals were determined using Matlab R2018b. The values are obtained for both the raw signal and the defected signal and is shown in table 9.7 and table 9.8 respectively.

Table 9.7. Determination of statistical parameter for raw signals obtained for 5 sec

Frequency (Hz)	Position	RMS	σ	Kurtosis	Skewness	Peak2rms	Shannon entropy	log energy entropy
550	Inlet tube	1.0367	1.0381	3.1776	0.1761	3.2291	-194.5642	-296.4825
	Center	1.0009	1.0012	3.0004	0.0421	3.0937	-147.0854	-244.6219
	Outlet tube	0.9792	0.9777	2.9561	-0.2029	2.8447	-119.0972	-221.4606
1400	Inlet tube	1.0293	1.0275	3.2657	0.4254	3.4682	-174.8823	-270.7914
	Center	0.974	0.9759	2.9687	0.0474	3.2427	-126.2008	-267.541
	Outlet tube	0.9622	0.9627	2.7253	-0.0138	2.7787	-114.4531	-217.4127
2200	Inlet tube	1.0224	1.0244	3.1008	0.1192	3.1945	-162.6105	-311.0646
	Center	0.9618	0.9594	2.793	0.0484	2.746	-123.7201	-271.1377
	Outlet tube	0.9024	0.9043	2.5582	0.0395	2.7347	-108.3663	-265.823

Table 9.8. Determination of statistical parameter for defected signals obtained for 5 sec

Frequency (Hz)	Position	RMS	σ	Kurtosis	Skewness	Peak2rms	Shannon entropy	log energy entropy
550	Inlet tube	1.0858	1.0883	3.6425	0.2992	3.5004	-224.5551	-274.2797
	Center	1.0075	1.008	3.3441	0.2605	3.2955	-163.0952	-229.9605
	Outlet tube	0.9139	0.9158	2.992	-0.034	3.0498	-92.7724	-229.5183
1400	Inlet tube	1.0057	1.0036	3.5818	0.1519	2.8741	-186.5833	-293.6581
	Center	1.0012	0.9996	3.2928	0.0276	2.7933	-131.604	-275.9934
	Outlet tube	0.95	0.9333	2.803	0.0049	2.7453	-89.4139	-243.3677
2200	Inlet tube	1.063	1.0655	3.5796	0.0537	3.3591	-182.0791	-290.6487
	Center	1.0319	1.0345	3.2216	0.0306	3.2845	-142.5908	-250.4374
	Outlet tube	0.9552	0.9499	2.708	-0.1631	3.0231	-95.1546	-240.3896

From Table 9.7 and 9.8, it is observed that the statistical parameters are decreasing for the signal taken at the inlet tube to the outlet tube.

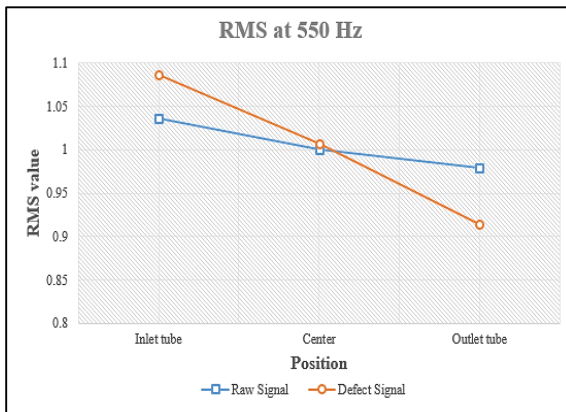
A decrease in the RMS (root mean square) value of a vibration signal indicate a reduction in the overall energy or amplitude of the signal. This can occur due to the presence of a fault or defect that is reducing the amount of vibration being transmitted through the system.

The peak-to-RMS (root mean square) value of a vibration signal is a measure of the amplitude of the highest peaks in the signal relative to its overall energy content. A decrease in the peak-to-RMS value of a vibration signal indicate a reduction in the severity or intensity of the vibrations being transmitted through the system. A decrease in the peak-to-RMS value of a vibration signal may not always be a cause for concern.

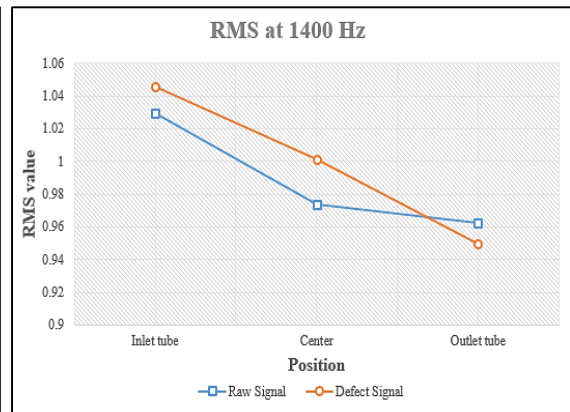
A decrease in kurtosis of a vibration signal indicates the reduction in the peakedness of the signal, which represents a decrease in the amplitude of impulsive events.

A positively skewed value observed for the vibration signal indicate the presence of a fault while a negative skewed value in the signal indicate the presence of misalignment.

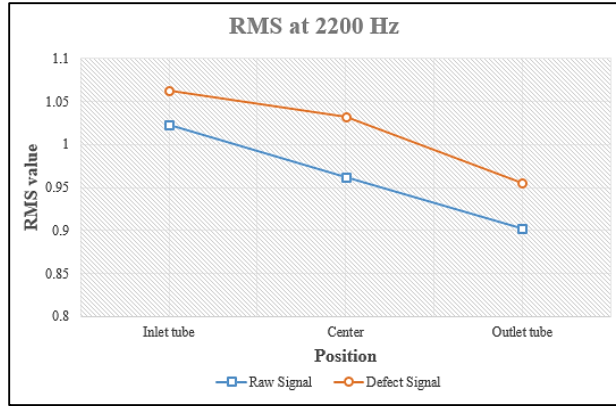
Shannon entropy, a measure of uncertainty, can take negative values for signals such as vibration signals if the signal is highly predictable or structured. In such cases, the entropy is low, and the negative entropy value reflects the high degree of order or regularity in the signal. On the other hand, a completely random signal would have a high entropy value, close to the maximum entropy, which is \log_2 of the number of states in the signal.



(a)

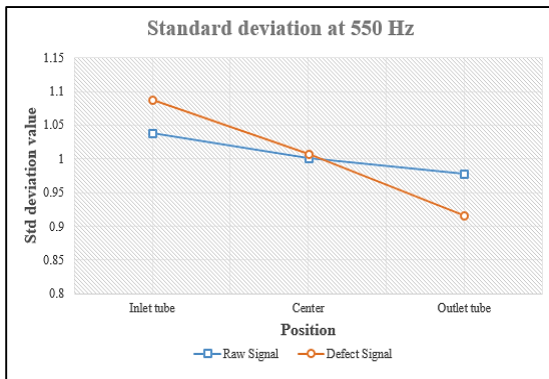


(b)

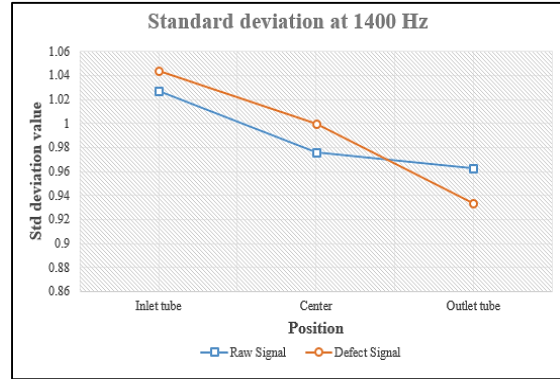


(c)

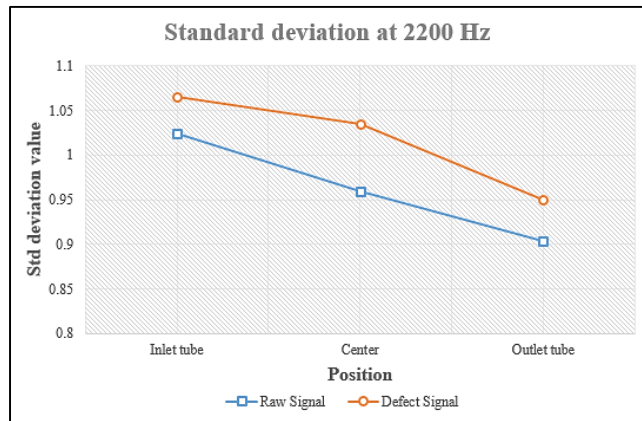
Figure 9.10. RMS curve for the signals at 550 Hz, 1400 Hz and 2200 Hz



(a)

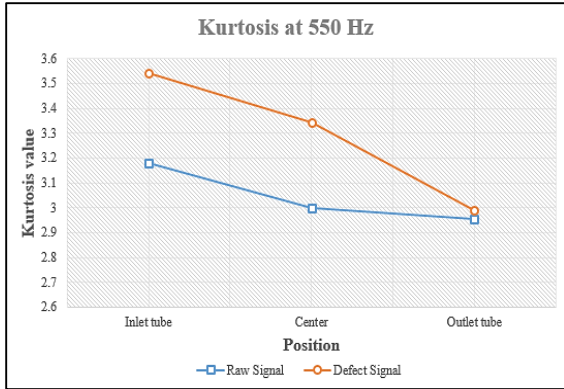


(b)

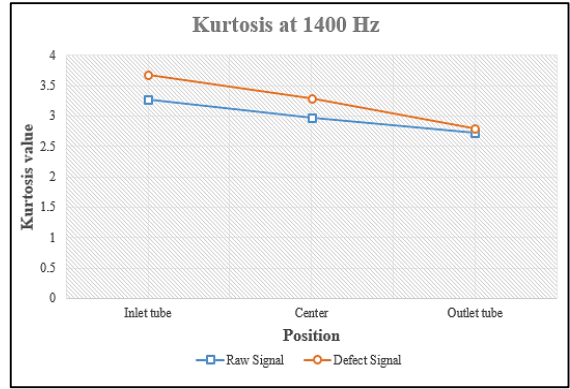


(c)

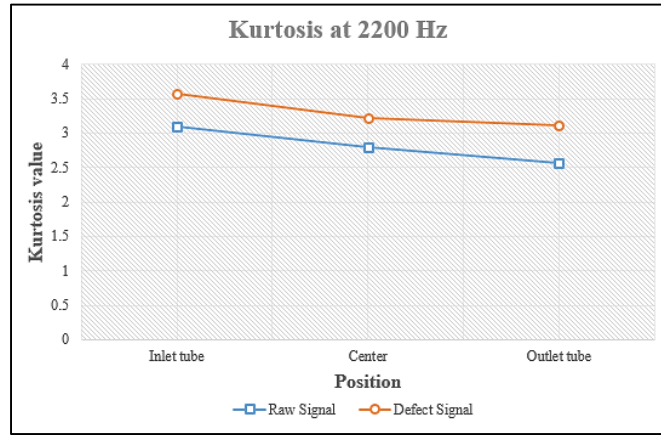
Figure 9.11. Standard deviation curve at frequencies of 550 Hz, 1400 Hz and 2200 Hz



(a)

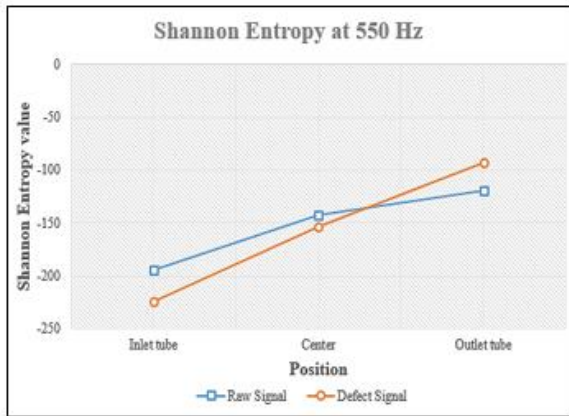


(b)

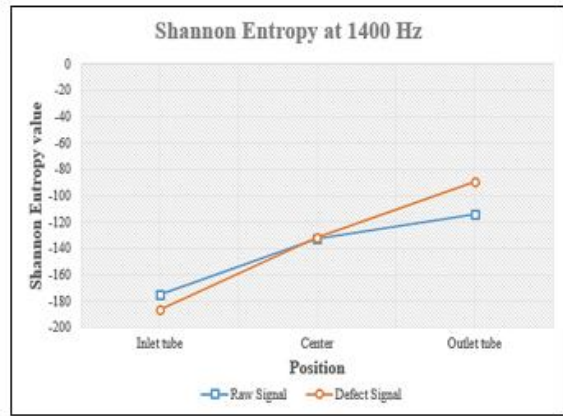


(c)

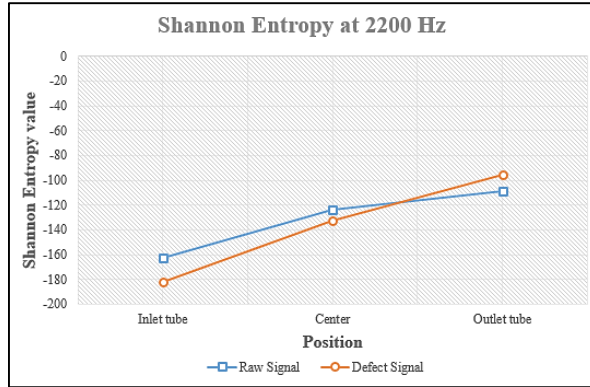
Figure 9.12. Kurtosis curve at frequencies of 550 Hz, 1400 Hz and 2200 Hz



(a)

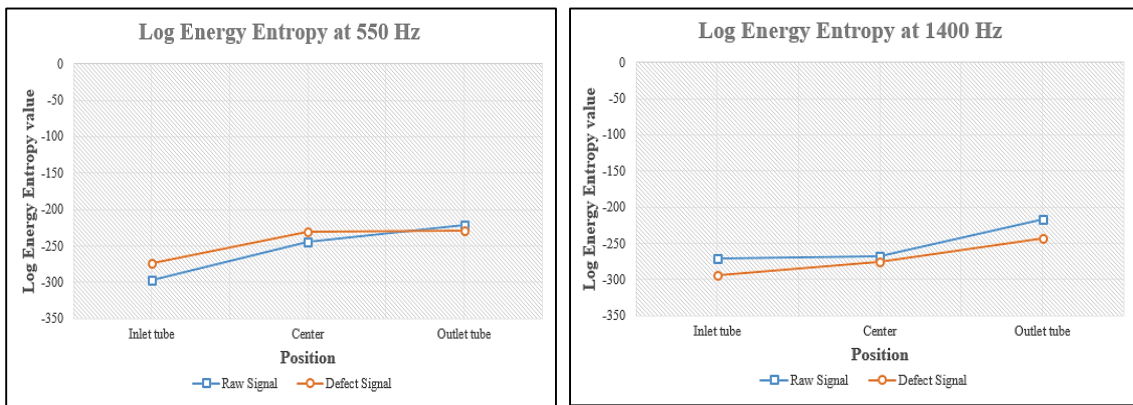


(b)



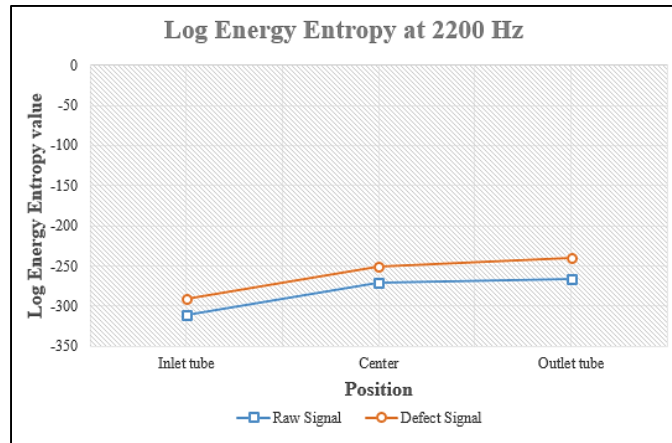
(c)

Figure 9.13. Shannon Entropy curve at frequencies of 550 Hz, 1400 Hz and 2200 Hz



(a)

(b)



(c)

Figure 9.14. Log Energy Entropy curve at frequencies of 550 Hz, 1400 Hz and 2200 Hz

Figure (9.9 – 9.14) represents the variation of the statistical parameters from the inlet tube to the outlet tube at frequencies of 550 Hz, 1400 Hz and 2200 Hz.

Sensitivity Analysis

Sensitivity analysis is a technique used to determine how changes in an input variable affect the output of a model or system. It helps to identify which variables have the greatest impact on the outcome, and can be used to assess the robustness of a model or system to changes in these variables [97]. Sensitivity analysis is commonly used in fields such as engineering, economics, and environmental science.

There are several methods for performing sensitivity analysis, including:

1. One-at-a-time (OAT) analysis: where one input variable is varied while holding all others constant.
2. Local sensitivity analysis: where the partial derivatives of the output with respect to each input variable are calculated.
3. Global sensitivity analysis: where the entire input space is explored using methods such as Monte Carlo simulation or Latin hypercube sampling.
4. Variance-based sensitivity analysis: where the total variance in the output is decomposed into contributions from each input variable.

The choice of method depends on the complexity of the model, the number of input variables, and the goals of the analysis. Once the sensitivity analysis is performed, the results can be used to identify which variables have the greatest impact on the output and to make decisions about how to modify the model or system to improve its performance.

For determining the sensitivity, chain base indexing concept is implemented in this study. Here the value of statistical parameter obtained at the inlet tube is considered as the reference value. Whereas variation of statistical parameters at the center and outlet tube of the muffler is determined by implementing the chain base indexing concept. Equation shows the relation used for chain indexing and table give the percentage change in statistical parameter value for the signals at those positions.

Applying the chain base index concept, percentage change in statistical parameter is calculated as shown in Eq. (66).

$$\% \text{ change in statistical parameter at center} = \frac{(\text{SE for signal taken at inlet tube} - \text{SE for signal taken at center})}{\text{SE for signal taken at inlet tube}} \times 100 \%$$

And

(66)

$$\% \text{ change in statistical parameter at outlet tube} = \frac{(\text{SE for signal taken at center} - \text{SE for signal taken at outlet tube})}{\text{SE for signal taken at center}} \times 100 \%$$

Table 9.9. Percentage change of statistical parameters

Frequency	Position	Shannon Entropy for raw signal	Percentage change	Shannon Entropy for defect signal	Percentage
550	Inlet tube	-194.5642		-224.5551	
550	Center	-147.0854	26.45852	-163.0952	31.82288
550	Outlet tube	-119.0972	16.76495	-92.7724	39.40214
1400	Inlet tube	-174.8823		-186.5833	
1400	Center	-146.2008	24.40584	-131.604	29.46636
1400	Outlet tube	-114.4531	13.42480	-89.4139	32.05837
2200	Inlet tube	-162.6105		-182.0791	
2200	Center	-123.7201	23.91629	-142.5908	27.17956
2200	Outlet tube	-108.3663	12.41011	-95.1546	28.23438

The table 9.9 shows that the percentage change in shannon entropy for the raw signal and defect signal from the inlet tube to the outlet tube is gradually decreasing. Further, it was observed that the percentage change in shannon entropy for the defect signals is more than raw signal at all the position. The percentage change is 31.82% and 39.4% at the center and outlet tube for the defected signal as compared to 26.46% and 16.76% respectively for the raw signals. However with the increase in frequency, the percentage change in shannon entropy was observed to be decreasing for both the raw and defected signals. A decrease in Shannon entropy value of the vibration signal indicate that the signal has become less random or more predictable. Due to the presence of sound absorption material and acoustic element which act as a damping elements, the energy loss due to the friction or air resistance. This leads to the decrease in entropy from the inlet to the outlet section.

Significance of Vibration analysis in reducing exhaust system noise

Vibration analysis was carried out on in each chamber of the muffler and the sensitivity analysis results helps us in knowing the importance of vibration analysis in muffler. Vibration analysis is done in order to see the statistical parameters for the acquired signals in different positions of the muffler. The sound pressure level obtained through simulation for the muffler is compared with the statistical parameters. It was observed that the sound

pressure level decreases from inlet to the exit of muffler and similarly the statistical parameters acquired through vibration also behaves in a similar manner. Thus this statistical parameters gives us a correlation with the SPL for the muffler. Experimentally, it is not possible to measure this sound pressure level at center i.e. at intermediate sections or at any position randomly. But vibration analysis could be performed anywhere on the chambers of the muffler. Thus vibration analysis could be considered as an alternative for measuring the behavior of reduction of noise towards the exit of muffler.

CHAPTER 10. CONCLUSIONS

Over the years, scientists and researchers are working on improving the performance of exhaust muffler through muffler design optimization. It is contributing towards providing us noise and pollution free environment. This research work is mainly divided into three sections in the process of developing an optimized muffler favorable reducing noise to a maximum amount. Section I discussed about an existing muffler and its optimization, section II discuss obtained the optimized reactive muffler and further converting it into an optimized hybrid muffler. Whereas section III develops a relation between the hybrid muffler and the vibration.

Section I: Existing muffler and optimized reactive muffler

Initially, from the literature a four-chambered reactive muffler was selected for the purpose of optimization. Aerodynamic performance analysis was performed for this muffler in ANSYS Fluent and a significant pressure drop of 6792.9 Pa from inlet and outlet of muffler was observed. Next, Comsol Multiphysics was used for performing the acoustic performance analysis and through it the maximum transmission loss of 71.04 dB was obtained at 1085 Hz. This result was validated through experimentation in Alfaacoustics Impedance tube setup and it showed a variation of only about 2.8% for the maximum transmission loss. Pilot experiments were then performed towards optimizing this existing four chambered reactive muffler. Initially, the number of baffles to be used inside the muffler is determined. Based on the widening of frequency band and suitable transmission loss, two baffles were finalized for usage in the optimized reactive muffler. Next, on the basis of pilot studies for maximum transmission loss, range of baffle plate positions, and positions of the holes were first decided. The range determined by these studies was 0 to 10 mm for the hole position (HP), 190 to 210 mm for the first baffle position from the input tube, and 90 to 110 mm for the second baffle position from the exit tube. The L9 orthogonal array was built by applying Taguchi's DOE approach and anticipating the nine trial tests that must be conducted in order to optimize the reactive muffler. Pressure acoustic frequency domain analysis provided the TL for these trails, which was then entered into MINITAB to get the S/N ratio. The parameters that were most ideal for achieving the highest value of TL was provided by the S/N ratio curve. The optimum parameters obtained through this analysis is L1=190 mm, L2=110 mm and HP=10 mm. After that, an ANOVA

analysis was performed, which supported the position of the baffles as the most important factors. Percentage contributions of performance for the first baffle near the intake and second baffle near the exit was found to be 15.91% and 83.04% respectively. The muffler with the ideal dimension was then put to the test in Comsol Multiphysics, and the findings were confirmed through experimental, with variation of only about 0.5%. The results of the simulation model and the experimental study were then compared for the present and optimized muffler designs. In simulation model maximum TL were found to be improved from 71.04 dB to 73.33 dB and in experimental validation from 69.26 dB to 72.94 dB for the optimized muffler at 1090 Hz.

Section II: Optimization of reactive muffler to hybrid muffler.

The optimized reactive muffler was then implemented with a layer of sound absorption material converting it into a hybrid muffler. Glasswool 701 was selected as the sound absorption material on the basis of pilot experiment performed for the absorption materials obtained through literature survey. Pilot experiments were then performed in terms of maximum transmission loss, towards optimizing this optimized reactive muffler. On the basis of pilot studies, the thickness of absorption material in each chamber of muffler were first decided. The range determined by these studies was 25 mm to 35 mm for all the three chambers of the optimized reactive muffler. The L16 orthogonal array was then built by applying Taguchi's DOE approach and anticipating the sixteen trial tests that must be conducted in order to optimize the muffler. Pressure acoustic frequency domain analysis was used to determine the TL for these trails and the results obtained were entered in MINITAB to get the S/N ratio. The parameters that were most ideal for achieving the highest value of TL was provided by the S/N ratio curve. This analysis showed that thickness in first chamber is zero, thickness in second and third chamber as 35 mm each are the most optimal parameters of the hybrid muffler. After that, an ANOVA analysis was performed, which supported the thickness of absorption material layer in each chamber as the most important factors. Percentage contributions of performance of thickness layer for the first, second and third chamber was found to be 75%, 19.67% and 4.42% respectively. The hybrid muffler with the ideal dimension was tested through simulation in Comsol Multiphysics and through experimentation in Impedance tube setup and variation of only about 2.23% is observed for maximum transmission loss. The results of the simulation

model and the experimental study were then compared for the optimized reactive muffler and hybrid muffler designs. In simulation model maximum TL were found to be improved from 73.33 dB to 77.59 dB, whereas in experimental validation it improved from 72.94 dB to 79.36 dB at 900 Hz for the hybrid muffler. Thus in terms of maximum transmission and better performance for wider frequencies, hybrid muffler is found to be performing better than optimized reactive muffler and existing four chambered muffler.

Section III: Developing relation between hybrid muffler and vibration.

During the experimentation of hybrid muffler, a vibration sensor i.e. accelerometer is also attached in the muffler at three different positions, one each at inlet tube, center and outlet tube respectively to acquire the vibration signals at those positions. FFT analysis was carried out to transform the time-domain signal to frequency-domain signal and it predicted 550 Hz, 1400 Hz and 2200 Hz as the most significant frequency to note spectral contents. Multi-resolution wavelet analysis was then performed in MATLAB and through maximum energy to entropy ratio, Fejer-Korovkin (fk) wavelet with $N=22$ was found to be most suitable wavelet for analyzing the signals. Statistical analysis was carried out to maintain a correlation between the sound pressure obtained through simulation and the statistical parameters. Almost all the statistical parameters were responded as maximum to the sound pressure level (SPL) of maximum and when SPL was minimum, the statistical parameters were found to be minimum. On the basis of percentage variation, Shannon entropy (SE) was found to be the most significant statistical parameter. Maximum percentage variation was found to be 68.47%, 65.29% and 62.15% for the SPL obtained through simulation and 58.69%, 52.08% and 47.74% for the SE obtained through vibration analysis. Thus the correlation between both the parameters are good and SPL can be verified, if we know the SE for it through vibration analysis. Due to this, vibration analysis could be taken as an alternative to measure sound pressure level at the middle section i.e. intermediate section which is not possible through experimentation. It can also be used for all other positions where SPL cannot be obtained through experimentation.

Application and advantage of this hybrid muffler

The hybrid muffler obtained through this research work produce maximum sound pressure level of 33.8 dB at the outlet tube of muffler, which is within the limit set by regulatory

bodies. Further this muffler is a three-chambered muffler as compared to existing muffler which is of four chamber. By reducing the number of chamber within the same space, the performance of this muffler is found to be better and within the limit set by regulatory bodies. Thus it reduced the design complexity and it would be helpful for the automotive manufacturer's to manufacture it easily at low cost. Further vibration analysis of the hybrid muffler detect the position where vibration is maximum and a possibility of failure, helping the designers to consider this parameter and design the muffler.

Future Scope of the study

In the present study, an existing muffler was optimized to a hybrid muffler where an already existing Glasswool absorption material was used. All the analysis related to it were carried out using pressure acoustic frequency domain analysis and experimentally validated. During this work, vibration signals were also acquired at specific positions at different frequencies. However, further studies could be carried out on few of the following research topics.

- Insertion Loss, which is one of the performance parameter could be used in future research work and identify the value of the mufflers used in this study. Separate experimental set up is required to measure these performance parameter.
- Research work could be carried out in developing and using an acoustic meta-material which would absorb the exhaust system noise as well as filter out the toxic exhaust gases. It would provide us noise and pollution free exhaust at the outlet of muffler.
- Develop an experimental technique to acquire the pressure fluctuation at any position inside the muffler and it should have a direct correlation with the statistical parameters.

REFERENCES

- [1] M. H. Morgan and H. L. Warren, *Vitruvius The ten books on architecture*. Harvard University Press, 1914.
- [2] D. Baumann and B. Hagg, “Musical acoustics in the middle ages,” *Early Music*, vol. 18, no. 2, pp. 199–212, 1990.
- [3] G. Galilei, “Dialogues concerning two new sciences.” The Macmillan Company, 1914.
- [4] P. Gassendi and M. Mersenne, “acoustics - Early experimentation,” *Britannica*, 2022. .
- [5] Lord Rayleigh, *The Theory of Sound*. Dovers Publication, 1945.
- [6] H. L. F. Helmholtz, *On the sensations of tone*. Forgotten Books, 1954.
- [7] R. P. Feynman, R. B. Leighton, and M. Sands, *The Feynman Lectures on Physics*, New Millen. Basic Books, New York, 1977.
- [8] R. B. Lindsay and R. S. Shankland, “Acoustics: Historical and Philosophical Development,” *Physics Today*, vol. 26, no. 12. pp. 55–56, 1973, doi: 10.1063/1.3128363.
- [9] R. B. Lindsay, *Acoustics : historical and philosophical development*. Dowden, Hutchinson & Ross, Stroudsburg, 1973.
- [10] L. E. Kinsler, A. R. Frey, A. B. Coppens, and J. V. Sanders, *Fundamentals of Acoustics*, 4th ed. John Wiley & Sons, Inc., 2000.
- [11] L. L. Beranek, *Acoustics*. Acoustical Society of America, New York, 1993.
- [12] G. B. Whitham, *Linear and nonlinear waves*. 1974.
- [13] G. J. . Ruijgrok, *Elements of Aviation Acoustics*. Delft University Press, Delft, 1990.
- [14] S. W. Rienstra and A. Hirschberg, *An Introduction to acoustics*. Eindhoven University of Technology, 2017.
- [15] A. R. Mohanty, “Acoustical Materials for automotive NVH reduction,” in *IUTAM Symposium on Designing for Quietness, Solid Mechanics and its application*, 2002, pp. 21–31.
- [16] G. A. Ambaye, “Time and frequency domain analysis of signals: a review,” *Int. J. Eng. Res. Technol.*, vol. 9, no. 12, pp. 271–276, 2020.
- [17] E. Di Giulio, M. Napolitano, A. Di Meglio, R. A. Romano, and R. Dragonetti, “Low

- frequency acoustic method to measure the complex density of porous materials,” *J. Acoust. Soc. Am.*, vol. 152, no. 4, pp. 2220–2226, 2022.
- [18] S. Lahdelma and E. Juuso, “Signal processing in vibration analysis,” *Fifth Int. Conf. Cond. Monit. Mach. Fail. Prev. Technol.*, no. July 2008, pp. 867–878, 2008.
- [19] H. Basheer and A. Khamis, “Forecasting of crude palm oil price using hybridizing wavelet and group method of data handling model,” *Malaysian J. Fundam. Appl. Sci.*, vol. 13, no. 4, pp. 642–648, 2017.
- [20] R. Polikar, *THE WAVELET TUTORIAL*, no. 552. 2004.
- [21] J. L. Taylor, *The Vibration analysis handbook*. Vibration Consultants, University of Michigan, 1994.
- [22] M.-J. Lai, “Popular Wavelet families and filters and their use,” in *Computational Complexity: Theory, Techniques, and Applications*, Springer New York, 2012, pp. 2168–2225.
- [23] S.-H. Wang, Y.-D. Zhang, Z. Dong, and P. Phillips, “Wavelet Families and variants,” in *Pathological Brain Detection*, Springer Singapore, 2018, pp. 85–104.
- [24] M. Chaudhary and A. Dhamija, “A brief study of various wavelet families and compression techniques,” *J. Glob. Res. Comput. Sci.*, vol. 4, no. 4, pp. 43–49, 2013.
- [25] M. Singh, S. Shoor, and H. Singh, “Shannon entropy a better indices for local defect detection and to study the effect of variable loading conditions for taper roller bearing,” *Int. J. Mech. Eng. Technol.*, vol. 9, no. 7, pp. 198–208, 2018.
- [26] P. Singh and S. Harsha, “Statistical and frequency analysis of vibrations signals of roller bearings using empirical mode decomposition,” *Inst. Mech. Eng.*, pp. 1–15, 2019.
- [27] D. Camarena-Martinez, M. Valtierra-Rodriguez, J. P. Amezcua-Sanchez, D. Granados-Lieberman, R. J. Romero-Troncoso, and A. Garcia-Perez, “Shannon Entropy and K -Means Method for automatic diagnosis of broken rotor bars in induction motors using vibration signals,” *Shock Vib.*, pp. 1–10, 2016.
- [28] G. D. N. P. Leite, A. M. Araujo, P. A. C. Rosas, T. Stosic, and B. Stosic, “Entropy measures for early detection of bearing faults,” *Physica A*, vol. 514, pp. 458–472, 2019.
- [29] M. L. Munjal, *Acoustics of Ducts and Mufflers with application to exhaust and*

- ventilation system design*. Inderscience Publication, John Wiley & Sons, 1987.
- [30] M. L. Munjal, *Acoustics of ducts and mufflers*. John Wiley & Son s Ltd, 2014.
- [31] M. O. Reeves and M. T. Reeves, “Exhaust muffler for engines,” 582485, 1897.
- [32] G. W. Moores, “Muffler,” 1,338,520., 1920.
- [33] S. Oldberg, “Silencer,” 2,038,309, 1936.
- [34] M. V Phelan, “Exhaust Muffler,” 3,109,510, 1963.
- [35] K. Kaari, “Muffler and exhaust systems,” 3361227, 1968.
- [36] E. Houdry, “Catalytic converter for exhaust gases,” 2674521, 1950.
- [37] E. J. Houdry, “Catalytic Muffler,” 3041149, 1962.
- [38] M. Shinhama, N. Hisashige, and F. Yokogawa, “Engine exhaust apparatus,” 5025890, 1991.
- [39] M. Fukuda, “Muffler,” 4589517, 1986.
- [40] A. Madi, I. L. Hernandez, and P. H. Rao, “Muffler With Internally Supported Tuner,” 16/733546, 2021.
- [41] V. D. Prajapati, “Design and analysis of automotive muffler,” *Int. J. Eng. Res. Technol.*, vol. 5, no. 05, pp. 384–389, 2016.
- [42] F. Sun, H. Chen, J. Wu, and K. Feng, “Sound absorbing characteristics of fibrous metal materials at high temperatures,” *Appl. Acoust.*, vol. 71, no. 3, pp. 221–235, 2010.
- [43] U. Kalita, A. Pratap, and S. Kumar, “Absorption Materials Used In Muffler A Review,” *Int. J. Mech. Ind. Technol.*, vol. 2, no. 2, pp. 31–37, 2015.
- [44] S. Amares, E. Sujatmika, T. W. Hong, R. Durairaj, and H. S. H. B. Hamid, “A Review: Characteristics of noise absorption material,” *J. Phys. Conf. Ser.*, vol. 908, no. 1, pp. 1–8, 2017.
- [45] X. Liu, X. Ma, C. Yu, and F. Xin, “Sound absorption of porous materials perforated with holes having gradually varying radii,” *Aerosp. Sci. Technol.*, vol. 120, p. 107229, 2022.
- [46] P. G. Peik, “Muffler,” US 2014666, 1935.
- [47] D. E. Sterrett, E. C. Pekarul, and T. P. Turner, “Multi-chamber muffler with selective sound absorbent material placement,” 5783782, 1998.
- [48] A. Selamet and P. M. Radavich, “The effect of length on the acoustic attenuation

- performance of concentric expansion chambers: an analytical, computational and experimental investigation,” *J. Sound Vib.*, vol. 201, no. 4, pp. 407–426, 1997.
- [49] A. Selamet, I. J. Lee, and N. T. Huff, “Acoustic attenuation of hybrid silencers,” *J. Sound Vib.*, vol. 262, no. 3, pp. 509–527, 2003.
- [50] E. Nousiainen, V. Hongisto, and M. Lindgren, “Acoustical characterization of fibrous materials by using measured flow resistivity data,” *InterNoise 2000, France*, pp. 1–4, 2000.
- [51] D. Potente, “General design principles for an automotive muffler,” in *Proceedings of Acoustics*, 2005, pp. 153–158.
- [52] S. Pal, T. S. Golan, V. Kumar, V. Jain, N. Ramdas, and O. P. Sharma, “Design of a Muffler & Effect of Resonator length for 3 Cylinder SI Engine,” *IOSR J. Mech. Civ. Eng.*, vol. 11, no. 3, pp. 85–91, 2014.
- [53] V. Sherekar and P. R. Dhamangaonkar, “Design principles for an automotive muffler,” *Int. J. Appl. Eng. Res.*, vol. 9, no. 4, pp. 483–489, 2014.
- [54] T. W. Le Roy, “Muffler characterization with implementation of the finite element method and experimental techniques,” Michigan Technological University, 2011.
- [55] A. Gadipalli, S. S. P. Thalla, A. Shaik, and G. S. Madhuri, “Study of backpressure in chambered exhaust muffler of single cylinder diesel engine,” *Int. J. Sci. Res. Rev.*, vol. 8, no. 5, pp. 529–534, 2019.
- [56] A. Abosrea, W. El-Sallamy, T. Osman, and T. Elnady, “Production cost development for commercial exhaust systems,” *Ain Shams Eng. J.*, vol. 9, no. 4, pp. 2725–2735, 2018.
- [57] F. J. H. Terashima, K. F. de Lima, N. Barbieri, R. Barbieri, and N. L. M. L. Filho, “A two-dimensional finite element approach to evaluate the sound transmission loss in perforated silencers,” *Appl. Acoust.*, vol. 192, p. 108694, 2022.
- [58] A. Vimaladass, “Investigation of Vehicle Muffler Acoustic Transmission Loss,” Kaunas University of Technology, 2022.
- [59] L. A. Al-Rahman, R. I. Raja, and R. A. Rahman, “Attenuation of noise by using absorption materials and barriers : A Review,” *Int. J. Eng. Technol.*, vol. 2, no. 7, pp. 1207–1217, 2012.
- [60] M. E. Delany and E. N. Bazley, “Acoustical properties of fibrous absorbent

- materials,” *Appl. Acoust.*, vol. 3, no. 2, pp. 105–116, 1970.
- [61] N. T. Huff, “Materials for absorptive silencer systems,” in *Proceedings of the 2001 Noise and Vibration Conference*, 2001, pp. 1680–1685.
- [62] Y. Nakagawa, “Sound absorbing material, muffler using the sound absorbing material and method for forming sound absorption layer thereof,” US 6,467,571 B2, 2002.
- [63] A. Zent and J. T. Long, “Automotive Sound Absorbing Material Survey Results,” *SAE Tech. Pap. Ser.*, 2007.
- [64] M. Sadouki, M. Fellah, Z. E. A. Fellah, E. Ogam, and C. Depollier, “Determination of the flow resistivity and thickness of porous materials with rigid frames via transmitted waves at Darcy ’ s regime,” *HAL open Sci.*, 2015.
- [65] Z. Ji, “Acoustic attenuation performance of a multi-chamber muffler with selective sound-absorbing material placement,” *SAE Tech. Pap. Ser.*, 2007.
- [66] J. F. Allard and N. Atalla, *Propagation of Sound in porous media Modelling Sound Absorption materials*, 1st ed. John Wiley & Son s Ltd, United Kingdom, 2009.
- [67] X. Sagartzazu, L. Hervella-Nieto, and J. M. Pagalday, “Review in sound absorbing materials,” *Arch. Comput. Methods Eng.*, vol. 15, no. 3, pp. 311–342, 2008.
- [68] Y. H. Guan, D. Zhao, and T. Sen Low, “Experimental evaluation on acoustic impedance and sound absorption performances of porous foams with additives with Helmholtz number,” *Aerosp. Sci. Technol.*, vol. 119, 2021.
- [69] N. Dauchez, S. Sahraoui, and N. Atalla, “Convergence of poroelastic finite elements based on Biot displacement formulation,” *J. Acoust. Soc. Am.*, vol. 109, no. 1, pp. 33–40, 2001.
- [70] X. Wang, *Automotive Tire Noise and Vibrations*, 1st ed. Butterworth-Heinemann, Elsevier, United States, 2020.
- [71] V. R. Deulgaonkar, S. P. Kallurkar, and A. G. Mattani, “Review and diagnostics of noise and vibrations in automobiles,” *Int. J. Mod. Eng. Res.*, vol. 1, no. 2, pp. 242–246, 2011.
- [72] K. S. P and A. G. Mattani, “Noise and Vibrations in Automobiles: Review and Diagnostics,” *Int. J. Mech. Prod. Eng. Res. Dev.*, vol. 1, no. 2, pp. 76–88, 2011.
- [73] A. R. Inamdar, P. A. Deshpande, and S. R. Gadekar, “Review on noise and vibration

- in automobiles,” in *4th International Conference on recent innovations in science engineering and management*, 2016, pp. 571–576.
- [74] D. D. Davis, G. M. Stokes, D. Moore, and G. L. Stevens, “Theoretical and Experimental Investigation of Mufflers with Comments on Engine-Exhaust Muffler Design,” *NACA Tech. Rep. 1192*, pp. 1–52, 1954.
- [75] B. C. Nakra, W. K. Sa’id, and A. Nassir, “Investigations on mufflers for internal combustion engines,” *Appl. Acoust.*, vol. 14, no. 2, pp. 135–145, 1981.
- [76] M. L. Munjal, “Advances in the acoustics of flow ducts and mufflers,” *Sadhana*, vol. 15, no. 2, p. 57, 1990.
- [77] S. Bilawchuk and K. R. Fyfe, “Comparison and implementation of the various numerical methods used for calculating transmission loss in silencer systems,” *Appl. Acoust.*, vol. 64, pp. 903–916, 2003.
- [78] M. B. Xu, A. Selamet, I. J. Lee, and N. T. Huff, “Sound attenuation in dissipative expansion chambers,” *J. Sound Vib.*, vol. 272, no. 3–5, pp. 1125–1133, 2004.
- [79] S. N. Y. Gerges, R. Jordan, F. A. Thieme, J. L. Bento Coelho, and J. P. Arenas, “Muffler modeling by transfer matrix method and experimental verification,” *J. Brazilian Soc. Mech. Sci. Eng.*, vol. 27, no. 2, pp. 132–140, 2005.
- [80] O. Z. Mehdizadeh and M. Paraschivoiu, “A three-dimensional finite element approach for predicting the transmission loss in mufflers and silencers with no mean flow,” *Appl. Acoust.*, vol. 66, no. 8, pp. 902–918, 2005.
- [81] Ii. Lee, “Acoustic characteristics of Perforated dissipative and hybrid silencers,” Ohio State University, 2005.
- [82] H. Erol and Ö. Ahmeto, “Acoustic attenuation in fully-filled perforated dissipative mufflers with extended inlet / outlet,” *ICSV13-Vienna*, vol. 1, pp. 1–7, 2006.
- [83] Z. Ji, S. Su, and C. Liu, “Acoustic attenuation performance analysis of three-pass perforated tube muffler with end-resonator,” *SAE Tech. Pap.*, vol. 1, no. 1, pp. 783–791, 2008.
- [84] K. S. Andersen, “Analyzing Muffler Performance Using the Transfer Matrix Method,” in *Proceedings of the COMSOL Conference*, 2008, pp. 1–7.
- [85] K. S. Andersen, “Analysis of exhaust elements using the transfer matrix method,” *SAE Tech. Pap.*, 2010.

- [86] R. B. Anderson, B. Yost, M. Stone, and T. Lei, "Impedance tube and sample holder," US 10 , 345 , 140 B1, 2019.
- [87] A. Allam and T. Elnady, "Characterization of mufflers," *Proc. 22nd Int. Congr. Acoust.*, 2016.
- [88] W. Elsahar and T. Elnady, "Measurement and Simulation of Two-Inlet Single-Outlet Mufflers," *SAE Int. J. Passeng. Cars - Mech. Syst.*, vol. 8, Jun. 2015.
- [89] T. Elnady, S. Allam, and M. Abom, "Modeling perforates in mufflers using two-ports," *J. Vib. Acoust.*, vol. 132, pp. 1–11, 2010.
- [90] P. Chaitanya and M. L. Munjal, "Tuning of the Extended Concentric Tube Resonators," *Symp. Int. Automot. Technol.*, 2011.
- [91] Y. L. Shao, "A study on exhaust muffler using a mixture of counter-phase counteract and split-gas rushing," *Procedia Eng.*, vol. 15, pp. 4409–4413, 2011.
- [92] Y. Zhang, P. Wu, Y. Ma, H. Su, and J. Xue, "Analysis on acoustic performance and flow field in the split-stream rushing muffler unit," *J. Sound Vib.*, vol. 430, pp. 185–195, 2018.
- [93] S. Kamarkhani and A. Mahmoudi Kohan, "Muffler design with baffle effect and performances on transmission loss," *Mech. Mech. Eng.*, vol. 22, no. 4, pp. 1337–1343, 2018.
- [94] M. A. Rojan, Z. Alias, S. A. Bakar, and S. Hashim, "Enhancement of MODENAS CT115'S motorcycle muffler performance by optimization of backpressure," *IOP Conf. Ser. Mater. Sci. Eng.*, vol. 670, pp. 1–5, 2019.
- [95] L. Zhang, H. M. Shi, X. H. Zeng, and Z. Zhuang, "Theoretical and experimental study on the transmission loss of a side outlet muffler," *Shock Vib.*, 2020.
- [96] J. K. Lee, K. S. Oh, and J. W. Lee, "Methods for evaluating in-duct noise attenuation performance in a muffler design problem," *J. Sound Vib.*, vol. 464, pp. 1–62, 2020.
- [97] J. K. Lee, I. Lee, and J. W. Lee, "Reliability-based acoustical topology optimization of mufflers under noise frequency and temperature uncertainties," *Mech. Syst. Signal Process.*, vol. 160, p. 107854, 2021.
- [98] J. W. Lee, "Optimal topology of reactive muffler achieving target transmission loss values: Design and experiment," *Appl. Acoust.*, vol. 88, pp. 104–113, 2015.
- [99] P. Xiao and M. G. Prasad, "Insertion loss studies of a baffle-simple expansion

- chamber system,” *J. Acoust. Soc. Am.*, vol. 97, no. 5, pp. 3255–3255, 1995.
- [100] S. Xiao, F. Yan, Z. Liu, and C. Lu, “Study on the acoustic performance of expansion muffler based on comprehensive analysis of acoustic modal and transmission loss,” *Int. Conf. Inf. Syst. Comput. Aided Educ.*, pp. 101–107, 2018.
- [101] H. Han, S.-S. Chae, and Y.-C. Kim, “Analytical design of muffler based on transmission loss calculation,” *FISITA World Automot. Congr.*, pp. 1–6, 2000.
- [102] J. Choi *et al.*, “Structural optimization of an automobile transmission case to minimize radiation noise using the model reduction technique,” *J. Mech. Sci. Technol.*, vol. 25, no. 5, pp. 1247–1255, 2011.
- [103] D. E. Sterrett, E. C. Pekar, and T. P. Turner, “Multi-chamber muffler with selective sound absorbent material placement,” US 5783782, 1998.
- [104] C. E. Nelson, “Silencer,” US 2072961, 1937.
- [105] U. Schmidt, “Sound muffling device,” US 2101460, 1937.
- [106] W. L. Manning, “Silencer,” US 2166417, 1939.
- [107] G. Wolfhugel, “Muffler,” US 4396090, 1983.
- [108] T. W. Hetherington, “Acoustic Muffler,” US 4846302, 1989.
- [109] D. Garey, “Light weight hybrid exhaust muffler,” US 4901816, 1990.
- [110] R. R. Udell, “Noise attenuation apparatus,” US 4930597, 1990.
- [111] L. Valdman, “Noise suppressing device,” WO 00/32910, 2000.
- [112] G. Zhang, “Muffler,” US 7779962 B2, 2010.
- [113] A. Craggs, “A finite element method for modelling dissipative mufflers with a locally reactive lining,” *J. Sound Vib.*, vol. 54, no. 2, pp. 285–296, 1977.
- [114] M. Chiu, “Optimization Design of Hybrid Mufflers on Broadband Frequencies Using the Genetic Algorithm,” *Arch. Acoust.*, vol. 36, no. 4, pp. 795–822, 2011.
- [115] M. C. Chiu, “Numerical assessment for a broadband and tuned noise using hybrid mufflers and a simulated annealing method,” *J. Sound Vib.*, vol. 332, no. 12, pp. 2923–2940, 2013.
- [116] P. Šteblaj, M. Čudina, P. Lipar, and J. Prezelj, “A muffler with adaptive acoustic properties,” *J. Mech. Eng.*, vol. 61, no. 10, pp. 553–560, 2015.
- [117] S. Pal, “Design and acoustic analysis of hybrid muffler,” *Int. J. Ignited Minds*, vol. 1, no. 4, pp. 1–10, 2015.

- [118] A. K. Gupta and D. A. Tiwari, "Performance of Transmission Loss on Hybrid Muffler by Using Rock Wool and Glass Fiber as a Absorbing Materials," *Int. J. Adv. Mater. Sci. Eng.*, vol. 4, no. 4, pp. 49–57, 2015.
- [119] A. K. Gupta, "Simulation and Experimental Validation of Sound Transmission Loss of Pure Reactive Muffler with Different Expansion Ratio," *Int. J. Adv. Res. Trends Eng. Technol.*, vol. 3, no. 4, pp. 49–52, 2016.
- [120] H. Huang, Z. Ji, and Z. Li, "Influence of perforation and sound-absorbing material filling on acoustic attenuation performance of three-pass perforated mufflers," *Adv. Mech. Eng.*, vol. 10, no. 1, pp. 1–11, 2018.
- [121] Y. Chang, M. Chiu, and S. Huang, "Numerical analysis of circular straight mufflers equipped with three chambers at high-order-modes," *Appl. Acoust.*, vol. 155, pp. 167–179, 2019.
- [122] U. Kalita and M. Singh, "Design and CFD Analysis on Flow Through a Reactive Muffler of Four-Cylinder Diesel Engine," in *Recent Trends in Engineering Design, Lecture Notes in Mechanical Engineering*, vol. 222, Springer Nature Singapore Pte Ltd, 2021, pp. 211–223.
- [123] U. Kalita and M. Singh, "Optimization of a reactive muffler used in four-cylinder petrol engine into hybrid muffler by using CFD analysis," *Mater. Today Proc.*, vol. 50, no. 5, pp. 1936–1945, 2022.
- [124] U. Kalita and M. Singh, "Prediction of transmission loss in muffler on varying the flow resistivity of absorption material," *J. Emerg. Technol. Innov. Res.*, vol. 6, no. 3, pp. 674–679, 2019.
- [125] M. M. Patne, S. Senthilkumar, and M. Jerome Stanley, "Numerical analysis on improving transmission loss of reactive muffler using various sound absorptive materials," *IOP Conf. Ser. Mater. Sci. Eng.*, vol. 993, no. 1, 2020.
- [126] T. Zaw, A. Abu, N. Fawazi, and A. M. Wahab, "Effects of Parameters of Helmholtz Resonator on Transmission Loss of Hybrid Muffler," *Int. J. Eng. Technol.*, vol. 7, pp. 151–157, 2018.
- [127] Y. Fan and Z. Ji, "Three-pass mufflers with perforated inlet/outlet tubes," *Appl. Acoust.*, vol. 156, pp. 217–228, 2019.
- [128] G. M. L. Gladwell and V. Mason, "Variational finite element calculation of the

- acoustic response of a rectangular panel,” *J. Sound Vib.*, vol. 14, no. 1, pp. 115–135, 1971.
- [129] C. J. Young and M. J. Crocker, “Prediction of transmission loss in mufflers by the finite-element method,” *J. Acoust. Soc. Am.*, vol. 57, no. 1, pp. 144–148, 1975.
- [130] A. Elsayed, C. Bastien, H. Medina, S. Jones, and H. Kassem, “Enhancing noise attenuation in exhaust mufflers on response to baffle configuration,” *Int. J. Eng. Manuf.*, vol. 7, no. 4, pp. 12–25, 2017.
- [131] J. G. Cherng, W. Wu, P. Ding, M. Hebbes, and H. Zhang, “Design Optimization of Vehicle Muffler Transmission Loss using Hybrid Method,” *SAE Tech. Pap.*, 2015.
- [132] X. Wang, *Vehicle noise and vibration refinement*. Woodhead Publishing Limited, CRC Press, New York, 2010.
- [133] K. S. Won and J. Choe, “Transmission loss analysis in a partitioned duct with porous boundaries based on combination of FEM and measurement of sound absorption coefficients,” *Appl. Acoust.*, vol. 165, p. 107291, 2020.
- [134] D. Wiemeler, A. Jauer, and J. F. Brand, “Flow noise level prediction methods of exhaust system tailpipe noise,” *SAE Tech. Pap.*, 2008.
- [135] J. Fang, Y. Zhou, P. Jiao, and Z. Ling, “Study on pressure loss for a muffler based on CFD and experiment,” in *International Conference on Measuring Technology and Mechatronics Automation*, 2009, pp. 887–890.
- [136] J. Fang, Y. Zhou, X. Hu, and L. Wang, “Measurement and Analysis of Exhaust Noise from Muffler on an Excavator,” *Int. J. Precis. Eng. Manuf.*, vol. 10, no. 5, pp. 59–66, 2009.
- [137] Y. Yao, S. Wei, J. Zhao, S. Chen, Z. Feng, and J. Yue, “Experiment and CFD analysis of reactive muffler,” *Res. J. Appl. Sci. Eng. Technol.*, vol. 6, no. 17, pp. 3282–3288, 2013.
- [138] L. Liu, Z. Hao, and C. Liu, “CFD analysis of a transfer matrix of exhaust muffler with mean flow and prediction of exhaust noise,” *J. Zhejiang Univ. Sci. A*, vol. 13, no. 9, pp. 709–716, 2012.
- [139] S.-J. Liu, J.-J. Zeng, W.-W. Han, Y. Chen, and J. Wang, “Intake and exhaust system performance of diesel engine based on CFD and steady flow test method,” *Trans. Chinese Soc. Intern. Combust. Engines*, vol. 34, pp. 68–73, Jan. 2016.

- [140] J. Xu and S. Zhou, "Analysis of flow field for automotive exhaust system based on computational fluid dynamics," *Open Mech. Eng. J.*, vol. 8, no. 1, pp. 587–593, 2014.
- [141] P. Wang, J. Li, and T. Wu, "Numerical Determination of Transfer Impedance for Perforates," *SAE Int. J. Passeng. Cars - Mech. Syst.*, vol. 8, no. 3, pp. 1003–1008, 2015.
- [142] P. Saripalli, "CFD Analysis on Flow Through a Resistance Muffler of LCV Diesel Engine," *Int. J. Sci. Technol. Soc.*, vol. 3, no. 4, p. 162, 2015.
- [143] C. G. Puneetha, H. Manjunath, and M. R. Shashidhar, "Backpressure Study in Exhaust Muffler of Single Cylinder Diesel Engine using CFD Analysis Shell Outlet pipe Inlet pipe Perforated pipe," *Altair Technol. Conf.*, pp. 1–14, 2015.
- [144] C. P. Om Ariara Guhan, G. Arthanareeswaren, and K. N. Varadarajan, "CFD Study on Pressure Drop and Uniformity Index of Three Cylinder LCV Exhaust System," *Procedia Eng.*, vol. 127, pp. 1211–1218, 2015.
- [145] C. P. O. A. Guhan, G. Arthanareeswaran, K. N. Varadarajan, and S. Krishnan, "ScienceDirect Exhaust System Muffler Volume Optimization of Light Commercial Vehicle Using CFD Simulation," *Mater. Today Proc.*, vol. 5, no. 2, pp. 8471–8479, 2018.
- [146] S. Talegaonkar, M. Agrewale, and K. C. Vora, "Design and Development of Tunable Exhaust Muffler for Race Car," *SAE Tech. Pap.*, Feb. 2016.
- [147] E. M. Milad and M. Jolgaf, "Acoustic Analysis of a Perforated-pipe Muffler Using ANSYS," *Univ. Bull.*, vol. 4, no. 19, pp. 45–56, 2017.
- [148] A. Prasad and R. C. Thiagarajan, "Acoustic Performance Design of Automotive Muffler ," 2015.
- [149] D. Tutunea, M. X. Calbureanu, and M. Lungu, "The computational fluid dynamics (CFD) study of fluid dynamics performances of a resistance muffler," *Int. J. Mech.*, vol. 7, no. 4, pp. 401–408, 2013.
- [150] S. D. Pangavhane, A. B. Ubale, V. A. Tandon, and D. R. Pangavhane, "Experimental and CFD analysis of a perforated inner pipe muffler for the prediction of Backpressure," *Int. J. Eng. Technol.*, vol. 5, no. 5, pp. 3940–3950, 2013.
- [151] P. C. Rao, B. M. Varma, and L. V. V. G. Rao, "Muffler Design , Development and

- Validation Methods,” vol. v, pp. 8626–8639, 2016, doi: 10.15680/IJRSET.2016.0505288.
- [152] V. M. Mundhe and E. R. Deore, “Design and analysis of perforated muffler in Automobile Exhaust System,” *Int. J. Multidiscip. Res. Dev. Vol.*, vol. 2, pp. 182–187, 2015.
- [153] M. M. Krishnan, G. A. Jose, S. D. Linston, and T. S. L. Prasath, “Acoustic Analysis of Reactive Muffler,” *Int. J. Mech. Eng.*, vol. 6, no. 3, pp. 1507–1514, 2021.
- [154] A. S. Bonnet-Bendhia, D. Drissi, and N. Gmati, “Simulation of muffler’s transmission losses by a homogenized finite element method,” *J. Comput. Acoust.*, vol. 12, no. 3, pp. 447–474, 2004.
- [155] S. Kore, A. Aman, and E. Direbsa, “Performance evaluation of a reactive muffler using CFD,” *J. EEA*, vol. 28, pp. 83–89, 2011.
- [156] S. M. Trivedi, “CFD Flow Analysis and Optimization of Exhaust Muffler,” *Int. J. Res. Appl. Sci. Eng. Technol.*, vol. V, no. VIII, pp. 86–91, 2017.
- [157] S. Dondapati, M. Trivedi, R. S. Dondapati, and D. Chandra, “Investigation on the mechanical stresses in a muffler mounting bracket using Root Cause Failure Analysis (RCFA), finite element analysis and experimental validation,” *Eng. Fail. Anal.*, vol. 81, pp. 145–154, 2017.
- [158] N. Patil and S. Chaudhary, “CFD analysis of exhaust backpressure for four-stroke CI engine,” *Int. J. Res. Trends Innov.*, vol. 3, no. 6, pp. 247–252, 2018.
- [159] P. Puhan, D. K. Sahu, and D. Mishra, “CFD Analysis of a perforated inner pipe exhaust muffler for the prediction of Transmission Loss and backpressure using reverse engineering,” in *Proceedings of the 7th International and 45th National Conference on Fluid Mechanics and Fluid Power*, 2018, pp. 1–4.
- [160] A. J. Torregrosa, A. Gil, L. M. García-Cuevas, P. Quintero, and F. D. Denia, “Prediction of the transmission loss in a flexible chamber,” *J. Fluids Struct.*, vol. 82, pp. 134–153, 2018.
- [161] C. George T and H. G. V. Raj, “Energy efficient design and modification of an automotive exhaust muffler for optimum noise , transmission loss , insertion loss and back pressure: A Review,” in *IOP Conf. Series: Materials Science and Engineering*, 2018, pp. 1–12.

- [162] C. Nardari, A. Mann, and T. Schindele, “Exhaust and Muffler Aeroacoustics Predictions using Lattice Boltzmann Method,” *SAE Tech. Pap.*, vol. 1, pp. 1–8, May 2018.
- [163] B. Mohamad, J. Karoly, A. Zelentsov, and S. Amroune, “A hybrid method technique for design and optimization of formula race car exhaust muffler,” *Int. Rev. Appl. Sci. Eng.*, vol. 11, no. 2, pp. 174–180, 2020.
- [164] P. P. Hujare, V. R. Mote, A. R. Mache, D. P. Hujare, and S. S. Kore, “Analysis for effect of pores on acoustic performance of reactive muffler,” *Noise Vib. Worldw.*, vol. 52, no. 9, pp. 285–292, 2021.
- [165] M. Saadabadi, M. Samimi, and H. Hosseinlghab, “Organized Computational Measurement to Design a High-Performance Muffler,” *Metrol. MDPI*, no. 3, pp. 254–279, 2023.
- [166] J. Song, Y. Liu, Z. Yu, and H. Jin, “Digital design and experimental testing of a compressor’s suction muffler transmission loss,” *Appl. Math. Nonlinear Sci.*, vol. 3, no. 2, pp. 571–582, 2023.
- [167] A. Kashikar, R. Suryawanshi, N. Sonone, R. Thorat, and S. Savant, “Development of muffler design and its validation,” *Appl. Acoust.*, vol. 180, p. 108132, 2021.
- [168] T. P. Bagchi, *TAGUCHI methods explained: Practical Steps to robust design*. 1993.
- [169] R. K. Roy, *Design of Experiments Using the Taguchi Approach: 16 Steps to Product and Process Improvement*. 2001.
- [170] P. Sandips, P. S. M, B. A. P, and A. D. Sahasrabudhe, “FEM Analysis and Optimization of Two Chamber Reactive Muffler by using Taguchi Method,” *Am. Int. J. Res. Sci. Technol. Eng. Math.*, pp. 21–28, 2013.
- [171] A. Kashikar, R. Suryawanshi, N. Sonone, R. Thorat, and S. Savant, “Development of muffler design and its validation,” *Appl. Acoust.*, vol. 180, p. 108132, 2021.
- [172] S. S. Gosavi, V. M. Juge, and M. M. M. Nadgouda, “Optimization of Suction Muffler Using Taguchi ’s DOE Method,” *Int. Compress. Eng. Conf.*, 2006.
- [173] T. C. Yang and S. S. Tsai, “Design optimization of an industrial muffler by taguchi method,” *Adv. Mater. Res.*, vol. 871, pp. 277–282, 2014.
- [174] S. Naikwad, A. Salunkhe, M. Bamane, and A. Bhoite, “Design, assessment and optimization of automotive muffler,” *Int. J. Innov. Res. Sci. Eng. Technol.*, vol. 6,

- no. 5, pp. 7384–7397, 2017.
- [175] T. C. Jagtap and S. N. Khairnar, “Performance evaluation of muffler by using fem and fft analyzer,” *Proc. 1st Shri Chhatrapati Shivaji Maharaj QIP Conf. Eng. Innov.*, pp. 252–255, 2018.
- [176] T. C. Jagtap, S. S. Raut, A. Ambesange, and S. N. Khairnar, “Vibration Analysis of muffler by using FEM and FFT analysis,” *IJARIE*, vol. 4, no. 2, pp. 2888–2894, 2018.
- [177] A. Ambesange and T. C. Jagtap, “Analysis of Exhaust Muffler By Using FEM & FFT Analyzer,” *IJARIE*, vol. 5, no. 5, pp. 401–406, 2019.
- [178] T. J. Sutton, S. J. Elliott, M. McDonald, and T. J. Saunders, “Active control of road noise inside vehicles,” *J. noise Control Eng.*, vol. 42, no. 4, pp. 137–146, 1994.
- [179] A. Frederick and S. Brady, “Vibration Analysis on an Automobile Muffler,” Miami University, 2003.
- [180] A. R. Simon, K. A. Reddy, and B. Prashanth, “Vibrational analysis of muffler,” *Int. J. Sci. Dev. Res.*, vol. 2, no. 2, pp. 59–64, 2017.
- [181] A. Mohanty and S. Fatima, “An overview of automobile noise and vibration control,” *Noise Notes*, vol. 13, no. 1, pp. 43–56, 2014.
- [182] K. P. K. Reddy, S. Fatima, and A. R. Mohanty, “A new sound quality metric for the design of engine exhaust mufflers,” in *Proceedings of the Institution of Mechanical Engineers, Part D: Journal of Automobile Engineering*, 2017, no. 1, pp. 1–10.
- [183] S. V. S. Sreeramagiri and T. Bhavani, “NVH And Structural Adaptations in Automobiles: A Perspective,” *Int. J. Eng. Res. Technol.*, vol. 10, no. 1, pp. 307–315, 2021.
- [184] A. R. Mohanty and S. P. Pattnaik, “An Optimal Design Methodology for a Family of Perforated Mufflers,” *SAE Tech. Pap.*, no. January, 2005.
- [185] N. Barbieri, R. Barbieri, and K. F. De Lima, “Errors in transmission loss prediction - the bispectrum and kurtosis approaches,” *Mech. Syst. Signal Process.*, vol. 18, no. 2, pp. 223–233, 2004.
- [186] R. Barbieri and N. Barbieri, “Finite element acoustic simulation based shape optimization of a muffler,” *Appl. Acoust.*, vol. 67, no. 4, pp. 346–357, 2006.
- [187] V. P. Patekar and R. B. Patil, “Vibrational analysis of automotive exhaust silencer

- based on FEM and FFT analyzer,” *Int. J. Emerg. Technol.*, vol. 3, no. 2, pp. 1–3, 2012.
- [188] Sunil and S. P. M, “Experimental Modal Analysis of Automotive Exhaust Muffler Using Fem and FFT Analyzer,” *Int. J. Recent Dev. Eng. Technol.*, vol. 3, no. 1, p. 185, 2014.
- [189] S. Mittal and D. K. C. More, “Design and vibrational characteristic analysis of exhaust manifold with experimental validation using FFT analyzer,” *Int. J. Adv. Res. Sci. Commun. Technol.*, vol. 7, no. 2, pp. 645–665, 2021.
- [190] B. J. Schwarz and M. H. Richardson, “Experimental Modal analysis,” *CSI Reliab. week*, pp. 1–12, 1999.
- [191] W. Jie and D. Yue, “The modal analysis of automotive exhaust muffler based on PRO/E and ANSYS,” in *3rd International Conference on Advanced Computer Theory and Engineering(ICACTE)*, 2010, vol. 6.
- [192] K. A. Reddy, “A Comprehensive Study of Acoustic Techniques in Different Mufflers,” *Int. J. Sci. Dev. Res.*, vol. 1, no. 8, pp. 345–350, 2016.
- [193] T. H. E. E. Parliament, T. H. E. Council, O. F. The, and E. Union, “Regulation (EU) No 540/2014 of the European Parliament and of the Council of 16 April 2014,” *Off. J. Eur. Union L 158/131*, vol. 2013, no. 540, 2014.
- [194] E. Ryan, “European communities (environmental noise) (amendment) regulations,” 2021.
- [195] European commission, “The noise policy of the European Union,” *European commission*, vol. 105, no. 2. pp. 1376–1376, 1999.
- [196] W. H. Organization, *Night noise guidelines for Europe*. 2009.
- [197] N. Garg and S. Maji, “A retrospective view of noise pollution control policy in India: Status, proposed revisions and control measures,” *Curr. Sci.*, vol. 111, no. 1, pp. 29–38, 2016.
- [198] I. V. Muralikrishna and V. Manickam, *Noise Pollution and Its Control*. 2017.
- [199] J. . Middelberg, T. J. Barber, S. . Leong, K. . Byrne, and E. Leonardi, “Computational Fluid Dynamics analysis of the acoustic performance of various simple expansion chamber mufflers,” in *Proceedings of Acoustics*, 2004, pp. 123–128.

- [200] Anant W. Wankhade and Dr. A. P. Bhattu, "Optimization and Experimental Validation of Elliptical Reactive Muffler with Central Inlet Central Outlet," *Int. J. Eng. Res.*, vol. V4, no. 05, pp. 1321–1328, 2015.
- [201] J. Ma and P. Guo, "Analysis of performance of automotive exhaust muffler based on ANSYS finite element," *Appl. Mech. Mater.*, vol. 509, pp. 118–122, 2014.
- [202] Z. Zhou, "Vibro-acoustic analysis for muffler design," *Sound Vib.*, vol. 48, no. 12, pp. 15–16, 2014.
- [203] M. Deaconu, D. Radulescu, and G. Vizitiu, "Acoustic study of different mufflers based on metamaterials using the black hole principle for aircraft industry," in *Euronoise 2018*, 2018, pp. 2271–2276.
- [204] A. P. Bhattu, "Analysis and optimal design of hybrid silencers," University of Pune, 2014.
- [205] K. M. Kumar, "Direct estimation of acoustic source characteristics of the internal combustion engine exhaust system and analysis of complex muffler configurations," IISC, Bangalore, 2018.
- [206] D. Neihguk and A. Prasad, "Effect of Manufacturing Defects in the form of Internal Leakages on the Acoustic Performance of Mufflers," *Proc. COMSOL Conf.*, pp. 2–6, 2016.
- [207] P. B. Bhadke and K. A. Mahajan, "Effect of change in diameter on muffler transmission loss using COMSOL," *IOSR J. Mech. Civ. Eng.*, pp. 41–46, 2017.
- [208] C. Multiphysics, "Absorptive Muffler," *COMSOL Multiphysics 6.1*. <https://www.comsol.com/model/absorptive-muffler-1367>.
- [209] C. Multiphysics, C. Software, and L. Agreement, "Muffler with Perforates," pp. 1–22, 2013.
- [210] P. Cawley and R. D. Adams, "The mechanics of the coin-tap method of non-destructive testing," *J. Sound Vib.*, vol. 122, no. 2, pp. 299–316, 1988.
- [211] P. Cawley and R. D. Adams, "Sensitivity of the coin-tap method of nondestructive testing," *Mater. Eval.*, vol. 47, no. 5, pp. 558–563, 1989.
- [212] P. Cawley, "A high frequency coin-tap method of non-destructive testing," *Mech. Syst. Signal Process.*, vol. 5, no. 1, pp. 1–11, 1991.
- [213] J. Gryzagoridis and D. Findeis, "Tap testing vs. Thermography," *54th Annu. Br.*

- Conf. Non-Destructive Testing, NDT 2015*, no. 1, pp. 1–8, 2015.
- [214] G. C. C. da Silva, M. A. de A. Nunes, R. V. Lopes, and A. B. A. Junior, “Design and construction of a low cost impedance tube for sound absorption coefficients measurements,” in *22nd International Congress of Mechanical Engineering*, 2013, pp. 105–115.
- [215] M. Suhanek, K. Jambrosic, and H. Domitrovic, “Student project of building an impedance tube,” in *Proceedings of Acoustics*, 2008, pp. 4479–4484.
- [216] D. W. Herrin, “Measurement of Sound Absorption and Impedance.”
- [217] S. P. Deshpande and M. D. Rao, “Development of a low cost impedance tube to measure acoustic absorption and transmission loss of materials,” *121st ASEE Annu. Conf. Expo.*, 2014.
- [218] Brüel & Kjær, “Product Data Impedance Tube Kit Type 4206,” pp. 145–180, 2019.
- [219] J. Chen and D. W. Herrin, “Description and validation of a muffler insertion loss flow rig,” *INTER-NOISE 2019 MADRID - 48th Int. Congr. Exhib. Noise Control Eng.*, 2019.
- [220] A. K. Gupta, “Studies on noise reduction of acoustic reactive mufflers,” Devi Ahilya Vishwavidyalaya Indore, 2015.
- [221] P. Shravage, “Muffler Test Rig,” *Alfaacoustics*. .
- [222] A. Internationals, “ASTM E2611 Standard Test Method for normal incidence determination of porous material acoustical properties based on the Transfer Matrix Method,” 2017.
- [223] A. Internationals, “ASTM E2611 Standard Test Method for Normal Incidence Determination of Porous Material Acoustical Properties Based on the Transfer Matrix Method,” 2019.
- [224] EUROPEAN STANDARD, “Acoustics - Determination of sound power levels and sound energy levels of noise sources using sound pressure - Engineering methods for an essentially free field over a reflecting plane (ISO 3744:2010),” 2010.
- [225] S. Das *et al.*, “A novel design for muffler chambers by incorporating baffle plate,” *Appl. Acoust.*, vol. 197, 2022.
- [226] A. Selamet, F. D. Denia, and A. J. Besa, “Acoustic behavior of circular dual-chamber mufflers,” *J. Sound Vib.*, vol. 265, pp. 967–985, 2003.

- [227] A. Selamat and Z. L. Ji, "Acoustic attenuation performance of circular expansion chambers with extended inlet / outlet," *J. Sound Vib.*, vol. 223, no. 2, pp. 197–212, 1999.
- [228] H. Arslan, M. Ranjbar, E. Secgin, and V. Celik, "Theoretical and experimental investigation of acoustic performance of multi- chamber reactive silencers," *Appl. Acoust.*, vol. 157, no. January, p. 106987, 2020.
- [229] P. S. Khanzode and M. V. Kulkarni, "Acoustic analysis and optimization of double expansion chamber reactive muffler for maximum transmission," *Int. J. Sci. Technol. Res.*, vol. 8, no. 9, pp. 2351–2355, 2019.
- [230] N. Sohei, N. Tsuyoshi, and Y. Takashi, "Acoustic analysis of elliptical muffler chamber having a perforated pipe," *J. Sound Vib.*, vol. 297, no. 3–5, pp. 761–773, 2006.

APPENDICES

1. Analytical method for calculating transmission loss

Initially, at $x = 0$ the equation for continuity of mass flow is given in Eq. 1.

$$\rho S_1(u_a + u_c) = \rho S_2(u_b + u_d) \quad (1)$$

Implementing $u = \pm \frac{p'}{\rho c}$ in the above Eq. 45, it reduce to

$$S_1(A - C) = S_2(B - D) \quad (2)$$

Equation for pressure is given in Eq. 3 and implementing particle velocity in it, it is deduced as shown in Eq. 4.

$$p'_a + p'_c = p'_b + p'_d \quad (3)$$

$$\text{i.e. } A + C = B + D \quad (4)$$

Similarly, at $x = 1$, the continuity equation and equation for pressure will be as shown from Eq. (5-8).

$$\rho S_2(u_b + u_d) = \rho S_1 u_f \quad (5)$$

$$S_2 \left(B e^{-i\frac{\omega l}{c}} - D e^{i\frac{\omega l}{c}} \right) = S_1 \cdot f \quad (6)$$

$$p'_b + p'_d = p'_f \quad (7)$$

$$B e^{-i\frac{\omega l}{c}} + D e^{i\frac{\omega l}{c}} = F \quad (8)$$

Solving the above Eqs. (3-8), we get Eq. 9.

$$\frac{A}{F} = \frac{\left(\frac{S_2}{S_1} + 1\right)^2}{4 \frac{S_2}{S_1}} e^{i\frac{\omega l}{c}} - \frac{\left(\frac{S_2}{S_1} - 1\right)^2}{4 \frac{S_2}{S_1}} e^{-i\frac{\omega l}{c}}$$

$$\text{i.e. } \frac{A}{F} = \cos \frac{\omega l}{c} + i \cdot \frac{1}{2} \left[\frac{S_1}{S_2} + \frac{S_2}{S_1} \right] \sin \frac{\omega l}{c} = \frac{A_i}{A_t} \quad (9)$$

Where A_i = Amplitude of incident pressure wave, A_t = Amplitude of transmitted pressure wave

Now, the transmission loss is determined as

$$\text{Transmission loss (TL)} = 10 \log_{10} \left| \frac{A_i}{A_t} \right|^2$$

$$\begin{aligned}
TL &= 10\log_{10} \left[1 + \frac{1}{4} \left(\frac{S_1}{S_2} - \frac{S_2}{S_1} \right)^2 \sin^2 kl \right] \\
TL &= 10\log_{10} \left[1 + \frac{1}{4} \left(m - \frac{1}{m} \right)^2 \sin^2 kl \right] \quad (10)
\end{aligned}$$

Where $m = \text{expansion ratio} = S_1/S_2$ and S_1, S_2 are the cross-section areas of inlet tube and chamber respectively.

k (wave number) $= \omega/c = 2\pi f/c$, $c = \text{speed of sound}$ and ω and f are angular velocities in rad/sec and Hz respectively, $l = \text{length of expansion chamber}$

This theory might be applicable to several types of reactive mufflers and the stages that make them up. The relationship between the three pressure waves at the junction of each chamber can be calculated using the amplitude ratios.

2. Transfer matrix method for calculating transmission loss

Transfer Matrix for the uniform tube

For a uniform tube, the transfer matrix can be obtained by using the standard wave equations. The sound pressure and the particle velocity for the uniform tube can be written as

$$\begin{aligned}
p_r &= A_r + B_r \\
v_r &= \frac{A_r - B_r}{Y_r}
\end{aligned}$$

Whereas

$$\begin{aligned}
p_{r-1} &= A_r \cdot e^{-jk_0 l_r} + B_r \cdot e^{jk_0 l_r} \\
&= (A_r + B_r) \cos k_0 l_r - j \cdot (A_r - B_r) \sin k_0 l_r
\end{aligned}$$

$$p_{r-1} = p_r \cdot \cos k_0 l_r - j \cdot v_r Y_r \sin k_0 l_r \quad (11)$$

$$\begin{aligned}
v_{r-1} &= \frac{A_r \cdot e^{-jk_0 l_r} - B_r \cdot e^{jk_0 l_r}}{Y_r} \\
&= \frac{A_r - B_r}{Y_r} \cdot \cos k_0 l_r - j \cdot \frac{A_r + B_r}{Y_r} \cdot \sin k_0 l_r
\end{aligned}$$

$$v_{r-1} = v_r \cos k_0 l_r - j \frac{p_r}{Y_r} \cdot \sin k_0 l_r \quad (12)$$

Eq. 11 and Eq. 12 are written in matrix form as

$$\begin{bmatrix} p_{r-1} \\ v_{r-1} \end{bmatrix} = \begin{bmatrix} \cos k_0 l_r & -j \cdot Y_r \sin k_0 l_r \\ -j \frac{1}{Y_r} \cdot \sin k_0 l_r & \cos k_0 l_r \end{bmatrix} \begin{bmatrix} p_r \\ v_r \end{bmatrix}$$

$$\text{i.e. } \begin{bmatrix} p_r \\ v_r \end{bmatrix} = \begin{bmatrix} \cos k_o l_r & j Y_r \sin k_o l_r \\ j \frac{1}{Y_r} \sin k_o l_r & \cos k_o l_r \end{bmatrix} \begin{bmatrix} p_{r-1} \\ v_{r-1} \end{bmatrix} \quad (13)$$

Here k_o is wave number of the uniform element and Eq. 14 gives us the relation for determining sound pressure and particle velocity for uniform tube or a distributed element.

Figure 12.1 illustrates the equivalent distributed element circuit using the usual wave relation, and Eq. (14), which is derived from Eq. 59, provides the transfer matrix [29], [54].

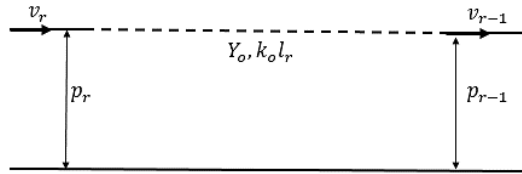


Figure 12.1. Equivalent circuit representation for a distributed element

$$\text{Transfer matrix } [T_d] = \begin{pmatrix} \cos(k_o l_r) & j Y_r \sin(k_o l_r) \\ \frac{j \sin(k_o l_r)}{Y_r} & \cos(k_o l_r) \end{pmatrix} \quad (14)$$

Here l_r = length of the element, Y_r = Characteristic impedance = c/S , where c = speed of sound, S = cross-sectional area.

Transfer matrix for lumped element

Figure 12.2 depicts the comparable circuit for an in-line lumped element using the usual wave relation.

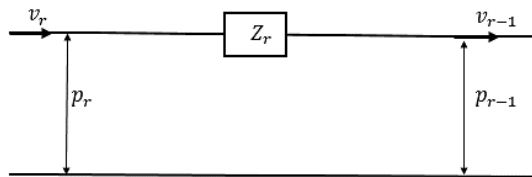


Figure 12.2. Equivalent circuit representation for an in-line lumped element

For an in-line lumped element, the standard wave relations are written as

$$p_r = p_{r-1} + Z_r \cdot v_{r-1}$$

$$v_r = v_{r-1}$$

In matrix form, it is written as

$$\begin{bmatrix} p_r \\ v_r \end{bmatrix} = \begin{bmatrix} 1 & Z_r \\ 0 & 1 \end{bmatrix} \begin{bmatrix} p_{r-1} \\ v_{r-1} \end{bmatrix}$$

When there is a quick area shift, such as when gases compress out of the muffler and into the tailpipe, in-line lumped elements are used. The transfer matrix for these elements is thus represented by Eq. 15 [29], [54].

$$\text{Transfer matrix } [T_i] = \begin{pmatrix} 1 & Z_r \\ 0 & 1 \end{pmatrix} \quad (15)$$

Here Z_r = Lumped impedance

Transfer matrix for shunt or branch lumped element

The analogous circuit for a branch or shunt lumped element using the conventional wave relation is depicted in Figure 12.3.

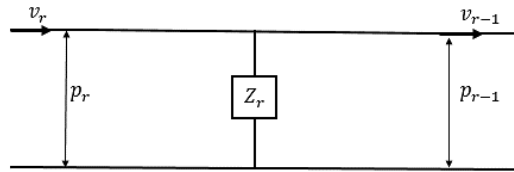


Figure 12.3. Equivalent circuit representation for a shunt lumped element

For a branch lumped element, the standard wave relations are written as

$$\begin{aligned} p_r &= p_{r-1} \\ v_r &= \frac{p_{r-1}}{Z_r} + v_{r-1} \end{aligned}$$

This can be written in matrix form as

$$\begin{bmatrix} p_r \\ v_r \end{bmatrix} = \begin{bmatrix} 1 & 0 \\ \frac{1}{Z_r} & 1 \end{bmatrix} \begin{bmatrix} p_{r-1} \\ v_{r-1} \end{bmatrix}$$

When any part of the muffler behaves like a Helmholtz resonator and the transfer matrix can be calculated using Eq. 16, a branch lumped element is used [29], [54].

$$\text{Transfer matrix } [T_s] = \begin{pmatrix} 1 & 0 \\ 1/Z_r & 1 \end{pmatrix} \quad (16)$$

Determining the TL in terms of four-pole parameters

The transmission loss of an element can be obtained through the four-pole parameters expressed in Eq. 10. These four-pole parameters for the overall transfer matrix of the system having element 2 to (r-1) can be obtained as shown in this section. For the r^{th} element, the transfer matrix expression is

$$\begin{bmatrix} p_{r-1} \\ v_{r-1} \end{bmatrix} = [T_r] \begin{bmatrix} p_r \\ v_r \end{bmatrix}$$

$$\begin{bmatrix} p_{r-1} \\ v_{r-1} \end{bmatrix} = \begin{bmatrix} E_{11} & E_{12} \\ E_{21} & E_{22} \end{bmatrix} \begin{bmatrix} p_r \\ v_r \end{bmatrix}$$

$$p_{r-1} = A_r + B_r$$

$$v_{r-1} = \frac{A_r - B_r}{Y_r}$$

$$p_1 = A_1 + B_1 = A_1 \text{ (as } B_1 = 0)$$

$$v_1 = \frac{A_1 - B_1}{Y_1} = \frac{A_1}{Y_1}$$

$$\text{Thus } A_r = [p_{r-1} + Y_r \cdot v_{r-1}] / 2$$

$$A_r = \left[\left(E_{11} A_1 + E_{12} \frac{A_1}{Y_1} \right) + Y_r \left(E_{21} A_1 + E_{22} \frac{A_1}{Y_1} \right) \right] / 2$$

$$\frac{A_r}{A_1} = \frac{1}{2} \left[\left(E_{11} + \frac{E_{12}}{Y_1} \right) + Y_r \left(E_{21} + \frac{E_{22}}{Y_1} \right) \right]$$

$$\text{i.e. } TL = 20 \log \left[\left(\frac{Y_1}{Y_r} \right)^{1/2} \left| \frac{1}{2} \left[\left(E_{11} + \frac{E_{12}}{Y_1} \right) + Y_r \left(E_{21} + \frac{E_{22}}{Y_1} \right) \right] \right| \right] \quad (17)$$

3. Aerodynamic performance analysis using finite element analysis

The finite element analysis is divided into three stages.

1. Preprocessing
2. Processing
3. Post-processing

Preprocessing: In this stage the problem that needs to be carried out is defined i.e. whether it is one-dimensional, two-dimensional or axis-symmetric three-dimensional case is identified. The geometry for the cross-section is constructed using the various tools available for it and afterwards meshing is performed in it.

Processing: This is the second stage where the different boundary conditions, constraints are implemented. The different aerodynamic parameters are implemented and the solution is processed.

Post-processing: This is the last stage of FEA, where the results obtained from solution is segregated in the form of graphical manner or numerical form and finally results are concluded.

In this study ANSYS is mainly used for determining the aerodynamic performance parameters i.e. back pressure or pressure drop for the various muffler models. The steps

followed for determining the aerodynamic performance parameter is thoroughly discussed in this section.

ANSYS Fluent module is used for obtaining the performance parameter and the principle steps followed in this process are as shown in Figure 6.1.

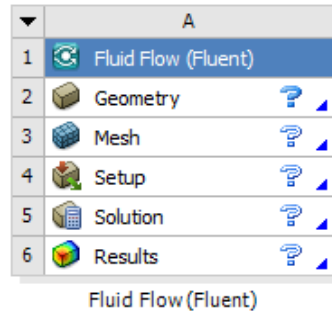


Figure 12.4. Steps for FEA in ANSYS Fluent

1. **Geometry:** The first step is to create the geometry of the muffler. Using the various sketching and modeling tools the muffler is constructed. During this process, the fluid and the solid domains should be clearly defined so that the flowing fluid passes through the acoustic elements properly.
2. **Mesh:** Construction the required model, next the model is discretize into 'n' number of small elements and nodes. Dividing the model into number of small finite elements is known as meshing. Depending on the size of each element, the model can be divided according to the need. Small size of each element for a particular cross-section will lead to increase in number of elements whereas large size of each element for that same cross-section will reduce the number of elements. Meshing mostly helps in predicting accurate result for the section. Fine meshing will lead to more accurate results as compared to an uneven meshing of the element.
3. **Setup:** In this step the total processing is followed. Initially the fluent launcher interface is opened and the option of two-dimensional or three-dimensional analysis is selected as shown in figure. Next the fluent interface is opened and in that step by step all the desired values and terms were selected as shown in Figure 6.2 and 6.3.

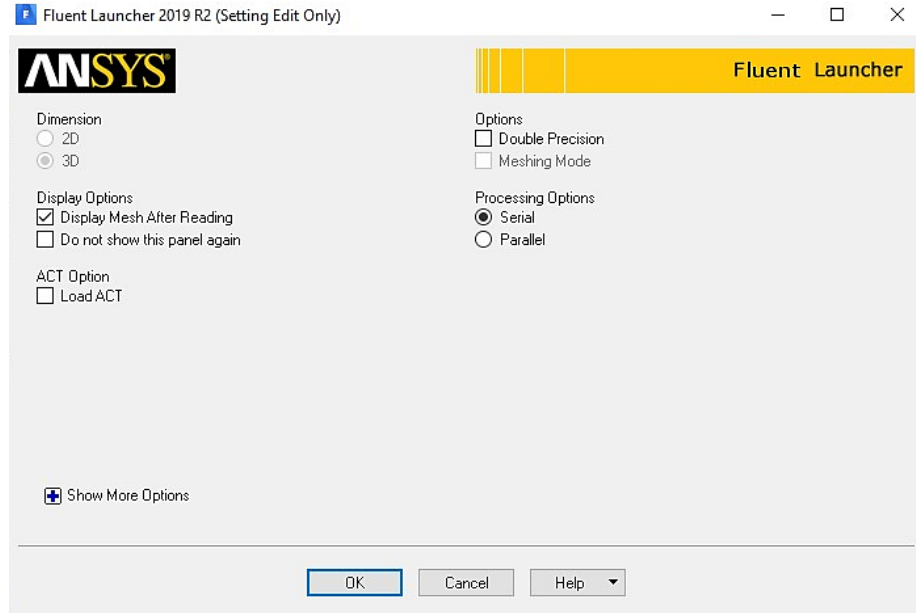


Figure 12.5. Fluent launcher interface for selecting module

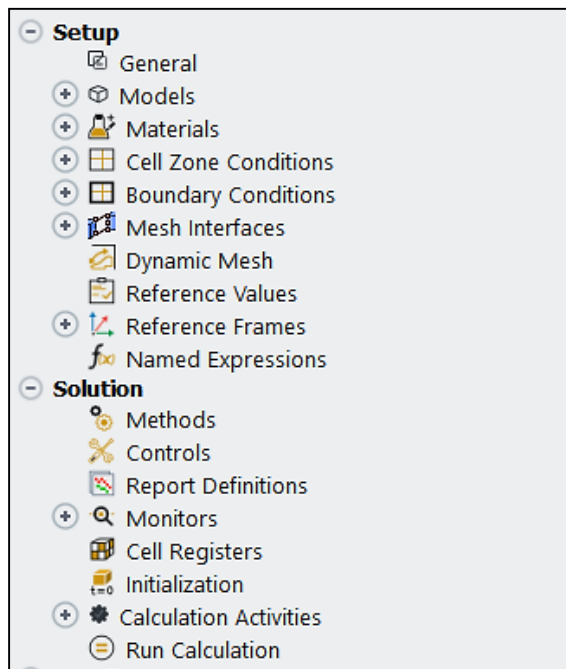


Figure 12.6. Steps used in setup and solution stage of fluent interface

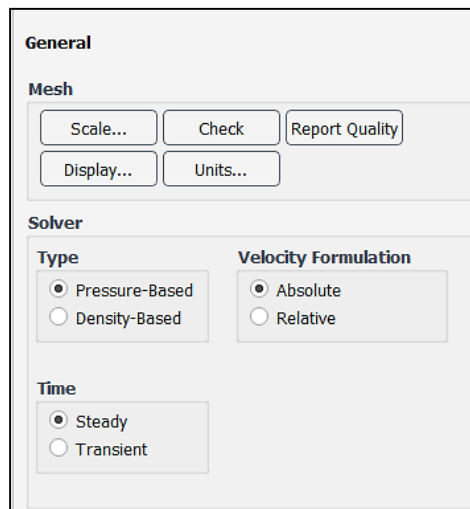
- i. **General:** type of solver, velocity formulation and type of fluid flow is selected.
- ii. **Model definition:** In this step, the type of flow equation, flow pattern and other physical properties applied to the muffler are selected.
- iii. **Materials:** According the domain and cross-section, the materials and its properties are implemented.

- iv. Cell zone condition: The type of domains applicable in each chamber are selected.
 - v. Boundary Condition: The boundary conditions applicable at the inlet section and at the outlet section of the muffler are fitted. In case of ducts or mufflers, velocity inlet and pressure outlet are the two main boundary conditions.
 - vi. Reference values: For processing the solution, the phase from which the reference values need to be considered is selected.
4. Solution: This is the processing stage where initially the method applicable for solving the process is selected. Then the different parameters that's need to be monitored are selected and afterwards it is initialized either through standard initialization or hybrid initialization. Next it is processed for calculation and the number of iterations that need to be carried out is implemented.
 5. Results: This is the post-processing stage where the results obtained from the solution is projected in plots and various contour diagrams. Pressure contour, velocity contour, acoustic power levels, streamline pattern are determined from the solution for the particular muffler.

4. Parameters used in the setup of aerodynamic performance analysis

The different conditions selected in setup for the aerodynamic analysis are discussed in this section step by step.

1. General



2. Models

Models

Models

Multiphase - Off

Energy - On

Viscous - Realizable k-e, Standard Wall Fn

Radiation - Off

Heat Exchanger - Off

Species - Off

Discrete Phase - Off

Solidification & Melting - Off

Acoustics - Broadband Noise Sources

Structure - Off

Eulerian Wall Film - Off

Electric Potential - Off

Model

Inviscid

Laminar

Spalart-Allmaras (1 eqn)

k-epsilon (2 eqn)

k-omega (2 eqn)

Transition k-kl-omega (3 eqn)

Transition SST (4 eqn)

Reynolds Stress (7 eqn)

Scale-Adaptive Simulation (SAS)

Detached Eddy Simulation (DES)

Large Eddy Simulation (LES)

k-epsilon Model

Standard

RNG

Realizable

Near-Wall Treatment

Standard Wall Functions

Scalable Wall Functions

Non-Equilibrium Wall Functions

Enhanced Wall Treatment

Menter-Lechner

User-Defined Wall Functions

Options

Viscous Heating

Curvature Correction

Production Limiter

Model Constants

C2-Epsilon
1.9

TKE Prandtl Number
1

TDR Prandtl Number
1.2

Energy Prandtl Number
0.85

Wall Prandtl Number
0.85

User-Defined Functions

Turbulent Viscosity
none

Prandtl Numbers

TKE Prandtl Number
none

TDR Prandtl Number
none

Energy Prandtl Number
none

Wall Prandtl Number
none

OK Cancel Help

Acoustics Model

Model

Off

Broadband Noise Sources

Model Constants

Far-Field Density (kg/m3)
1.225

Far-Field Sound Speed (m/s)
340

Reference Acoustic Power (w)
1e-12

Number of Realizations
200

Number of Fourier Modes
50

OK Apply Cancel Help

3. Materials

Create/Edit Materials

Name
air

Chemical Formula

Material Type
fluid

Fluent Fluid Materials
air

Mixture
none

Order Materials by

Name

Chemical Formula

Fluent Database...

User-Defined Database...

Properties

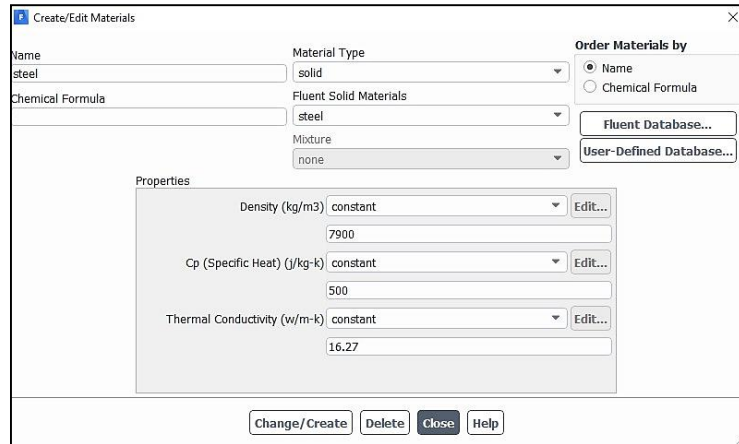
Density (kg/m3) constant Edit...
1.225

Cp (Specific Heat) (j/kg-k) constant Edit...
1006.43

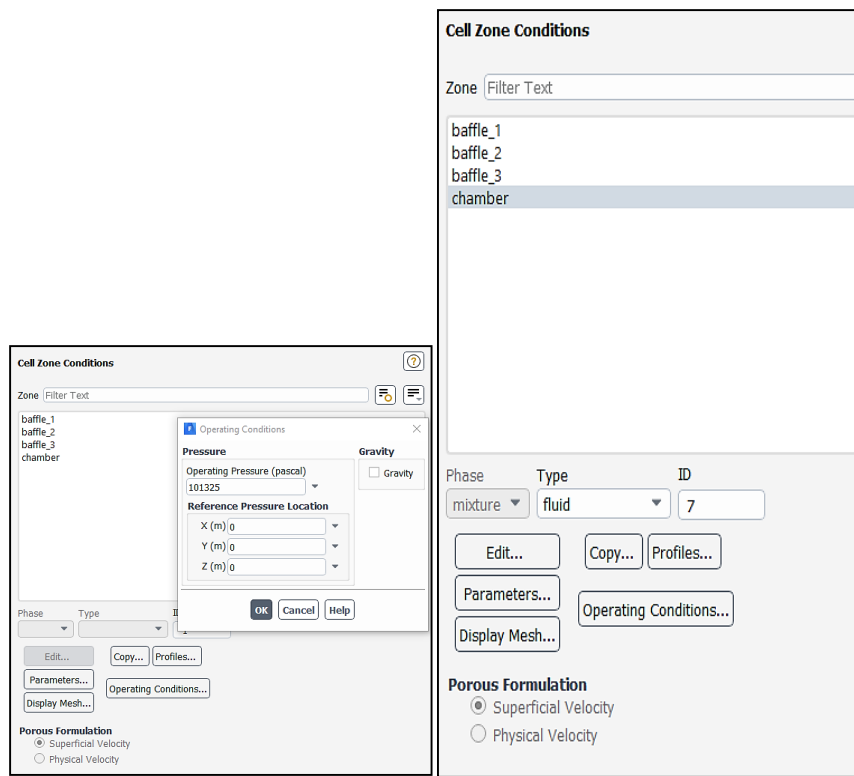
Thermal Conductivity (w/m-k) constant Edit...
0.0242

Viscosity (kg/m-s) constant Edit...

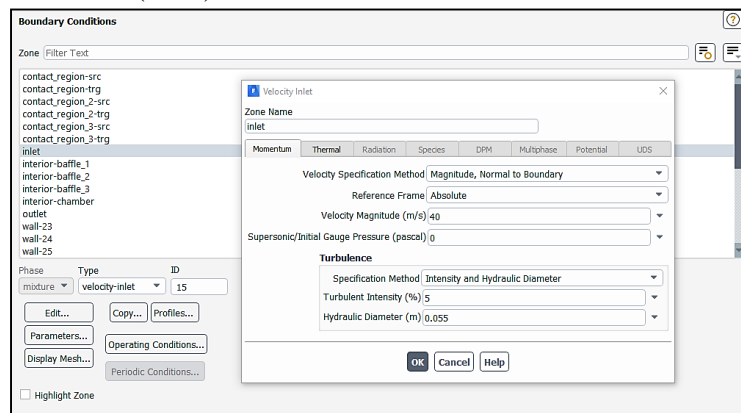
Change/Create Delete Close Help

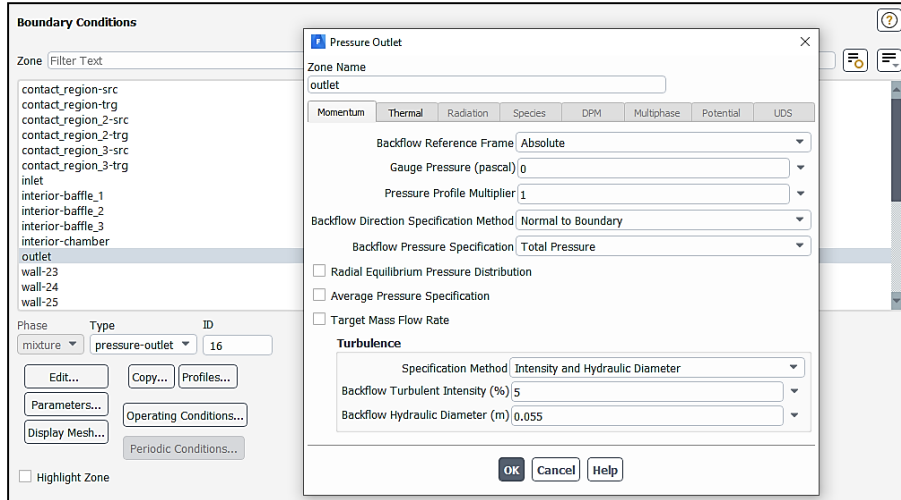


4. Cell zone conditions

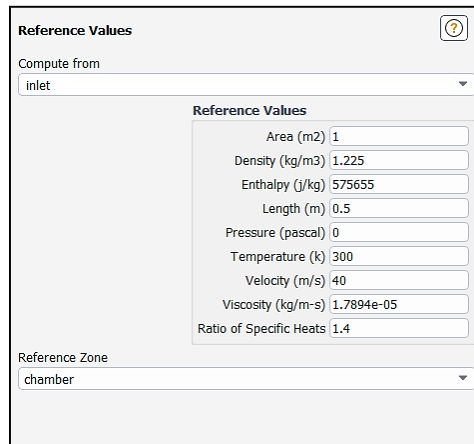


5. Boundary Conditions (B.C.)

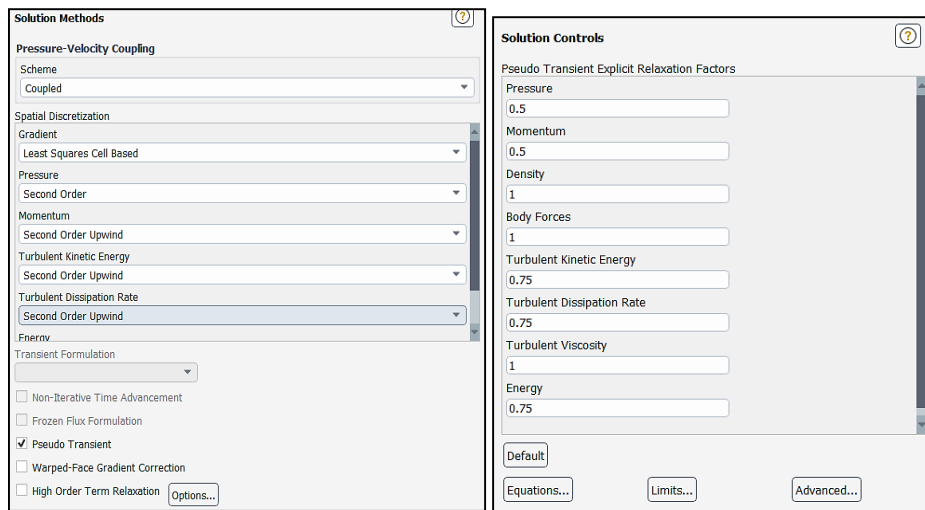




6. Reference Values : Values taken by selecting inlet section



Step 4: Solutions



Solution Initialization ?

Initialization Methods

Hybrid Initialization
 Standard Initialization

Compute from
inlet

Reference Frame

Relative to Cell Zone
 Absolute

Initial Values

Gauge Pressure (pascal)
0

X Velocity (m/s)
0

Y Velocity (m/s)
0

Z Velocity (m/s)
-40

Turbulent Kinetic Energy (m2/s2)
6

Turbulent Dissipation Rate (m2/s3)
627.2606

Temperature (k)

Initialize Reset Patch...

Run Calculation ?

Check Case... Update Dynamic Mesh...

Pseudo Transient Options

Fluid Time Scale

Time Step Method Timescale Factor
 User Specified 1
 Automatic

Length Scale Method Verbosity
Conservative 0

Solid Time Scale

Time Step Method Timescale Factor
 User Specified 1
 Automatic

Options

Data Sampling for Steady Statistics

Sampling Interval
1 Sampling Options...

Iterations Sampled 0

Number of Iterations Reporting Interval
150 1

Profile Update Interval
1

Data File Quantities... Acoustic Signals...
Acoustic Sources FFT...

Calculate

5. TL for the trial experiments of optimized reactive muffler

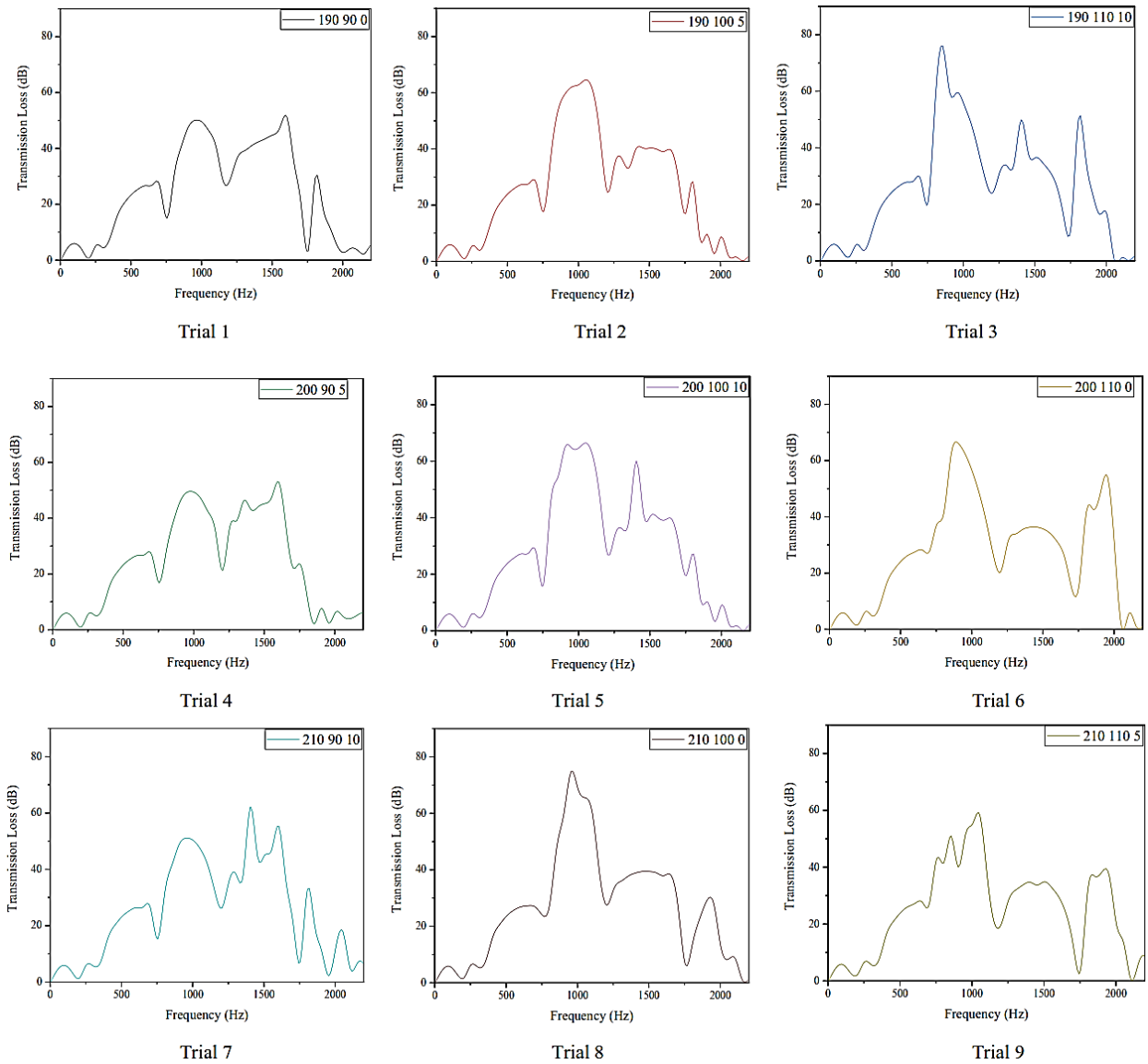


Figure 12.7. TL curve for all the trial experiments

LIST OF ABBREVIATIONS

BEM	Boundary Element Method
CF	Correction Factor
CFD	Computational Fluid Dynamics
FEM	Finite Element Method
IL	Insertion Loss
LD	Level Difference
SPL	Sound Pressure Level
TL	Transmission Loss
TMM	Transfer Matrix Method

NOMENCLATURE

ρ_0	Density of fluid
σ	Flow resistivity
f	Frequency
Z_c	Complex impedance
k_c	Complex wave number
γ	Specific heat
P	Back pressure
C_s	Speed of sound
G	Specific gas constant
K	Bulk modulus
η	Dynamic viscosity
Pr	Prandtl number
k	Thermal conductivity
ϕ	Porosity
V_f	Volume quotient
V_t	Total volume
ω	Angular frequency
Δp	Pressure difference
Q	Volumetric flow
k_i	Intrinsic permeability
S	Section of the material
l	Thickness of the material
α_∞	Tortuosity
R_{e0}	Resistivity without porous material
R_e	Resistivity with porous material
$n(\omega)$	Refraction index
c_0	Speed of sound in acoustic medium
$c(\omega)$	Speed of sound in porous medium
δ	Maximum viscous layer

Λ	Characteristic viscosity
Λ'	Thermal characteristic length
f_{Tt}	Transition frequency
ε	Porosity of the surface
R_h	Radius of the hole
d_h	Diameter of the hole
P_s	Muffler resistance
p_i	Inlet pressure
p_o	Outlet pressure
W_i	Incident power
W_t	Transmitted power
S_i	Inlet area
S_o	Outlet area
Δ	Determinant
$E_{11}, E_{12}, E_{21}, E_{22}$	4 pole parameters
Z_m	Impedance of absorption material
Y_m	Complex characteristic impedance
Ω_a	Domain for air
Ω_b	Domain for porous material

LIST OF PUBLICATIONS

1. Paper Title: Optimization of reactive muffler through pressure acoustic analysis and Taguchi approach.
Journal: **Journal of the Brazilian Society of Mechanical Sciences and Engineering (Scopus and WOS)**
Volume 45, Article number: 98 (2023)
Publication date: 19th January, 2023
DOI: <https://doi.org/10.1007/s40430-023-04023-1>
2. Paper Title: Optimization of absorption material layer thickness in different chambers of hybrid muffler using Taguchi approach.
Journal: **Sadhana-Academy Proceedings in Engineering Sciences (Scopus and WOS)**
Volume 47, Article number: 257 (2022)
Publication date: 28th November, 2022
DOI: <https://doi.org/10.1007/s12046-022-02039-2>
3. Paper title: Optimization of a Reactive muffler used in four-cylinder petrol engine into Hybrid muffler by using CFD analysis
Conference Proceeding: **Materials Today: Proceedings. (Scopus Indexed)**
Volume 50, Issue 5
Publication date: 25th October, 2021
<https://doi.org/10.1016/j.matpr.2021.09.319>
4. Paper title: Design and CFD analysis on flow through a reactive muffler of four-cylinder diesel engine
Conference Proceeding: Recent trends in Engineering Design” **Lecture Notes in Mechanical Engineering-Springer, (Scopus Indexed)**
Volume 340
Publication date: 26st June, 2021
DOI: [10.1007/978-981-16-1079-0_22](https://doi.org/10.1007/978-981-16-1079-0_22)
5. Paper title: Acoustic performance analysis of muffler by varying sound absorption materials.
Conference Proceeding: **Materials Today: Proceedings. (Scopus Indexed)**
Article in press
Publication date: 3rd March, 2023
<https://doi.org/10.1016/j.matpr.2023.02.272>
6. Paper title: A Review on mufflers used in automotive vehicles.
Journal: **International Journal of Engineering Research in Mechanical and Civil Engineering (IJERMCE)**

Volume 8, Issue 12.
Publication: 31st December, 2021

7. Paper title: Prediction of transmission loss on a simple expansion chamber muffler.
Journal: **Journal of Emerging Technologies and Innovative Research (JETIR)**
(UGC)
Volume 5, Issue 12.
Publication: 31st December, 2018

8. Paper title: Prediction of transmission loss in muffler on varying the flow resistivity of absorption material.
Journal: **Journal of Emerging Technologies and Innovative Research (JETIR)**
(UGC)
Volume 6, Issue 3.
Publication: 31st March, 2019

LIST OF CONFERENCES

1. Paper title : Acoustic performance analysis of muffler by varying sound absorption materials.
Conference : **2nd International Conference on Recent Advances in Modeling and Simulations Techniques in Engineering and Sciences (RAMSTES-2022)**
Manipal University, Jaipur. 9th – 11th November, 2022.
2. Paper title: Optimization of a Reactive muffler used in four-cylinder petrol engine into Hybrid muffler by using CFD analysis
Conference : **2nd International Conference on Functional Materials, Manufacturing and Performances (ICFMMP)**
Lovely Professional University, Punjab, 17– 18th September, 2021
3. Paper title: Design and CFD analysis on flow through a reactive muffler of four-cylinder diesel engine
Conference : **International Conference on Advances in Sustainable Technologies – ICAST 2020**
Lovely Professional University, Punjab, 6th - 7th November, 2020
4. Paper title: Aerodynamic Performance analysis of Muffler used in exhaust system of automotive vehicles
Conference : **International Conference on Materials for Emerging Technologies (ICMET 2021)**
Lovely Professional University, Punjab, 18 – 19th February, 2022
5. Paper Title : Optimization of a Reactive muffler through acoustic performance analysis
Conference : **International Conference on Materials for Emerging Technologies (ICMET 2021)**
Lovely Professional University, Punjab, 18 – 19th February, 2022

LIST OF PATENTS

1. Title of Invention: A NOVEL MUFFLER TEST RIG FOR ALL SIZES OF MUFFLER

Application No. : 202011005584 A

Publication Date : 04/09/2020

2. Title of Invention: MUFFLER TEST RIG DEVICE WITH PRESSURE MONITORING IN EACH CHAMBER

Application No. : 202211067029 A

Publication Date : 02/12/2022

3. Title of Invention: MUFFLER TEST RIG WITH VIBRATION ANALYZER

Application No. : 202211066105 A

Publication Date : 25/11/2022

LIST OF CERTIFICATION COURSES

NOISE MANAGEMENT AND CONTROL



NPTEL Online Certification

(Funded by the Ministry of HRD, Govt. of India)



This certificate is awarded to
UJJAL KALITA
for successfully completing the course
Noise Management and Control
with a consolidated score of **49 %**


Online Assignments	18.38/25	Proctored Exam	30.75/75
--------------------	----------	----------------	----------



Prof. T. V. Prabhakar
Chairman
Center for Continuing Education, IITK

Total number of candidates certified in this course: **201**

Jul-Oct 2018
(12 week course)



Prof. Satyaki Roy
NPTEL Coordinator
IIT Kanpur



Indian Institute of Technology Kanpur




FREE ONLINE EDUCATION
swayam
The Best Merit, Smart Merit

Roll No: NPTEL18ME63S21420045


To validate and check scores: <http://npTEL.ac.in/noc>

ACOUSTICS MATERIALS AND METAMATERIALS



NPTEL Online Certification

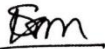
(Funded by the MoE, Govt. of India)



This certificate is awarded to
UJJAL KALITA
for successfully completing the course
Acoustic Materials and Metamaterials
with a consolidated score of **49 %**

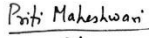
Online Assignments	19.46/25	Proctored Exam	30/75
--------------------	----------	----------------	-------

Total number of candidates certified in this course: **23**




Prof. Sanjeev Manhas
Coordinator, Continuing Education Centre
IIT Roorkee


Jan-Mar 2023
(8 week course)



Prof. Priti Maheshwari
NPTEL Coordinator
IIT Roorkee




Indian Institute of Technology Roorkee



FREE ONLINE EDUCATION
swayam
The Best Merit, Smart Merit

Roll No: NPTEL23ME03S44770185

To validate the certificate 

No. of credits recommended: 2 or 3